

# Synchrony affects Taylor's law in theory and data: Supporting information

Daniel C. Reuman, Lei Zhao, Lawrence W. Sheppard, Philip C. Reid, Joel E. Cohen

Section S1 states the general framework for the main mathematical analysis. Section S2 carries out the main analysis, which covers the case that the  $Y_i$  (see main text for a definition of  $Y_i$ ) are identically distributed but not necessarily independent. Section S3 analyzes (via the results of section S2) and simulates case studies of distributions  $Y = (Y_1, \dots, Y_n)$  constructed by transforming multi-variate Gaussian random variables, and with identically distributed  $Y_i$ . Section S4 considers case studies of distributions constructed by transforming Gaussian variables so that the resulting distributions have non-identically distributed  $Y_i$ . Section S5 considers case studies using an alternate construction of  $Y$  with identically distributed  $Y_i$ . Section S6 has plotting methods. Section S7 has details of data. Sections S8-S10 contain plots associated with sections S3-S5. Remaining sections have additional figures and tables.

## Contents

<b>S1 Framework for mathematical analysis of spatial Taylor's law</b>	<b>4</b>
<b>S2 Mathematical analysis of the identically distributed case</b>	<b>6</b>
<b>S3 Cases: Distributions constructed using Gaussian copulas and identically distributed marginals</b>	<b>11</b>
<b>S4 Cases: Distributions constructed using Gaussian copulas and non-identically distributed marginals</b>	<b>14</b>
<b>S5 Cases: Distributions constructed using sums and identically distributed marginals</b>	<b>15</b>
<b>S6 Methods for the omnibus plots</b>	<b>20</b>
<b>S7 Data details</b>	<b>21</b>
<b>S8 Figures, distributions constructed using Gaussian copulas and identically distributed marginals</b>	<b>23</b>
<b>S9 Figures, distributions constructed using Gaussian copulas and non-identically distributed marginals</b>	<b>55</b>
<b>S10 Figures, distributions constructed using sums and identically distributed marginals</b>	<b>87</b>
<b>S11 Figures testing spatial Taylor's law for empirical data</b>	<b>113</b>
<b>S12 Figures testing spatial Taylor's law for randomized or partially sorted data</b>	<b>119</b>
<b>S13 Other figures</b>	<b>121</b>
<b>S14 Tables</b>	<b>124</b>

## List of Figures

S1	Omnibus plots, ID Gaussian copula approach, Poisson . . . . .	23
S2	Omnibus plots, ID Gaussian copula approach, Poisson . . . . .	24
S3	Omnibus plots, ID Gaussian copula approach, negative binomial . . . . .	25
S4	Omnibus plots, ID Gaussian copula approach, negative binomial . . . . .	26
S5	Omnibus plots, ID Gaussian copula approach, negative binomial . . . . .	27
S6	Omnibus plots, ID Gaussian copula approach, negative binomial . . . . .	28
S7	Omnibus plots, ID Gaussian copula approach, negative binomial . . . . .	29
S8	Omnibus plots, ID Gaussian copula approach, negative binomial . . . . .	30
S9	Omnibus plots, ID Gaussian copula approach, negative binomial . . . . .	31
S10	Omnibus plots, ID Gaussian copula approach, negative binomial . . . . .	32
S11	Omnibus plots, ID Gaussian copula approach, gamma . . . . .	33
S12	Omnibus plots, ID Gaussian copula approach, gamma . . . . .	34
S13	Omnibus plots, ID Gaussian copula approach, gamma . . . . .	35
S14	Omnibus plots, ID Gaussian copula approach, gamma . . . . .	36
S15	Omnibus plots, ID Gaussian copula approach, gamma . . . . .	37
S16	Omnibus plots, ID Gaussian copula approach, gamma . . . . .	38
S17	Omnibus plots, ID Gaussian copula approach, exponential . . . . .	39
S18	Omnibus plots, ID Gaussian copula approach, exponential . . . . .	40
S19	Omnibus plots, ID Gaussian copula approach, chi-squared . . . . .	41
S20	Omnibus plots, ID Gaussian copula approach, chi-squared . . . . .	42
S21	Omnibus plots, ID Gaussian copula approach, normal . . . . .	43
S22	Omnibus plots, ID Gaussian copula approach, normal . . . . .	44
S23	Omnibus plots, ID Gaussian copula approach, normal . . . . .	45
S24	Omnibus plots, ID Gaussian copula approach, normal . . . . .	46
S25	Omnibus plots, ID Gaussian copula approach, normal . . . . .	47
S26	Omnibus plots, ID Gaussian copula approach, normal . . . . .	48
S27	Omnibus plots, ID Gaussian copula approach, log-normal . . . . .	49
S28	Omnibus plots, ID Gaussian copula approach, log-normal . . . . .	50
S29	Omnibus plots, ID Gaussian copula approach, log-normal . . . . .	51
S30	Omnibus plots, ID Gaussian copula approach, log-normal . . . . .	52
S31	Omnibus plots, ID Gaussian copula approach, log-normal . . . . .	53
S32	Omnibus plots, ID Gaussian copula approach, log-normal . . . . .	54
S33	Omnibus plots, non-ID Gaussian copula approach, Poisson . . . . .	55
S34	Omnibus plots, non-ID Gaussian copula approach, Poisson . . . . .	56
S35	Omnibus plots, non-ID Gaussian copula approach, gamma . . . . .	57
S36	Omnibus plots, non-ID Gaussian copula approach, gamma . . . . .	58
S37	Omnibus plots, non-ID Gaussian copula approach, gamma . . . . .	59
S38	Omnibus plots, non-ID Gaussian copula approach, gamma . . . . .	60
S39	Omnibus plots, non-ID Gaussian copula approach, gamma . . . . .	61
S40	Omnibus plots, non-ID Gaussian copula approach, gamma . . . . .	62
S41	Omnibus plots, non-ID Gaussian copula approach, exponential . . . . .	63
S42	Omnibus plots, non-ID Gaussian copula approach, exponential . . . . .	64
S43	Omnibus plots, non-ID Gaussian copula approach, chi-squared . . . . .	65
S44	Omnibus plots, non-ID Gaussian copula approach, chi-squared . . . . .	66
S45	Omnibus plots, non-ID Gaussian copula approach, normal . . . . .	67

S46	Omnibus plots, non-ID Gaussian copula approach, normal . . . . .	68
S47	Omnibus plots, non-ID Gaussian copula approach, normal . . . . .	69
S48	Omnibus plots, non-ID Gaussian copula approach, normal . . . . .	70
S49	Omnibus plots, non-ID Gaussian copula approach, normal . . . . .	71
S50	Omnibus plots, non-ID Gaussian copula approach, normal . . . . .	72
S51	Omnibus plots, non-ID Gaussian copula approach, log-normal . . . . .	73
S52	Omnibus plots, non-ID Gaussian copula approach, log-normal . . . . .	74
S53	Omnibus plots, non-ID Gaussian copula approach, log-normal . . . . .	75
S54	Omnibus plots, non-ID Gaussian copula approach, log-normal . . . . .	76
S55	Omnibus plots, non-ID Gaussian copula approach, log-normal . . . . .	77
S56	Omnibus plots, non-ID Gaussian copula approach, log-normal . . . . .	78
S57	Omnibus plots, non-ID Gaussian copula approach, negative binomial . . . . .	79
S58	Omnibus plots, non-ID Gaussian copula approach, negative binomial . . . . .	80
S59	Omnibus plots, non-ID Gaussian copula approach, negative binomial . . . . .	81
S60	Omnibus plots, non-ID Gaussian copula approach, negative binomial . . . . .	82
S61	Omnibus plots, non-ID Gaussian copula approach, negative binomial . . . . .	83
S62	Omnibus plots, non-ID Gaussian copula approach, negative binomial . . . . .	84
S63	Omnibus plots, non-ID Gaussian copula approach, negative binomial . . . . .	85
S64	Omnibus plots, non-ID Gaussian copula approach, negative binomial . . . . .	86
S65	Omnibus plots, sums approach, Poisson . . . . .	87
S66	Omnibus plots, sums approach, Poisson . . . . .	88
S67	Omnibus plots, sums approach, negative binomial . . . . .	89
S68	Omnibus plots, sums approach, negative binomial . . . . .	90
S69	Omnibus plots, sums approach, negative binomial . . . . .	91
S70	Omnibus plots, sums approach, negative binomial . . . . .	92
S71	Omnibus plots, sums approach, negative binomial . . . . .	93
S72	Omnibus plots, sums approach, negative binomial . . . . .	94
S73	Omnibus plots, sums approach, negative binomial . . . . .	95
S74	Omnibus plots, sums approach, negative binomial . . . . .	96
S75	Omnibus plots, sums approach, gamma . . . . .	97
S76	Omnibus plots, sums approach, gamma . . . . .	98
S77	Omnibus plots, sums approach, gamma . . . . .	99
S78	Omnibus plots, sums approach, gamma . . . . .	100
S79	Omnibus plots, sums approach, gamma . . . . .	101
S80	Omnibus plots, sums approach, gamma . . . . .	102
S81	Omnibus plots, sums approach, exponential . . . . .	103
S82	Omnibus plots, sums approach, exponential . . . . .	104
S83	Omnibus plots, sums approach, chi-squared . . . . .	105
S84	Omnibus plots, sums approach, chi-squared . . . . .	106
S85	Omnibus plots, sums approach, normal . . . . .	107
S86	Omnibus plots, sums approach, normal . . . . .	108
S87	Omnibus plots, sums approach, normal . . . . .	109
S88	Omnibus plots, sums approach, normal . . . . .	110
S89	Omnibus plots, sums approach, normal . . . . .	111
S90	Omnibus plots, sums approach, normal . . . . .	112
S91	Figure testing TL for aphid data . . . . .	113
S92	Figure testing TL for CPR data . . . . .	114
S93	Figure testing TL for CalCOFI data . . . . .	115
S94	Figure testing TL for CalCOFI data . . . . .	116
S95	Figure testing TL for CalCOFI data . . . . .	117

S96	Figure testing TL for CalCOFI data . . . . .	118
S97	Figure testing TL for randomized data . . . . .	119
S98	Figure testing TL for sorted data . . . . .	120
S99	Main text figure 2 with numbered points . . . . .	121
S100	Related to main text figure 3 . . . . .	122
S101	Temperature and nutrient depth gradients, CalCOFI . . . . .	123

## List of Tables

S1	Taxa and depth indices . . . . .	124
S2	Aphid sampling sites . . . . .	125
S3	Summary of analytic and numerical results with hyperlinks . . . . .	126
S4	Summary of empirical and randomization results with hyperlinks . . . . .	127

## S1 Framework for mathematical analysis of spatial Taylor’s law

Suppose the population size or density in location  $i$  at time  $t$  is modeled by the non-negative real-valued random variable  $Y_i(t)$  for  $i = 1, \dots, n$ . Assume that the stochastic process  $Y(t) = (Y_1, \dots, Y_n)$  is stationary and ergodic. Roughly speaking, a “stationary” stochastic process is one whose joint probability distribution is not affected by shifts in time, so that mechanisms of population dynamics are not shifting in time. And an “ergodic” process is one for which statistical characteristics can be deduced from a single, sufficiently long realization of the process, so that, for instance, long-term statistical outcomes are independent of initial conditions. Precise definitions are in standard texts [Brillinger, 2001]. These are common features or assumptions of ecological models [Nisbet and Gurney, 1982, Caswell, 2001, Turchin, 2003]. Define the spatial sample mean and sample variance as the random variables  $m(t) = \frac{1}{n} \sum_{i=1}^n Y_i(t)$  and  $v(t) = \frac{1}{n-1} \sum_{i=1}^n (Y_i(t) - \frac{1}{n} \sum_{j=1}^n Y_j(t))^2 = \frac{1}{n-1} \sum_{i=1}^n Y_i(t)^2 - \frac{n}{n-1} m(t)^2$ , which are also ergodic stationary stochastic processes. We are interested in the  $\log(v)$ -versus- $\log(m)$  scatter plot for a finite-duration realization of these processes (ignoring times  $t$  for which  $m(t)$  or  $v(t)$  was zero), and particularly in the slope and intercept of an ordinary linear regression through such a plot,

$$b = \frac{\text{cov}_t(\ln(m(t)), \ln(v(t)))}{\text{var}_t(\ln(m(t)))}, \quad (1)$$

$$\ln(a) = E_t(\ln(v(t))) - bE_t(\ln(m(t))). \quad (2)$$

These are the basic quantities in spatial TL. The subscripts  $t$  indicate that the covariance, variance, and expected value (mean) are sample quantities computed through time for the finite-duration realization. By ergodicity of  $Y$  and consistency of the sample mean, variance, and covariance, for large samples, we instead consider

$$b = \frac{\text{cov}(\ln(m), \ln(v))}{\text{var}(\ln(m))}, \quad (3)$$

$$\ln(a) = E(\ln(v)) - bE(\ln(m)), \quad (4)$$

where the covariance, variance, and expected value are computed for the marginal distributions of the processes  $m$  and  $v$  conditional on positive values of these quantities. We assume these quantities are finite.

Suppose the population correlations  $\rho_{ij} = \text{cor}(Y_i, Y_j)$  exist for all  $i, j = 1, \dots, n$ . These temporal correlations between populations represent spatial synchrony between locations  $i$  and  $j$  (again making use of ergodicity, and consistency of the sample covariance and variance). The synchrony  $\Omega = \frac{1}{n^2} \sum_{i,j} \rho_{ij}$  is an average correlation across all pairs of sampling locations (including comparisons of a location with itself, which give  $\rho_{ii} = 1$ ), and is commonly used in empirical studies. We will analyze the influence of  $\Omega$  on  $b$ .

$\Omega$  is naturally interpretable as a measure of average synchrony for the following additional reasons. First, letting  $Z_i = Y_i / \sqrt{\text{var}(Y_i)}$ , we have

$$\Omega = \frac{1}{n^2} \sum_{ij} \text{cor}(Y_i, Y_j) \quad (5)$$

$$= \frac{1}{n^2} \sum_{ij} \text{cor}(Z_i, Z_j) \quad (6)$$

$$= \frac{1}{n^2} \sum_{ij} \text{cov}(Z_i, Z_j) \quad (7)$$

$$= \frac{1}{n^2} \text{cov} \left( \sum_i Z_i, \sum_j Z_j \right) \quad (8)$$

$$= \text{var} \left( \frac{1}{n} \sum_i Z_i \right) \quad (9)$$

$$= \frac{\text{var} \left( \frac{1}{n} \sum_i Z_i \right)}{\frac{1}{n} \sum_i \text{var}(Z_i)}, \quad (10)$$

where equation (10) is the variance of a mean divided by the mean of the variances. This well known measure of synchrony is readily interpretable as the extent to which oscillations in local (normalized) time series reinforce each other or cancel in the average time series. Second, equation (10) and the definition of  $\Omega$  show that  $0 \leq \Omega \leq 1$ . The value 0 occurs when the variability in the  $Z_i$  exactly cancels, i.e.,  $\text{var} \left( \frac{1}{n} \sum_i Z_i \right) = 0$  and  $\frac{1}{n} \sum_i Z_i = \frac{1}{n} \sum_i E(Z_i)$ , perfect asynchrony. The value 1 occurs when  $Z_i = Z_j$  for all  $i, j$ , perfect synchrony. The summation  $\frac{1}{n(n-1)} \sum_{i \neq j} \rho_{ij}$  is an alternative measure of synchrony but may be less natural because it can take negative values (its minimum is  $-1/(n-1)$ ). The difference between this measure and  $\Omega$  is essentially in whether 0 should represent perfect asynchrony (independence) or perfect antisynchrony (cancelation).

To understand the relationship between synchrony and TL for large samples under assumptions of stationarity and ergodicity, it is sufficient to work with the marginal distribution  $Y$ , instead of with the process  $Y(t)$ . We therefore consider families of distributions of the form  $Y = (Y_1, \dots, Y_n)$  such that for each  $i$ , all members of the family have the same marginals  $Y_i$ , and we consider how  $\Omega$  and  $b$  covary through the family. In the theoretical development, marginals are kept constant to understand the influence of synchrony  $\Omega$  in isolation from other potential influences on  $b$ .

To describe the intuition of the mathematical analyses that will be described in detail in section S2, we need a lemma, taken directly from Cohen and Xu [2015]. They cite Oehlert [1992] and Hosmer et al. [2008] pp. 355-358.

**Lemma 1.** *Let  $X$  be a real-valued random variable with finite mean  $E(X)$  and finite variance  $\text{var}(X)$ . If a real-valued function  $f$  of real  $x$  is twice differentiable at  $E(X)$ , then the delta method gives*

$$f(X) \approx f(E(X)) + (X - E(X))f'(E(X)) \quad (11)$$

$$E(f(X)) \approx f(E(X)) + \frac{f''(E(X))}{2} \text{var}(X) \quad (12)$$

$$\text{var}(f(X)) \approx [f'(E(X))]^2 \text{var}(X). \quad (13)$$

We now use the lemma with  $f(x) = \ln(x)$ :

$$\ln(m) \approx \ln(\mathbb{E}(m)) + \frac{m - \mathbb{E}(m)}{\mathbb{E}(m)} \quad (14)$$

$$\ln(v) \approx \ln(\mathbb{E}(v)) + \frac{v - \mathbb{E}(v)}{\mathbb{E}(v)} \quad (15)$$

$$\text{var}(\ln(m)) = \frac{\text{var}(m)}{\mathbb{E}(m)^2}, \quad (16)$$

where the approximation is good as long as  $m$  and  $v$  do not vary too much around  $\mathbb{E}(m)$  and  $\mathbb{E}(v)$ , relative to the range of  $x$  for which first- and second-order Taylor expansions of  $\ln(x)$  at  $\mathbb{E}(m)$  and  $\mathbb{E}(v)$  are good approximations. Therefore,

$$\frac{\text{cov}(\ln(m), \ln(v))}{\text{var}(\ln(m))} \approx \frac{\mathbb{E}(m)}{\mathbb{E}(v)} \frac{\text{cov}(m, v)}{\text{var}(m)}. \quad (17)$$

But  $\mathbb{E}(v) = \frac{1}{n-1} \sum_{i=1}^n \mathbb{E}(Y_i^2) - \frac{n}{n-1} \mathbb{E}(m^2)$  and  $\text{var}(m) = \mathbb{E}(m^2) - \mathbb{E}(m)^2$ , so  $\mathbb{E}(m^2) = \text{var}(m) + \mathbb{E}(m)^2$  and  $\mathbb{E}(v) = \frac{1}{n-1} \sum_{i=1}^n \mathbb{E}(Y_i^2) - \frac{n}{n-1} (\text{var}(m) + \mathbb{E}(m)^2) = \frac{n}{n-1} (A - \text{var}(m))$  where  $A = \frac{1}{n} \sum_{i=1}^n \mathbb{E}(Y_i^2) - \mathbb{E}(m)^2$ . Thus

$$\frac{\text{cov}(\ln(m), \ln(v))}{\text{var}(\ln(m))} \approx \frac{(n-1)\mathbb{E}(m)}{n} \frac{\text{cov}(m, v)}{(A - \text{var}(m))\text{var}(m)}. \quad (18)$$

The first factor on the right of this approximation depends only on  $n$  and the marginals  $Y_i$  and not on their correlations. The quantity  $A$  also depends only on marginals. The quantity  $\text{var}(m)$ , however, equals  $\frac{1}{n^2} \sum_{i,j} \text{cov}(Y_i, Y_j)$ , which relates to synchrony  $\Omega$  and is similar in form to  $\Omega$ . The expression in (18) therefore provides the intuition behind our analysis: if synchrony ( $\Omega$  or  $\text{var}(m)$ ) changes and the marginals  $Y_i$  remain fixed, then (18) suggests that the slope  $b$  will be affected. Since the denominator of (18) is a  $\cap$ -shaped function of  $\text{var}(m)$ ,  $b$  may be a  $\cup$ -shaped function of synchrony, decreasing as synchrony increases for small values of synchrony, and increasing again for larger values of synchrony. These are hypotheses rather than conclusions because  $\text{cov}(m, v)$  in the numerator of (18) may also covary with synchrony.

## S2 Mathematical analysis of the identically distributed case

### S2.1 Setup of an identically distributed model

Assume the  $Y_i$  are all identically distributed (but not necessarily independent) with finite  $\mathbb{E}(Y_i) = M > 0$  and finite  $\text{var}(Y_i) = V > 0$ . Let  $\mu_{ij} = \mathbb{E}((Y_i - M)(Y_j - M))$ ,  $\mu_{ijk} = \mathbb{E}((Y_i - M)(Y_j - M)(Y_k - M))$ ,  $\mu_{ijkl} = \mathbb{E}((Y_i - M)(Y_j - M)(Y_k - M)(Y_l - M))$ , and assume these are all finite. Then  $\rho_{ij} = \text{cor}(Y_i, Y_j) = \frac{\mu_{ij}}{\sqrt{V}}$ . Also define  $\rho_{ijk} = \frac{\mu_{ijk}}{\mu_{iii}}$ . As in section S1, define  $m = \frac{1}{n} \sum_{i=1}^n Y_i$  and  $v = \frac{1}{n-1} \sum_{i=1}^n (Y_i - \frac{1}{n} \sum_{j=1}^n Y_j)^2 = \frac{1}{n-1} \sum_{i=1}^n Y_i^2 - \frac{n}{n-1} m^2$  to be the spatial sample mean and variance, and define  $\Omega = \frac{1}{n^2} \sum_{i,j} \rho_{ij}$  as synchrony. We aim to understand the influence of  $\rho_{ij}$  and  $\Omega$  on the quantities

$$b = \frac{\text{cov}(\ln(m), \ln(v))}{\text{var}(\ln(m))}. \quad (19)$$

$$\ln(a) = \mathbb{E}(\ln(v)) - b\mathbb{E}(\ln(m)). \quad (20)$$

The following analytic development uses as a guide and generalizes the analysis in the supporting information of Cohen and Xu [2015]. The important generalization here is that we no longer assume independence (across space) of the random variables representing populations. Cohen and Xu [2015] also had unequal numbers of sites  $n_j$  measured for each time  $j$ , but we assume  $n_j = n$  for all  $j$ .

## S2.2 Preparatory lemmas

**Lemma 2.** For the random variable  $m$  and  $f(x) = \ln(x)$ , the approximations from the delta method are

$$\ln(m) \approx \ln(M) + \frac{m - M}{M} \quad (21)$$

$$E(\ln(m)) \approx \ln(M) - \frac{1}{2M^2}V\Omega \quad (22)$$

$$\text{var}(\ln(m)) \approx \frac{V\Omega}{M^2}, \quad (23)$$

where  $\Omega = \frac{1}{n^2}\Sigma_{ij}\rho_{ij}$ .

*Proof.* In the formulas of lemma 1, let  $X = m$  and  $f(x) = \ln(x)$ . Then  $f'(x) = \frac{1}{x}$ ,  $f''(x) = \frac{-1}{x^2}$ ,  $E(m) = M$ , and  $\text{var}(m) = \frac{1}{n^2}\Sigma_{ij}\mu_{ij} = V\Omega$ . Plugging into the formulas gives the desired results.  $\blacksquare$

If  $\rho_{ij} = 0$  for all  $i \neq j$  then  $\Omega = \frac{1}{n}$  and the results of lemma 2 reduce to those of lemma 1 of Cohen and Xu [2015] with  $n_j$  set to  $n$  for all  $j$ .

**Lemma 3.** For the random variable  $v$  and  $f(x) = \ln(x)$ , we have

$$E(v) = \frac{nV(1 - \Omega)}{n - 1} \quad (24)$$

$$\ln(v) \approx \ln(E(v)) + \frac{v - E(v)}{E(v)} \quad (25)$$

$$E(\ln(v)) \approx \ln(E(v)) - \frac{(n - 1)^2 \text{var}(v)}{2n^2V^2(1 - \Omega)^2} \quad (26)$$

$$\text{var}(\ln(v)) \approx \frac{(n - 1)^2 \text{var}(v)}{n^2V^2(1 - \Omega)^2} \quad (27)$$

$$\text{var}(v) = \frac{n^2 \sum_{ij} \mu_{iijj} - 2n \sum_{ijk} \mu_{iijk} + \sum_{ijkl} \mu_{ijkl}}{n^2(n - 1)^2} - (E(v))^2. \quad (28)$$

*Proof.*

$$E(v) = \frac{1}{n - 1} \sum_{i=1}^n E(Y_i^2) - \frac{n}{n - 1} E(m^2) \quad (29)$$

$$= \frac{1}{n - 1} \sum_{i=1}^n (V + M^2) - \frac{n}{n - 1} (\text{var}(m) + M^2) \quad (30)$$

$$= \frac{1}{n - 1} \sum_{i=1}^n (V + M^2) - \frac{n}{n - 1} (V\Omega + M^2) \quad (31)$$

$$= \frac{n}{n - 1} (V + M^2) - \frac{n}{n - 1} (V\Omega + M^2) \quad (32)$$

$$= \frac{Vn(1 - \Omega)}{n - 1}. \quad (33)$$

Now plugging into one of the formulas of lemma 1 with  $X = v$  and  $f(x) = \ln(x)$  gives the approximate equations for  $\ln(v)$ ,  $E(\ln(v))$ , and  $\text{var}(\ln(v))$  in terms of  $\text{var}(v)$ . To work out  $\text{var}(v)$  in terms of the moments and co-moments of the  $Y_i$ , note

$$\text{var}(v) = E(v^2) - E(v)^2 \quad (34)$$

$$= E(v^2) - \left( \frac{nV(1 - \Omega)}{n - 1} \right)^2. \quad (35)$$

Define  $Z_i = Y_i - M$ . Then

$$v = \frac{1}{n-1} \sum_{i=1}^n Z_i^2 - \frac{n}{n-1} \left( \frac{1}{n} \sum_{i=1}^n Z_i \right)^2 \quad (36)$$

$$= \frac{n \sum_{i=1}^n Z_i^2 - (\sum_{i=1}^n Z_i)^2}{n(n-1)}. \quad (37)$$

Squaring this and taking the expectation gives

$$\mathbb{E}(v^2) = \frac{n^2 \mathbb{E}((\sum_{i=1}^n Z_i^2)^2) - 2n \mathbb{E}((\sum_{i=1}^n Z_i^2)(\sum_{i=1}^n Z_i)^2) + \mathbb{E}((\sum_{i=1}^n Z_i)^4)}{n^2(n-1)^2} \quad (38)$$

$$= \frac{n^2 \sum_{ij} \mu_{iijj} - 2n \sum_{ijk} \mu_{iijk} + \sum_{ijkl} \mu_{ijkl}}{n^2(n-1)^2}. \quad (39)$$

Plugging this into (35) gives the result for  $\text{var}(v)$ . ■

If the  $Y_i$  are independent, then the results of lemma 3 reduce to those of lemma 2 of Cohen and Xu [2015] with  $n_j$  set to  $n$  for all  $j$ .

The approximations of lemmas 2 and 3 are better when the spreads of the random variables  $m$  and  $v$  are small relative to the curvature of the natural logarithm at  $\mathbb{E}(m)$  and  $\mathbb{E}(v)$ , respectively. Typically, larger values of  $n$  will reduce the spread, but this spread will not necessarily decline to zero in the limit of large  $n$ . So approximations will not necessarily become arbitrarily good for larger  $n$ . For instance,  $\text{var}(m) = V\Omega = \frac{V}{n^2} \sum_{ij} \rho_{ij}$ . If  $\rho_{ij} = \rho$  for all  $i \neq j$ , this expression reduces to  $\text{var}(m) = \frac{V}{n^2} (n+n(n-1)\rho) = V(\frac{1}{n} + \frac{n-1}{n}\rho)$ , which goes to  $V\rho$  as  $n$  goes to infinity.

The delta method approximations (21) and (25) are considered “good” when  $\sqrt{\text{var}(m)}$  and  $\sqrt{\text{var}(v)}$  are smaller than a value proportional to one over the square root of the curvature of  $\ln(x)$  at  $\mathbb{E}(m)$  and  $\mathbb{E}(v)$ , respectively. The proportionality constant used here controls the “goodness” threshold desired. The curvature of  $\ln(x)$  is asymptotically  $1/x^2$  for large  $x$ , so comparing  $\sqrt{\text{var}(m)}$  and  $\sqrt{\text{var}(v)}$  to  $\mathbb{E}(m)$  and  $\mathbb{E}(v)$ , respectively, indicates the quality of the delta method approximations. We have formulas for all these quantities. Approximations are asymptotically perfect in any limit which causes the ratios  $\sqrt{\text{var}(m)}/\mathbb{E}(m) = \sqrt{V\Omega}/M$  and  $\sqrt{\text{var}(v)}/\mathbb{E}(v)$  to decline to zero.

**Lemma 4.** *The covariance of  $m$  and  $v$  is*

$$\text{cov}(m, v) = \frac{1}{n(n-1)} \left( \sum_{ij} \mu_{iijj} - \frac{1}{n} \sum_{ijk} \mu_{iijk} \right). \quad (40)$$

*Proof.* In the iid case, the result is  $\text{cov}(m, v) = \frac{\mu_{iiii}}{n}$ , as proved (though not originally) by Zhang [2007] and cited by Cohen and Xu [2015] (their lemma 3). The quantity  $\mu_{iiii}$  does not depend on  $i$  because the  $Y_i$  are identically distributed. Cohen and Xu [2015] denote this quantity  $\mu_3$ . The beginning of the proof of Zhang [2007] also holds in our non-independent case:  $\text{cov}(m, v) = \frac{1}{n(n-1)}(I_1 - I_2)$ , where  $I_1$  and  $I_2$  are defined by Zhang [2007] as

$$I_1 = \mathbb{E}(\sum_{i=1}^n Z_i \sum_{j=1}^n Z_j^2) \quad (41)$$

$$I_2 = \frac{1}{n} \mathbb{E}(\sum_{i=1}^n Z_i (\sum_{j=1}^n Z_j)^2) \quad (42)$$

where  $Z_i = Y_i - M$ . We then compute

$$I_1 - I_2 = \sum_{ij} \mathbb{E}(Z_i Z_j^2) - \frac{1}{n} \sum_{ijk} \mathbb{E}(Z_i Z_j Z_k), \quad (43)$$

and therefore (40) holds. This expression reduces to the earlier result of Cohen and Xu [2015] in the iid case. ■

### S2.3 The main theorem and interpretation

**Theorem 5.** Given the definitions and assumptions listed in section S2.1, and with the expression for  $\text{var}(v)$  given in lemma 3,

$$b \approx \tilde{b} \equiv \left( \frac{M\mu_{iii}}{V^2} \right) \left( \frac{\Sigma_{ij}\rho_{ijj} - \frac{1}{n}\Sigma_{ijk}\rho_{ijk}}{n^2(1-\Omega)\Omega} \right) \quad (44)$$

$$= \left( \frac{M\mu_{iii}}{V^2} \right) \left( \frac{n-1}{n^2(1-\Omega)\Omega} \right) \left( \frac{1}{n-1}\Sigma_{ij}\rho_{ijj} - \frac{1}{n(n-1)}\Sigma_{ijk}\rho_{ijk} \right) \quad (45)$$

$$= \frac{M}{V^2} \left( \frac{\mathbb{E} \left( \sum_i (Y_i - M) \sum_j (Y_j - M)(Y_j - m) \right)}{n^2(1-\Omega)\Omega} \right) \quad (46)$$

$$\ln(a) \approx \ln \left( \frac{nV(1-\Omega)}{n-1} \right) - \frac{(n-1)^2 \text{var}(v)}{2n^2V^2(1-\Omega)^2} - \tilde{b} \left( \ln(M) - \frac{1}{2M^2}V\Omega \right). \quad (47)$$

Approximations are better, respectively asymptotically perfect, when the delta method approximations (21) and (25) are better, respectively asymptotically perfect, and this occurs as described in the text following lemma 3.

The first factor of (44) is the iid result for  $b$  of Cohen and Xu [2015]. In the iid case,  $\rho_{ij} = 0$  for all  $i \neq j$ , and  $\rho_{ijk} = 0$  whenever  $i, j$  and  $k$  are not all equal, and (44) reduces to

$$b \approx \left( \frac{M\mu_{iii}}{V^2} \right) \frac{n - \frac{1}{n}n}{n^2(1 - \frac{1}{n})\frac{1}{n}} = \frac{M\mu_{iii}}{V^2} \quad (48)$$

which is the result of Cohen and Xu [2015]. This result holds for weaker assumptions than the full independence assumed by Cohen and Xu [2015], namely,  $\rho_{ij} = 0$  for  $i \neq j$ ,  $\rho_{ijk} = 0$  for  $i, j, k$  not all equal. The denominator of the second factor of (44) depends only on synchrony, and therefore suggests how synchrony affects the TL slope. The numerator of the second factor of (44) depends only on the third-order moments and co-moments. The iid result of Cohen and Xu [2015] shows that third-order moments affect TL slope, but our result shows that co-moments are also involved when they are non-zero.

Equation (45) emphasizes the separate effects of synchrony ( $\Omega$ ) and the third-order co-moments, as follows. If  $\rho_{ij} = 0$  for all  $i \neq j$  (no synchrony) then the second factor in (45) is 1. If  $\rho_{ijk} = 0$  whenever  $i, j$ , and  $k$  are not all equal, then the third factor in (45) is 1. So the second factor gives the effects of synchrony on TL slope and the third factor gives the effects of higher moments. The second factor of (45) has its minimum for  $\Omega = \frac{1}{2}$ . So (45) may suggest that TL slope may be shallower for larger values of synchrony up to  $\Omega = \frac{1}{2}$ , and then for  $\Omega > \frac{1}{2}$ , TL slope should get steeper again. However, this will hold only if the  $\rho_{ijk}$  do not change simultaneously to counteract the effects of  $\Omega$ , which they can (see Results and below for examples).

Equation (46) offers an alternative interpretation and is in some ways more intuitive because only two subscript indices appear explicitly instead of the three in (44) and (45). The expression  $\sum_i (Y_j - M)(Y_j - m)$  is proportional to a hybrid form of the sample variance: typically sample variance uses  $M$  in both factors or  $m$  in both factors, whereas this expression uses one of each.

Our theorem provides some simple intuition about why higher synchrony reduced the spatial TL slope  $b$ . Independent draws  $y_1, \dots, y_n$  from a right-skewed probability density function  $\psi(y)$  will tend to produce larger sample variances when they produce larger sample means [Cohen and Xu, 2015] because the probability mass in the right portion of the distribution is more “spread out” than that in the left portion. For instance, as a simplified illustration, consider  $n$  independent draws conditional on all values being smaller than the median  $M_d$  of  $\psi(y)$ ; compared to  $n$  independent draws conditional on all values being bigger than  $M_d$ . This is the same as drawing instead from the distributions  $\psi_{<}(y)$  or  $\psi_{>}(y)$ , where the subscripts refer to density functions that are proportional to  $\psi(y)$  below (respectively, above)  $M_d$ ,

but that have been set to zero above (respectively, below)  $M_d$ . The right skew of  $\psi(y)$  means that not only the mean but also the variance of  $\psi_<(y)$  should be less than the mean and variance, respectively, of  $\psi_>(y)$ . This thought experiment shows that synchrony mitigates the influence of higher means on higher variances by forcing the points  $y_1, \dots, y_n$  to be positively correlated, reducing the variance of the sample when the mean is larger. If the range of variation of the sample mean is small (e.g., because the variability of the sample mean decreases as the sample size increases), the log(variance)-versus-log(mean) plot should be linear as a tangent approximation to whatever the smooth underlying non-linear relation may be, as Cohen and Xu [2015] pointed out.

*Proof.* Starting with the numerator of (19), by lemmas 2 and 3, we have

$$\text{cov}(\ln(m), \ln(v)) \approx \text{cov}\left(\ln(M) + \frac{m - M}{M}, \ln\left(\frac{nV(1 - \Omega)}{n - 1}\right) + \frac{v - \frac{nV(1 - \Omega)}{n - 1}}{\frac{nV(1 - \Omega)}{n - 1}}\right) \quad (49)$$

$$\approx \text{cov}\left(\frac{m - M}{M}, \frac{v - \frac{nV(1 - \Omega)}{n - 1}}{\frac{nV(1 - \Omega)}{n - 1}}\right) \quad (50)$$

$$= \frac{n - 1}{MnV(1 - \Omega)} \text{cov}\left(m - M, v - \frac{nV(1 - \Omega)}{n - 1}\right) \quad (51)$$

$$= \frac{n - 1}{MnV(1 - \Omega)} \text{cov}(m, v). \quad (52)$$

By lemma 4, this is

$$\text{cov}(\ln(m), \ln(v)) \approx \frac{\Sigma_{ij}\mu_{ijj} - \frac{1}{n}\Sigma_{ijk}\mu_{ijk}}{Mn^2V(1 - \Omega)}. \quad (53)$$

The denominator of (19) was given in lemma 2, so

$$b \approx \frac{\Sigma_{ij}\mu_{ijj} - \frac{1}{n}\Sigma_{ijk}\mu_{ijk}}{Mn^2V(1 - \Omega)\text{var}(\ln(m))} \quad (54)$$

$$\approx \frac{M(\Sigma_{ij}\mu_{ijj} - \frac{1}{n}\Sigma_{ijk}\mu_{ijk})}{n^2V^2(1 - \Omega)\Omega} \quad (55)$$

$$= \left(\frac{M}{V^2}\right) \left(\frac{\Sigma_{ij}\mu_{ijj} - \frac{1}{n}\Sigma_{ijk}\mu_{ijk}}{n^2(1 - \Omega)\Omega}\right) \quad (56)$$

$$= \left(\frac{M\mu_{iii}}{V^2}\right) \left(\frac{\Sigma_{ij}\rho_{ijj} - \frac{1}{n}\Sigma_{ijk}\rho_{ijk}}{n^2(1 - \Omega)\Omega}\right), \quad (57)$$

giving (44). Then (45) follows by algebraic manipulation and (46) follows from

$$\sum_{ij} \mu_{ijj} - \frac{1}{n} \sum_{ijk} \mu_{ijk} = \frac{1}{n} \sum_{ijk} \mu_{ijj} - \frac{1}{n} \sum_{ijk} \mu_{ijk} = \frac{1}{n} \sum_{ijk} (\mu_{ijj} - \mu_{ijk}). \quad (58)$$

But

$$\mu_{ijj} - \mu_{ijk} = E((Y_i - M)[(Y_j - M)^2 - (Y_j - M)(Y_k - M)]) \quad (59)$$

$$= E((Y_i - M)(Y_j - M)[(Y_j - M) - (Y_k - M)]) \quad (60)$$

$$= E((Y_i - M)(Y_j - M)(Y_j - Y_k)). \quad (61)$$

Therefore

$$\sum_{ij} \mu_{ijj} - \frac{1}{n} \sum_{ijk} \mu_{ijk} = \frac{1}{n} \sum_{ijk} (\mu_{ijj} - \mu_{ijk}) \quad (62)$$

$$= E \left( \sum_i (Y_i - M) \sum_j (Y_j - M) \frac{1}{n} \sum_k (Y_j - Y_k) \right) \quad (63)$$

$$= E \left( \sum_i (Y_i - M) \sum_j (Y_j - M) (Y_j - m) \right). \quad (64)$$

Plugging this in to (56) gives (46). The expression for  $\ln(a)$  follows by plugging results of lemmas 2 and 3 into (20). ■

### S3 Cases: Distributions constructed using Gaussian copulas and identically distributed marginals

We want to construct a multivariate random variable  $(Y_1, \dots, Y_n)$  such that the  $Y_i$  are identically distributed with some given distribution, and such that we can control the correlation between  $Y_i$  and  $Y_j$ , for all  $i \neq j$ , with a parameter,  $\rho$ . One of many ways to do this follows. Let  $X = (X_1, \dots, X_n)$  be a multivariate normal random variable with mean  $(0, \dots, 0)$  and covariance matrix with diagonal entries 1 and off-diagonal entries  $\rho \geq 0$ . We let  $Y_i = \varphi(X_i)$ , where  $\varphi$  is a transformation that transforms a standard normal variable to one distributed as desired. By construction the  $Y_i$  are identically distributed, and larger values of  $\rho$  mean larger values of  $\text{cor}(Y_i, Y_j)$ , which is common to all pairs  $i, j$  with  $i \neq j$ . This amounts to controlling the dependence among the  $Y_i$  using Gaussian copulas. Simulating draws from  $(Y_1, \dots, Y_n)$  is straightforward and reasonably efficient within any computing system containing a multivariate random normal distribution sampler (e.g., the R programming language, which has the function `rmvnorm` in the package `mvtnorm`). Simulations were thus used to evaluate the relationship between mean-variance relationships (e.g., TL) and synchrony for  $Y_i$  Poisson, negative binomial, gamma, exponential, chi-squared, normal, and log-normal distributions. Plots were generated as described in section S6, see figures S1 on page 23 to S32 on page 54. These are discussed in batches by marginal distribution family below. There are multiple parameterizations of the negative binomial and gamma distributions. For the negative binomial distribution, we used the probability density function (pdf)  $\psi(k) = \binom{k+r-1}{k} (1-p)^r p^k$ . For the gamma distribution, we used  $\psi(x) = \frac{\beta^\alpha}{\Gamma(\alpha)} x^{\alpha-1} \exp(-\beta x)$ , for shape and rate parameters  $\alpha$  and  $\beta$ .

For Poisson and negative binomial marginals (figures S1 on page 23 through S10 on page 32), although substantial curvature and heteroskedasticity and noticeable granularity in  $\log(v)$ -versus- $\log(m)$  plots were evident for marginal distributions with small means, TL was typically otherwise approximately valid, i.e.,  $\log(v)$ -versus- $\log(m)$  were reasonably linear. There was a general tendency for  $b$  to be smaller for larger values of  $\rho$ .

For  $Y_i$  a gamma distribution (or other continuous distributions - see below), approximate partially analytic results can also be obtained using (56). The moments  $M$ ,  $V$ , and  $\mu_{iii}$  are well known in this case. The moments  $\mu_{ij}$ ,  $\mu_{ijj}$  and  $\mu_{ijk}$ , for  $i, j, k$  distinct, were computed numerically by evaluating the integrals corresponding to their definitions, for instance,

$$\mu_{ijk} = E((Y_i - M)(Y_j - M)(Y_k - M)) \quad (65)$$

$$= \int_{-\infty}^{\infty} \int_{-\infty}^{\infty} \int_{-\infty}^{\infty} (\varphi(x_i) - M)(\varphi(x_j) - M)(\varphi(x_k) - M) \Psi(x_i, x_j, x_k) dx_i dx_j dx_k, \quad (66)$$

where  $\Psi$  is the pdf of  $X$ . This calculation used the function `cuhre` in the `R2Cuba` package in the R programming language. That function reports estimates of error in its computations, which were retained

and propagated through subsequent algebraic manipulations to yield estimates of the resulting error in calculating (56). Typically errors were very small. A similar approach could not easily have been used for the Poisson or negative binomial distributions (above), because the performance of the R2Cuba package for non-continuous pdfs was not expected to be sufficient.

For gamma marginals (figures S11 on page 33 to S16 on page 38), the approximation (56) always captured the decline in the slope  $b$  with larger values of  $\rho$ . The approximation was quantitatively accurate for larger values of  $\alpha$  and smaller values of  $\rho$ . Statistically significant curvature or heteroskedasticity were sometimes evident in  $\log(v)$ -versus- $\log(m)$  for smaller values of  $\alpha$  and larger values of  $\rho$ , but curvature was a much smaller feature of  $\log(v)$ -versus- $\log(m)$  plots than was the overall trend. In all cases the slope  $b$  was markedly smaller for larger values of  $\rho$ .

Results for distributions with exponential marginals (figures S17 on page 39 to S18 on page 40) were similar to the gamma results in all respects, except that modest, statistically significant curvature or heteroskedasticity of the  $\log(v)$ -versus- $\log(m)$  relationship was detectable for all values of the exponential parameter  $\lambda$  considered, except at the lowest values of  $\rho$ . The approximation (56) always captured the decline in the slope  $b$  with larger values of  $\rho$ , but it was quantitatively accurate only for the smallest values of  $\rho$ .

Results for distributions with chi-squared marginals (figures S19 on page 41 to S20 on page 42) were similar to the gamma results in all respects, as expected since the chi-squared is a special case of the gamma. Modest but significant curvature and heteroskedasticity of the  $\log(v)$ -versus- $\log(m)$  relationship was visible for smaller degrees of freedom,  $k$ .

For  $Y_i$  a normal or log-normal distribution, the moments  $M$ ,  $V$ ,  $\mu_{iii}$ ,  $\mu_{ij}$ ,  $\mu_{ijj}$  and  $\mu_{ijk}$  for  $i, j, k$  distinct are known in closed form, facilitating approximate analytic results via (56). These moments for  $Y_i$  a normal distribution are in standard statistics texts, and lead to  $b \approx 0$  via equation (56). For the log-normal distribution obtained using  $\varphi(x) = \exp(\mu + \sigma x)$ , it is well-known that  $M = \exp(\mu + \sigma^2/2)$ ,  $V = (\exp(\sigma^2) - 1) \exp(2\mu + \sigma^2)$ , and  $\mu_{iii} = \exp(3\mu + 3\sigma^2/2)(\exp(\sigma^2) - 1)^2(\exp(\sigma^2) + 2)$ . Letting  $Z_i = \mu + \sigma X_i$ , it is also well known that the moment generating function for  $Z = (Z_1, \dots, Z_n)$  is  $M_Z(t_n) = E(\exp(t_n^T Z)) = \exp(t_n^T \vec{\mu} + \frac{1}{2} t_n^T \Sigma t_n)$ , where  $t_n$  is an  $n$ -dimensional vector of non-negative integers,  $\vec{\mu} = (\mu, \dots, \mu)$ , a superscript  $T$  denotes transpose, and  $\Sigma$  is the covariance matrix of  $Z$  (an  $n$ -by- $n$  matrix with diagonal entries  $\sigma^2$  and off-diagonal entries  $\sigma^2 \rho$ ). Applying the earlier expression for  $E(Y_i) = M = \exp(\mu + \sigma^2/2)$  and using the moment generating function,

$$\mu_{ij} = E((Y_i - E(Y_i))(Y_j - E(Y_j))) \quad (67)$$

$$= E(Y_i Y_j) - E(Y_i)E(Y_j) \quad (68)$$

$$= E(Y_i Y_j) - \exp(2\mu + \sigma^2) \quad (69)$$

$$= E(\exp(Z_i) \exp(Z_j)) - \exp(2\mu + \sigma^2) \quad (70)$$

$$= E(\exp(Z_i + Z_j)) - \exp(2\mu + \sigma^2) \quad (71)$$

$$= E(\exp((e_i + e_j)^T Z)) - \exp(2\mu + \sigma^2) \quad (72)$$

$$= \exp((e_i + e_j)^T \vec{\mu} + \frac{1}{2} (e_i + e_j)^T \Sigma (e_i + e_j)) - \exp(2\mu + \sigma^2) \quad (73)$$

$$= \exp(2\mu + \sigma^2)[\exp(\sigma^2 \rho) - 1], \quad (74)$$

where  $e_i$  is the  $n$ -dimensional vector consisting of all zeros except for a 1 in the  $i$ th component. We use

the same techniques to calculate  $\mu_{ijk}$ . For  $i, j, k$  distinct and skipping algebraic manipulations, we have

$$\mu_{ijk} = E((Y_i - E(Y_i))(Y_j - E(Y_j))(Y_k - E(Y_k))) \quad (75)$$

$$= E(Y_i Y_j Y_k) - E(Y_i Y_j)E(Y_k) - E(Y_i Y_k)E(Y_j) - E(Y_j Y_k)E(Y_i) + 2E(Y_i)E(Y_j)E(Y_k) \quad (76)$$

$$= E(Y_i Y_j Y_k) - 3E(Y_i Y_j)E(Y_k) + 2 \exp(3\mu + 3\sigma^2/2) \quad (77)$$

$$= E(Y_i Y_j Y_k) - 3 \exp((e_i + e_j)^T \vec{\mu} + \frac{1}{2}(e_i + e_j)^T \Sigma(e_i + e_j)) \exp(\mu + \sigma^2/2) + 2 \exp(3\mu + 3\sigma^2/2) \quad (78)$$

$$= E(Y_i Y_j Y_k) - 3 \exp(2\mu + \sigma^2 + \rho\sigma^2) \exp(\mu + \sigma^2/2) + 2 \exp(3\mu + 3\sigma^2/2), \quad (79)$$

where

$$E(Y_i Y_j Y_k) = E(\exp(Z_i + Z_j + Z_k)) \quad (80)$$

$$= \exp((e_i + e_j + e_k)^T \vec{\mu} + \frac{1}{2}(e_i + e_j + e_k)^T \Sigma(e_i + e_j + e_k)) \quad (81)$$

$$= \exp(3\mu + (3\sigma^2 + 6\rho\sigma^2)/2). \quad (82)$$

Combining gives  $\mu_{ijk} = \exp(3\mu + (3\sigma^2 + 6\rho\sigma^2)/2) - 3 \exp(2\mu + \sigma^2 + \rho\sigma^2) \exp(\mu + \sigma^2/2) + 2 \exp(3\mu + 3\sigma^2/2)$ . Using the same approach, it is straightforward to compute, for  $i \neq j$ ,  $\mu_{ijj} = \exp(3\mu + 5\sigma^2/2 + 2\rho\sigma^2) - 2 \exp(3\mu + 3\sigma^2/2 + \rho\sigma^2) - \exp(3\mu + 5\sigma^2/2) + 2 \exp(3\mu + 3\sigma^2/2)$ . This leads to

$$b \approx \left( \frac{1}{n\Omega} \right) \left( \frac{\exp(\sigma^2(\rho + 1)) - 2 \exp(2\rho\sigma^2) - n + \exp(2\sigma^2) + n \exp(2\rho\sigma^2)}{(\exp(\sigma^2) - 1)(\exp(\sigma^2) + 2)} \right), \quad (83)$$

the first factor of which indicates that  $b$  decreases as  $\Omega$  increases as long as the numerator of the second factor does not modify or eliminate that apparent relationship.

Results for distributions with normal marginals (figures S21 on page 43 through S26 on page 48) always showed no relationship between  $\log(v)$  and  $\log(m)$ . The value  $b \approx 0$  was always obtained, as expected.

Results for distributions with log-normal marginals (figures S27 on page 49 through S32 on page 54) always supported TL (the  $\log(v)$ -versus- $\log(m)$  relationship was always approximately linear, with statistical tests generally failing to reject the hypotheses of linearity and homoskedasticity), and  $b$  was smaller for larger values of  $\rho$ . For  $\sigma = 0.1$ , (56) was a qualitatively and quantitatively good approximation. For  $\sigma = 0.5$ , equation (56) qualitatively reflected the same dependence of  $b$  on  $\rho$  as simulations, but was not quantitatively accurate. For larger values of  $\sigma$ , (56) was neither qualitatively nor quantitatively accurate.

We carried out independent tests of the accuracy of the delta method approximations for the continuous distributions considered above using the ideas in the text immediately preceding lemma 4. As explained there, the delta method approximations were considered “good” when  $\sqrt{\text{var}(m)} = \sqrt{V\Omega}$  and  $\sqrt{\text{var}(v)}$  are smaller than values proportional to  $E(m) = M$  and  $E(v)$ , respectively, where the level of “goodness” required is determined by the choice of the constant of proportionality. We used proportionality constant 0.5, requiring  $\sqrt{V\Omega} \leq M/2$  and  $\sqrt{\text{var}(v)} \leq E(v)/2$  for the approximation to be deemed adequate. All the quantities in these inequalities are simple functions of the moments already computed as described in the previous paragraphs, except for  $\text{var}(v)$ . Rather than using lemma 3 to approximate  $\text{var}(v)$ , which would have required that we compute fourth-order moments numerically, we used the sample variance of all sample variances computed in the numeric analysis (see section S6). A second, numeric method of assessing the accuracy of the delta method approximations was also used, described in section S6. Results of assessing the accuracy of delta method approximations are shown on plots in sections S8 and S10, as described in section S6.

## S4 Cases: Distributions constructed using Gaussian copulas and non-identically distributed marginals

As in section S3, we constructed a multivariate random variable  $Y = (Y_1, \dots, Y_n)$  using techniques that amount to the use of Gaussian copulas, but we no longer required that the  $Y_i$  are identically distributed. We did require that they all come from the same family of distributions, e.g., they are all normally distributed, or all gamma distributed, etc.

Letting  $X = (X_1, \dots, X_n)$  be a multivariate normal random variable with mean  $(0, \dots, 0)$  and covariance matrix with diagonal entries 1 and off-diagonal entries  $\rho$ , we let  $Y_i = \varphi_i(X_i)$ , where  $\varphi_i$  are transformations that produce the desired marginal distributions. The parameter  $\rho$  controls the degree of synchrony. Simulations were used to evaluate the effects of synchrony on  $\log(v)$ -versus- $\log(m)$  relationships for  $Y_i$  obeying gamma, normal, exponential, log-normal, chi-squared, Poisson, and negative binomial distributions.

The initial general procedure for gamma, normal, exponential, and log-normal marginals was to consider  $Y$  such that  $Y_i$  is distributed in the same way as  $f_i Y_1$  for  $f_i > 0$  for  $i = 2, \dots, n$ . For each of these families of distributions, requiring that  $Y_1$  is in the family is sufficient to guarantee that  $Y_i$  is also in the family. This is not true for the negative binomial, Poisson, or chi-squared families. They are treated in different ways, described below.

For gamma distributions, for a variety of different  $Y_1$ , we used  $f_i = 1 + (i - 1)/4$  (results in figures S35 on page 57 through S40 on page 62). For exponential distributions, for a variety of different  $Y_1$ , we used  $f_i = i$  (results in figure S41 on page 63 through S42 on page 64). We also used  $f_i = i$  for normal distributions (results in figures S45 on page 67 through S50 on page 72) and for log-normal distributions (results in figures S51 on page 73 through S56 on page 78).

In all cases, TL was qualitatively validated: although more than 5% of tests for heteroskedasticity or curvature often rejected their null hypotheses with 95% confidence, curvature and heteroskedasticity were modest, and visually undetectable in most  $\log(v)$ -versus- $\log(m)$  plots. In all cases, TL slope initially decreased as  $\rho$  increased from 0. For larger values of  $n$ , this initial decrease was steeper. For  $\rho \gg 0$ ,  $\log(v)$ -versus- $\log(m)$  simulations clustered very tightly around a linear regression line, i.e., residuals were very small.

For all the distributions, in the limit as  $\rho \rightarrow 1$ , we approach the case  $Y_i = f_i Y_1$ . In this case,  $m = \text{mean}_i(Y_i) = \text{mean}_i(f_i Y_1) = Y_1 \text{mean}_i(f_i)$ , and  $v = \text{var}_i(Y_i) = \text{var}_i(f_i Y_1) = Y_1^2 \text{var}_i(f_i)$ . Therefore,  $\log(v) = 2 \log(Y_1) + \log(\text{var}_i(f_i))$ ,  $\log(m) = \log(Y_1) + \log(\text{mean}_i(f_i))$ , and  $\log(v) = 2 \log(m) - 2 \log(\text{mean}_i(f_i)) + \log(\text{var}_i(f_i))$ . Thus in the limit as  $\rho \rightarrow 1$ , we expect a perfect TL, with slope 2, as the plots cited above showed: middle panels in plots showed TL slopes approaching 2, while TL root mean square errors approached zero, as  $\rho$  approached 1. Sometimes the TL slope approached 2 from above, sometimes from below. Sometimes the overall pattern of dependence of TL slope on  $\rho$  was U-shaped, i.e., exhibiting an initial decrease, followed by a minimum, followed by an increase. Sometimes the overall pattern was a monotonic decline.

For the negative binomial distribution, it is not true that if  $Y_1$  is in the family, then  $f_i Y_1$  is in the family for a positive constant  $f_i$ . To provide examples with negative binomial marginals, we constructed negative binomial distributions  $Y_i$  with means  $\mu_i$  and standard deviations  $\sigma_i$  such that  $\mu_i = f_i \mu_1$  and  $\sigma_i = f_i \sigma_1$  for positive constants  $f_i$ ,  $i = 2, \dots, n$ . For a variety of negative binomial distributions  $Y_1$  (with parameters  $r_1$  and  $p_1$ ) in separate runs, we used the well-known formulas for the mean and standard deviation of a negative binomial distribution,  $\mu_1 = \frac{r_1 p_1}{1-p_1}$  and  $\sigma_1 = \sqrt{\frac{r_1 p_1}{(1-p_1)^2}}$ . We then assigned  $\mu_i = \mu_1 + (i - 1)/4$  for  $i = 2, \dots, n$  when  $n$  was 25, and  $\mu_i = \mu_1 + (i - 1)/16$  for  $i = 2, \dots, n$  when  $n$  was 100, implicitly defining the  $f_i = \mu_i / \mu_1$ . We then defined  $\sigma_i = f_i \sigma_1$ , and let  $Y_i$  be the negative binomial distribution with mean  $\mu_i$  and standard deviation  $\sigma_i$ , for  $i = 1, \dots, n$ . It is straightforward to show that there is exactly one such a negative binomial distribution. Results are in figures S57 on page 79 to S64 on page 86.

It is not possible to have Poisson or chi-squared distributions  $Y_i$  with  $\mu_i = f_i \mu_1$  and  $\sigma_i = f_i \sigma_1$ . This would make  $\mu_i$  proportional to  $\sigma_i$ . But for the Poisson family,  $\mu_i = \lambda_i$  and  $\sigma_i = \sqrt{\lambda_i}$ , so  $\sigma_i = \sqrt{\mu_i}$ , and for

the chi-squared family,  $\mu_i = k_i$  and  $\sigma_i = \sqrt{2k_i}$ , so  $\sigma_i = \sqrt{2\mu_i}$ , showing that proportionality does not occur in these families. If  $Y_1$  is a chi-squared distribution, and therefore is also a gamma distribution, then  $f_i Y_1$  is a gamma distribution; but it is not necessarily also a chi-squared distribution. We nevertheless tried Poisson distributions with a variety of choices for  $\lambda_1$  and with  $\lambda_i = \lambda_1 + i - 1$ . Results are in figures S33 on page 55 to S34 on page 56. We also tried chi-squared distributions with a variety of choices for  $k_1$  and with  $k_i = k_1 + i - 1$ . Results are in figures S43 on page 65 to S44 on page 66.

For Poisson and chi-squared examples, TL was a reasonable approximation, and the slope  $b$  declined steeply as  $\rho$  increased from 0 and continued to decline across the whole range of  $\rho$ . Negative binomial examples often strongly violated the linear hypothesis of TL for larger values of  $\rho$ .

## S5 Cases: Distributions constructed using sums and identically distributed marginals

We applied the well-known “common elements” method [Fischer, 1933] of constructing a multivariate random variable  $(Y_1, \dots, Y_n)$  such that the  $Y_i$  are identically distributed according to some specified distribution, and such that  $\text{cor}(Y_i, Y_j) = \rho$  for  $i \neq j$ . For several common distributions, we defined independent random variables  $X$ ,  $X_i$ , for  $i = 1, \dots, n$  and let  $Y_i = X + X_i$ . Because  $X$  is a summand in all the  $Y_i$ , the  $Y_i$  are correlated as desired. The approach leads to analytic results about the relationship between the  $\log(v)$ -versus- $\log(m)$  relationship and synchrony.

To generate Poisson-distributed  $Y_i$  with parameters  $E(Y_i) = \text{var}(Y_i) = \lambda$  for all  $i$ , let  $X$  and  $X_i$  for  $i = 1, \dots, n$  be independent Poisson random variables with parameters  $E(X) = \text{var}(X) = \lambda\rho$  and  $E(X_i) = \text{var}(X_i) = \lambda(1 - \rho)$ , respectively. Defining  $Y_i = X + X_i$ , it is well-known that  $Y_i$  is Poisson distributed, because the summands are independent, and  $E(Y_i) = E(X) + E(X_i) = \lambda\rho + \lambda(1 - \rho) = \lambda$ , as desired. Also, for  $i \neq j$ ,

$$\text{cor}(Y_i, Y_j) = \frac{\text{cov}(Y_i, Y_j)}{\lambda} = \frac{\text{cov}(X + X_i, X + X_j)}{\lambda} = \frac{E(X)}{\lambda} = \rho, \quad (84)$$

as desired. Simulating draws from  $(Y_1, \dots, Y_n)$  is straightforward and computationally efficient.

To evaluate the formulas of theorem 5, we need the moments  $M$ ,  $V$ ,  $\mu_{ij}$ ,  $\mu_{iii}$ ,  $\mu_{ijj}$ , and  $\mu_{ijk}$  for  $i$ ,  $j$ , and  $k$  distinct. By construction,  $M = V = \lambda$  and  $\mu_{ij} = \rho\lambda$ . The third central moment of a Poisson distribution of mean  $\lambda$  is well known,  $\mu_{iii} = \lambda$ . The moments

$$\mu_{ijj} = \rho \quad (85)$$

$$\mu_{ijk} = \rho \quad (86)$$

were computed by starting with the definitions  $\mu_{ijj} = E((Y_i - \lambda)(Y_j - \lambda)^2)$  and  $\mu_{ijk} = E((Y_i - \lambda)(Y_j - \lambda)(Y_k - \lambda))$ , substituting  $Y_i = X_i + X$ , and using the Matlab symbolic mathematics toolbox.

Plugging the moments into (56) and simplifying gives

$$b \approx \left( \frac{M\mu_{iii}}{V^2} \right) \left( \frac{1}{n\Omega} \right) = \frac{1}{n\Omega}, \quad (87)$$

which decreases with increasing  $\Omega$ . The decline of  $b$  with increasing  $\Omega$  is more rapid for larger values of  $n$ .

We assessed the accuracy of the delta method approximations analytically. As explained in the text immediately preceding lemma 4, we say that the delta method approximations are “good” when  $\sqrt{\text{var}(m)} = \sqrt{V\Omega}$  and  $\sqrt{\text{var}(v)}$  are smaller than values proportional to  $E(m) = M = \lambda$  and  $E(v)$ , respectively, where the level of “goodness” required is determined by the choice of the constant of proportionality. We used proportionality constant 0.5, requiring  $\sqrt{V\Omega} \leq M/2$  and  $\sqrt{\text{var}(v)} \leq E(v)/2$  for the approximation to be deemed adequate. The first inequality becomes  $\Omega \leq \lambda/4$  and the second becomes  $\text{var}(v) \leq E(v)^2/4$ . To analyze the second inequality, we produced analytic expressions for the moments

$\mu_{iiii}$ ,  $\mu_{iiji}$ ,  $\mu_{iijj}$ ,  $\mu_{iiij}$ ,  $\mu_{iijk}$  and  $\mu_{ijkl}$  (for  $i, j, k, l$  distinct) appearing in (28) for  $\text{var}(v)$ , beginning from the definitions of these quantities, and using the Matlab symbolic mathematics toolbox. Moments were

$$\mu_{iiii} = \lambda(3\lambda + 1) \quad (88)$$

$$\mu_{iiji} = \lambda(2\lambda\rho^2 + \rho + \lambda) \quad (89)$$

$$\mu_{iijj} = \lambda\rho(3\lambda + 1) \quad (90)$$

$$\mu_{iiij} = \lambda\rho(\lambda + 2\lambda\rho + 1) \quad (91)$$

$$\mu_{iijk} = \lambda\rho(3\lambda\rho + 1). \quad (92)$$

We plugged these into (28) and simplified, obtaining  $(\lambda(1 - \rho)(n + 2\lambda n - 2\lambda n\rho - 1))/(n(n - 1)) \leq (\lambda(1 - \rho))^2/4$  as an explicit form of the inequality  $\text{var}(v) \leq E(v)^2/4$ . For verification, we also assessed the accuracy of the delta method approximations numerically, as described in section S6.

Plots for Poisson examples are in figures S65 on page 87 to S66 on page 88. We conclude that 1) the analytic approximation illustrates the overall shape of the relationship between  $b$  and  $\Omega$ , 2) larger values of synchrony  $\Omega$  decreased values of the slope  $b$  of the  $\log(v)$ -versus- $\log(m)$  relationship, 3) the slope  $b$  goes to zero for large  $\Omega$ , and 4) the decrease in  $b$  with increasing  $\Omega$  happens faster for larger  $n$ , as predicted by the analytic results.

However, additional observations eclipsed these. Simulations often did not obey TL for  $\Omega > 0$ : the relationship between  $\log(v)$  and  $\log(m)$  was, for many parameters, nonlinear and/or heteroskedastic. The above conclusions pertain to the  $\log(v)$ -versus- $\log(m)$  relationship, which was often not described by TL (which postulates linearity). The example  $\log(v)$ -versus- $\log(m)$  plots in figures S65 on page 87 to S66 on page 88 show that values of  $\Omega > 0$  modified the TL pattern that occurs for  $\Omega = 0$  by smearing points rightward in  $\log(v)$ -versus- $\log(m)$  space, decreasing  $b$ .

The same analytic strategy was applied to other distributions. Let  $X$  be negative binomially distributed with parameters  $r_X = \rho r$  and  $p$ , and let the  $X_i$  be independent (with respect to each other and  $X$ ) negative binomials with parameters  $r_i = r - r_X = r(1 - \rho)$  and  $p$ . Defining  $Y_i = X + X_i$ , it is known that  $Y_i$  is negative binomial with parameters  $r_X + r_i = r$  and  $p$ , as desired; it is also easy to show, since the variance of a negative binomial with parameters  $r$  and  $p$  is  $pr/(1-p)^2$ , that  $\text{cor}(Y_i, Y_j) = \rho$ , as desired. Simulating draws from  $(Y_1, \dots, Y_n)$  is straightforward and computationally efficient. Standard formulas for negative binomial moments provide

$$M = pr/(1 - p) \quad (93)$$

$$V = pr/(p - 1)^2 \quad (94)$$

$$\mu_{iii} = (pr(p + 1))/(1 - p)^3 \quad (95)$$

$$\mu_{iiii} = pr(4p + 3pr + p^2 + 1)/(p - 1)^4. \quad (96)$$

Additional moments were computed by starting with their definitions, inserting  $Y_i = X_i + X$ , and using the Matlab symbolic mathematics toolbox,

$$\mu_{ij} = (pr\rho)/(p - 1)^2 \quad (97)$$

$$\mu_{ijk} = (pr\rho(p + 1))/(1 - p)^3 \quad (98)$$

$$\mu_{iij} = (pr\rho(p + 1))/(1 - p)^3 \quad (99)$$

$$\mu_{iiji} = pr(p^2\rho + 2rpp\rho^2 + 4pp\rho + rp\rho + \rho)/(p - 1)^4 \quad (100)$$

$$\mu_{iiij} = pr\rho(4p + 3pr + p^2 + 1)/(p - 1)^4 \quad (101)$$

$$\mu_{iijk} = pr\rho(4p + pr + p^2 + 2pr\rho + 1)/(p - 1)^4 \quad (102)$$

$$\mu_{ijkl} = pr\rho(4p + p^2 + 3pr\rho + 1)/(p - 1)^4, \quad (103)$$

where  $i, j, k, l$  are distinct. These formulas were substituted into (56) and the result was algebraically simplified to

$$b \approx \left( \frac{M\mu_{iii}}{V^2} \right) \left( \frac{1}{n\Omega} \right) = \frac{p+1}{n\Omega}, \quad (104)$$

which again displays a decreasing dependence on synchrony, with a faster decrease for larger values of  $n$ . The above expressions were also substituted into  $\text{var}(m) \leq E(m)^2/4$  and  $\text{var}(v) \leq E(v)^2/4$  to obtain the following constraints required for adequate accuracy of the delta method approximations:

$$\frac{pr(n\rho - \rho + 1)}{n(p-1)^2} \leq \left( \frac{pr}{2(1-p)} \right)^2 \quad (105)$$

$$\frac{pr(1-\rho)(n-4p+4np+np^2-p^2+2npr-2npr\rho-1)}{n(n-1)(p-1)^4} \leq \left( \frac{pr(1-\rho)}{2(p-1)^2} \right)^2. \quad (106)$$

The same numeric and plotting code (see section S6) that was applied to the Poisson distribution was also applied to the negative binomial. Figures S67 on page 89 to S74 on page 96 lead to similar conclusions about the relationship between  $b$  and  $\Omega$ , but, as in the Poisson case, simulations often did not obey TL for  $\Omega > 0$ , and larger values of  $\Omega$  destroyed the TL pattern by smearing points right in  $\log(v)$ -versus- $\log(m)$  space instead of modifying the slope while preserving linearity.

The same analytic strategy was applied to the gamma distribution. Let  $X$  be gamma distributed with shape and rate parameters  $\rho\alpha$  and  $\beta$ , and let the  $X_i$  be independent (with respect to each other and  $X$ ) gammas with parameters  $\alpha(1-\rho)$  and  $\beta$ . It is known that that  $Y_i = X + X_i$  is gamma distributed, with shape parameter equal to the sum of the shape parameters of  $X$  and  $X_i$ ,  $\alpha$ , and rate parameter equal to the common rate parameter for the summands,  $\beta$ . It is straightforward to see that  $\text{cor}(Y_i, Y_j) = \rho$  for  $i \neq j$ , as desired. Simulating draws from  $(Y_1, \dots, Y_n)$  is again straightforward and computationally efficient. Moments were from standard formulas or were computed by inserting  $Y_i = X + X_i$  into the moment definitions and computing:

$$M = \alpha/\beta \quad (107)$$

$$V = \alpha/\beta^2 \quad (108)$$

$$\mu_{ij} = \alpha\rho/\beta^2 \quad (109)$$

$$\mu_{iii} = 2\alpha/\beta^3 \quad (110)$$

$$\mu_{ijk} = 2\alpha\rho/\beta^3 \quad (111)$$

$$\mu_{ijj} = 2\alpha\rho/\beta^3 \quad (112)$$

$$\mu_{iiii} = 3\alpha(\alpha+2)/\beta^4 \quad (113)$$

$$\mu_{iiji} = \alpha(2\alpha\rho^2 + 6\rho + \alpha)/\beta^4 \quad (114)$$

$$\mu_{iiij} = 3\alpha\rho(\alpha+2)/\beta^4 \quad (115)$$

$$\mu_{iijk} = \alpha\rho(\alpha+2\alpha\rho+6)/\beta^4 \quad (116)$$

$$\mu_{ijkl} = 3\alpha\rho(\alpha\rho+2)/\beta^4. \quad (117)$$

In these formulas,  $i, j, k$  and  $l$  are distinct. The moments were substituted into (56) and the result was algebraically simplified to give

$$b \approx \left( \frac{M\mu_{iii}}{V^2} \right) \left( \frac{1}{n\Omega} \right) = \frac{2}{n\Omega}, \quad (118)$$

which again displays a decreasing dependence on synchrony, with a faster decrease for larger values of  $n$ . The above expressions were also substituted into  $\text{var}(m) \leq E(m)^2/4$  and  $\text{var}(v) \leq E(v)^2/4$  to obtain the

constraints required for adequate accuracy of the delta method approximations:

$$\frac{\alpha(n\rho - \rho + 1)}{\beta^2 n} \leq \frac{\alpha^2}{4\beta^2} \quad (119)$$

$$\frac{2\alpha(1-\rho)(3n + \alpha n - \alpha n\rho - 3)}{\beta^4 n(n-1)} \leq \left(\frac{\alpha(1-\rho)}{2\beta^2}\right)^2. \quad (120)$$

The same numeric and plotting code (section S6) yielded outputs in figures S75 on page 97 to S80 on page 102.

It is well known that the exponential and chi-squared distributions are special cases of the gamma distribution, therefore these cases were explored with the same formulas and plotting code described above, with outputs in figures S81 on page 103 to S84 on page 106. The same conclusions about the dependence of  $b$  on  $\Omega$  as for the Poisson and negative binomial distributions hold here. However, as in those cases, simulations often did not obey TL for  $\Omega > 0$ , and increasing synchrony destroyed TL by smearing points toward the right in  $\log(v)$ -versus- $\log(m)$  space, producing smaller values of  $b$ .

The same analytic strategy was applied to the normal distribution (parameters  $\mu$ , the mean, and  $\sigma$ , the standard deviation). The results were, for distinct  $i, j, k$ ,

$$M = \mu \quad (121)$$

$$V = \sigma^2 \quad (122)$$

$$\mu_{ij} = \rho\sigma^2 \quad (123)$$

$$\mu_{iii} = 0 \quad (124)$$

$$\mu_{ijk} = 0 \quad (125)$$

$$\mu_{ijj} = 0 \quad (126)$$

$$\mu_{iiii} = 3\sigma^4 \quad (127)$$

$$\mu_{iiji} = \sigma^4(2\rho^2 + 1) \quad (128)$$

$$\mu_{iiij} = 3\rho\sigma^4 \quad (129)$$

$$\mu_{iijk} = \rho\sigma^4(2\rho + 1) \quad (130)$$

$$\mu_{ijkl} = 3\rho^2\sigma^4 \quad (131)$$

$$b \approx 0, \quad (132)$$

subject to the requirements

$$\frac{\sigma^2(n\rho - \rho + 1)}{n} \leq \mu^2/4 \quad (133)$$

$$\frac{2\sigma^4(\rho - 1)^2}{n-1} \leq \frac{\sigma^4(1-\rho)^2}{4} \quad (134)$$

for the delta method approximations to be adequate. This result reflects the fact, evident from (56), that TL slope is zero whenever there is no skewness in the common marginal distribution  $Y_i$ . Plots for the normal distribution are in figures S85 on page 107 to S90 on page 112.

The following result encompasses the examples described above and illuminates them.

**Proposition 6.** *Let  $P \subseteq [0, 1]$  and suppose we have independent random variables  $X(\rho)$ ,  $X_i(\rho)$  for  $\rho \in P$  and  $i = 1, \dots, n$  such that for each  $\rho$  the  $X_i(\rho)$  for  $i = 1, \dots, n$  are identically distributed. Let  $Y_i(\rho) = X(\rho) + X_i(\rho)$  and assume  $\text{cor}(Y_i(\rho), Y_j(\rho)) = \rho$  and  $E(Y_i(\rho)) = M$  and  $\text{var}(Y_i(\rho)) = V$  for all  $\rho$  and  $i \neq j$ , for constants  $M$  and  $V$ . Let  $m(\rho) = \text{mean}_i(Y_i(\rho))$  and  $v(\rho) = \text{vari}_i(Y_i(\rho))$  be the sample mean and variance. Then  $E(v(\rho))$  decreases and  $\text{var}(m(\rho))$  increases as  $\rho$  increases. Furthermore,*

$$b(\rho) \approx \frac{M(n-1)\mu_3^{(X_i(\rho))}}{n^2 V^2(1 - \Omega(\rho))\Omega(\rho)} \quad (135)$$

where  $b(\rho)$  and  $\Omega(\rho)$  are the TL slope and synchrony defined previously, and  $\mu_3^{(X_i(\rho))}$  is the third central moment of  $X_i(\rho)$ . If  $\mu_3^{(X_i(\rho))}$  is proportional to  $1 - \rho$  then  $b(\rho)$  is approximately proportional to  $\frac{1}{\Omega(\rho)}$ .

*Proof.* We omit the explicit dependence of  $X$ ,  $X_i$ ,  $Y_i$ , etc. on  $\rho$ . Using the independence of the  $X$ ,  $X_i$  and the assumption that the  $X_i$  for  $i = 1, \dots, n$  are identically distributed for any given  $\rho$ ,

$$\text{cor}(Y_i, Y_j) = \frac{\text{cov}(Y_i, Y_j)}{\sqrt{\text{var}(Y_i)\text{var}(Y_j)}} \quad (136)$$

$$= \frac{\text{var}(X)}{\text{var}(Y_i)} \quad (137)$$

$$= \frac{\text{var}(X)}{V} \quad (138)$$

$$= \rho, \quad (139)$$

so  $\text{var}(X) = \rho V$ . Also by independence,  $V = \text{var}(Y_i) = \text{var}(X + X_i) = \text{var}(X) + \text{var}(X_i)$ , so  $\text{var}(X_i) = V - \rho V = V(1 - \rho)$ . Thus  $E(v) = E(\text{var}_i(Y_i)) = E(\text{var}_i(X + X_i)) = E(\text{var}_i(X_i)) = \text{var}(X_i) = V(1 - \rho)$ , which decreases as  $\rho$  increases. Next,

$$\text{var}(m) = \text{var}(\text{mean}_i(Y_i)) \quad (140)$$

$$= \text{var}(\text{mean}_i(X + X_i)) \quad (141)$$

$$= \text{var}(X + \text{mean}_i(X_i)) \quad (142)$$

$$= \text{var}(X) + \text{var}(\text{mean}_i(X_i)) \quad (143)$$

$$= \text{var}(X) + \frac{1}{n^2} \sum_{i=1}^n \text{var}(X_i) \quad (144)$$

$$= \frac{V}{n}((n-1)\rho + 1), \quad (145)$$

which increases as  $\rho$  increases.

Combining (19) and (52),

$$b \approx \frac{n-1}{MnV(1-\Omega)} \frac{\text{cov}(m, v)}{\text{var}(\ln(m))}. \quad (146)$$

By lemma 2, this becomes

$$b \approx \frac{M(n-1)\text{cov}(m, v)}{nV^2(1-\Omega)\Omega}. \quad (147)$$

But

$$\text{cov}(m, v) = \text{cov}(X + \text{mean}_i(X_i), \text{var}_i(X_i)) \quad (148)$$

$$= \text{cov}(m_{X_i}, v_{X_i}), \quad (149)$$

where  $m_{X_i} = \text{mean}_i(X_i)$  and  $v_{X_i} = \text{var}_i(X_i)$ . Because the  $X_i$  are independent and identically distributed, it is known [Zhang, 2007, Cohen and Xu, 2015] that  $\text{cov}(m_{X_i}, v_{X_i}) = \frac{\mu_3^{(X_i)}}{n}$ . Therefore  $\text{cov}(m, v) = \frac{\mu_3^{(X_i)}}{n}$ , and combining this expression with (147) gives (135). The last statement of the theorem follows because

$$1 - \Omega = 1 - \frac{1}{n^2} \sum_{ij} \text{cor}(Y_i, Y_j) \quad (150)$$

$$= \left( \frac{n-1}{n} \right) (1 - \rho). \quad (151)$$

■

The theorem pertains in its entirety to the Poisson, negative binomial, gamma, and normal examples examined above because in these cases,  $\mu_3^{(X_i)}$  is  $\lambda(1 - \rho)$ ,  $\frac{(1+p)pr(1-\rho)}{(1-p)^3}$ ,  $\frac{2\alpha(1-\rho)}{\beta^3}$ , and 0, respectively, each of which is proportional to  $1 - \rho$ . The “rightward smearing” of points in  $\log(v)$ -versus- $\log(m)$  space that occurred as synchrony increased from 0 in the examples above corresponds to the increases in  $\text{var}(m)$  with increasing  $\rho$  in proposition 6.

The analytic strategy we applied above to Poisson, negative binomial, gamma, and normal examples cannot be applied to the log-normal distribution because it is not true that the sum of two independent log-normally distributed random variables is another log-normally distributed random variable. However, a slightly modified strategy could be applied, because the product of two independent log-normally distributed random variables is another log-normally distributed random variable. We did not carry out such an analysis.

For the examples considered in this section,  $\mu_{ijj} = \mu_{ijk}$  (for the Poisson, see (85) and (86); for the negative binomial, see (98) and (99); for the gamma, which encompasses chi-squared and exponential, see (111) and (112); for the normal, see (125) and (126)). More generally:

**Proposition 7.** *Let  $X$  and  $X_i$  for  $i = 1, \dots, n$  be independent random variables and let the  $X_i$  be identically distributed. Let  $Y_i = X + X_i$ . Then  $\mu_{ijj} = \mu_{ijk}$  for all  $i, j, k$  distinct.*

*Proof.* Using the definitions

$$\mu_{ijj} = E((Y_i - E(Y_i))(Y_j - E(Y_j))(Y_j - E(Y_j))) \quad (152)$$

$$\mu_{ijk} = E((Y_i - E(Y_i))(Y_j - E(Y_j))(Y_k - E(Y_k))) \quad (153)$$

and substituting  $Y_i = X + X_i$  and using the Matlab symbolic manipulation toolbox, we get

$$\mu_{ijj} = 2E(X)^3 - 3E(X^2)E(X) + E(X^3) \quad (154)$$

$$\mu_{ijk} = 2E(X)^3 - 3E(X^2)E(X) + E(X^3). \quad (155)$$

■

## S6 Methods for the omnibus plots

For all distributions  $Y$  considered, simulation-based results were generated and plotted, and for some of them approximate analytic or semi-analytic results were also plotted. The assumption of TL that the  $\log(v)$ -versus- $\log(m)$  relationship is linear was also tested. An omnibus plot summarizing these results was generated for each example considered. Components of the plot are described here.

*Simulation-based results.* Given a random vector  $Y(\rho) = (Y_1(\rho), \dots, Y_n(\rho))$  for a fixed  $\rho$ , 5000 independent realizations were generated in 50 blocks of  $N = 100$  realizations each. For each realization, the sample mean,  $m$ , and the sample variance,  $v$ , were computed, producing 50 blocks of 100 pairs  $(m, v)$ . For each of a few example values of  $\rho$  (e.g., 0, 0.1, 0.5, 0.9),  $\log(v)$  was plotted as a function of  $\log(m)$  using all 5000 pairs  $(m, v)$  except those for which either  $m$  or  $v$  was 0. The plots were placed at the top of the omnibus plot. Axes were the same on all top panels within a plot, to facilitate comparison. Axis number labels are only shown on alternate top panels within a plot.

For each block separately, the slope  $b$  was computed through ordinary linear regression of  $\log(v)$  against  $\log(m)$ , again omitting pairs for which  $m$  or  $v$  was 0. The value of  $\Omega$  was also computed for each block (separately) as the average Pearson correlation coefficient between realizations of  $Y_i$  and  $Y_j$  in that block, the average being computed over pairs  $i$  and  $j$ , including cases with  $i = j$  (which necessarily produced a correlation of 1). The average (across blocks)  $b$  value was plotted against the average (across blocks)  $\Omega$  value, as  $\rho$  ranged from 0 to 0.9 in increments of 0.1, with error bars plotted for both quantities based on standard deviations (across blocks). For each block, residuals of the  $\log(v)$ -versus- $\log(m)$  regression were

computed and used to generate a root mean squared error (RMSE). The mean (across blocks) RMSE was plotted against  $\Omega$ . Both  $b$  and RMSE were plotted against  $\Omega$  in the central panel of the omnibus plot.

*Analytic results.* When possible (e.g., figures S11 on page 33 through S32 on page 54), the approximation (56) was computed for each value of  $\rho$ , either analytically or semi-analytically (here “semi-analytic” refers to calculations for which the constituent moments of (56) were calculated numerically, though with negligible error, see, e.g., (66)), and plotted against  $\rho$  in red on the central panel of the omnibus plot. Whether the approximation (56) could be computed depended on whether the moments in that expression could be evaluated either analytically or numerically. Calculation of moments from samples was not used because it is unreliable for reasonable numbers of samples for some of the required moments and distributions. How we evaluated moments, when available, is described on a case-by-case basis in sections above. When the inequalities  $\sqrt{\text{var}(m)} \leq E(m)/2$  and  $\sqrt{\text{var}(v)} \leq E(v)/2$  were satisfied (see section S3), a red downward-pointing triangle was superimposed on the point, indicating an independent validation of the approximations underlying (56) for that point. The quality of the delta-method approximations underlying (56) was also evaluated numerically by testing the quality of the approximations (21) and (25). When the correlations of the left and right sides of those formulas, across all 5000 samples from  $Y$ , were greater than 0.75, a red upward-pointing triangle was superimposed on the point.

*Assumptions of Taylor’s law.* For each value of  $\rho$ , the fraction of 5000 samples from  $Y$  producing  $m = 0$  was plotted on the bottom panel of the omnibus plot, as was the fraction of samples producing  $v = 0$ . Samples with either  $m = 0$  or  $v = 0$  were omitted from the estimation and testing of Taylor’s law. The  $\log(v)$ -versus- $\log(m)$  relationship is conditional on positive  $m$  and  $v$ .

TL postulates a linear relationship between  $\log(v)$  and  $\log(m)$ , so linearity was evaluated. For each block, the linear relationship  $\log(v) = b\log(m) + c$  was tested against a quadratic alternative,  $\log(v) = a\log(m)^2 + b\log(m) + c$  using a standard  $F$ -test, and the  $p$ -value was recorded. The fraction of blocks for which this  $p$ -value was less than 0.05 was plotted against  $\Omega$  on the bottom panel of the omnibus plot. When this value substantially exceeded the type-I error rate of 0.05, significant curvature existed in the  $\log(v)$ -versus- $\log(m)$  relationship. This curvature could be modest (assessed visually through the example panels at the top of the omnibus plot) even when significant.

Homoskedasticity of the  $\log(v)$ -versus- $\log(m)$  relationship was also tested. For each block, absolute residuals from the regression  $\log(v) = b\log(m) + c$  were computed and regressed against predictions of the same linear model. The  $p$ -value was recorded for the test of the null hypothesis that the slope of this latter regression was 0, a non-zero slope indicating heteroskedasticity. The fraction of blocks for which this  $p$ -value was less than 0.05 was plotted against  $\rho$  on the bottom panel of the omnibus plot. When this value substantially exceeded 0.05, significant heteroskedasticity existed in the  $\log(v)$ -versus- $\log(m)$  relationship.

## S7 Data details

Rothamsted Insect Survey (RIS) runs a network of suction traps that sample flying aphids [Macaulay et al., 1988, Harrington, 2014, Bell et al., 2015]. Daily aphid counts are collected throughout the flight season for many species at multiple locations. Twenty species (table S1) and 11 locations (table S2) were selected in advance of any analyses. Species were selected for their commonness (necessary for analyses of synchrony) and their importance as pests and as models for studies of population dynamics. Locations were selected for long duration of operation. The total count for a species over all days for a year was taken as the count for that species and year. RIS suction trap locations were chosen decades ago to give optimal coverage of the UK, subject to resource limitations. Nevertheless, relative to the whole UK, there are some gaps in the network of 11 traps we used, in Wales, Northern Ireland, and central southern England. After processing, time series were annual, from 1976 through 2010. See Sheppard et al. [2015] for additional details.

The Continuous Plankton Recorder (CPR) survey, now operated by the Sir Alister Hardy Foundation for Ocean Science (SAHFOS), has sampled the seas around the UK and elsewhere for plankton abundances

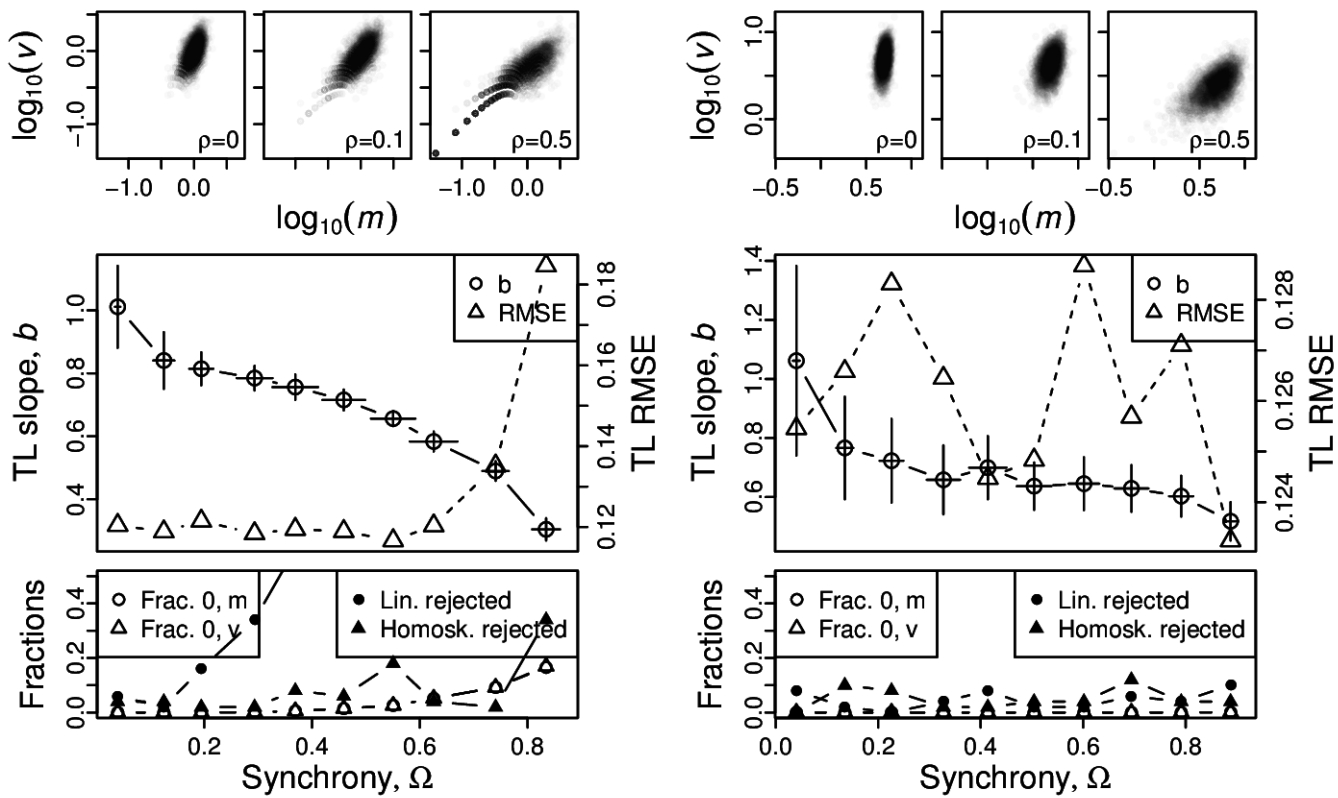
since before World War II, using a sampling device towed behind commercial ships [Batten et al., 2003, Beaugrand and Reid, 2003, Raittos et al., 2013]. The device is towed at about 7 m depth. Water is filtered through a moving band of silk, which is later cut into sections representing samples of 3 cubic meters of sea water over 10 nautical miles, thereby producing spatiotemporal data through repeat tows. Minimal changes have been made to the sampling device and analysis procedure over the history of the survey, to ensure consistency [Batten et al., 2003]. The resulting database contains estimates of the abundance of more than 500 taxa on a very large number of transects. We examined 22 phytoplankton and zooplankton taxa (table S1), selected prior to any analyses for their common occurrence and their importance for marine ecosystems. Samples are typically taken along standard routes approximately once a month, but precise times and locations are irregular, being influenced by ship availability and weather. Samples were compiled into 26 annual time series for  $2 \times 2$  degree areas of sea around the UK. Time series were from 1958 through 2013.

The California Cooperative Oceanic Fisheries Investigations (CalCOFI) has surveyed the California Current System off southern California since 1949 on a monthly-to-quarterly basis. Chlorophyll-*a* has been regularly measured since 1984 [Mantayla et al., 2008]. Time series from spring sampling for the 28 years from 1984 to 2011 were used (average of March-May sampling). Eighteen of 73 sampling stations were omitted, including 7 coastal stations and another 11 stations which are too shallow or have too many gaps in the time series. The remaining 55 sites were divided into four groups based on distance from shore, with group 1 near to shore (average 87.7 km) and group 4 far from shore (average 539.3 km). For each site and sampling occasion, chlorophyll samples were drawn from 0, 10, 20, 30, 50, 75, 100, 125, 150, and 200 m depths. Samples were filtered through Whatman GF/F filters and cold-extracted in a 90% acetone solution in the dark and under refrigeration and then measured fluorometrically using an acidification technique. Sampling and measuring protocols are described in detail on the CalCOFI web site (<http://calcofi.org/ccpublications/calcofi-methods.html>).

CalCOFI data can be downloaded from their website. SAHFOS and RIS data can be obtained by contacting those institutes and going through their long-established data sharing procedures.

## S8 Figures, distributions constructed using Gaussian copulas and identically distributed marginals

A, B



C, D

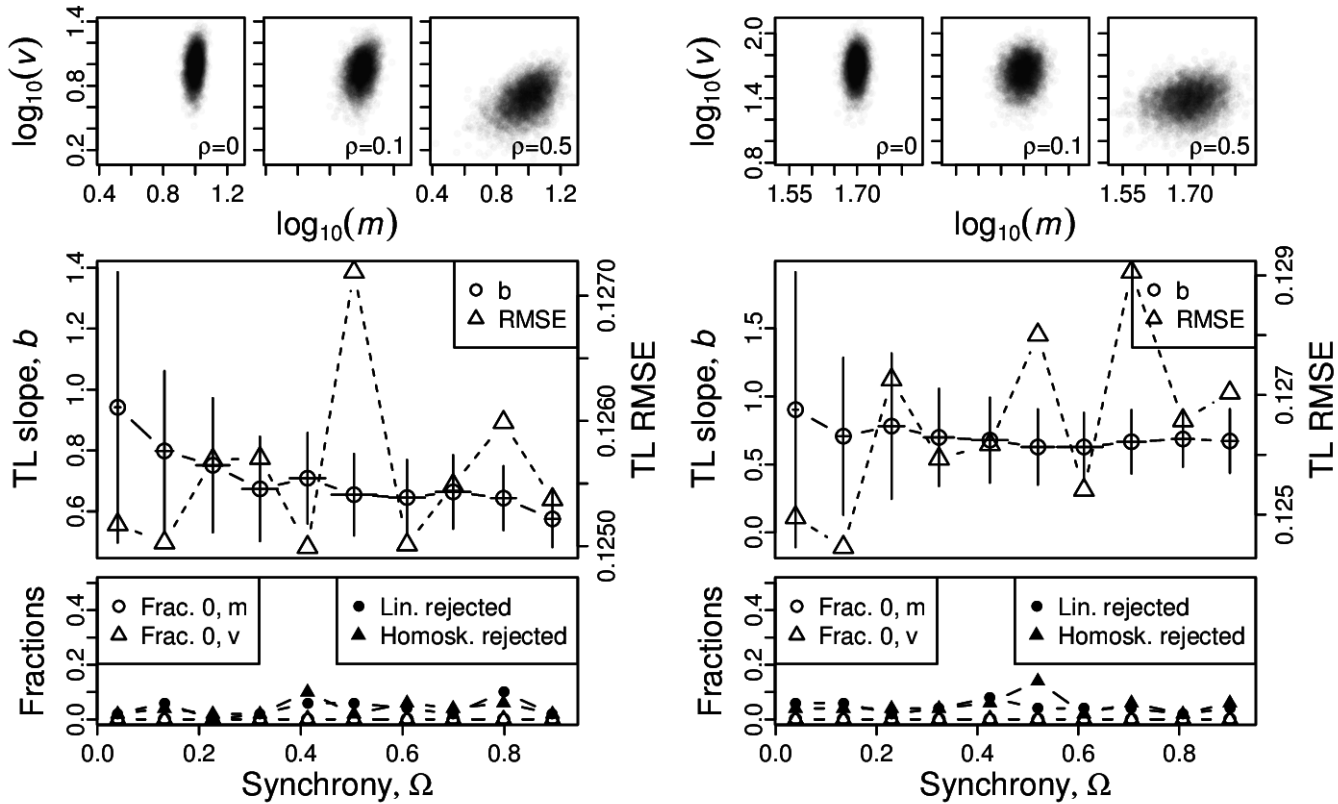
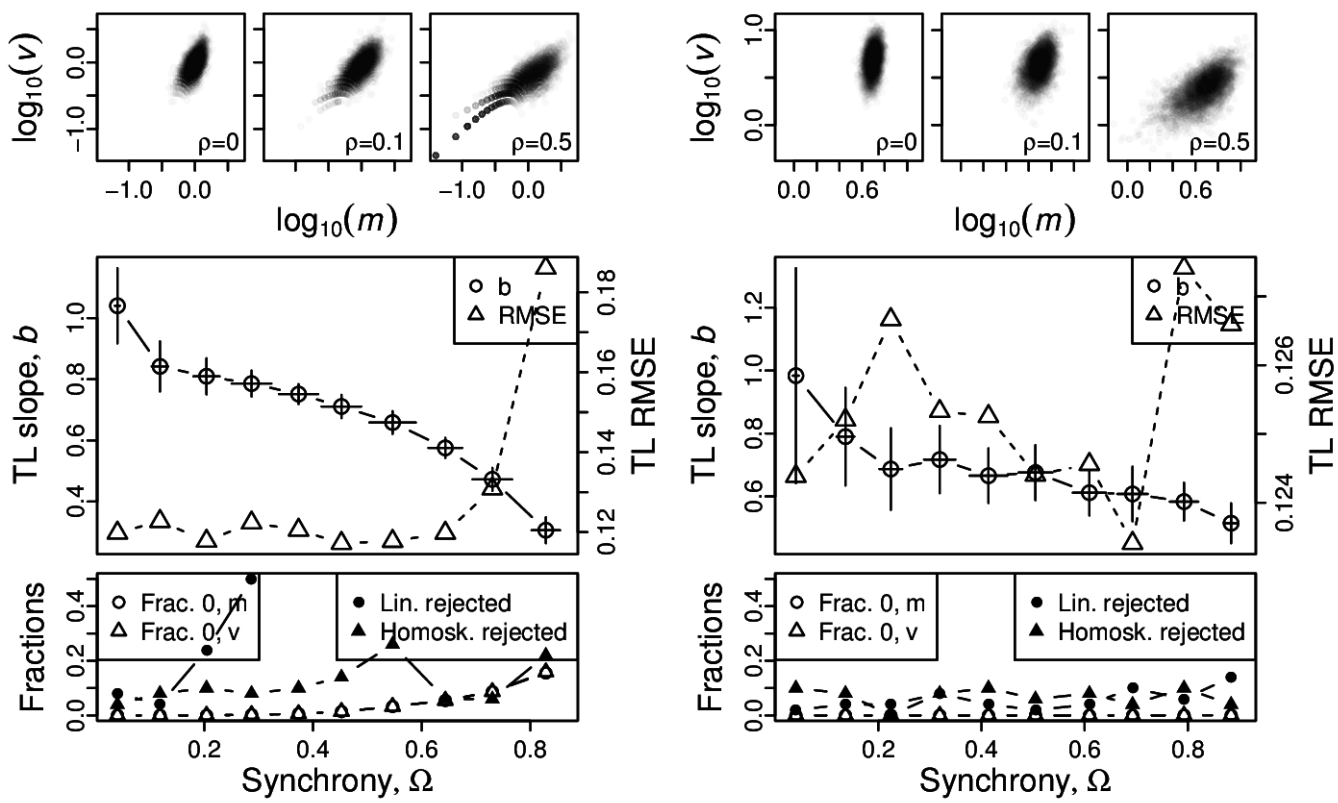


Figure S1: Omnibus plots (see section S6) for identically distributed Poisson marginals under the set up of section S3, for  $n = 25$ , for  $\lambda = 1$  (A),  $\lambda = 5$  (B),  $\lambda = 10$  (C), and  $\lambda = 50$  (D).

A, B



C, D

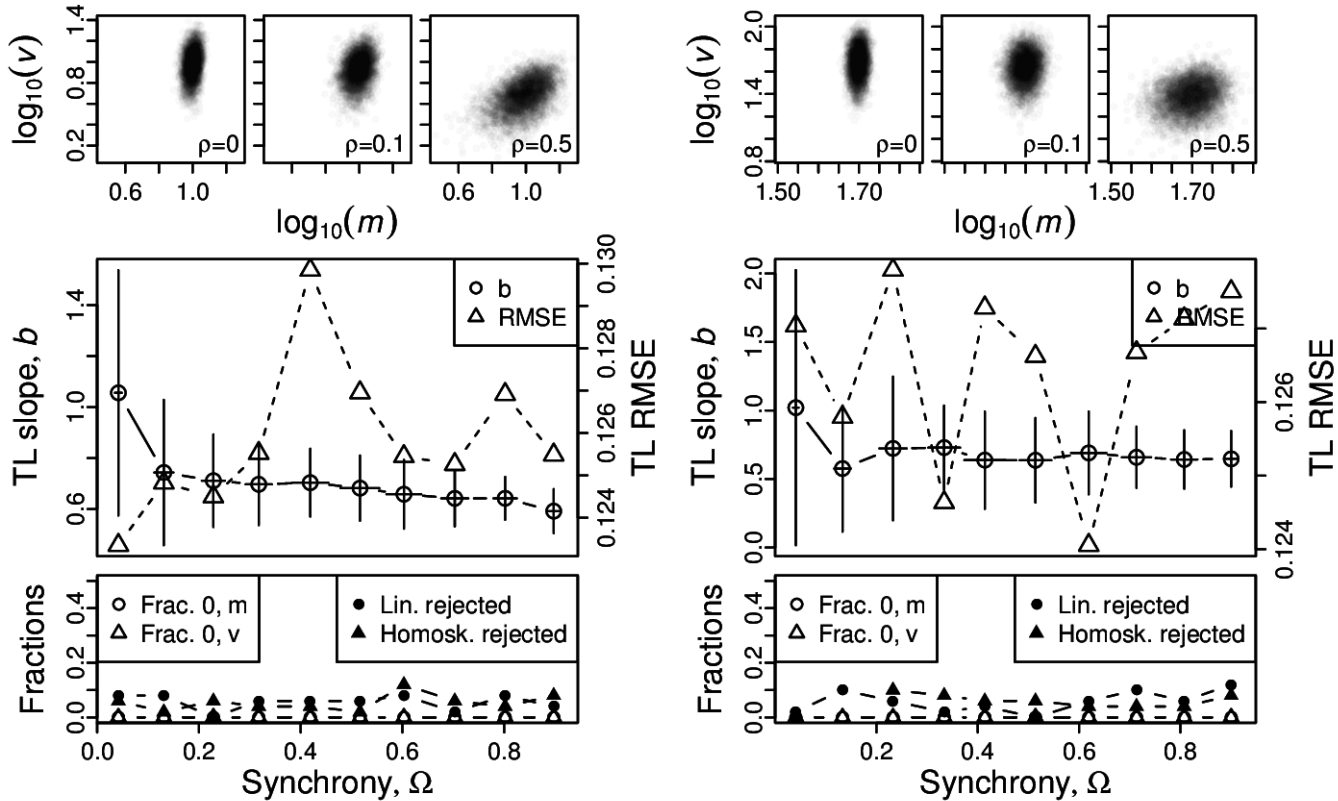
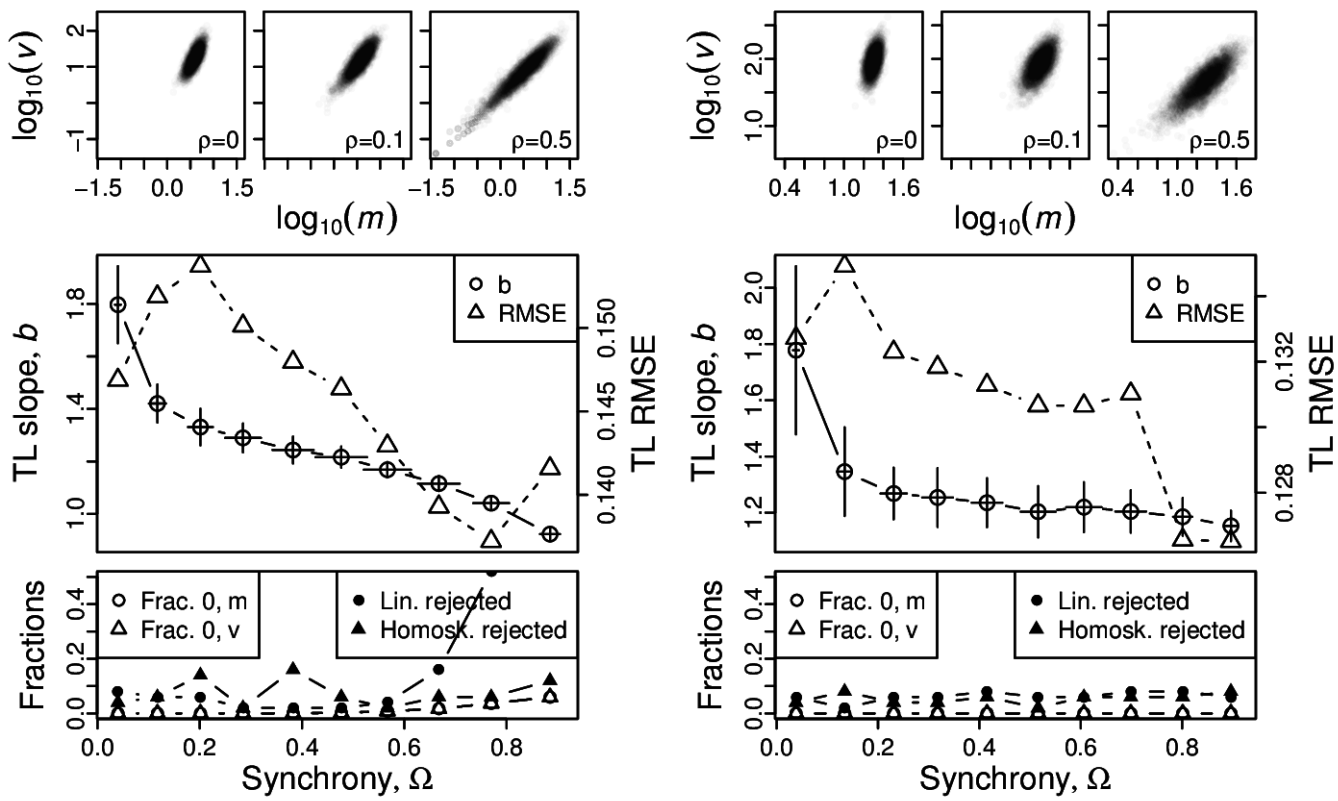


Figure S2: Omnibus plots (see section S6) for identically distributed Poisson marginals under the set up of section S3, for  $n = 100$ , for  $\lambda = 1$  (A),  $\lambda = 5$  (B),  $\lambda = 10$  (C), and  $\lambda = 50$  (D).

A, B



C, D

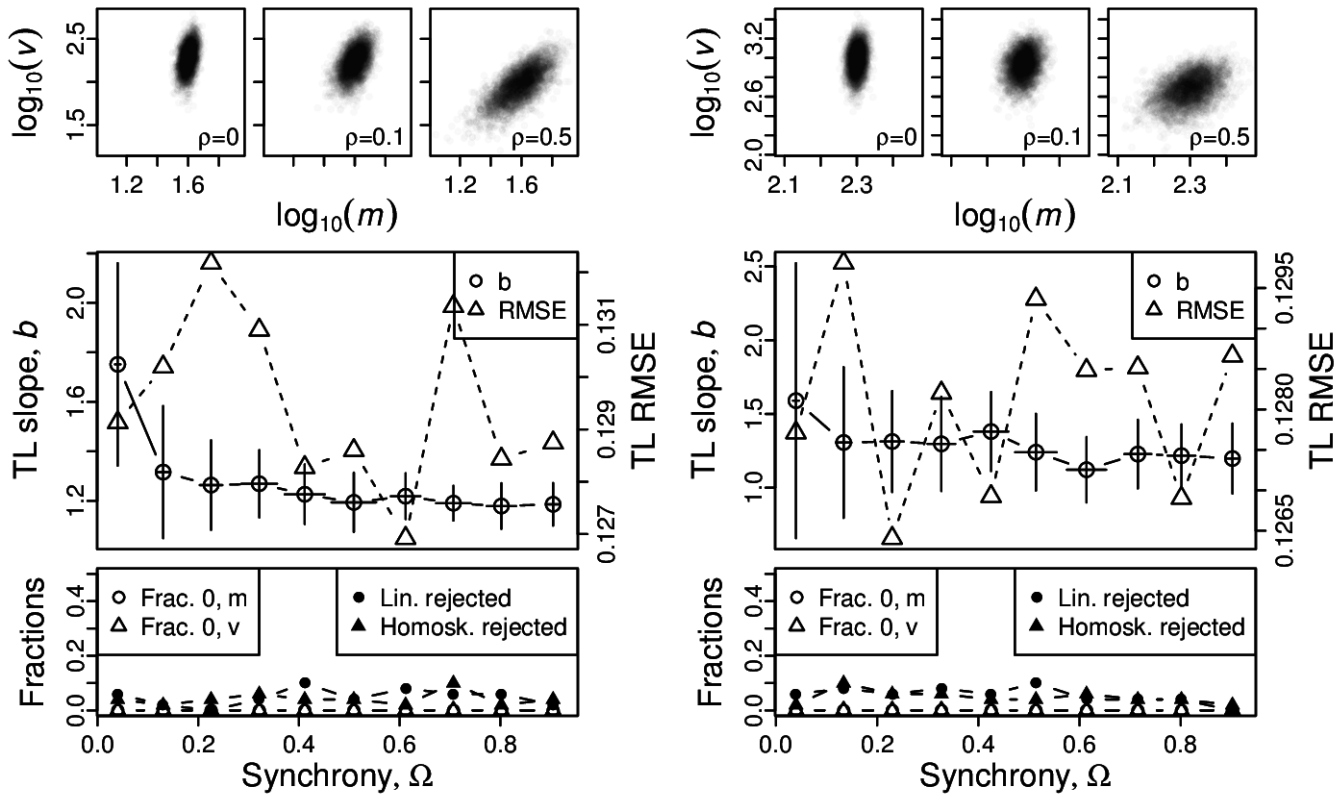
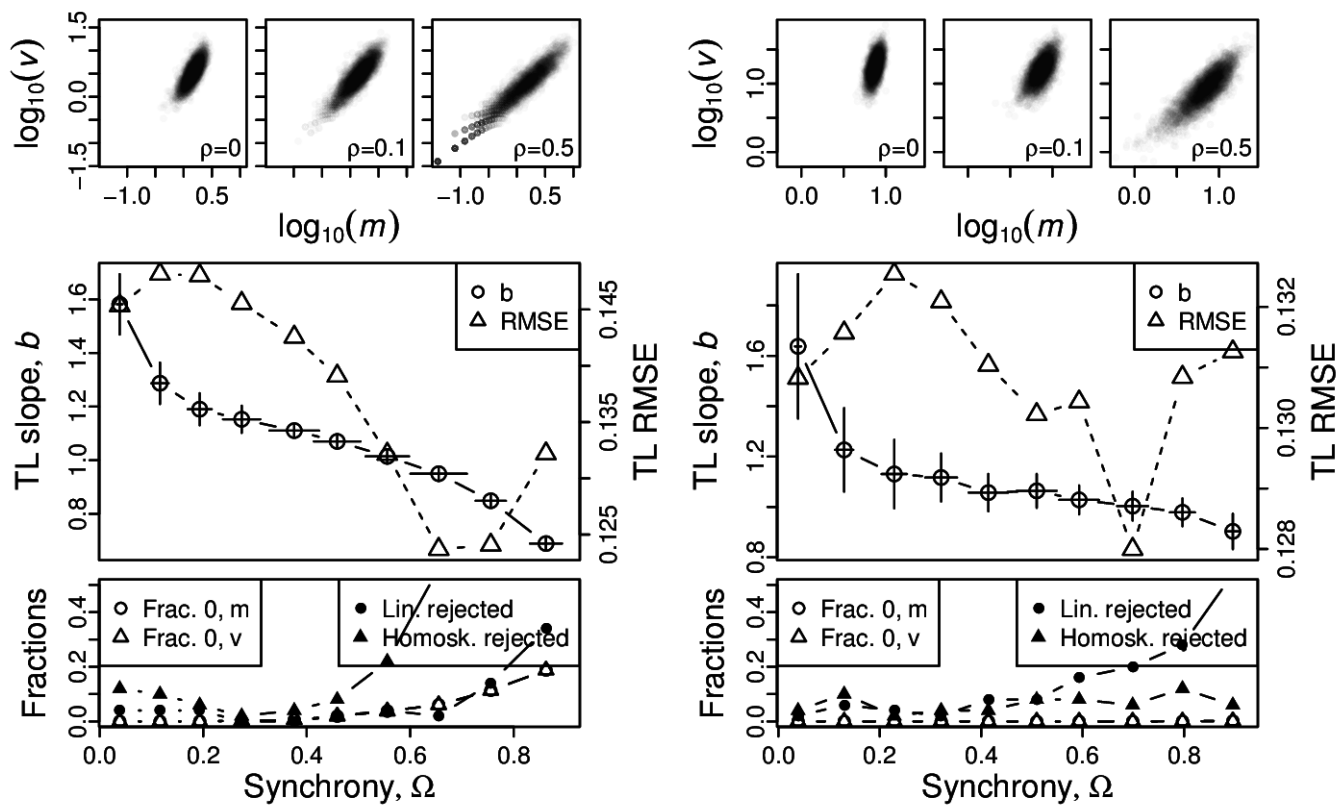


Figure S3: Omnibus plots (see section S6) for identically distributed negative binomial marginals under the set up of section S3, for  $n = 25$  and  $p = 0.2$ , for  $r = 1$  (A),  $r = 5$  (B),  $r = 10$  (C), and  $r = 50$  (D).

A, B



C, D

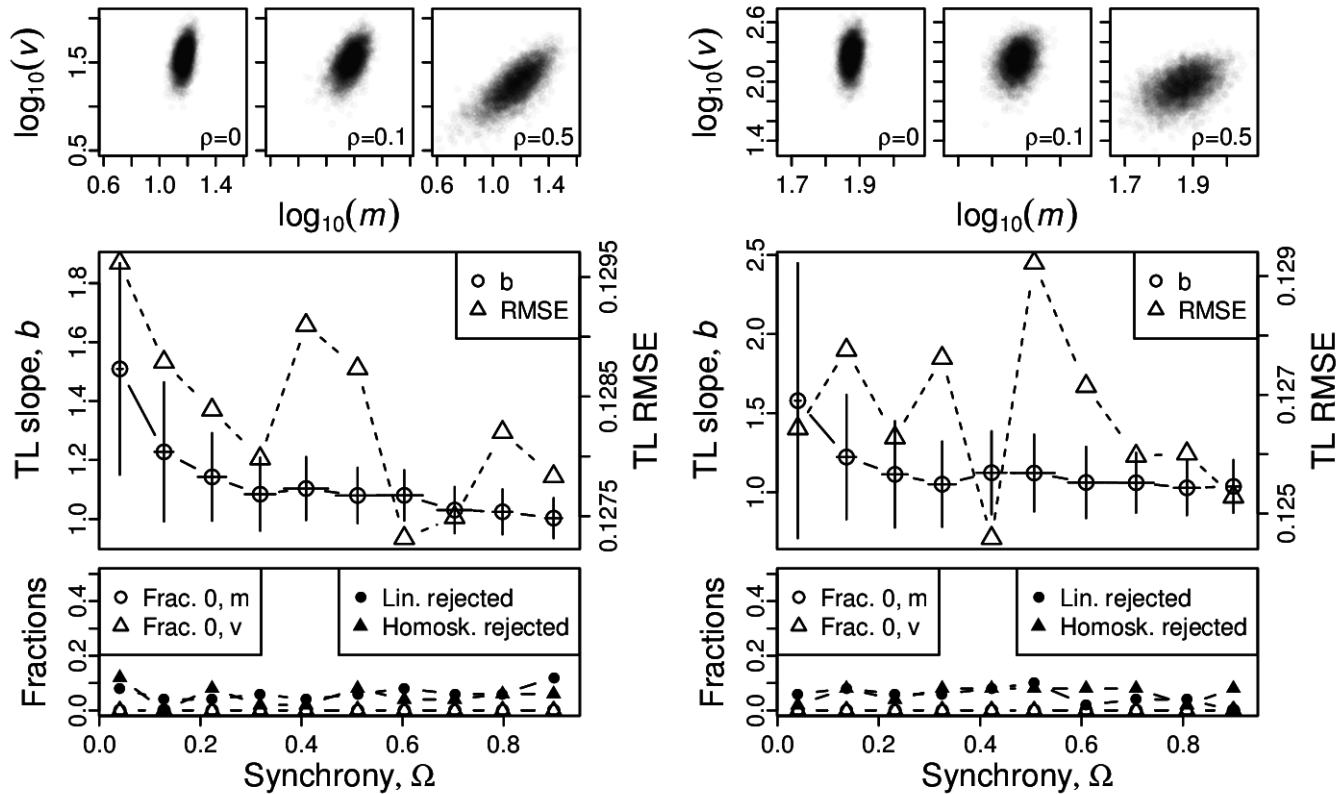
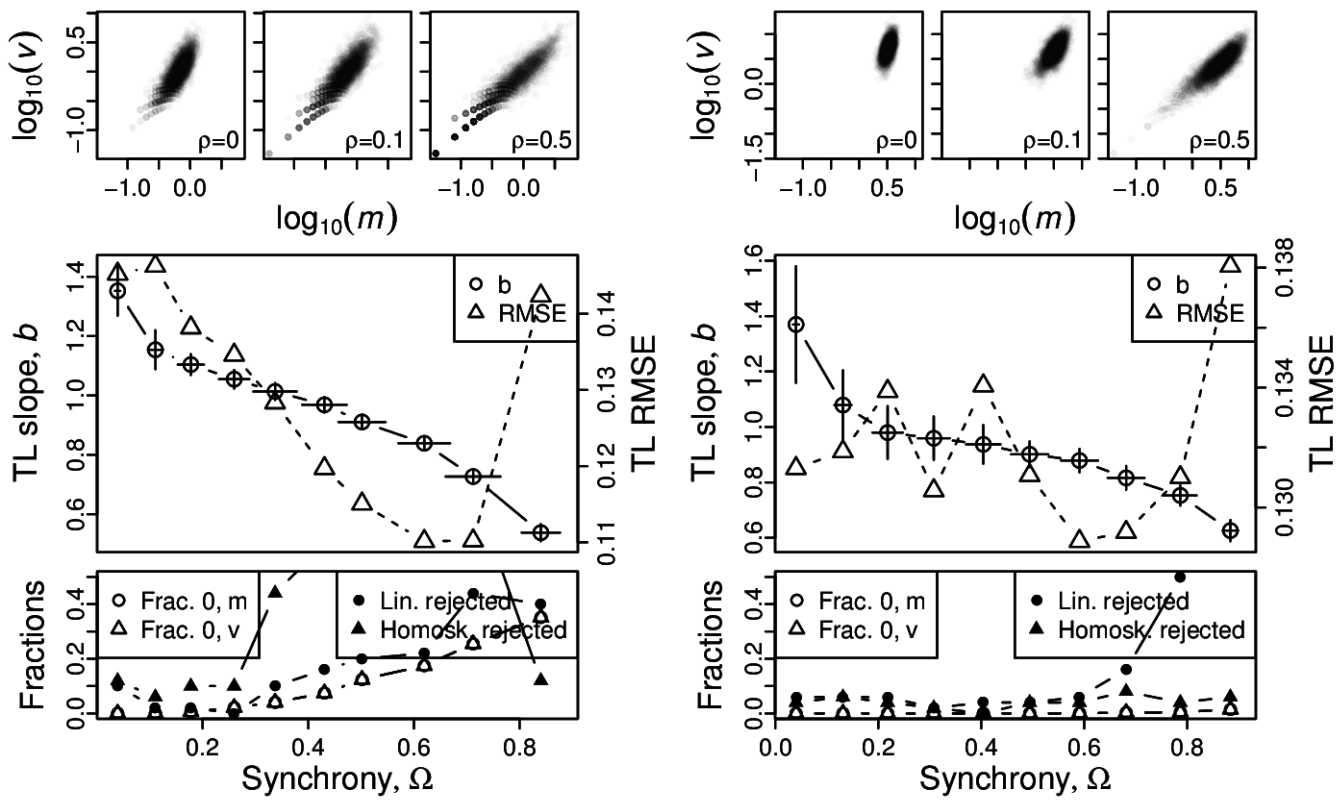


Figure S4: Omnibus plots (see section S6) for identically distributed negative binomial marginals under the set up of section S3, for  $n = 25$  and  $p = 0.4$ , for  $r = 1$  (A),  $r = 5$  (B),  $r = 10$  (C), and  $r = 50$  (D).

A, B



C, D

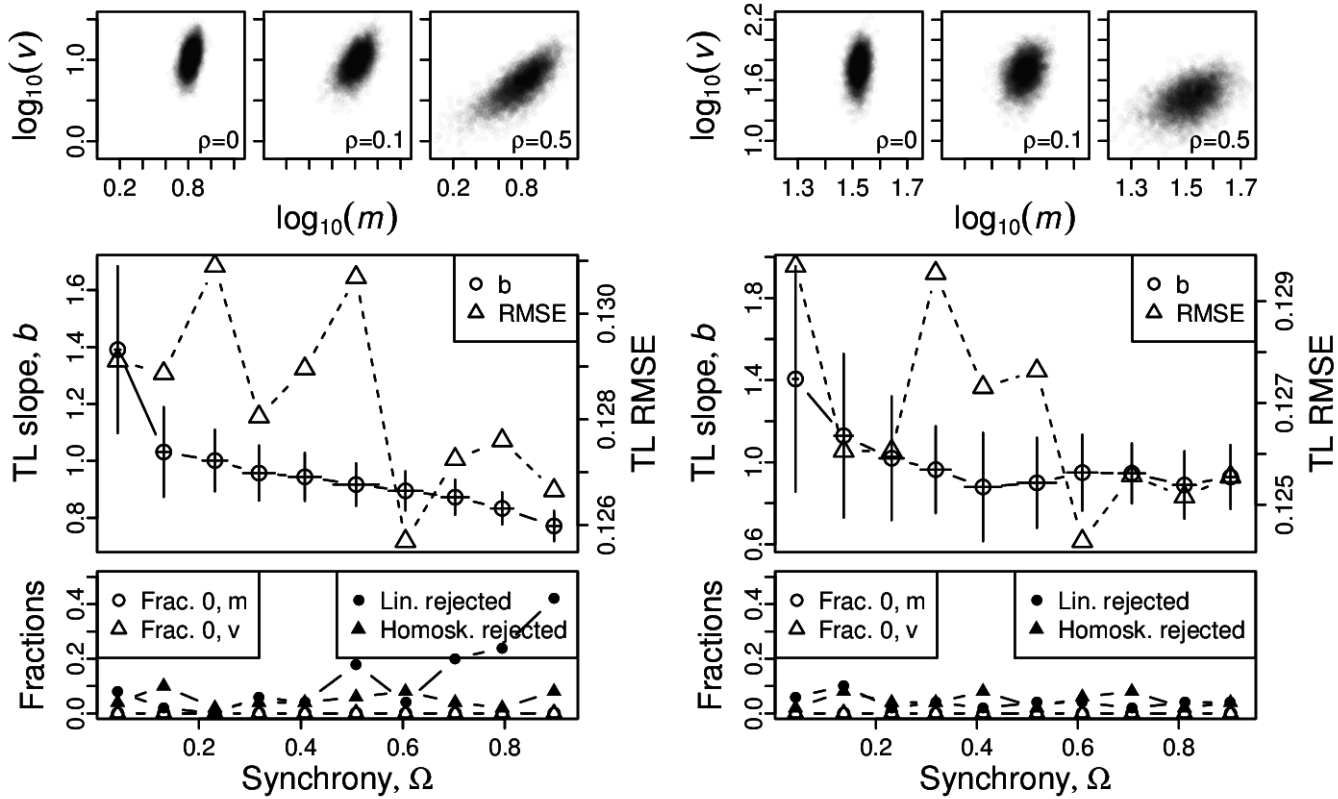
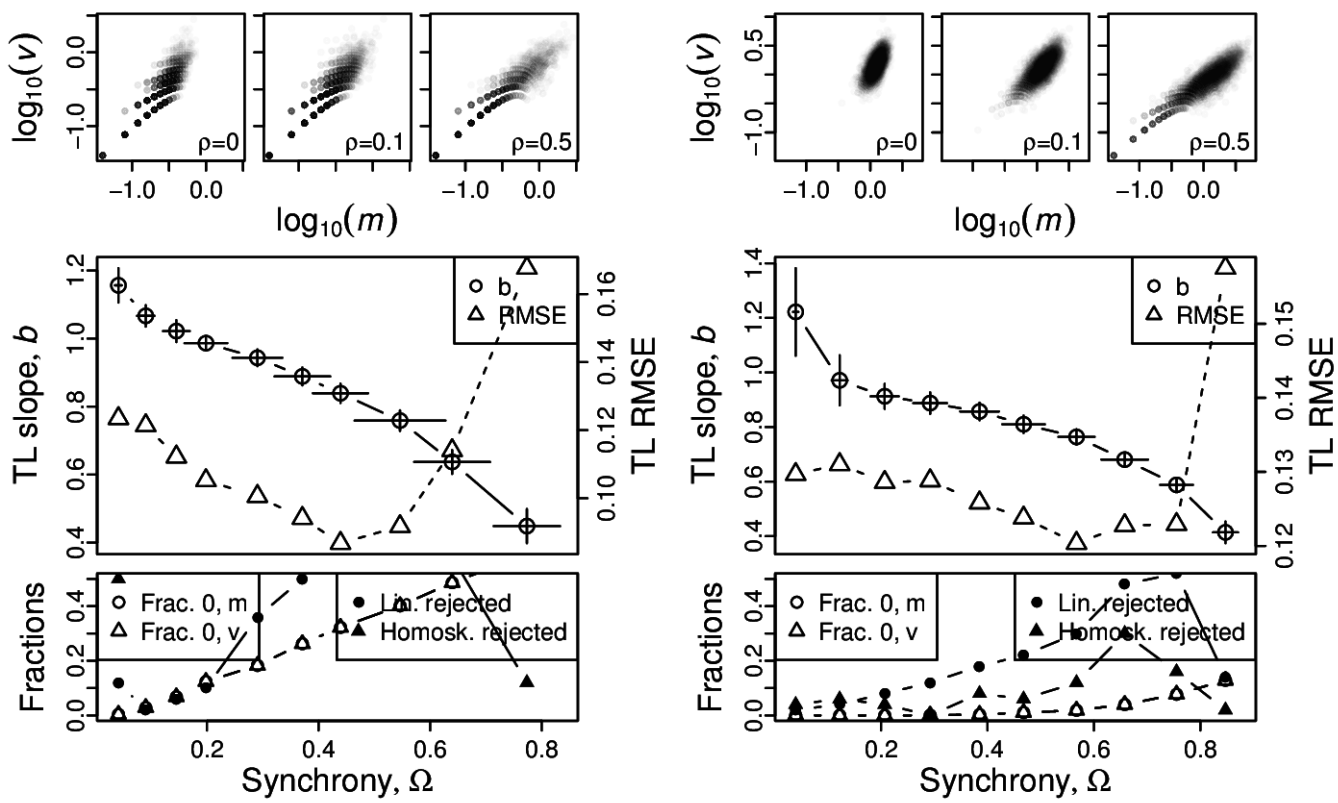


Figure S5: Omnibus plots (see section S6) for identically distributed negative binomial marginals under the set up of section S3, for  $n = 25$  and  $p = 0.6$ , for  $r = 1$  (A),  $r = 5$  (B),  $r = 10$  (C), and  $r = 50$  (D).

A, B



C, D

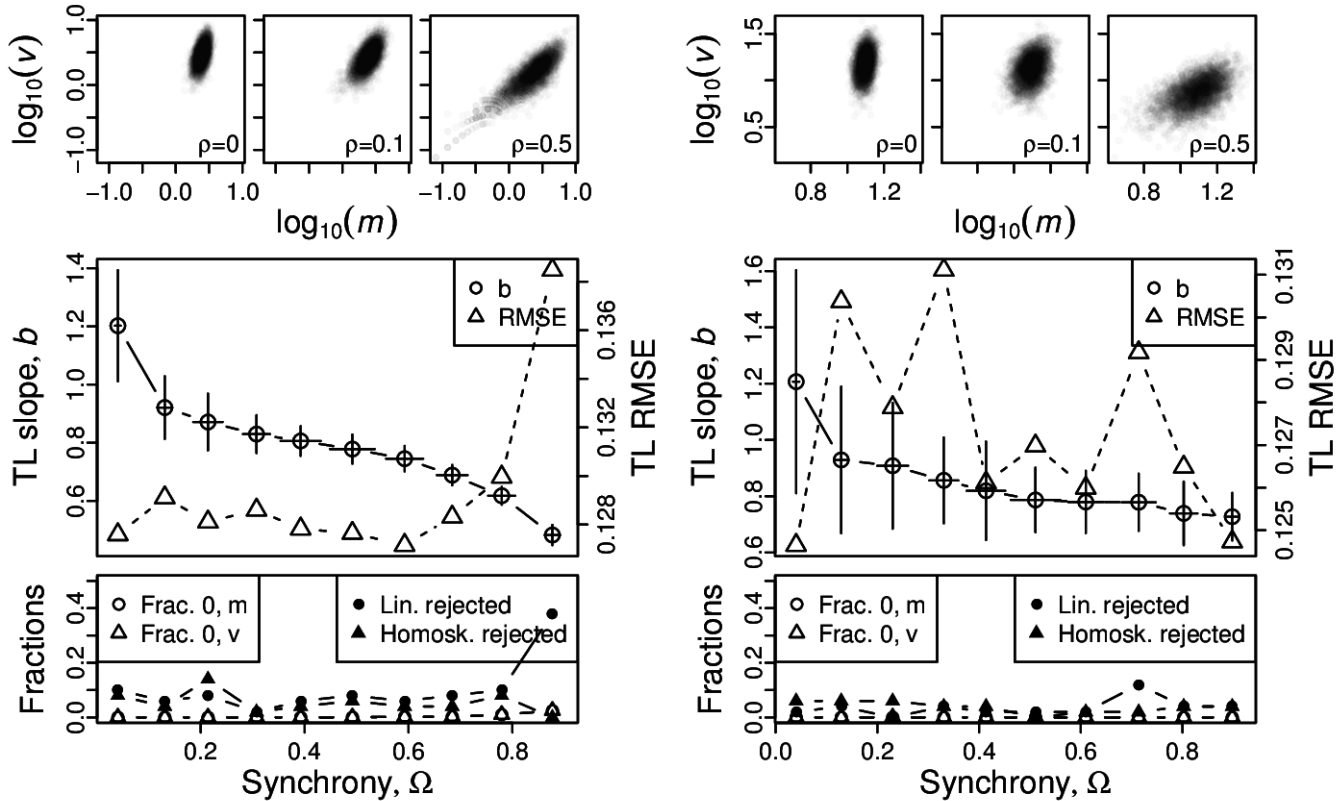
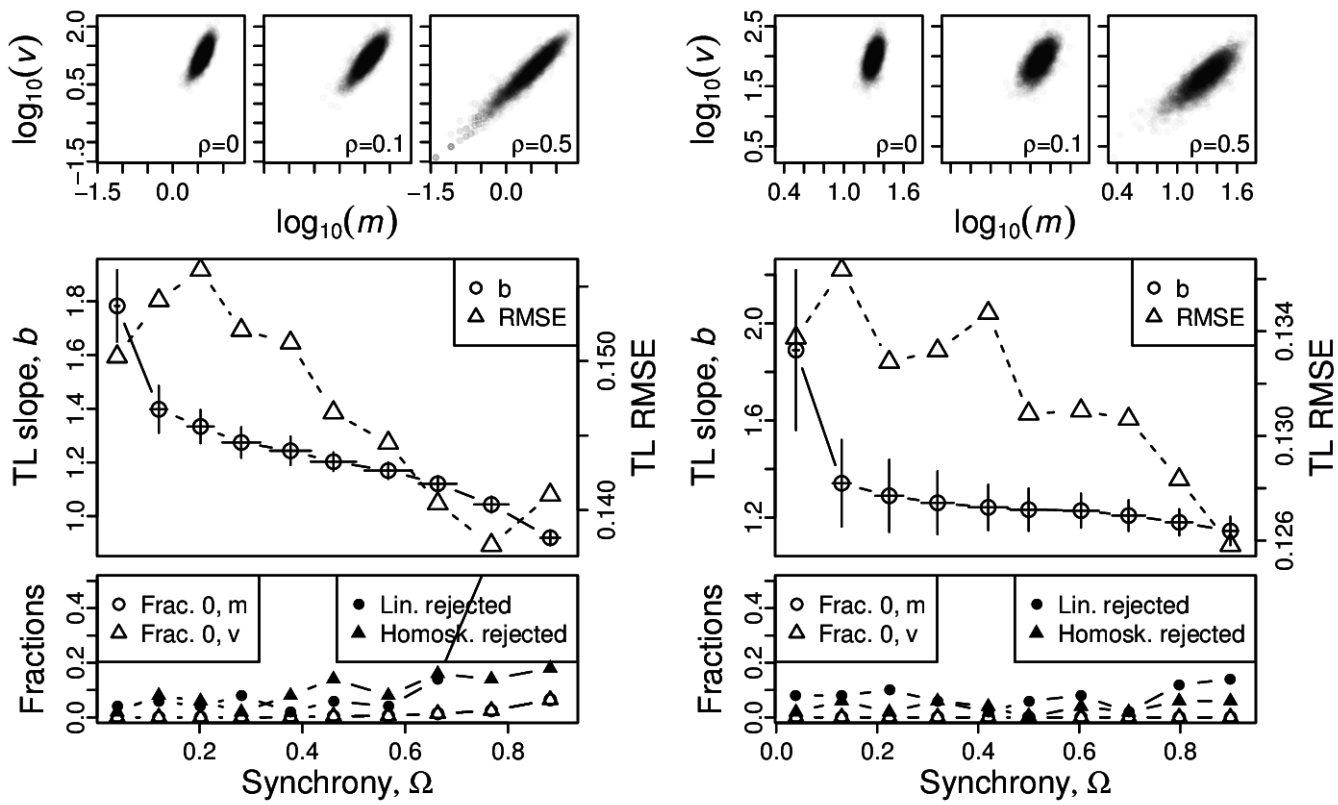


Figure S6: Omnibus plots (see section S6) for identically distributed negative binomial marginals under the set up of section S3, for  $n = 25$  and  $p = 0.8$ , for  $r = 1$  (A),  $r = 5$  (B),  $r = 10$  (C), and  $r = 50$  (D).

A, B



C, D

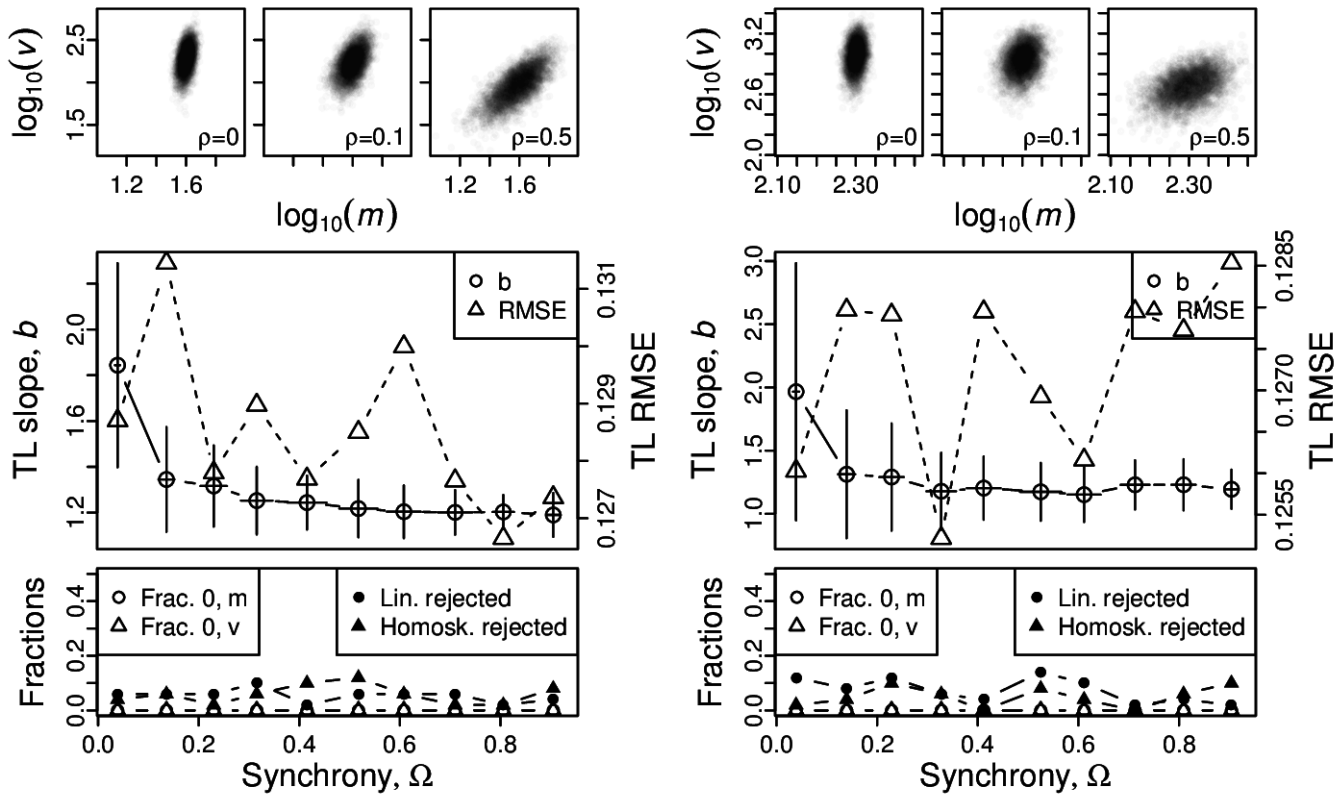


Figure S7: Omnibus plots (see section S6) for identically distributed negative binomial marginals under the set up of section S3, for  $n = 100$  and  $p = 0.2$ , for  $r = 1$  (A),  $r = 5$  (B),  $r = 10$  (C), and  $r = 50$  (D).

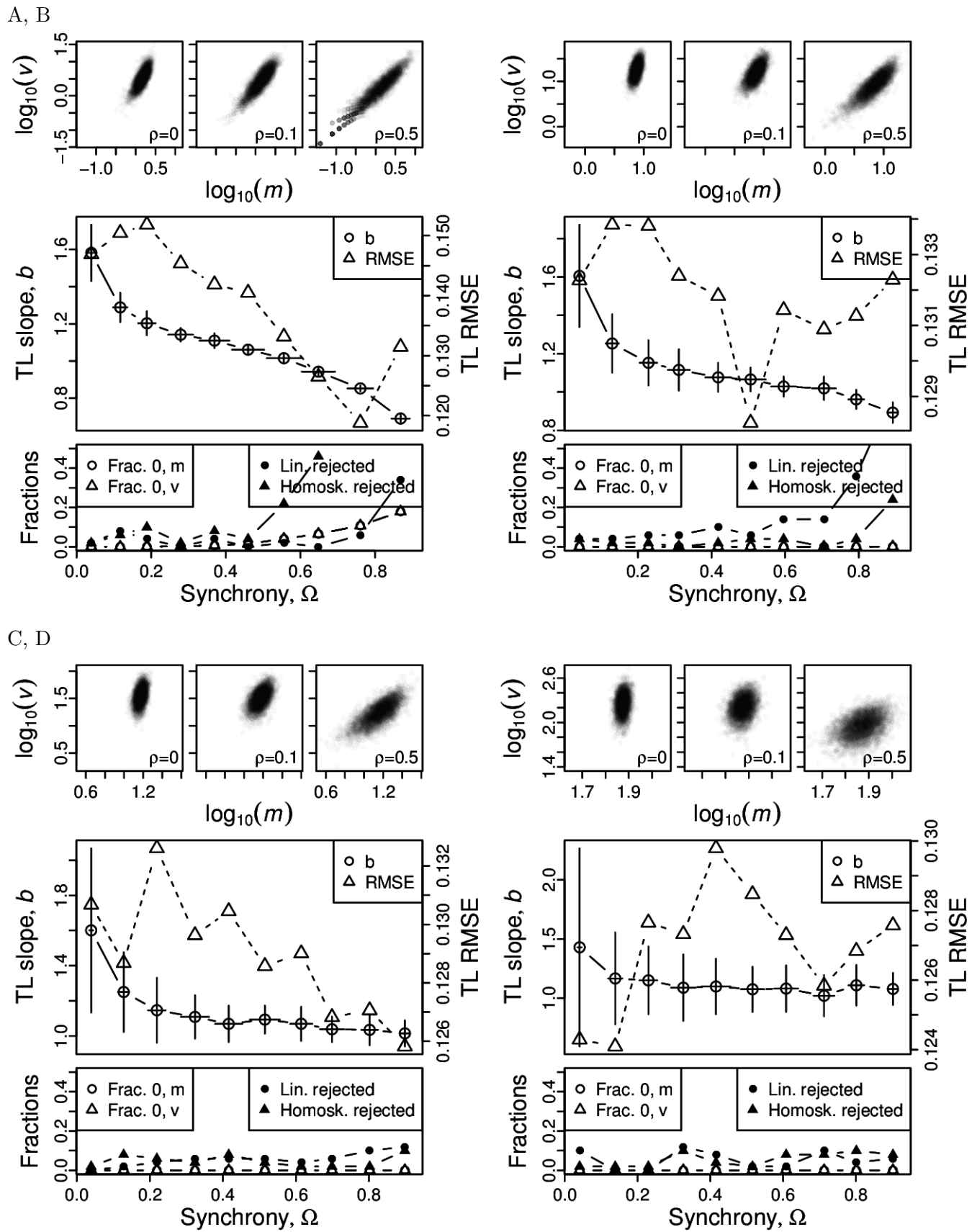
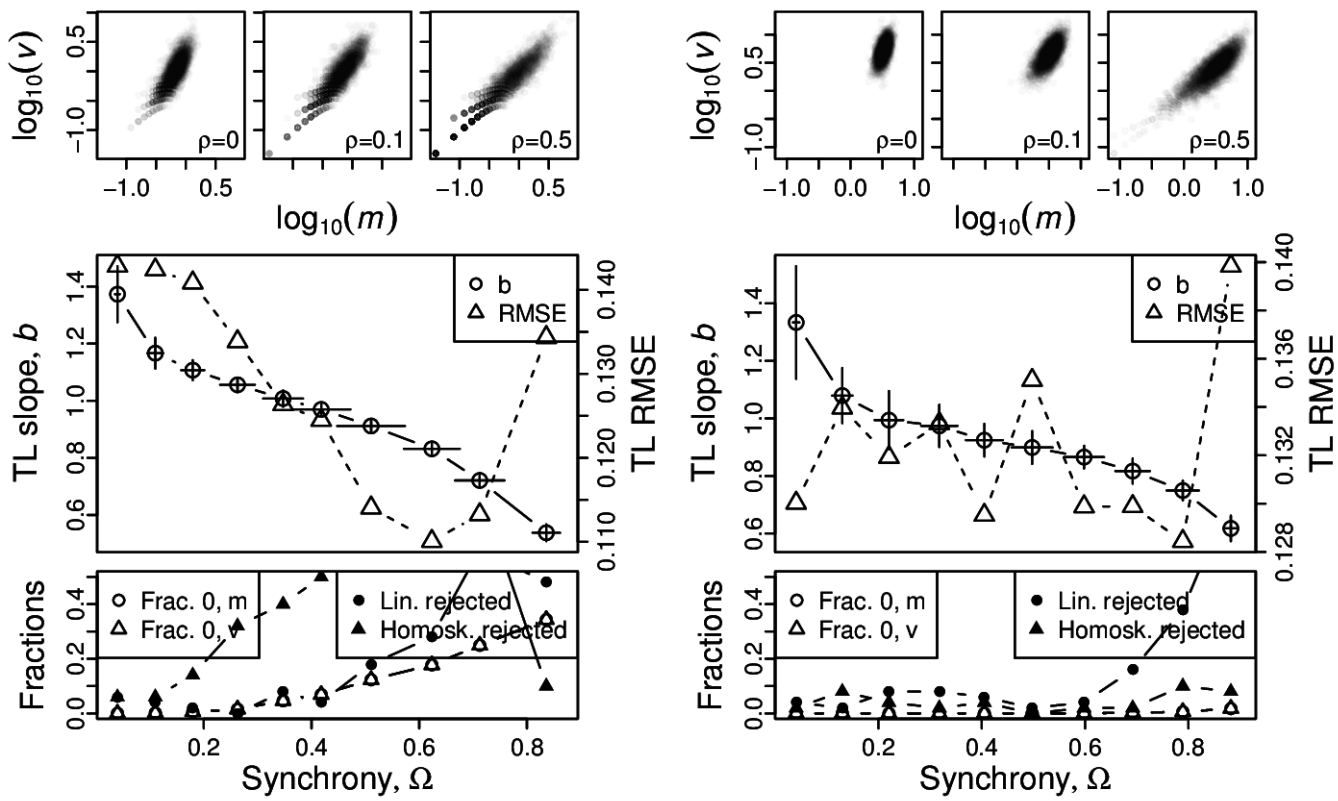


Figure S8: Omnibus plots (see section S6) for identically distributed negative binomial marginals under the set up of section S3, for  $n = 100$  and  $p = 0.4$ , for  $r = 1$  (A),  $r = 5$  (B),  $r = 10$  (C), and  $r = 50$  (D).

A, B



C, D

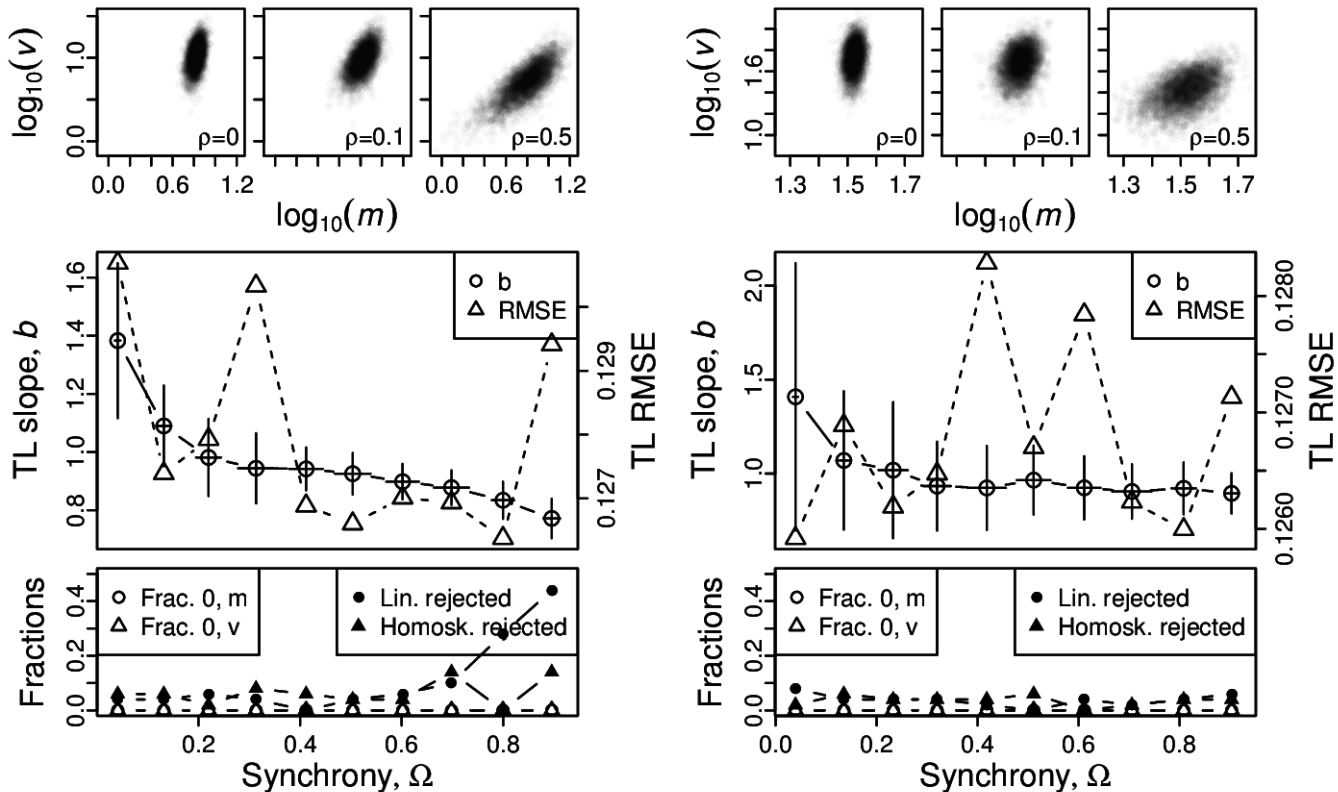
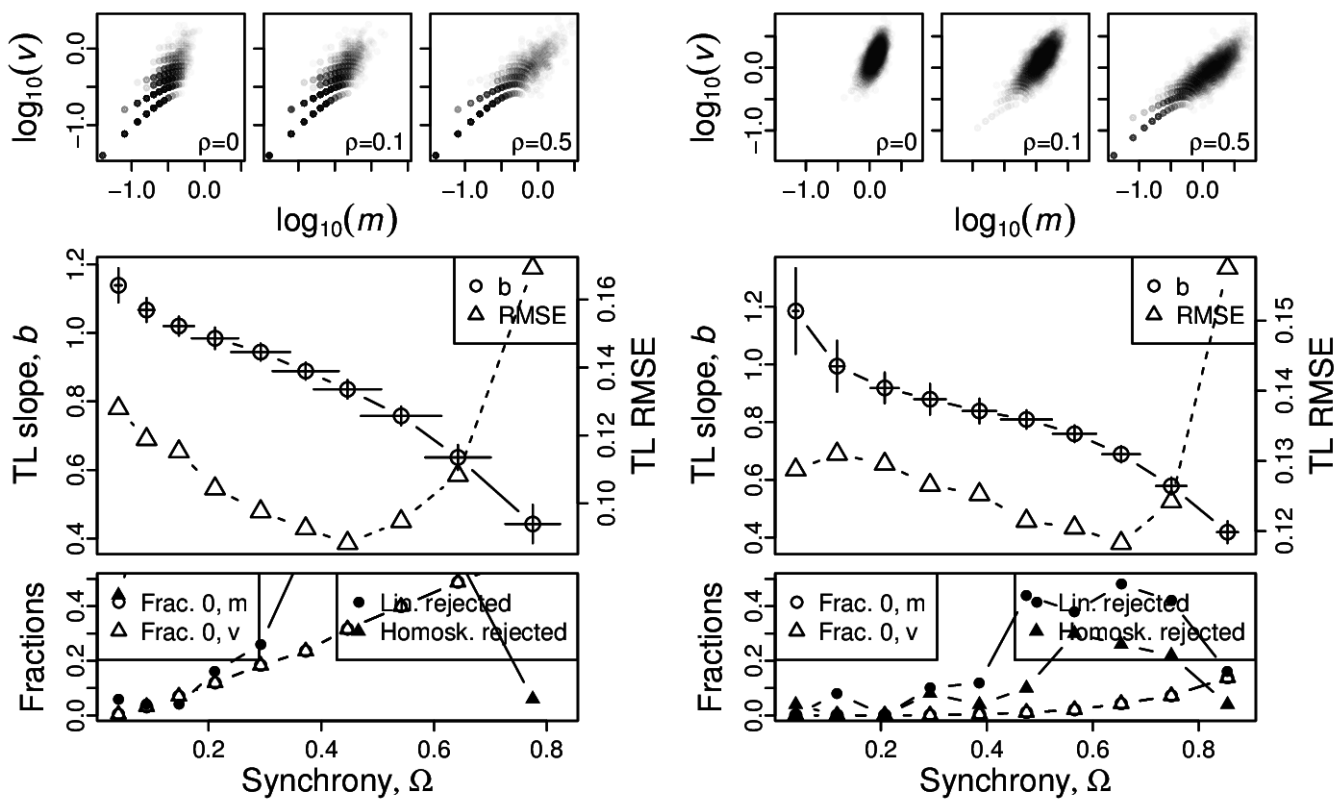


Figure S9: Omnibus plots (see section S6) for identically distributed negative binomial marginals under the set up of section S3, for  $n = 100$  and  $p = 0.6$ , for  $r = 1$  (A),  $r = 5$  (B),  $r = 10$  (C), and  $r = 50$  (D).

A, B



C, D

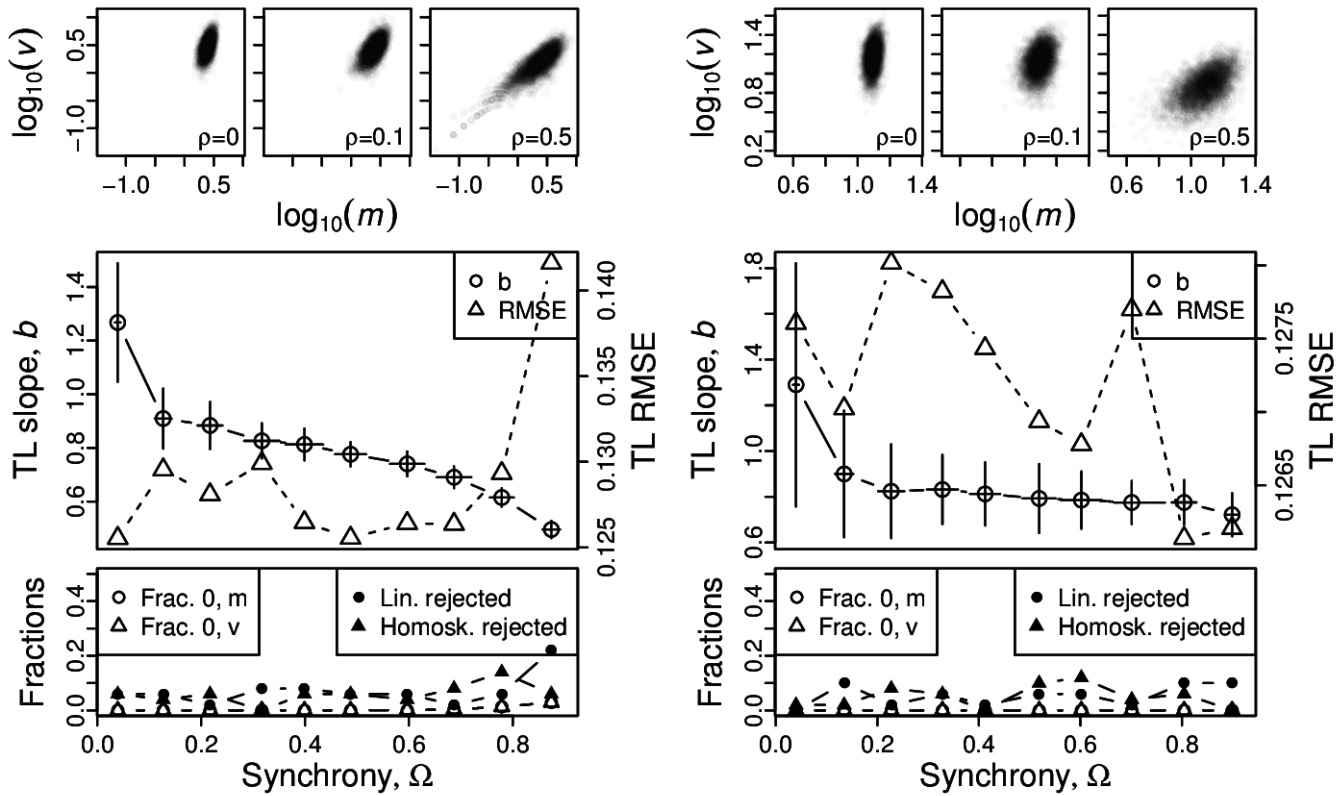
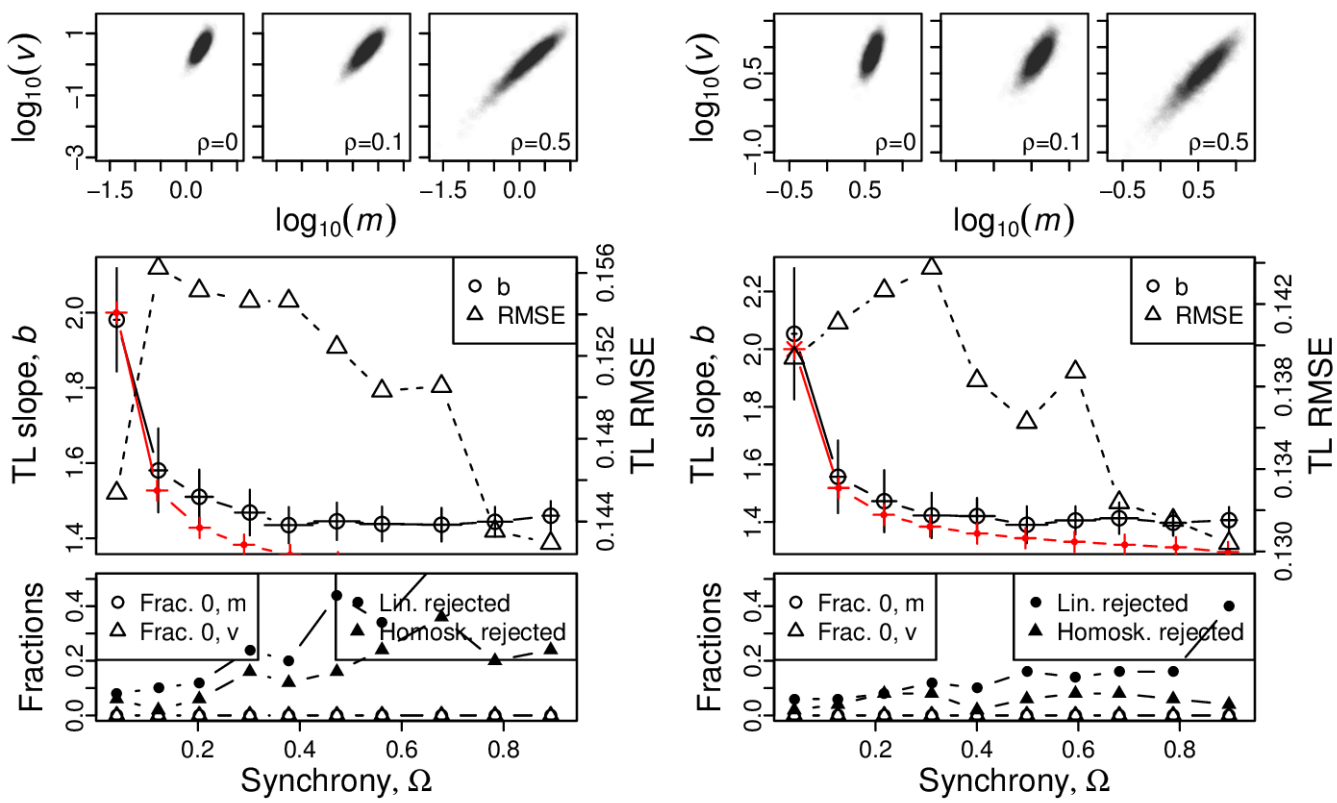


Figure S10: Omnibus plots (see section S6) for identically distributed negative binomial marginals under the set up of section S3, for  $n = 100$  and  $p = 0.8$ , for  $r = 1$  (A),  $r = 5$  (B),  $r = 10$  (C), and  $r = 50$  (D).

A, B



C, D

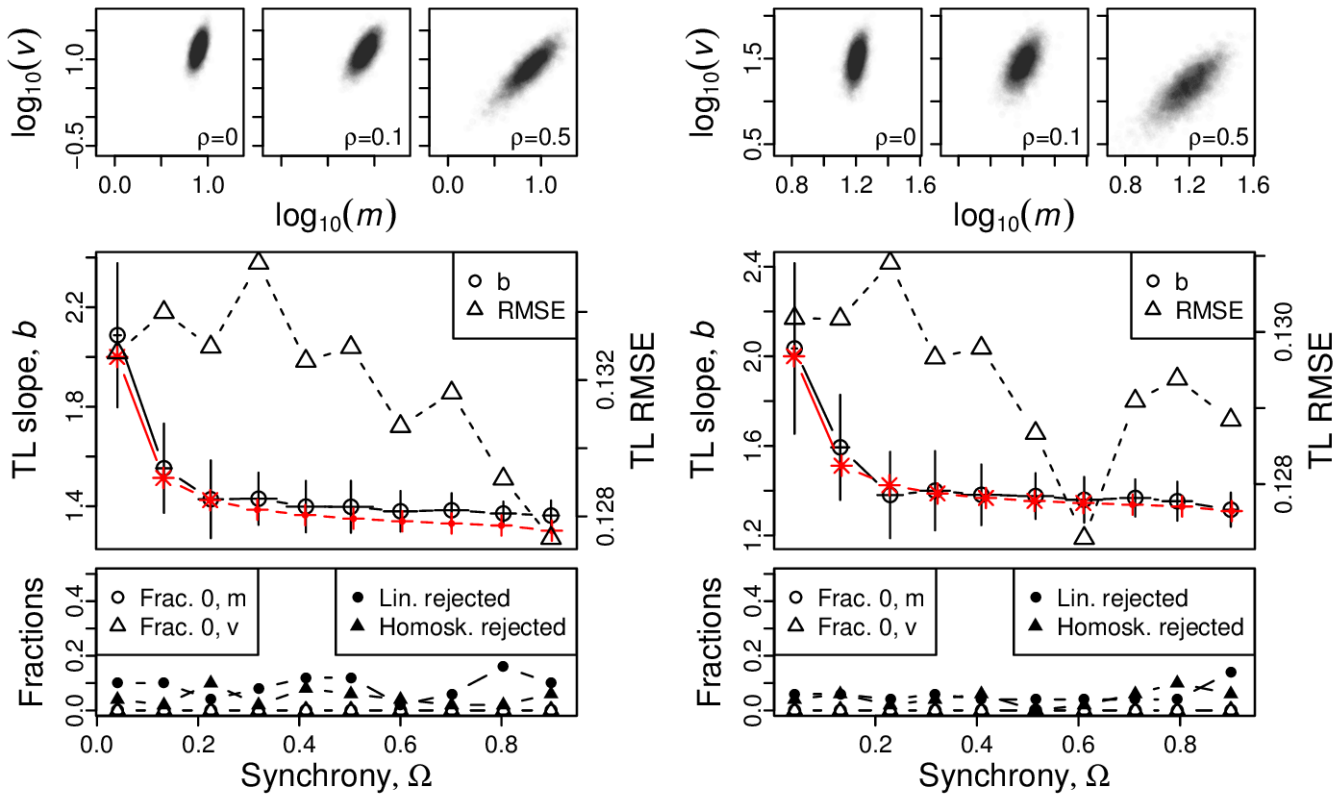
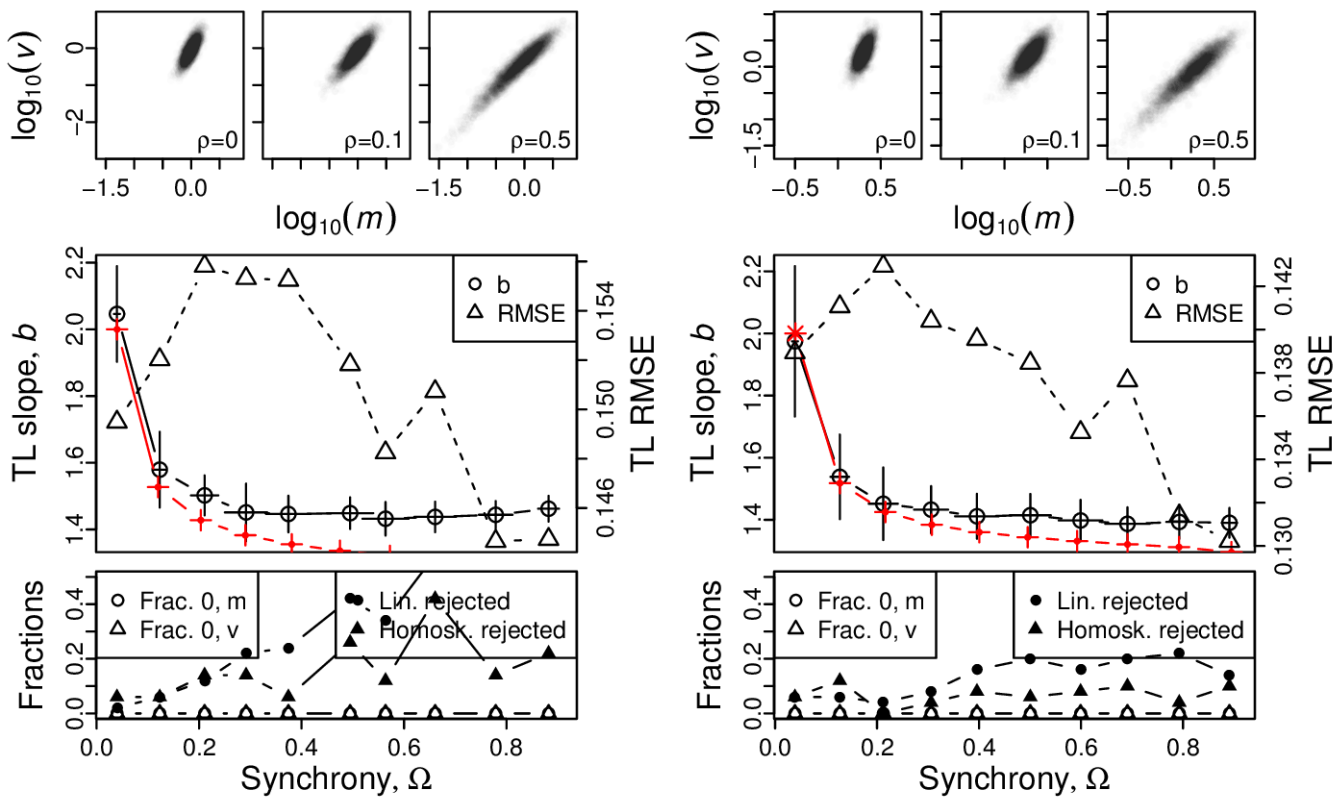


Figure S11: Omnibus plots (see section S6) for identically distributed gamma marginals under the set up of section S3, for  $n = 25$  and  $\beta = 0.5$ , for  $\alpha = 1$  (A),  $\alpha = 2$  (B),  $\alpha = 4$  (C), and  $\alpha = 8$  (D).

A, B



C, D

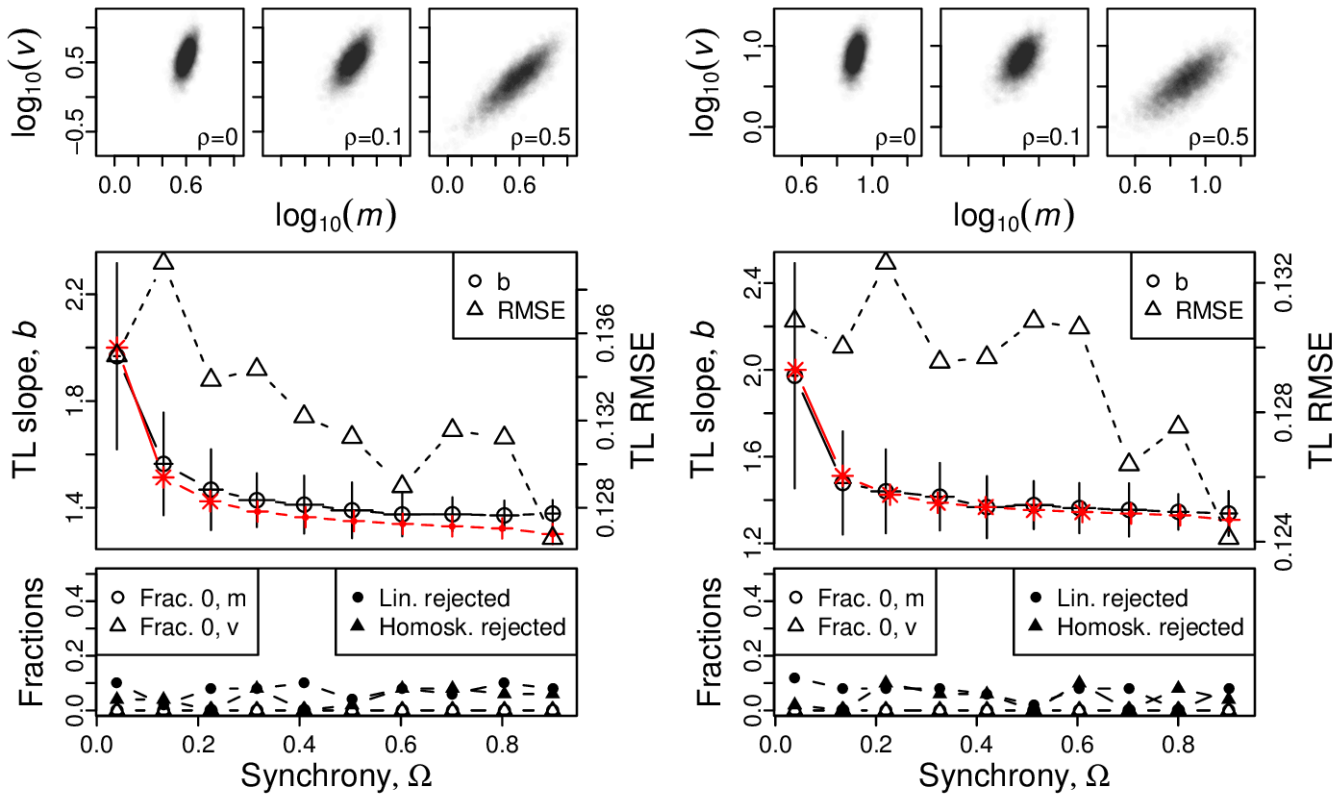
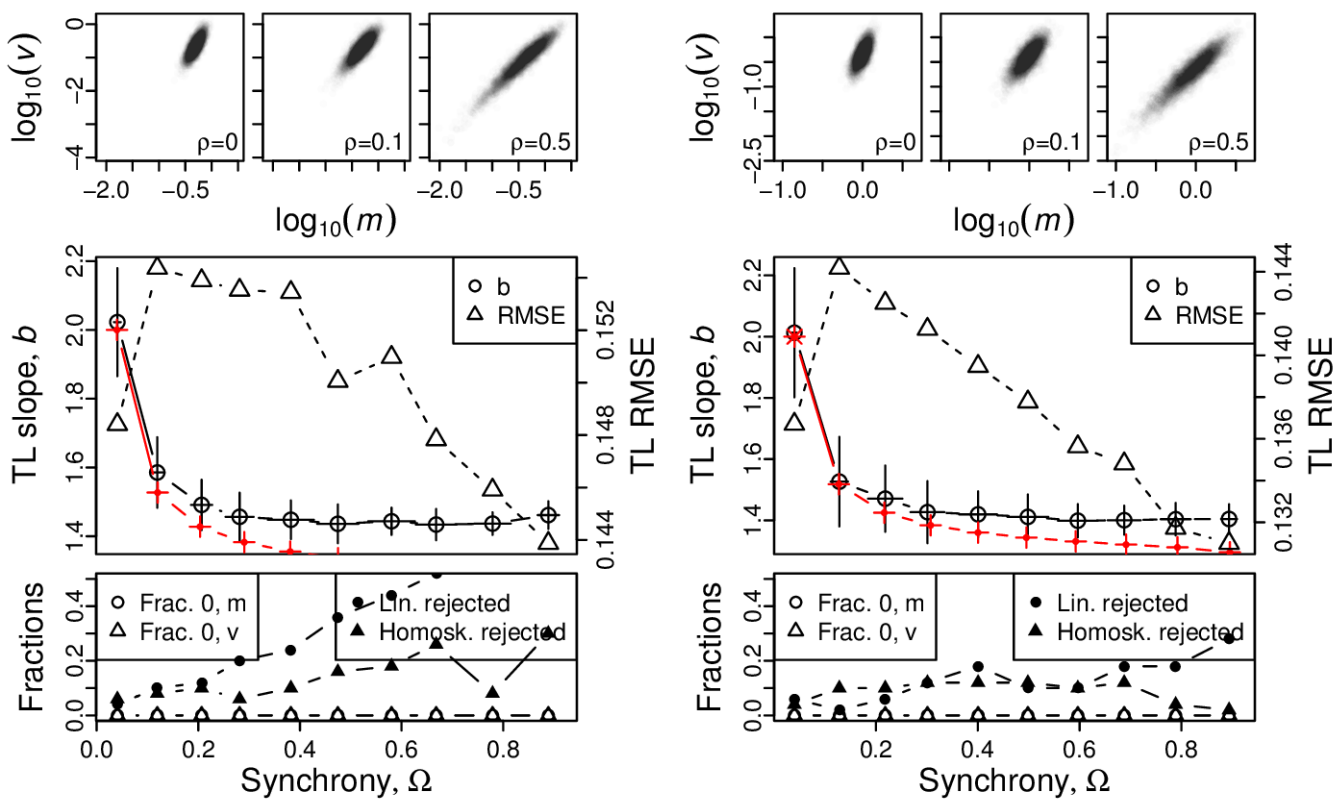


Figure S12: Omnibus plots (see section S6) for identically distributed gamma marginals under the set up of section S3, for  $n = 25$  and  $\beta = 1$ , for  $\alpha = 1$  (A),  $\alpha = 2$  (B),  $\alpha = 4$  (C), and  $\alpha = 8$  (D).

A, B



C, D

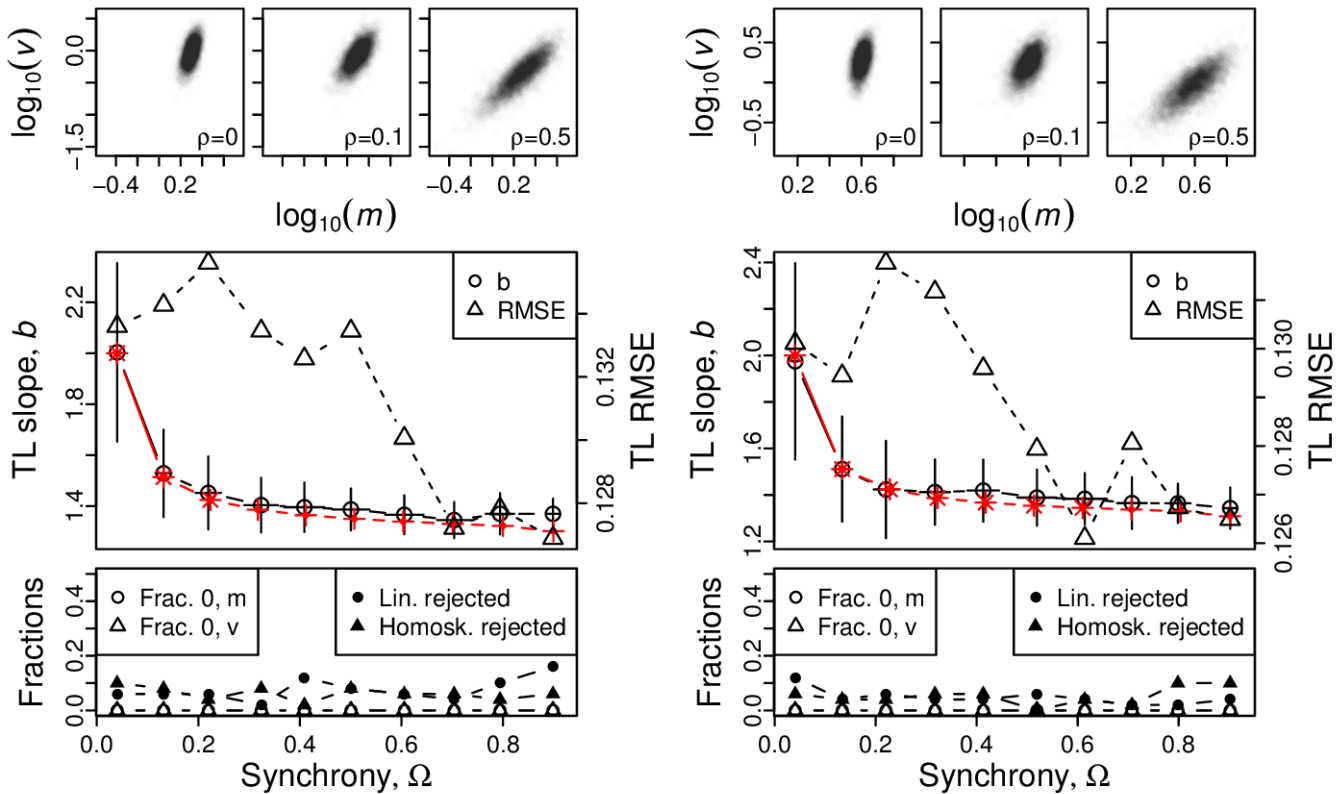
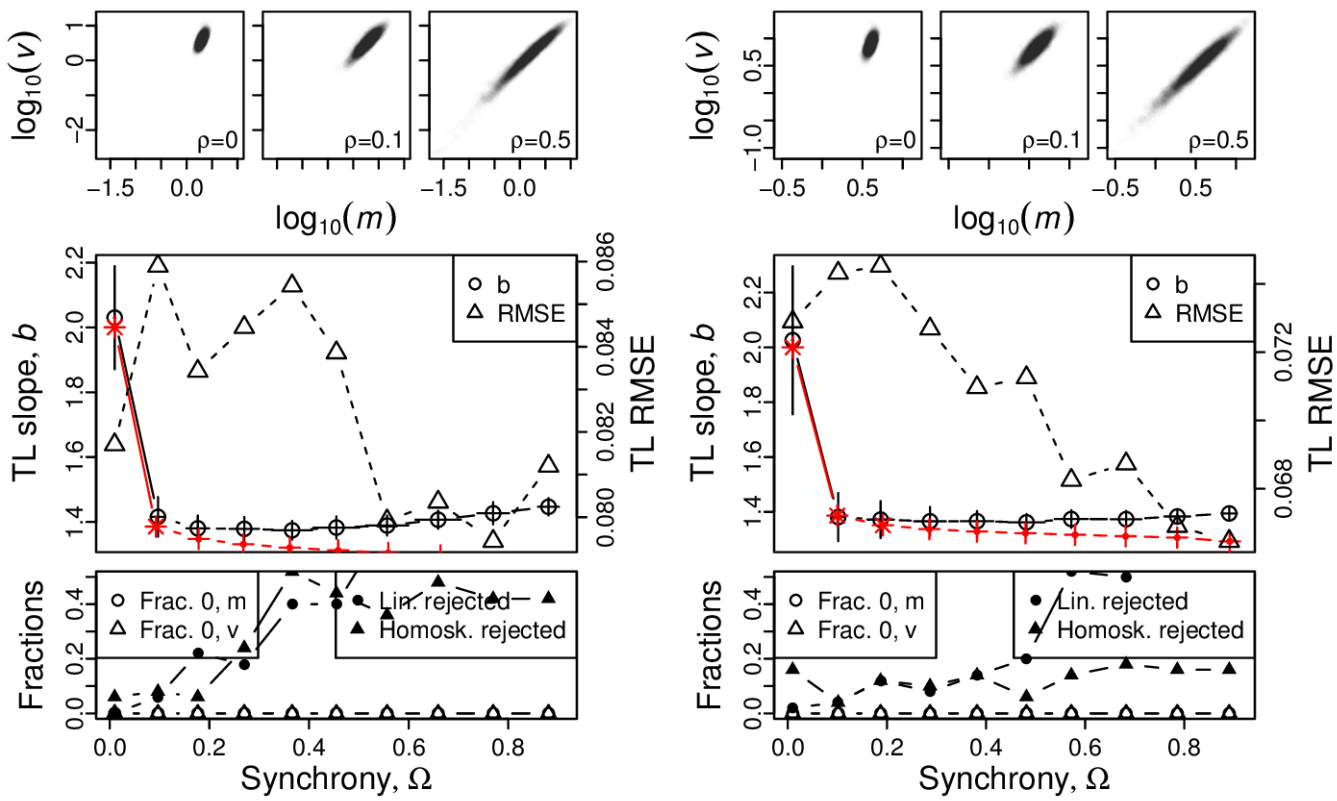


Figure S13: Omnibus plots (see section S6) for identically distributed gamma marginals under the set up of section S3, for  $n = 25$  and  $\beta = 2$ , for  $\alpha = 1$  (A),  $\alpha = 2$  (B),  $\alpha = 4$  (C), and  $\alpha = 8$  (D).

A, B



C, D

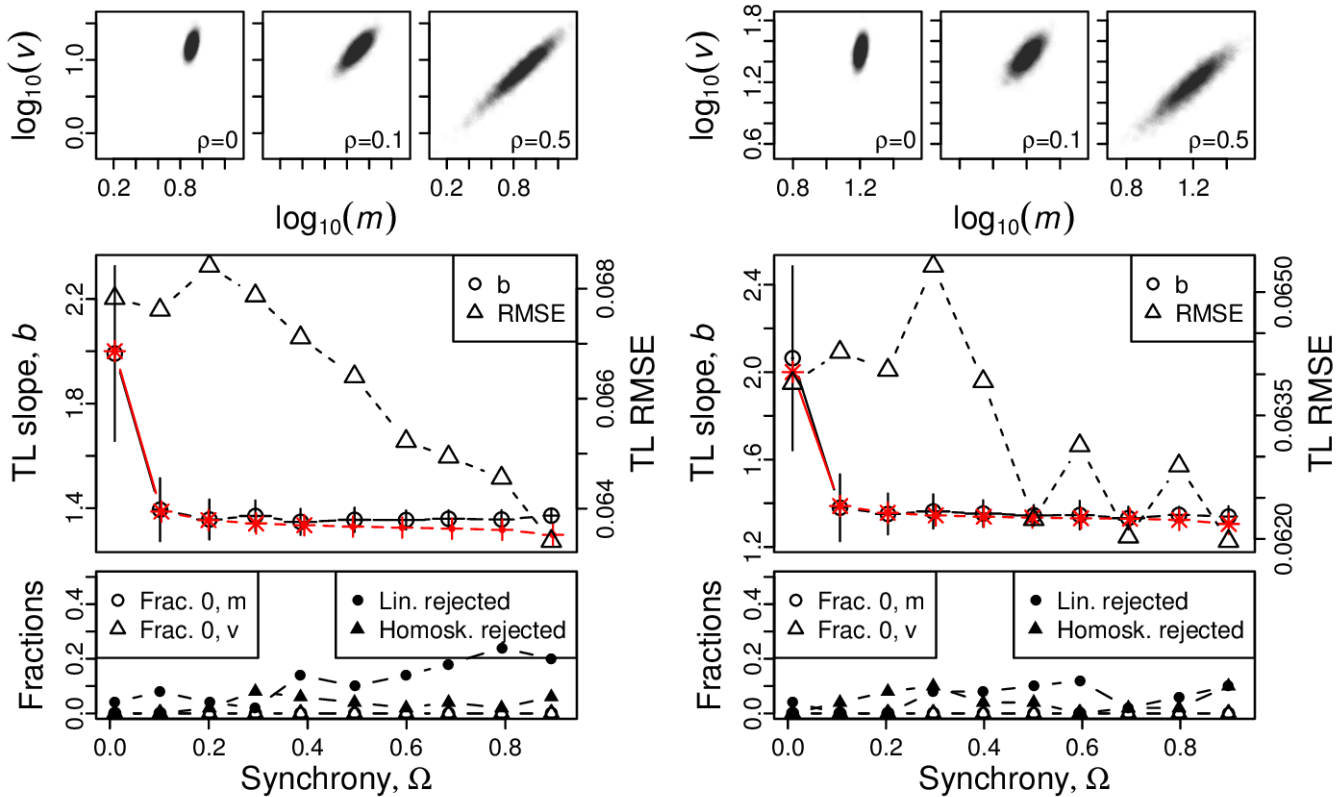
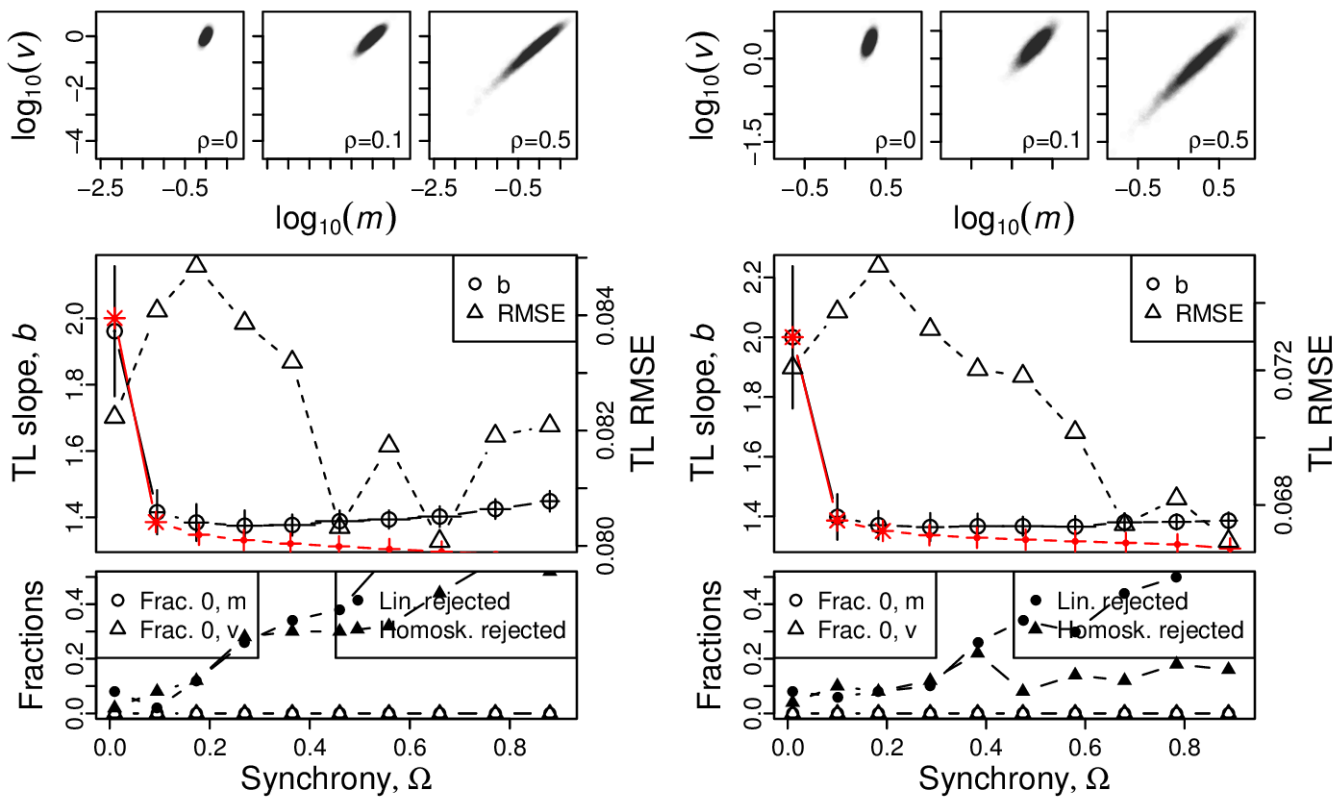


Figure S14: Omnibus plots (see section S6) for identically distributed gamma marginals under the set up of section S3, for  $n = 100$  and  $\beta = 0.5$ , for  $\alpha = 1$  (A),  $\alpha = 2$  (B),  $\alpha = 4$  (C), and  $\alpha = 8$  (D).

A, B



C, D

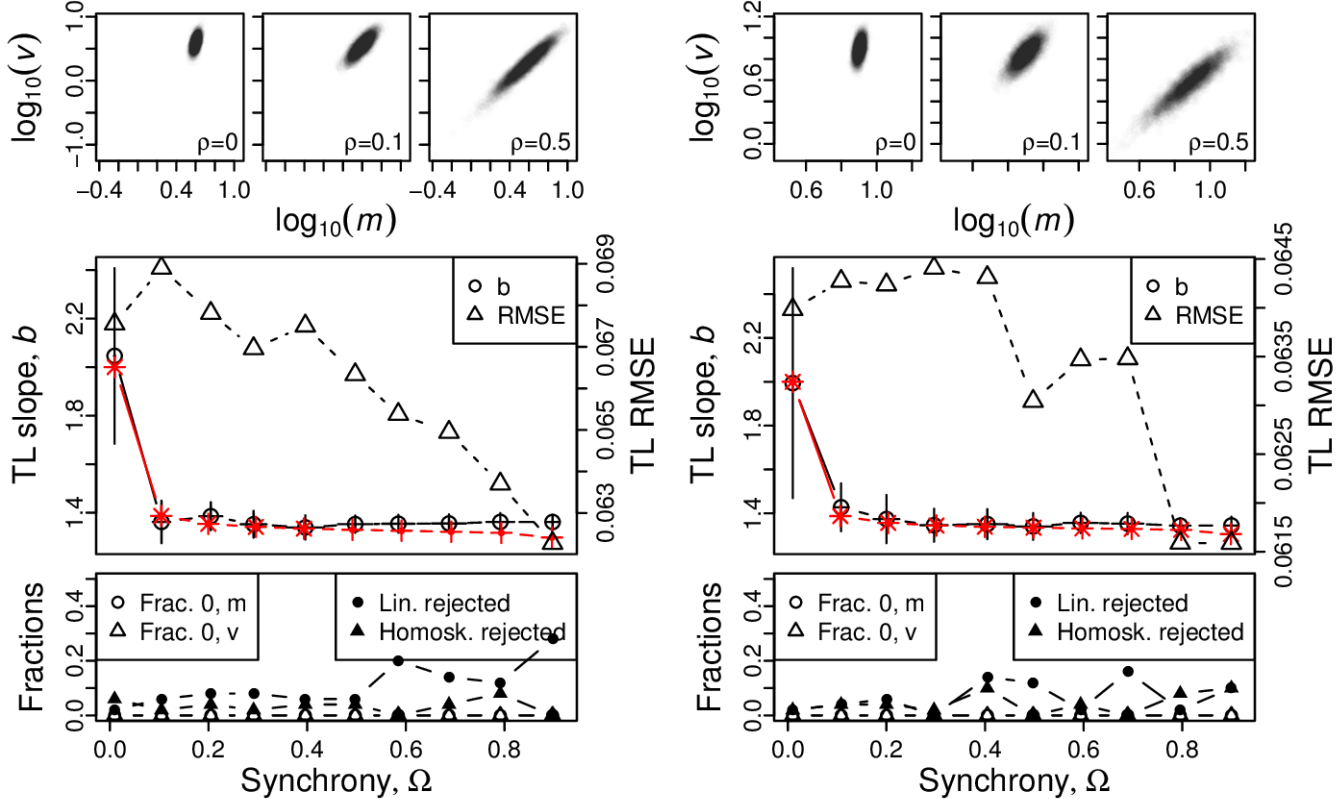
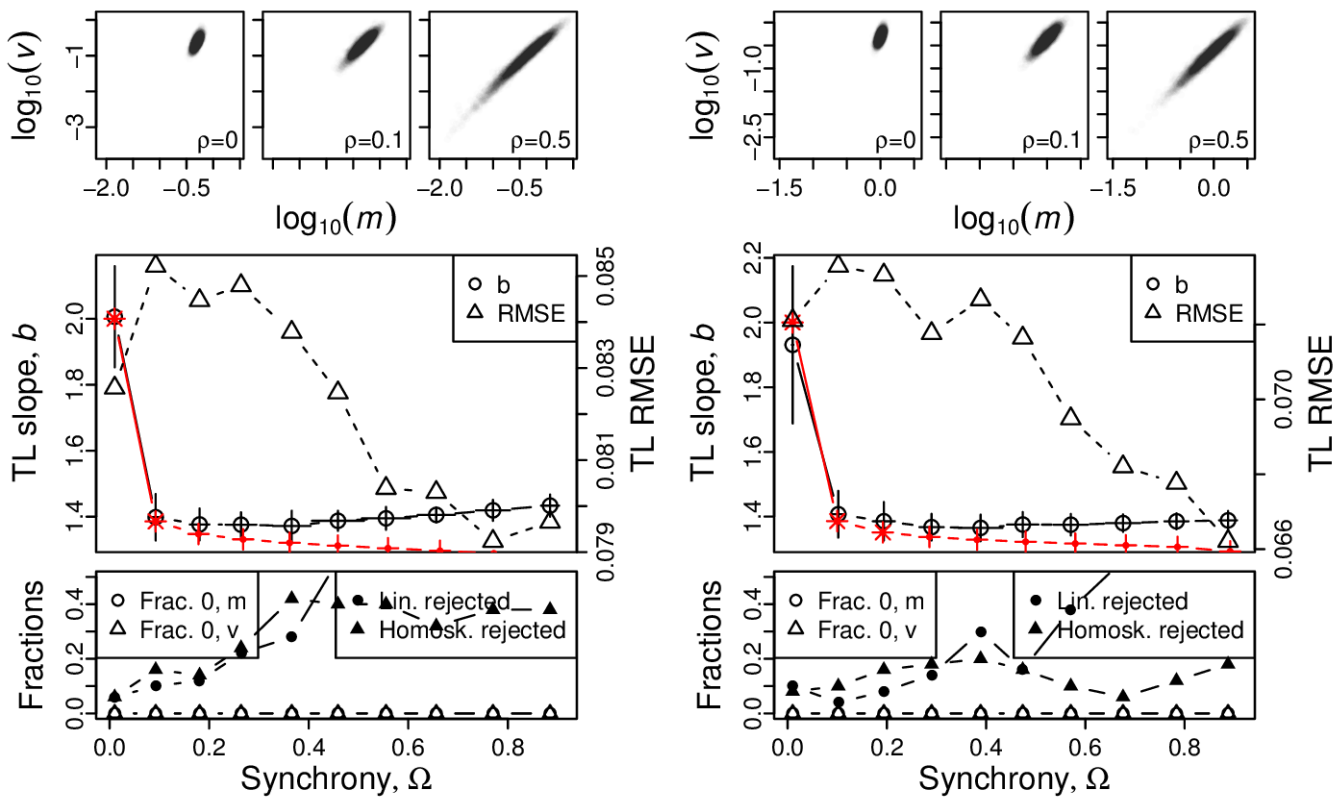


Figure S15: Omnibus plots (see section S6) for identically distributed gamma marginals under the set up of section S3, for  $n = 100$  and  $\beta = 1$ , for  $\alpha = 1$  (A),  $\alpha = 2$  (B),  $\alpha = 4$  (C), and  $\alpha = 8$  (D).

A, B



C, D

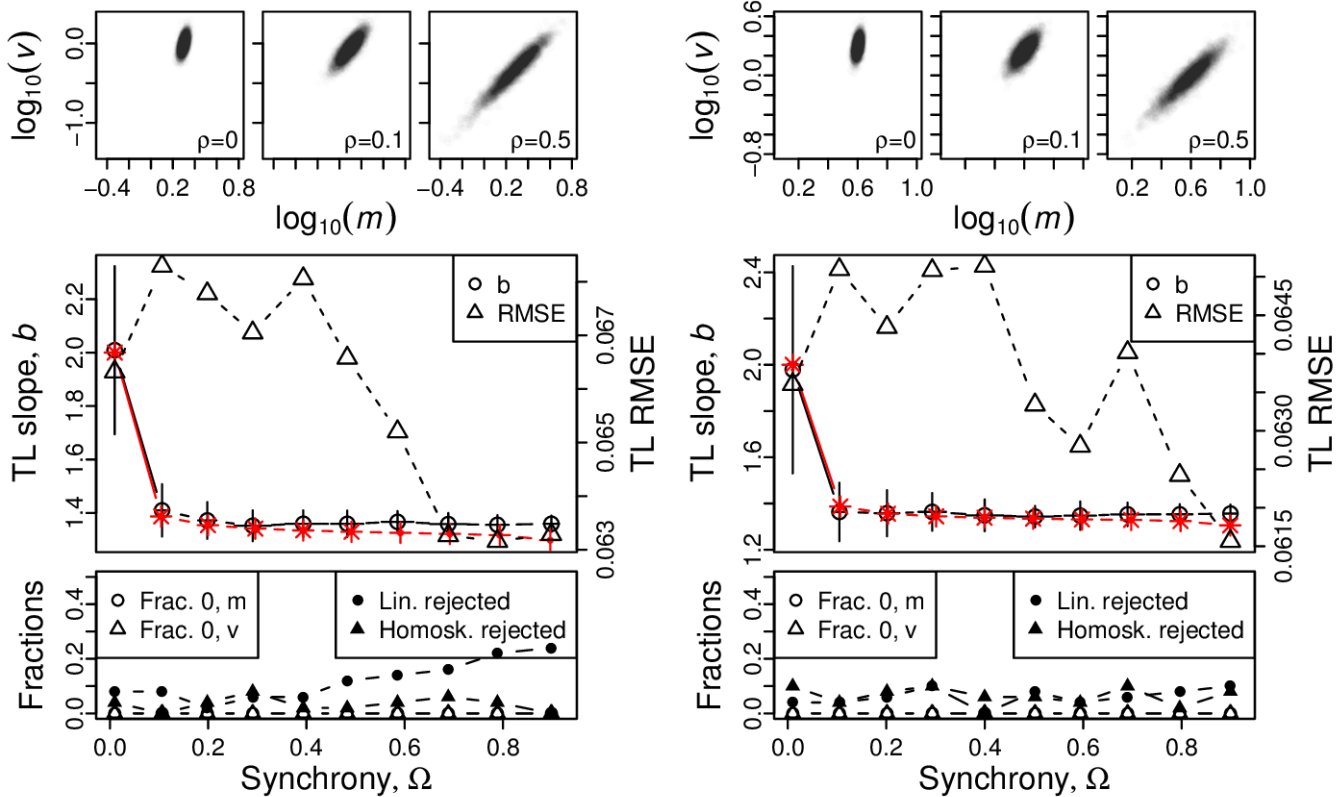
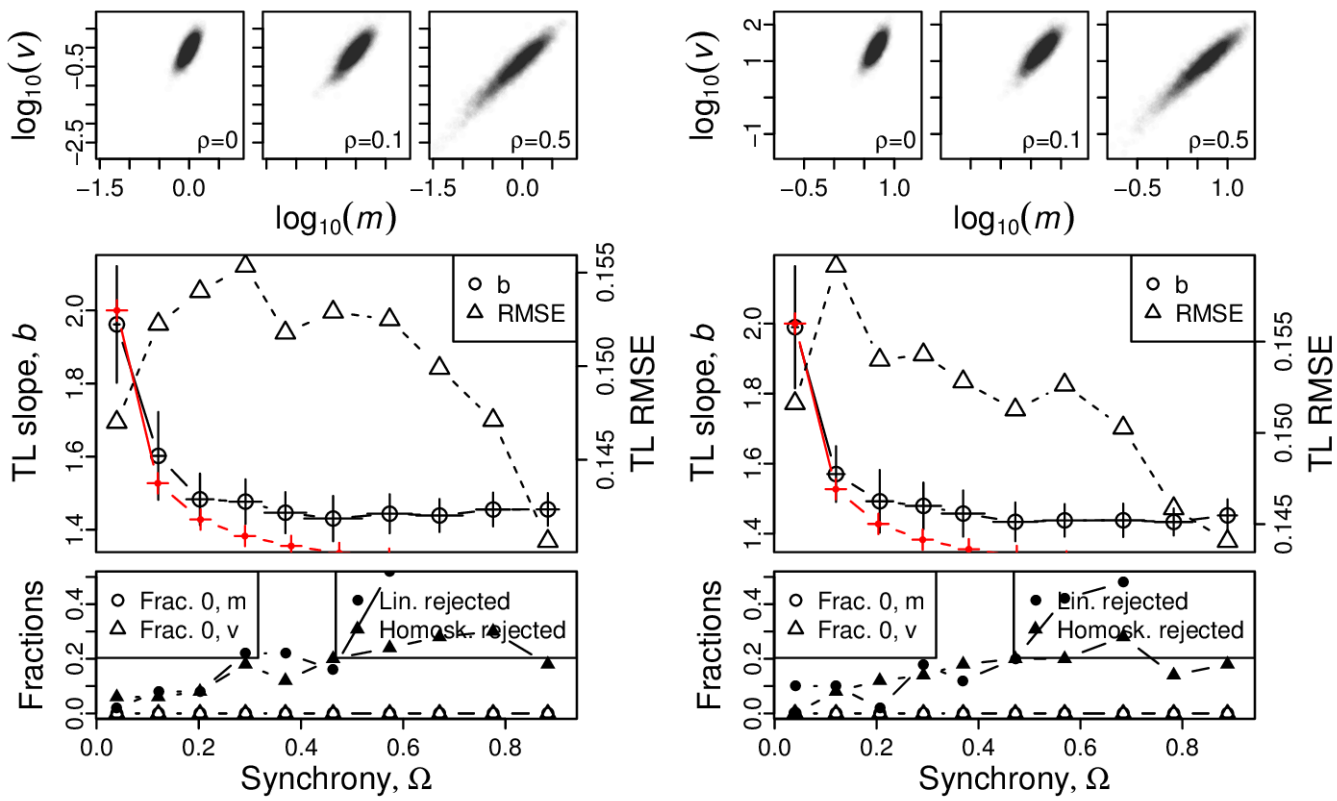


Figure S16: Omnibus plots (see section S6) for identically distributed gamma marginals under the set up of section S3, for  $n = 100$  and  $\beta = 2$ , for  $\alpha = 1$  (A),  $\alpha = 2$  (B),  $\alpha = 4$  (C), and  $\alpha = 8$  (D).

A, B



C, D

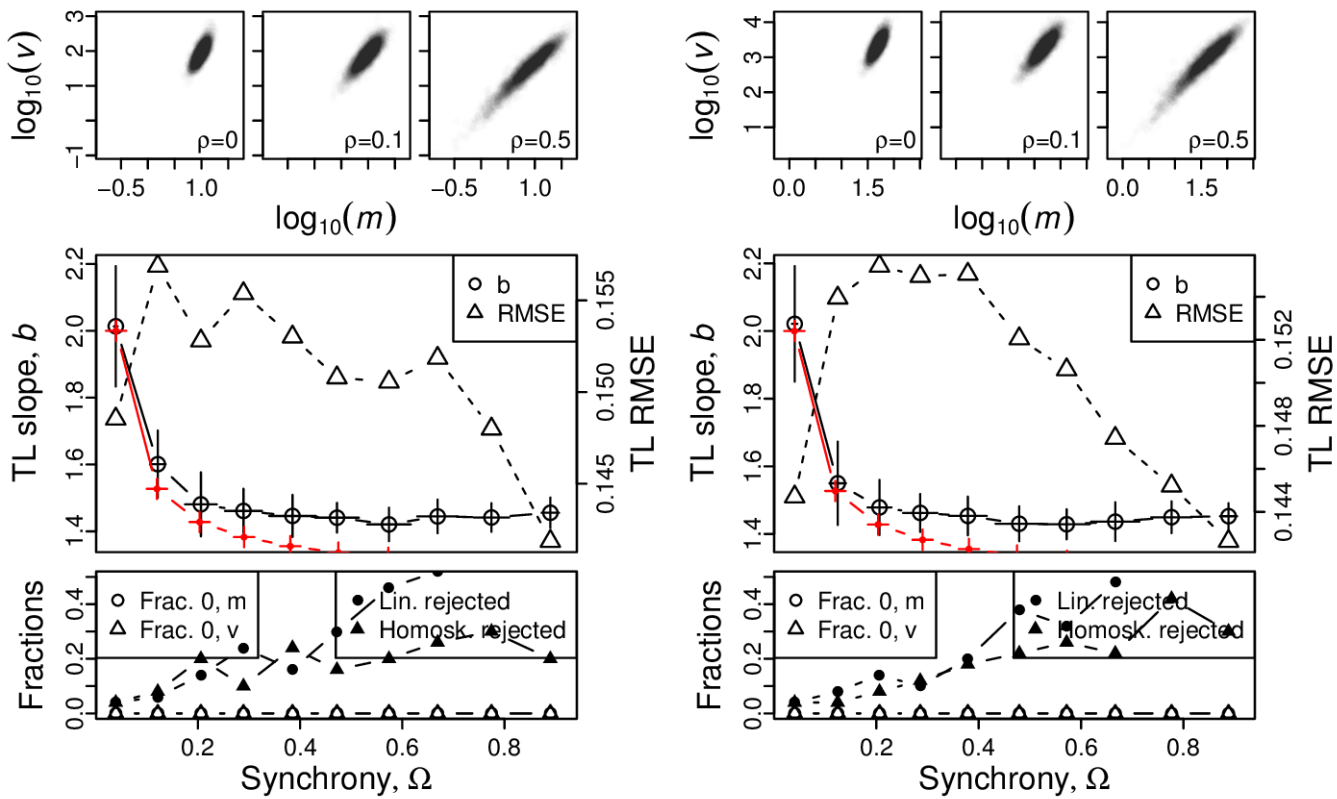
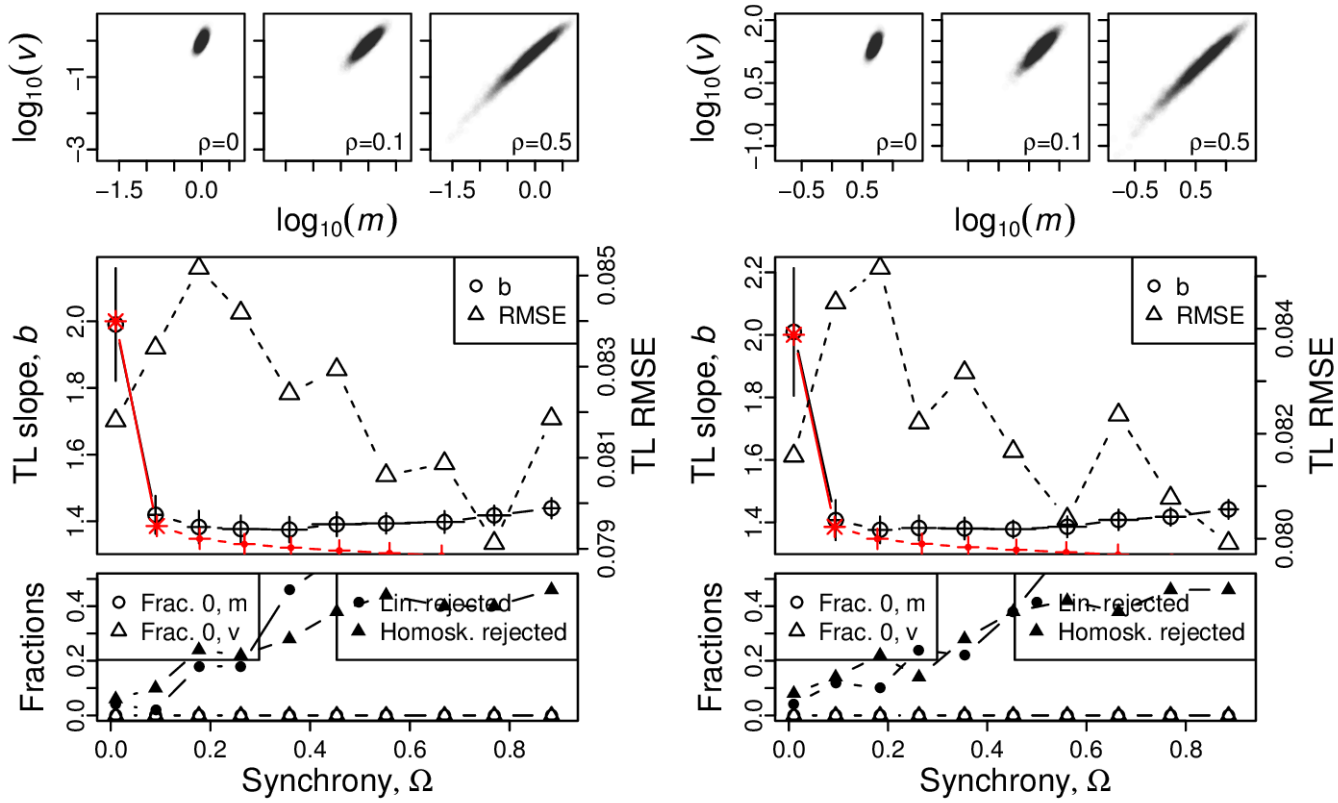


Figure S17: Omnibus plots (see section S6) for identically distributed exponentially distributed marginals under the set up of section S3, for  $n = 25$ , for  $1/\lambda = 1$  (A),  $1/\lambda = 5$  (B),  $1/\lambda = 10$  (C), and  $1/\lambda = 50$  (D).

A, B



C, D

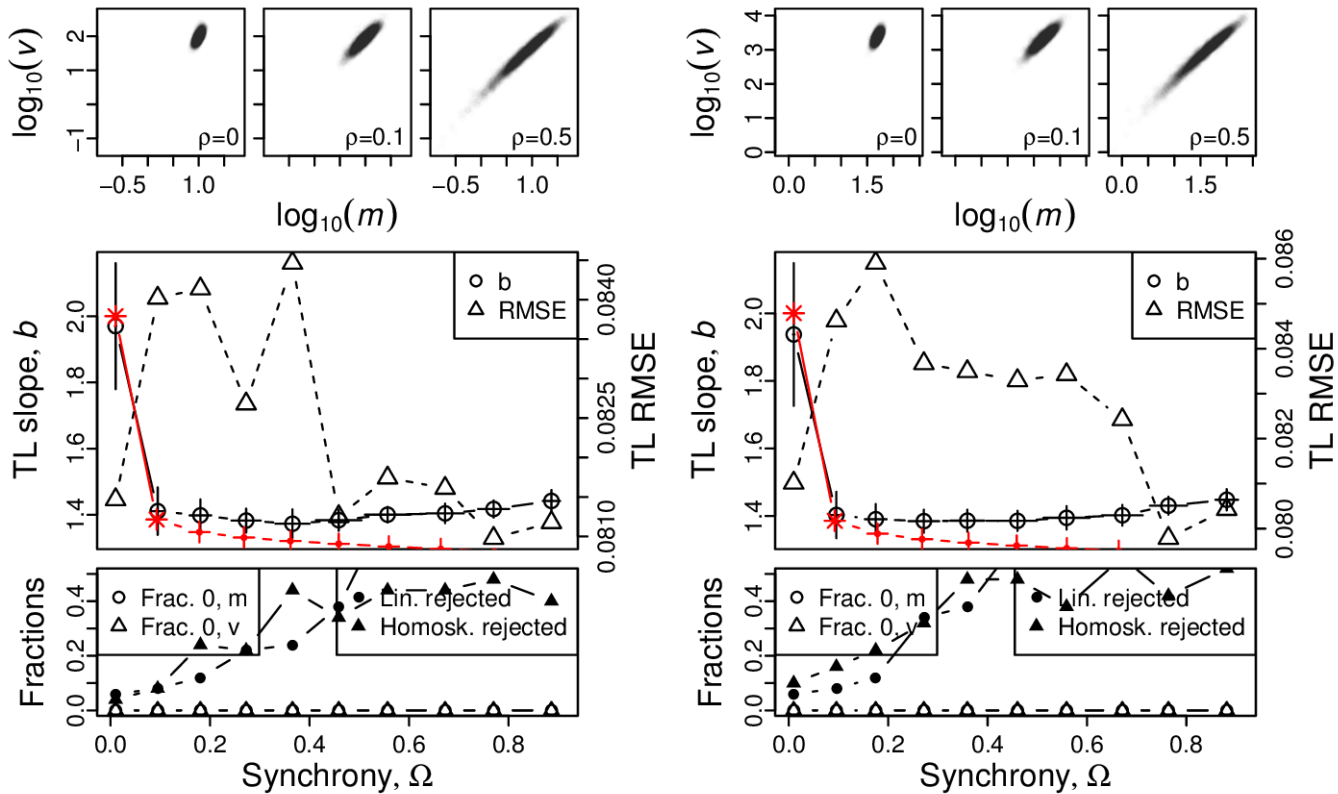
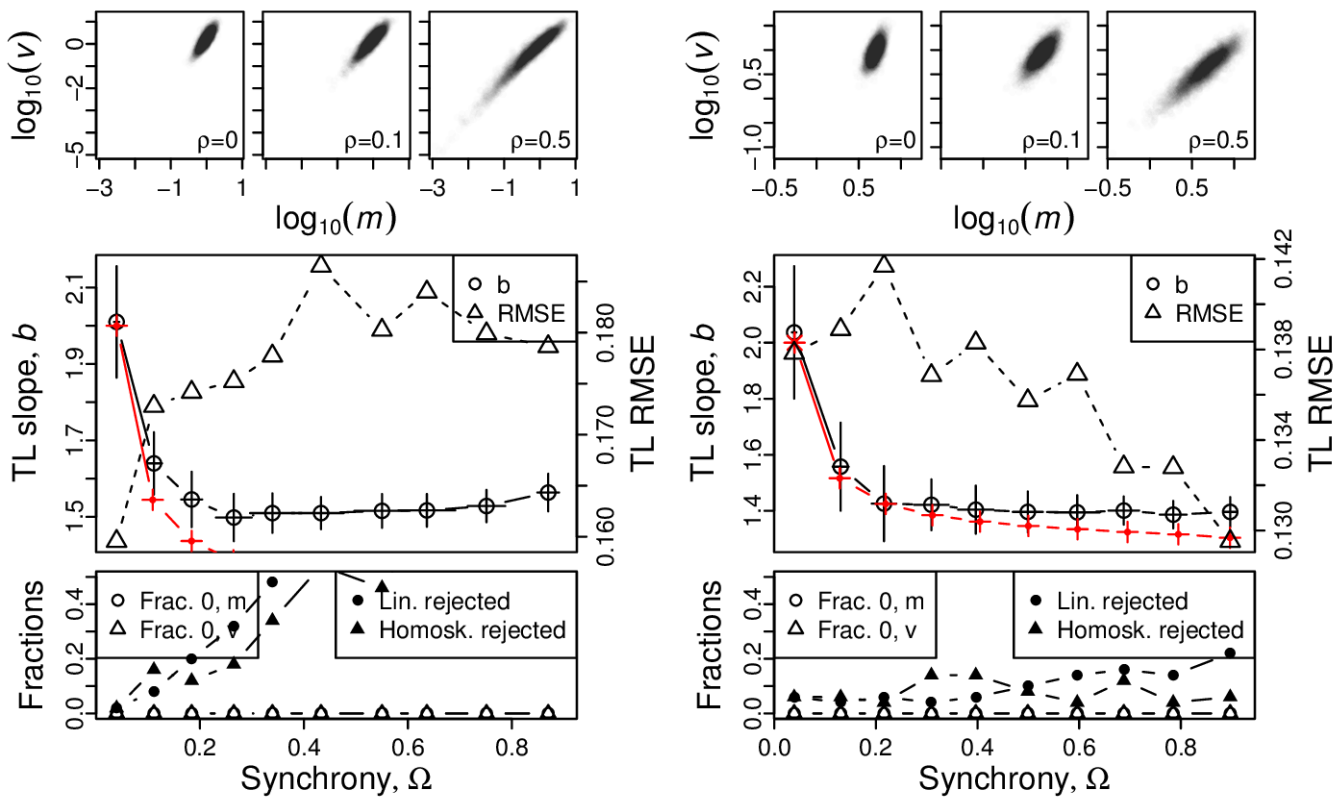


Figure S18: Omnibus plots (see section S6) for identically distributed exponentially distributed marginals under the set up of section S3, for  $n = 100$ , for  $1/\lambda = 1$  (A),  $1/\lambda = 5$  (B),  $1/\lambda = 10$  (C), and  $1/\lambda = 50$  (D).

A, B



C, D

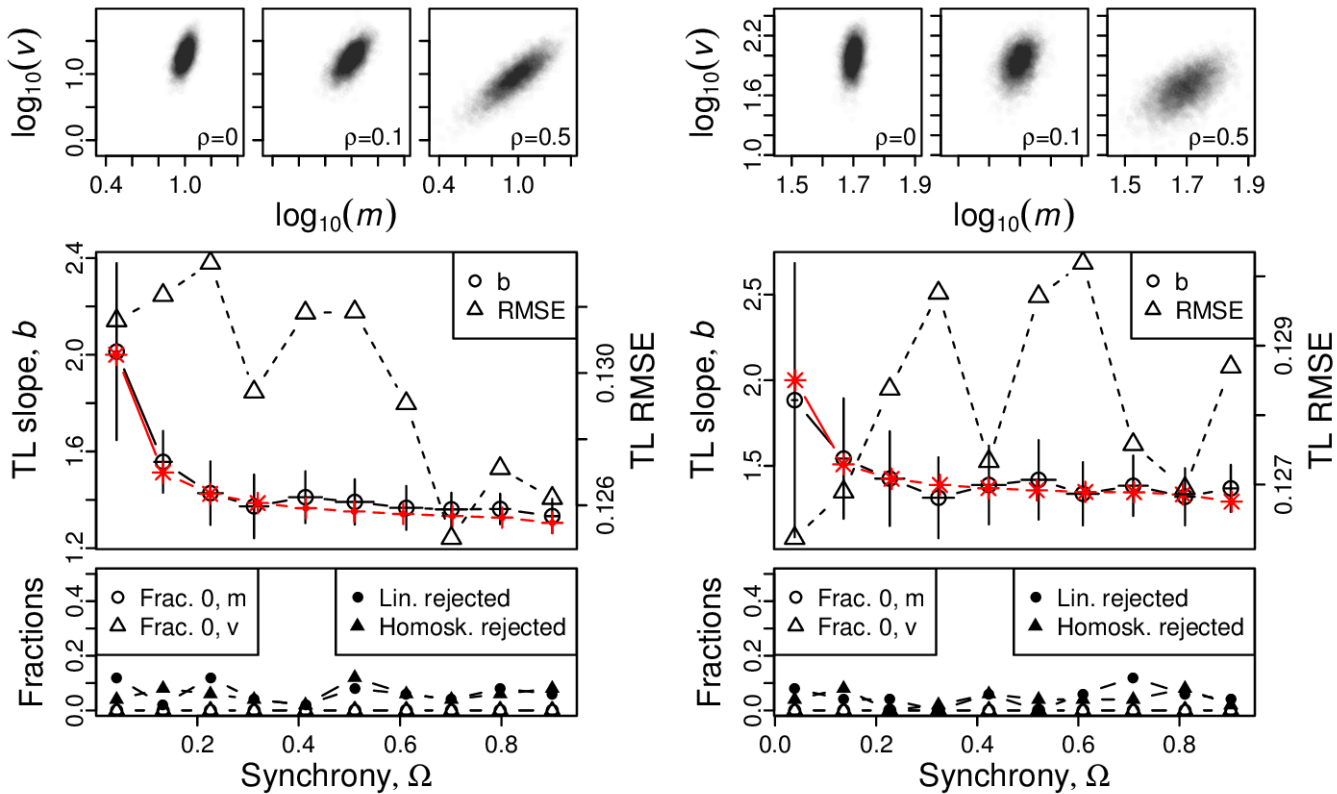
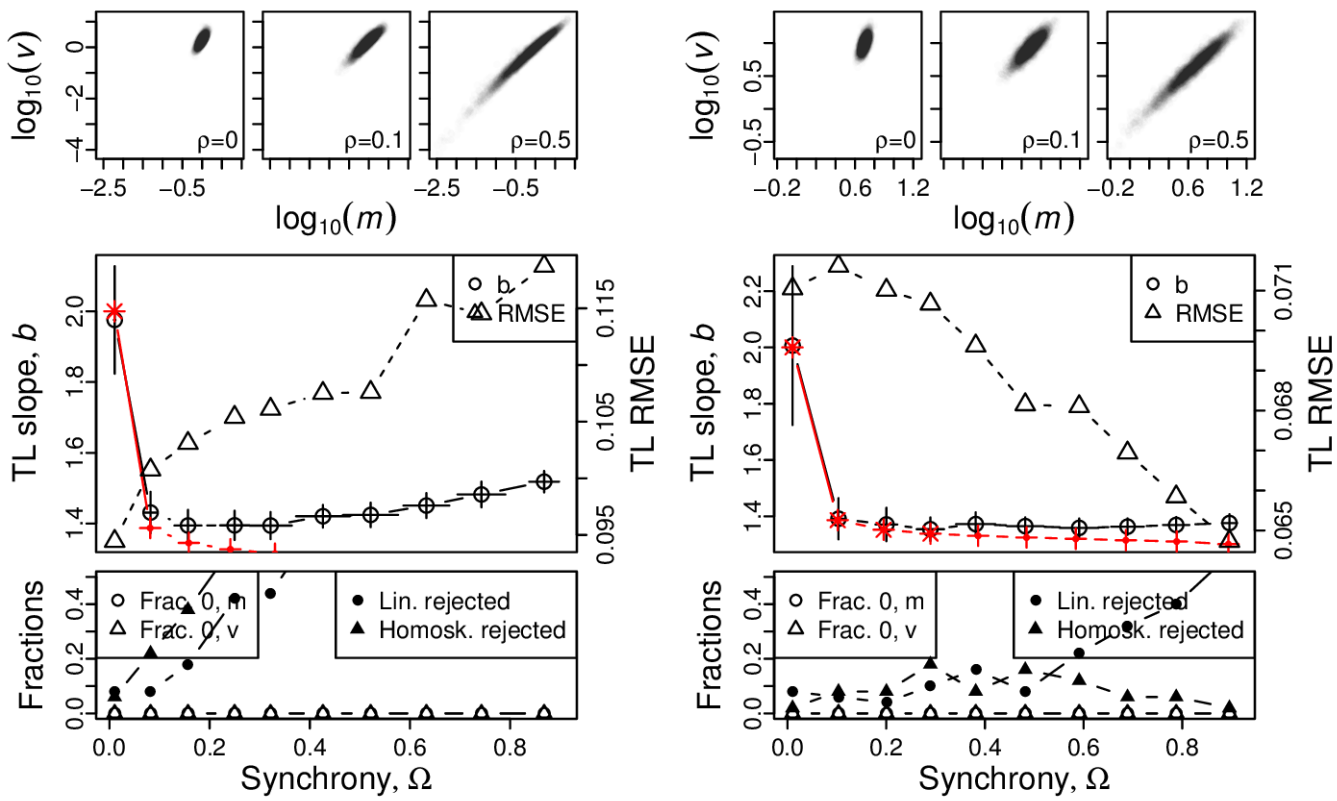


Figure S19: Omnibus plots (see section S6) for identically distributed chi-squared marginals under the set up of section S3, for  $n = 25$ , for  $k = 1$  (A),  $k = 5$  (B),  $k = 10$  (C), and  $k = 50$  (D).

A, B



C, D

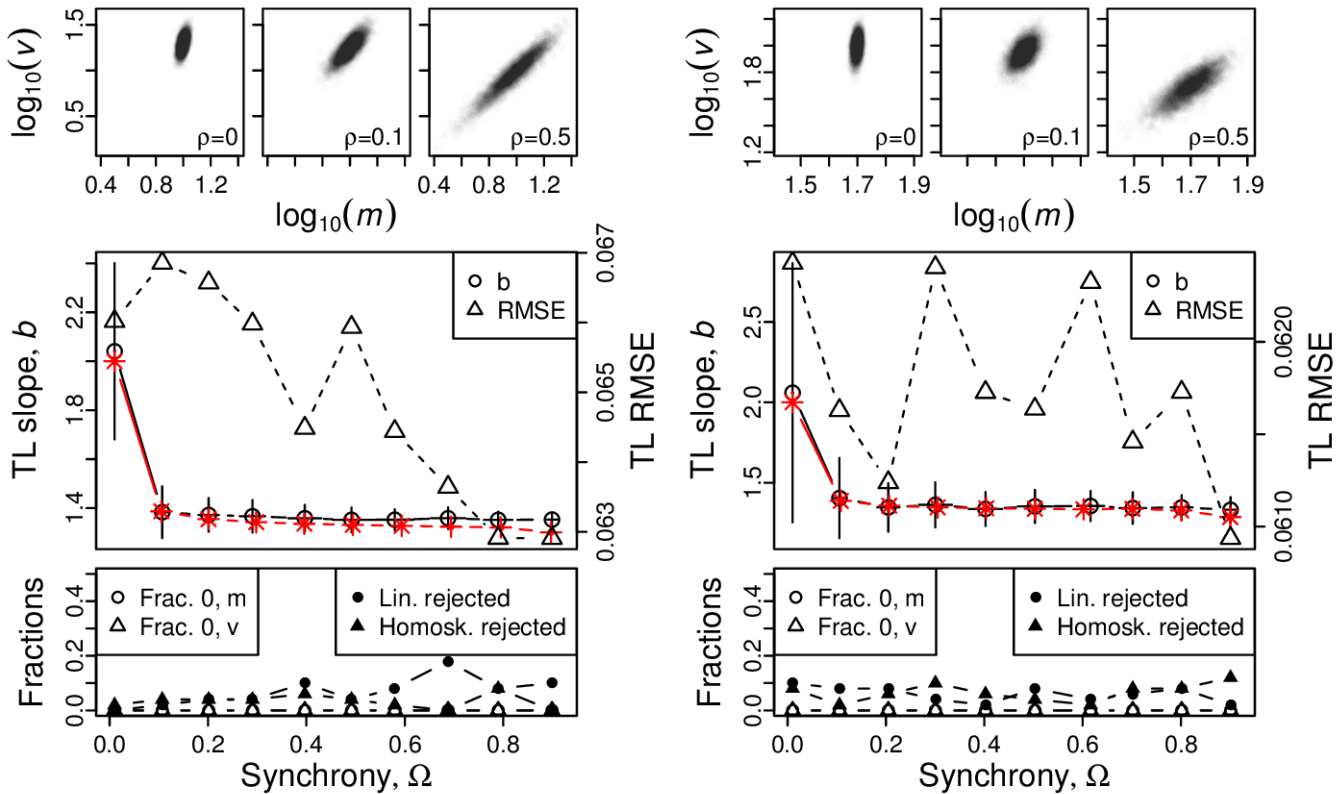
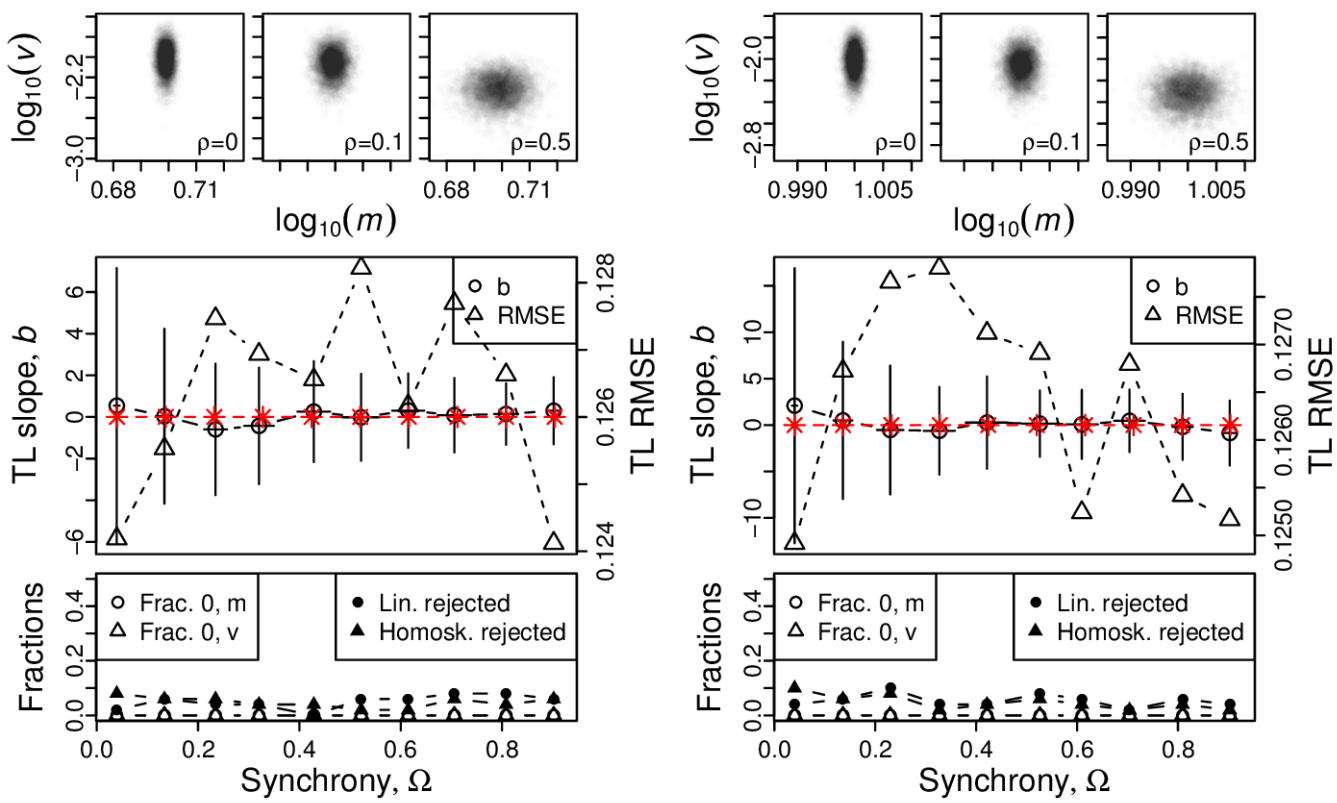


Figure S20: Omnibus plots (see section S6) for identically distributed chi-squared marginals under the set up of section S3, for  $n = 100$ , for  $k = 1$  (A),  $k = 5$  (B),  $k = 10$  (C), and  $k = 50$  (D).

A, B



C, D

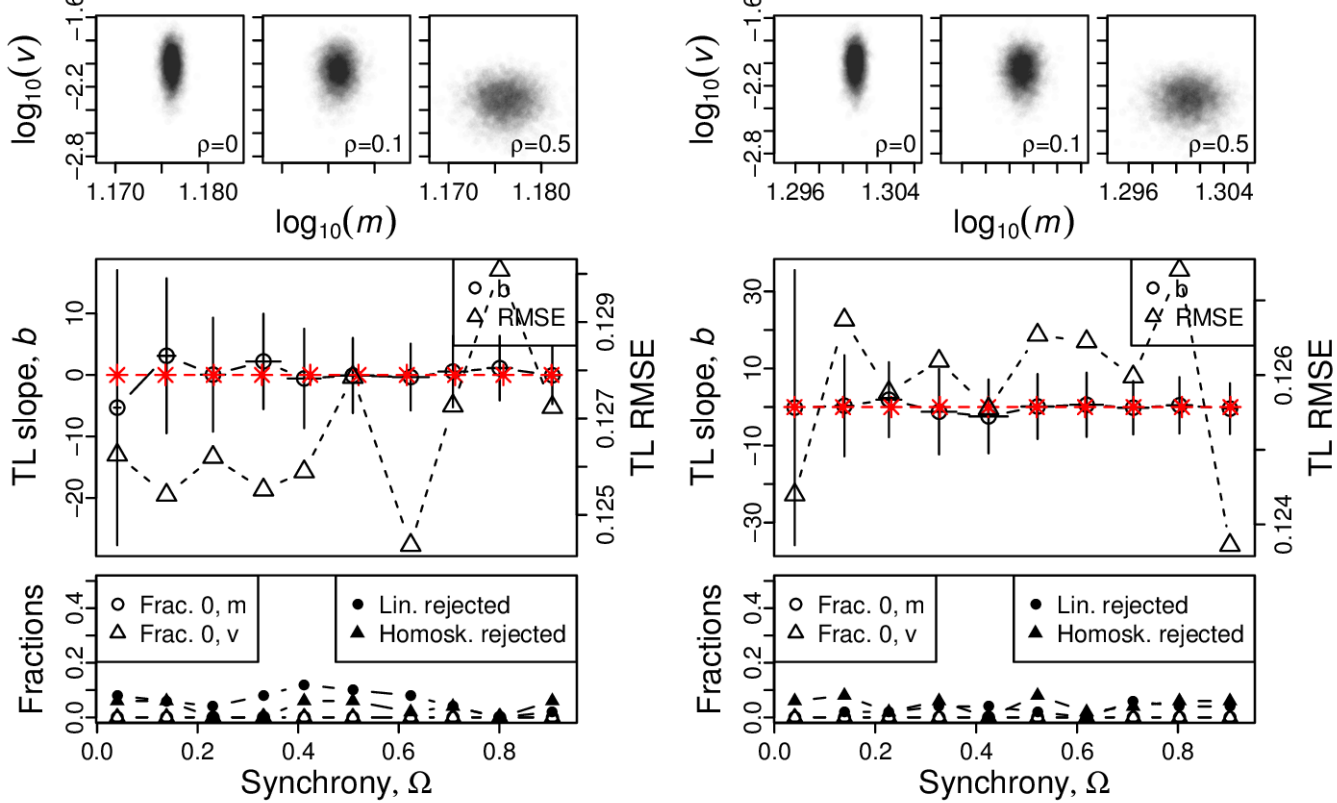
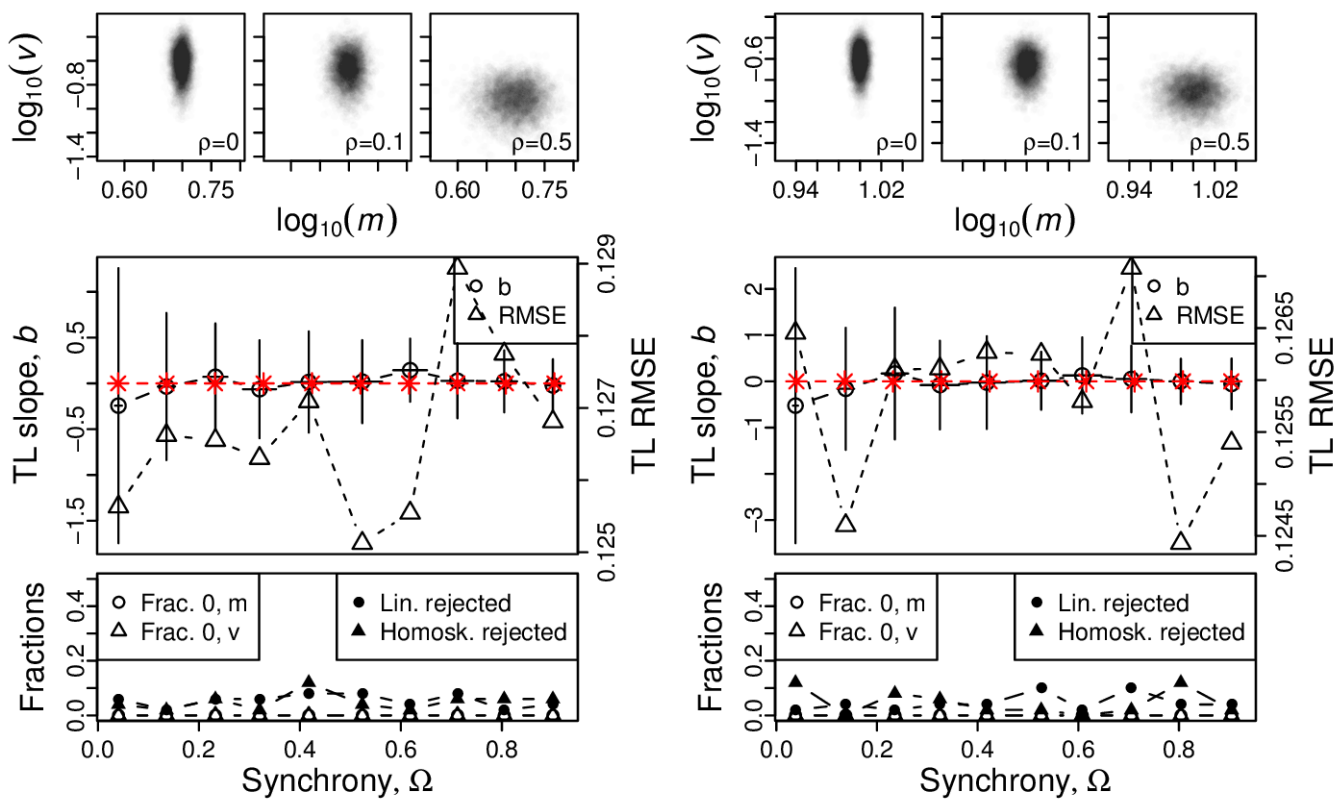


Figure S21: Omnibus plots (see section S6) for identically distributed normal marginals under the set up of section S3, for  $n = 25$  and  $\sigma = 0.1$ , for  $\mu = 5$  (A),  $\mu = 10$  (B),  $\mu = 15$  (C), and  $\mu = 20$  (D).

A, B



C, D

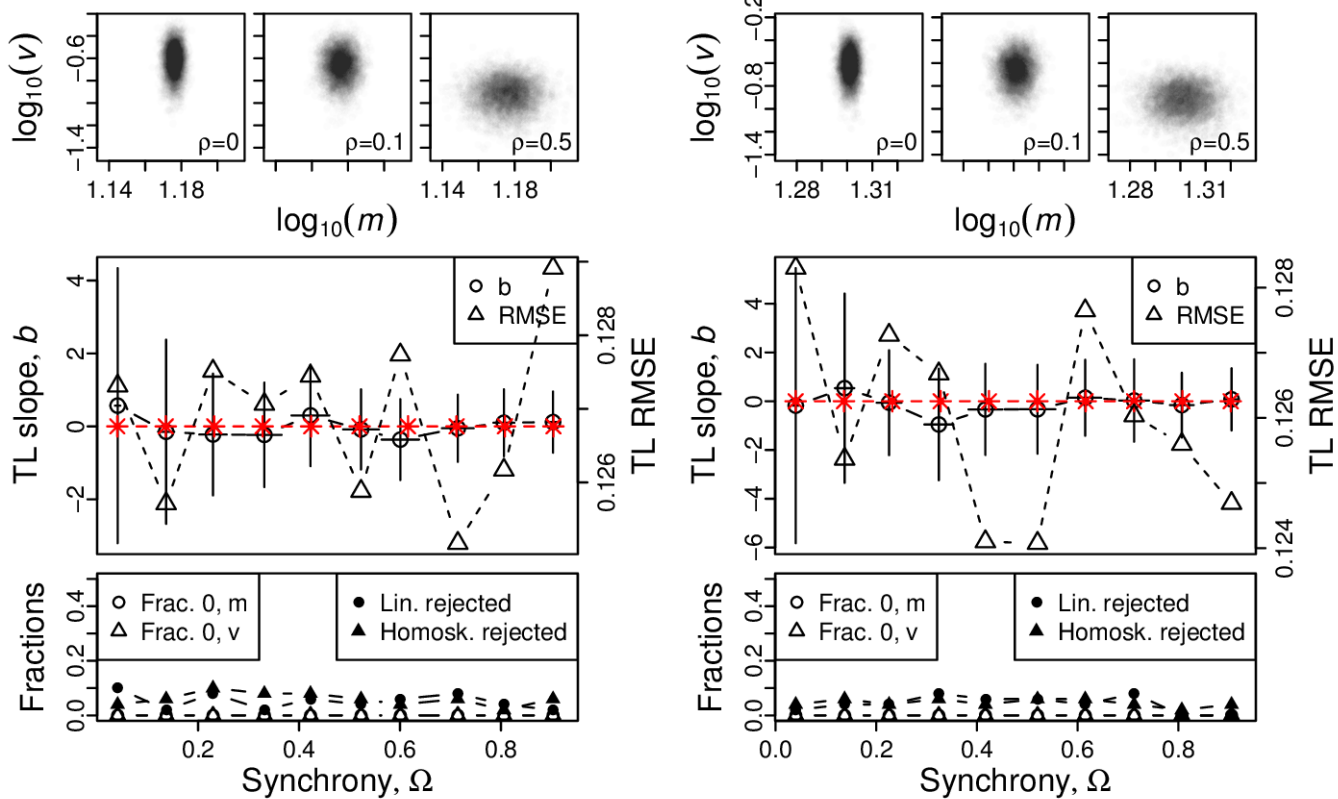
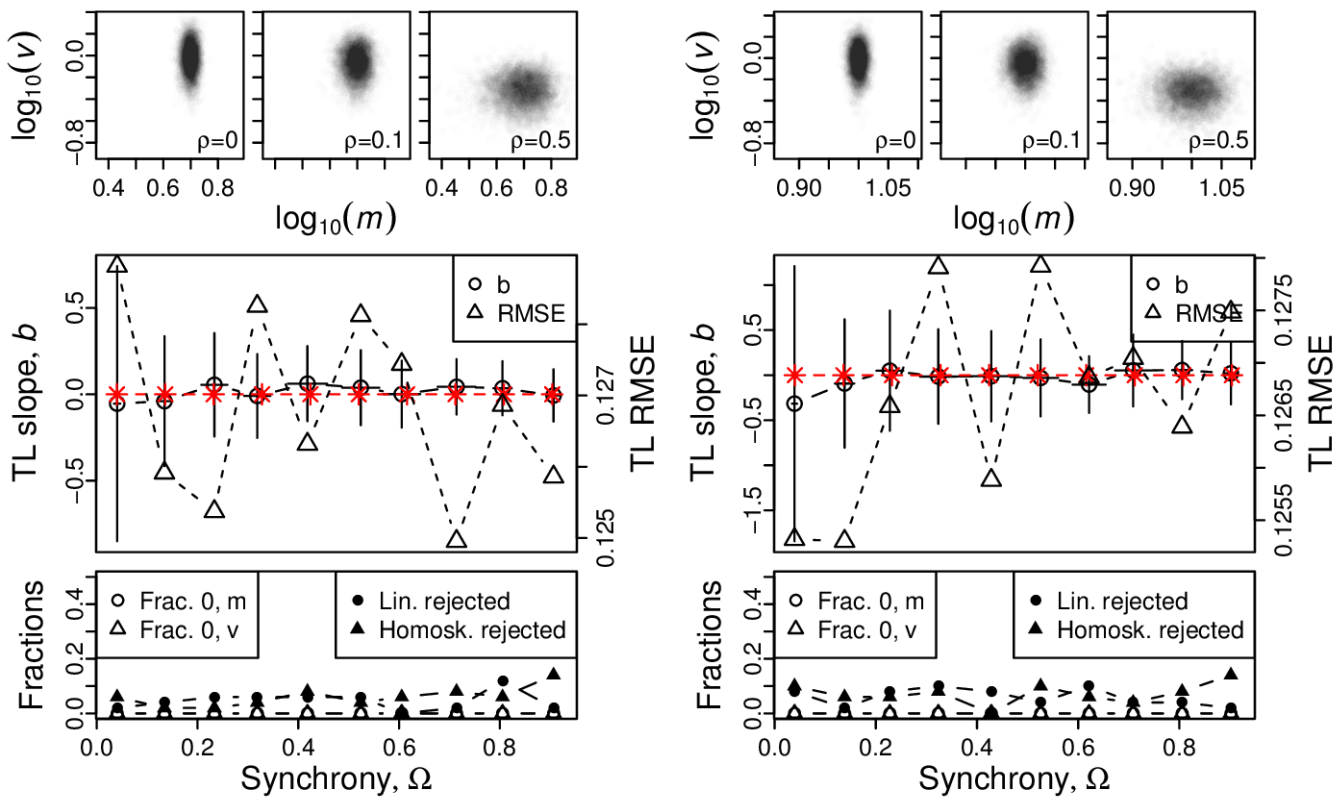


Figure S22: Omnibus plots (see section S6) for identically distributed normal marginals under the set up of section S3, for  $n = 25$  and  $\sigma = 0.5$ , for  $\mu = 5$  (A),  $\mu = 10$  (B),  $\mu = 15$  (C), and  $\mu = 20$  (D).

A, B



C, D

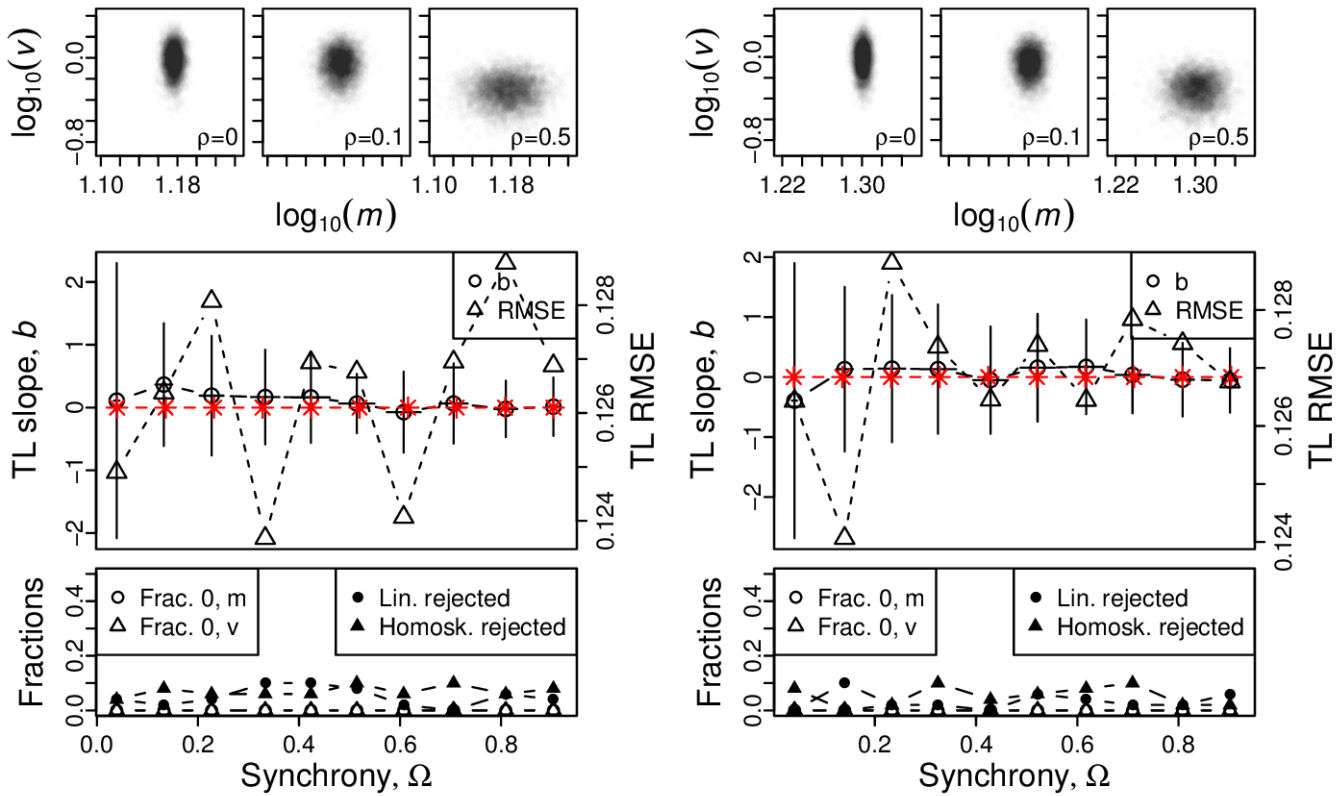


Figure S23: Omnibus plots (see section S6) for identically distributed normal marginals under the set up of section S3, for  $n = 25$  and  $\sigma = 1$ , for  $\mu = 5$  (A),  $\mu = 10$  (B),  $\mu = 15$  (C), and  $\mu = 20$  (D).

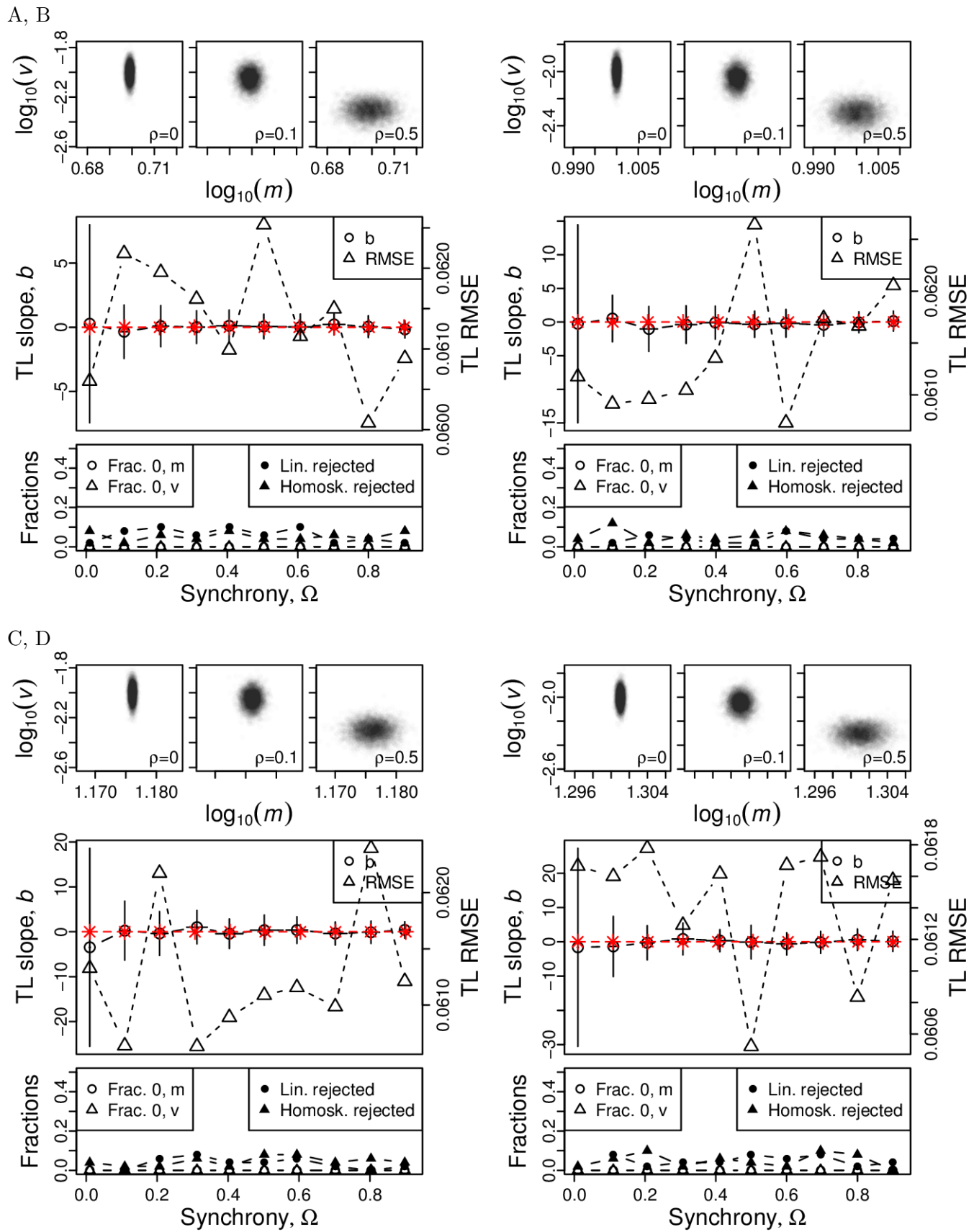
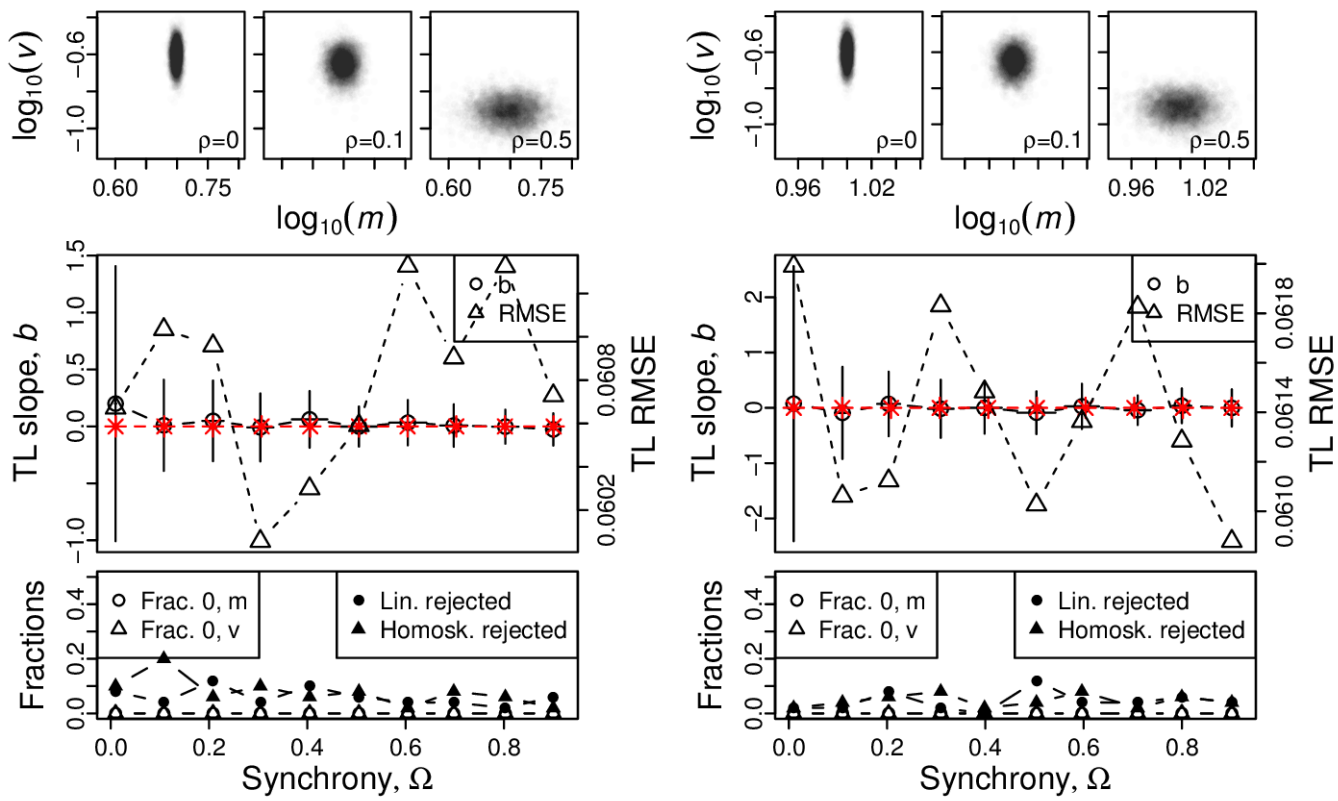


Figure S24: Omnibus plots (see section S6) for identically distributed normal marginals under the set up of section S3, for  $n = 100$  and  $\sigma = 0.1$ , for  $\mu = 5$  (A),  $\mu = 10$  (B),  $\mu = 15$  (C), and  $\mu = 20$  (D).

A, B



C, D

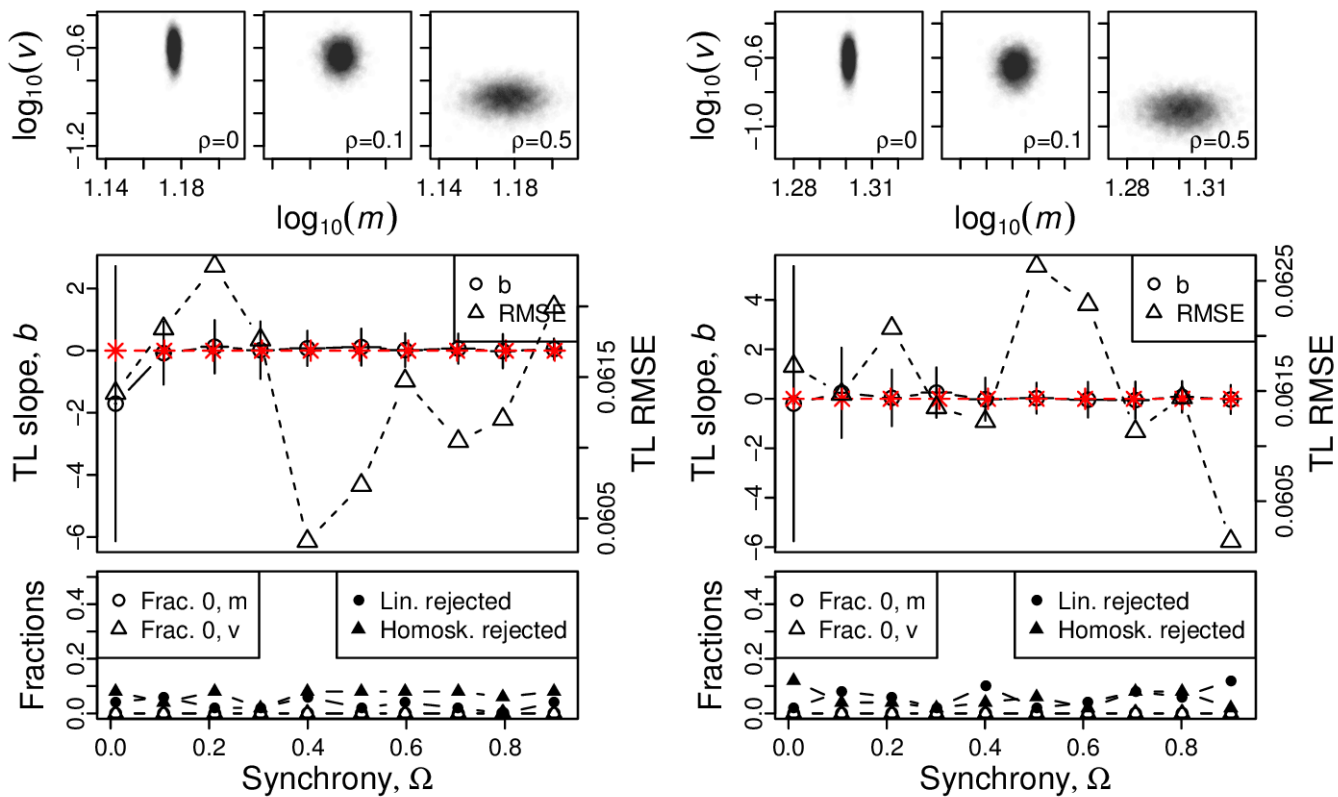
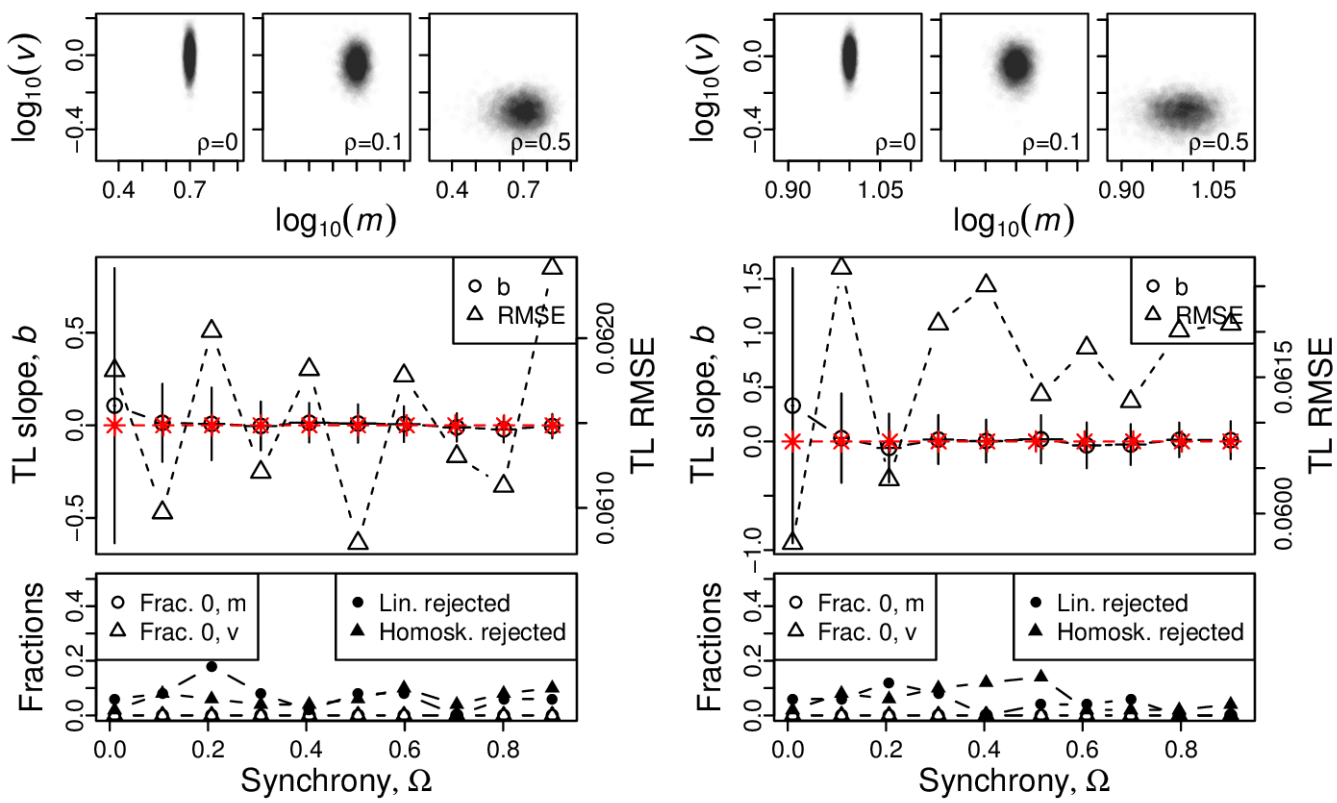


Figure S25: Omnibus plots (see section S6) for identically distributed normal marginals under the set up of section S3, for  $n = 100$  and  $\sigma = 0.5$ , for  $\mu = 5$  (A),  $\mu = 10$  (B),  $\mu = 15$  (C), and  $\mu = 20$  (D).

A, B



C, D

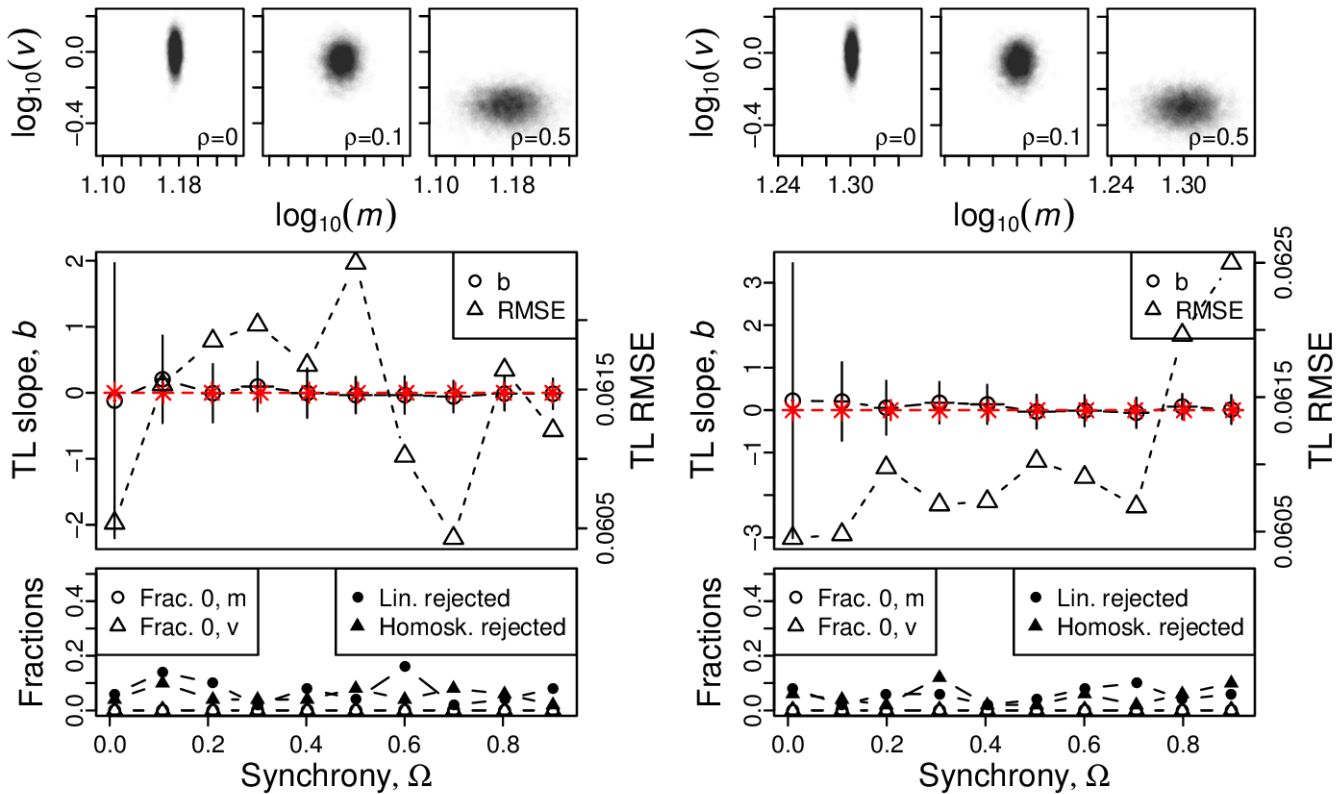


Figure S26: Omnibus plots (see section S6) for identically distributed normal marginals under the set up of section S3, for  $n = 100$  and  $\sigma = 1$ , for  $\mu = 5$  (A),  $\mu = 10$  (B),  $\mu = 15$  (C), and  $\mu = 20$  (D).

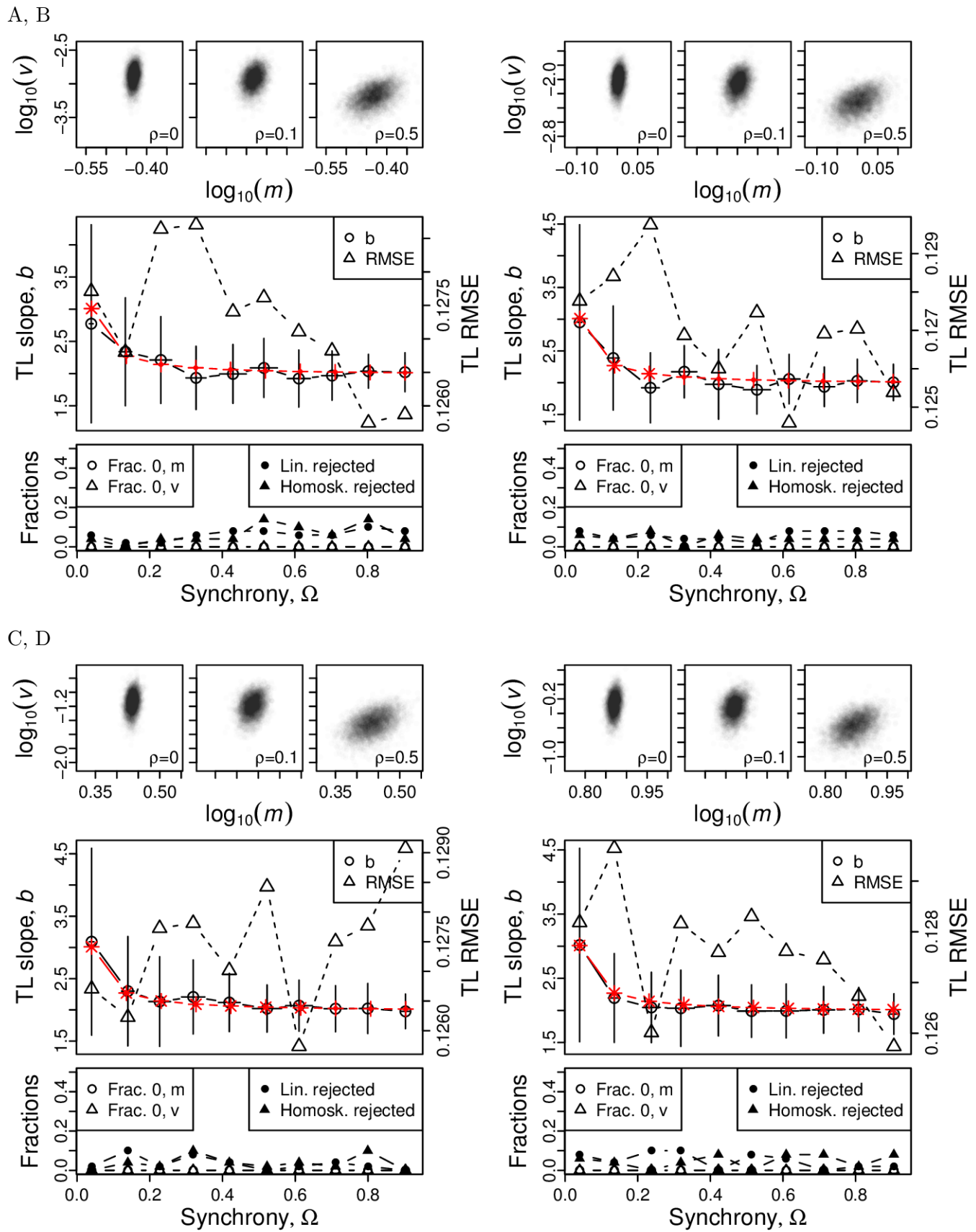
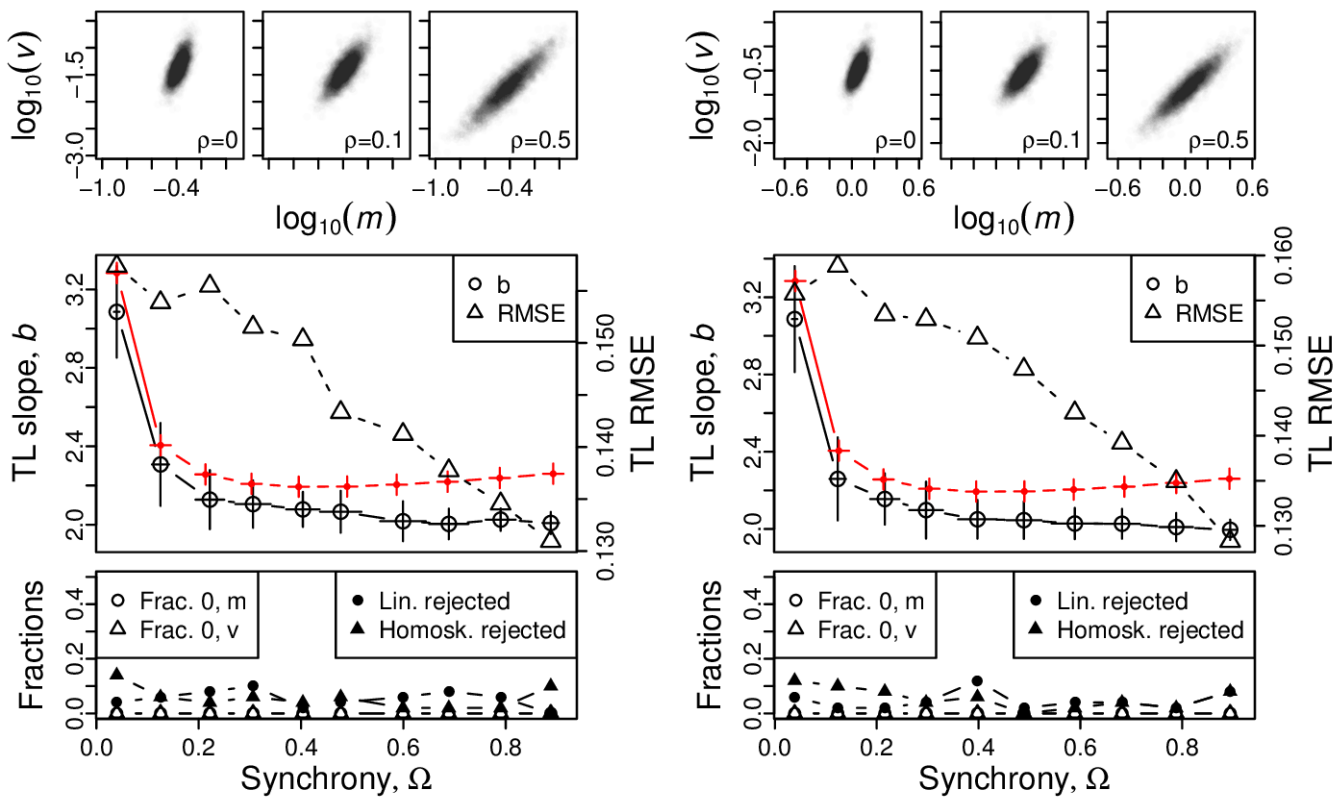


Figure S27: Omnibus plots (see section S6) for identically distributed log-normal marginals under the set up of section S3, for  $n = 25$  and  $\sigma = 0.1$ , for  $\mu = -1$  (A),  $\mu = 0$  (B),  $\mu = 1$  (C), and  $\mu = 2$  (D).

A, B



C, D

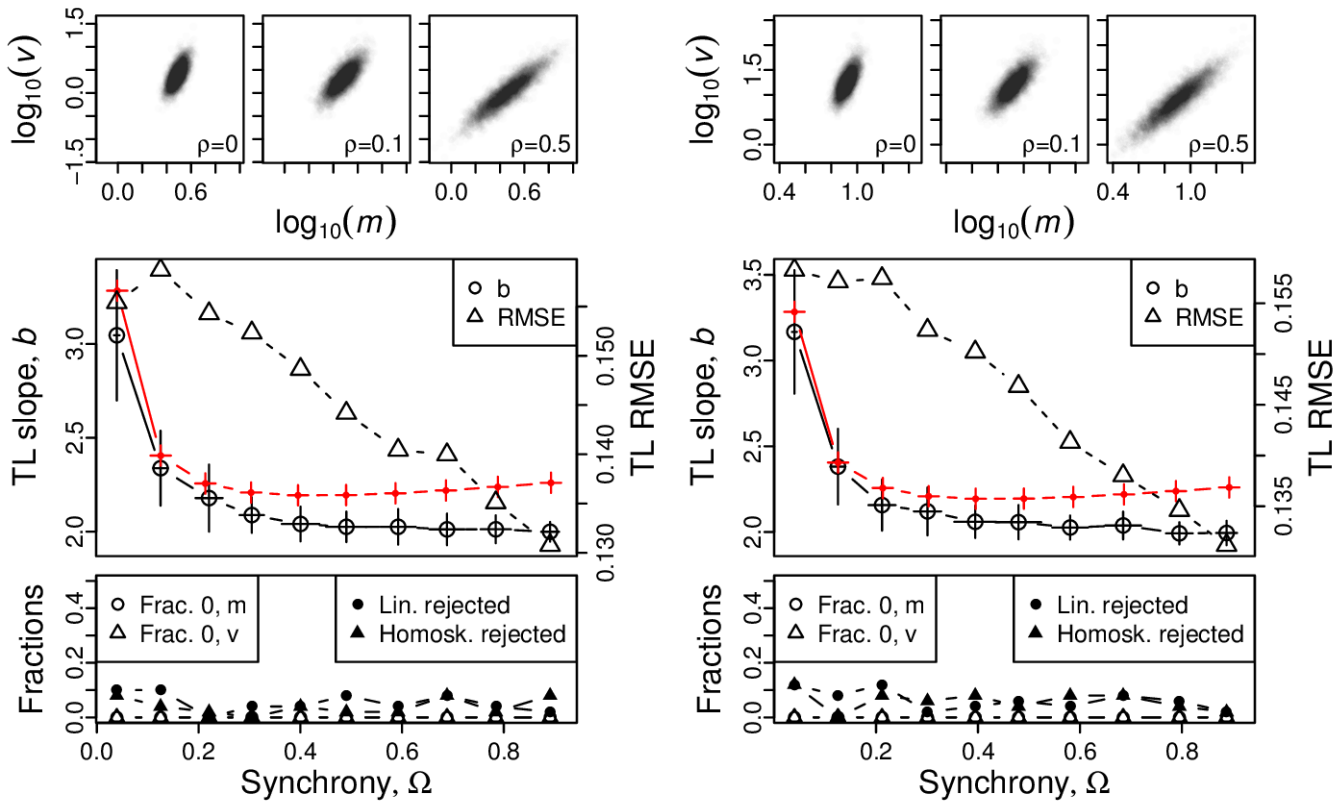
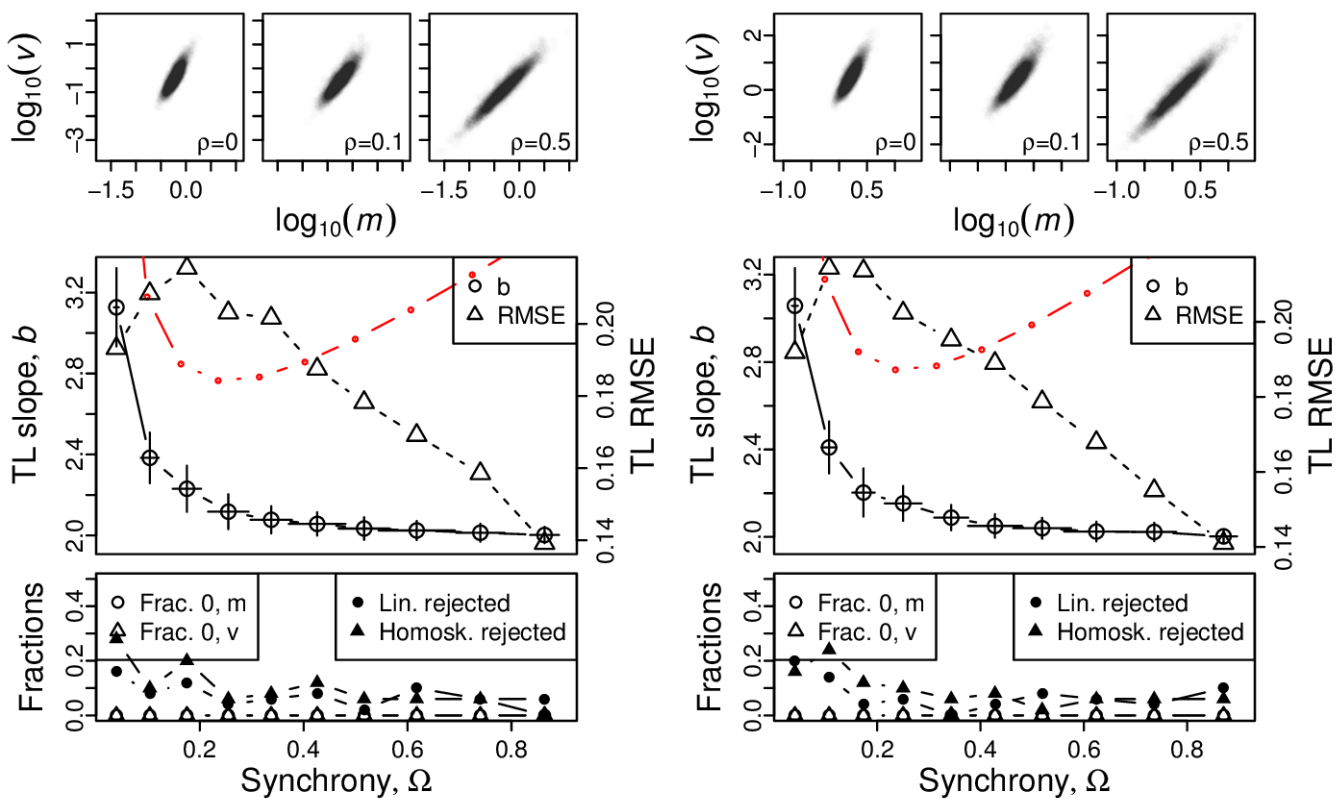


Figure S28: Omnibus plots (see section S6) for identically distributed log-normal marginals under the set up of section S3, for  $n = 25$  and  $\sigma = 0.5$ , for  $\mu = -1$  (A),  $\mu = 0$  (B),  $\mu = 1$  (C), and  $\mu = 2$  (D).

A, B



C, D

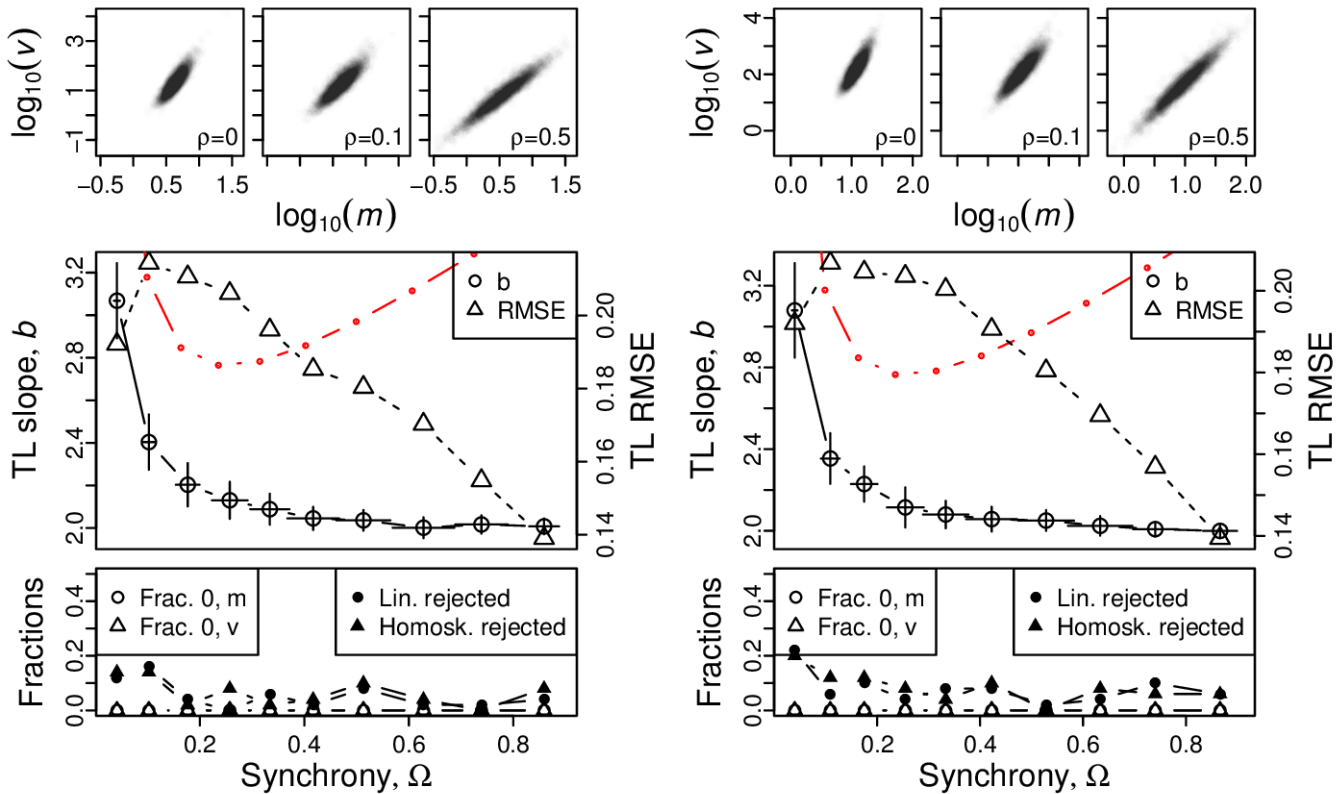
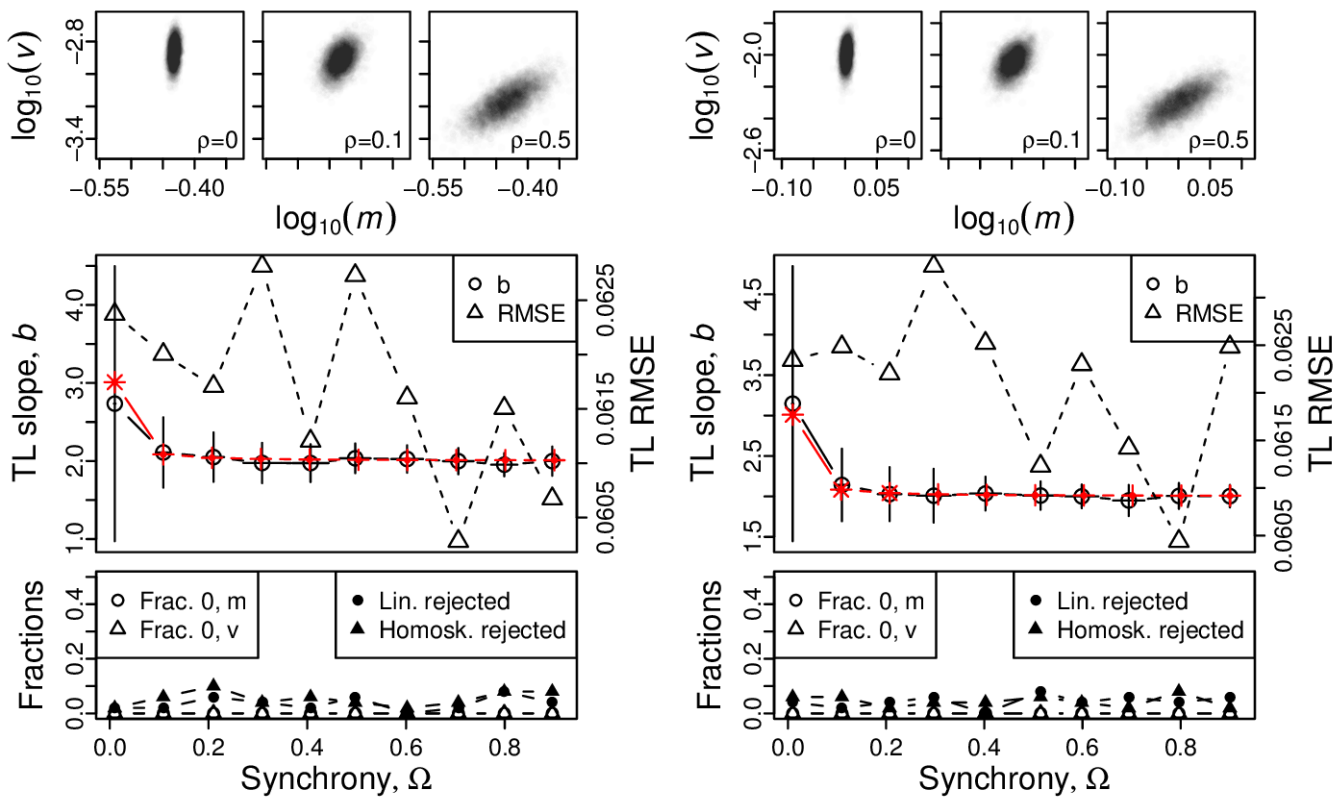


Figure S29: Omnibus plots (see section S6) for identically distributed log-normal marginals under the set up of section S3, for  $n = 25$  and  $\sigma = 1$ , for  $\mu = -1$  (A),  $\mu = 0$  (B),  $\mu = 1$  (C), and  $\mu = 2$  (D).

A, B



C, D

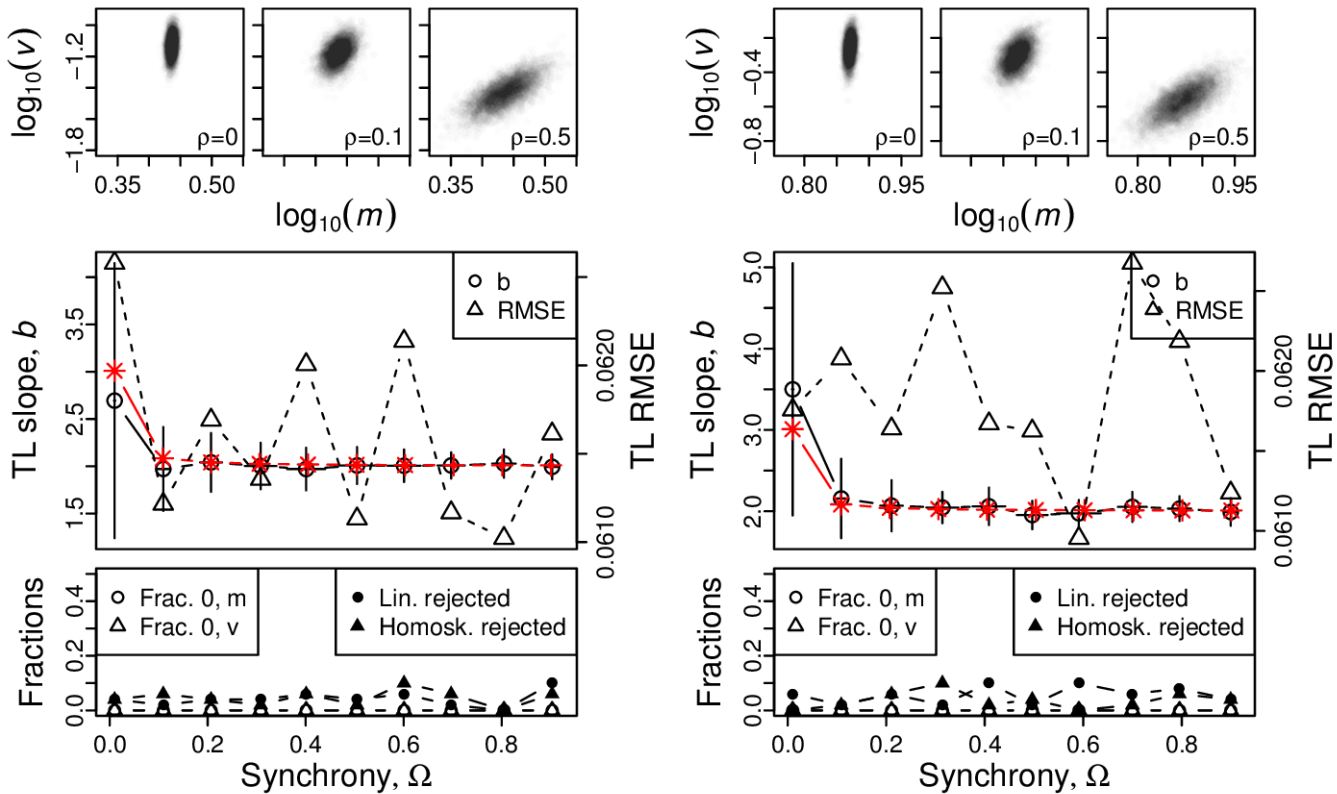
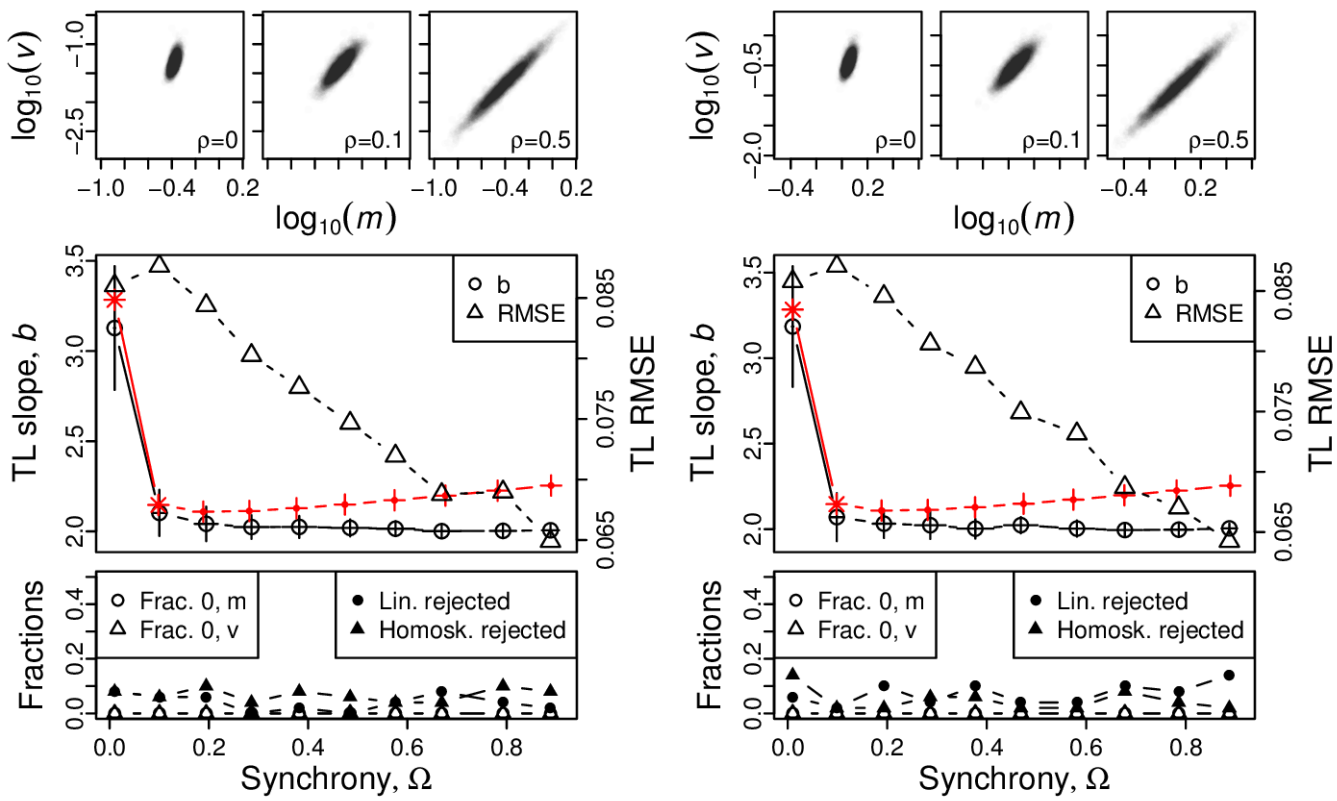


Figure S30: Omnibus plots (see section S6) for identically distributed log-normal marginals under the set up of section S3, for  $n = 100$  and  $\sigma = 0.1$ , for  $\mu = -1$  (A),  $\mu = 0$  (B),  $\mu = 1$  (C), and  $\mu = 2$  (D).

A, B



C, D

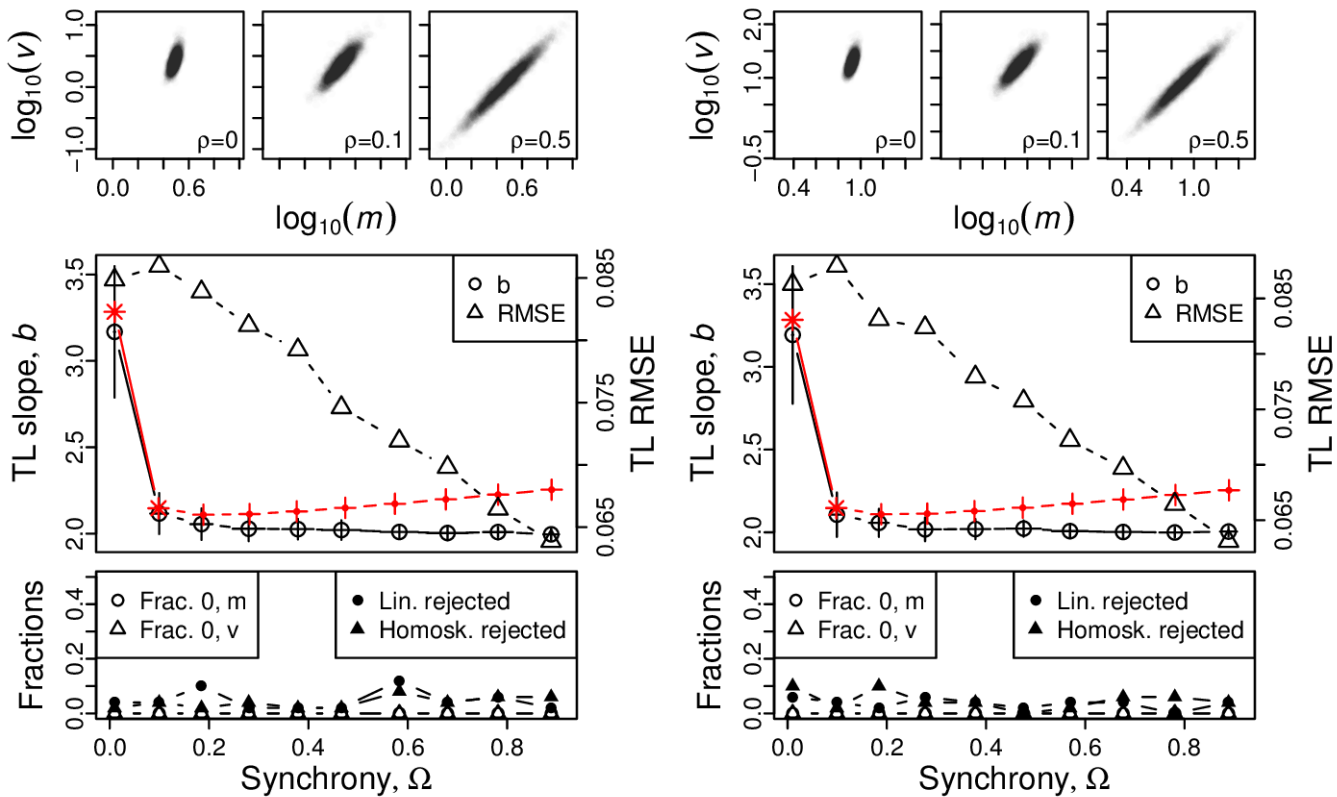
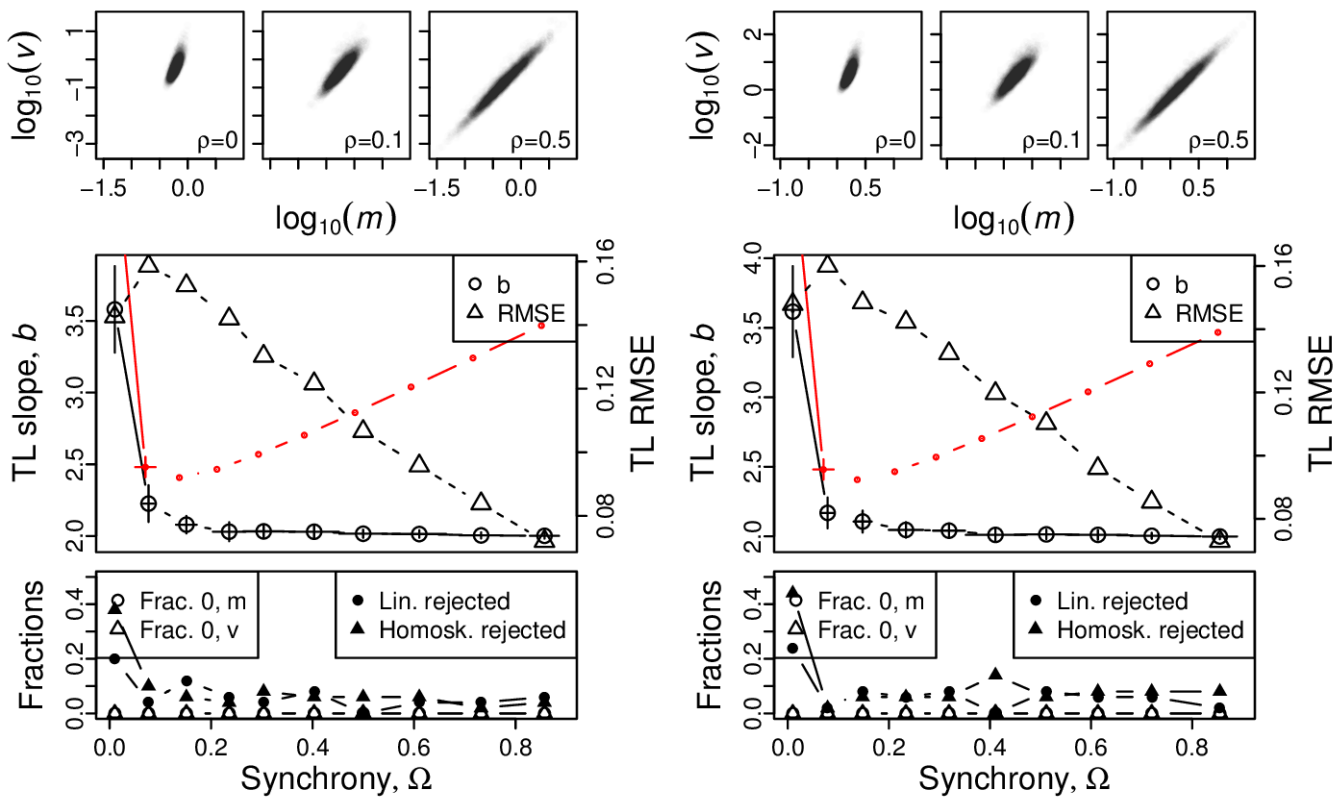


Figure S31: Omnibus plots (see section S6) for identically distributed log-normal marginals under the set up of section S3, for  $n = 100$  and  $\sigma = 0.5$ , for  $\mu = -1$  (A),  $\mu = 0$  (B),  $\mu = 1$  (C), and  $\mu = 2$  (D).

A, B



C, D

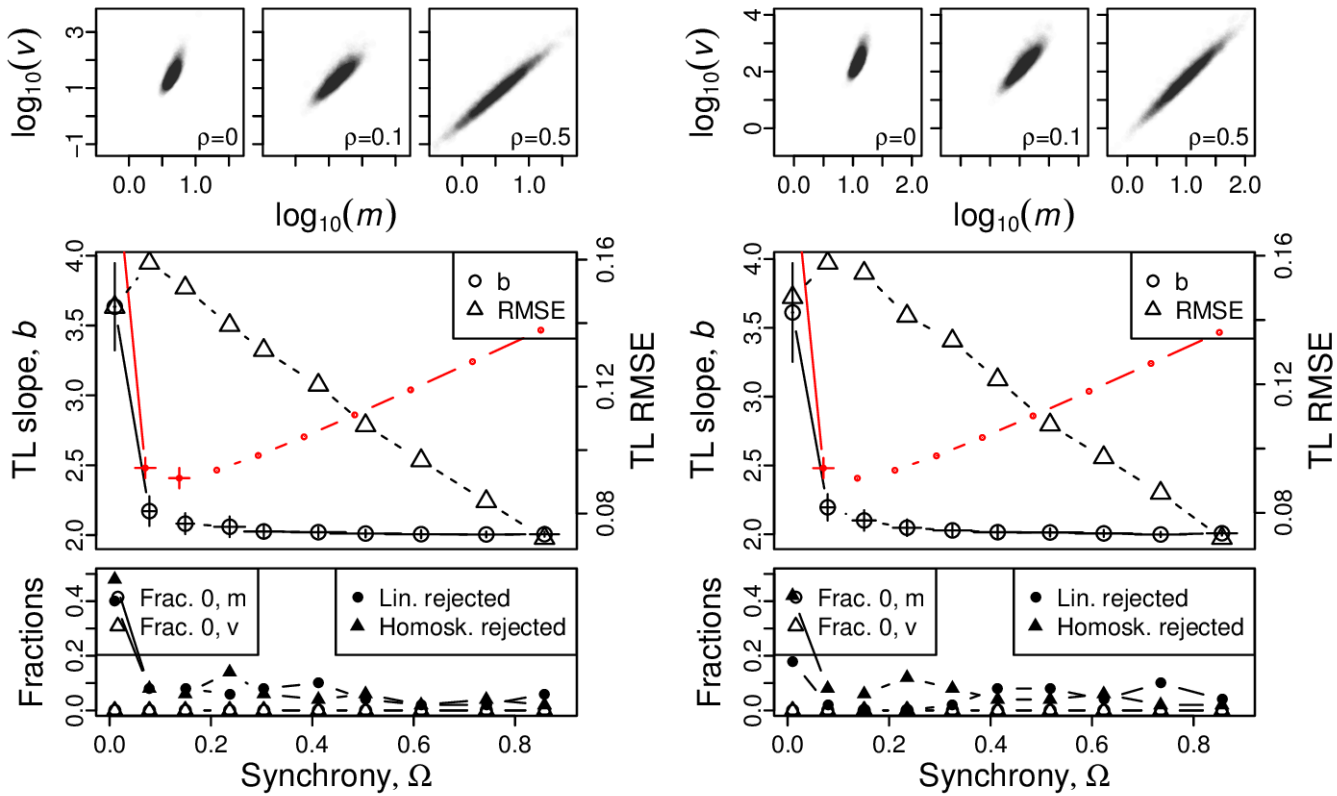
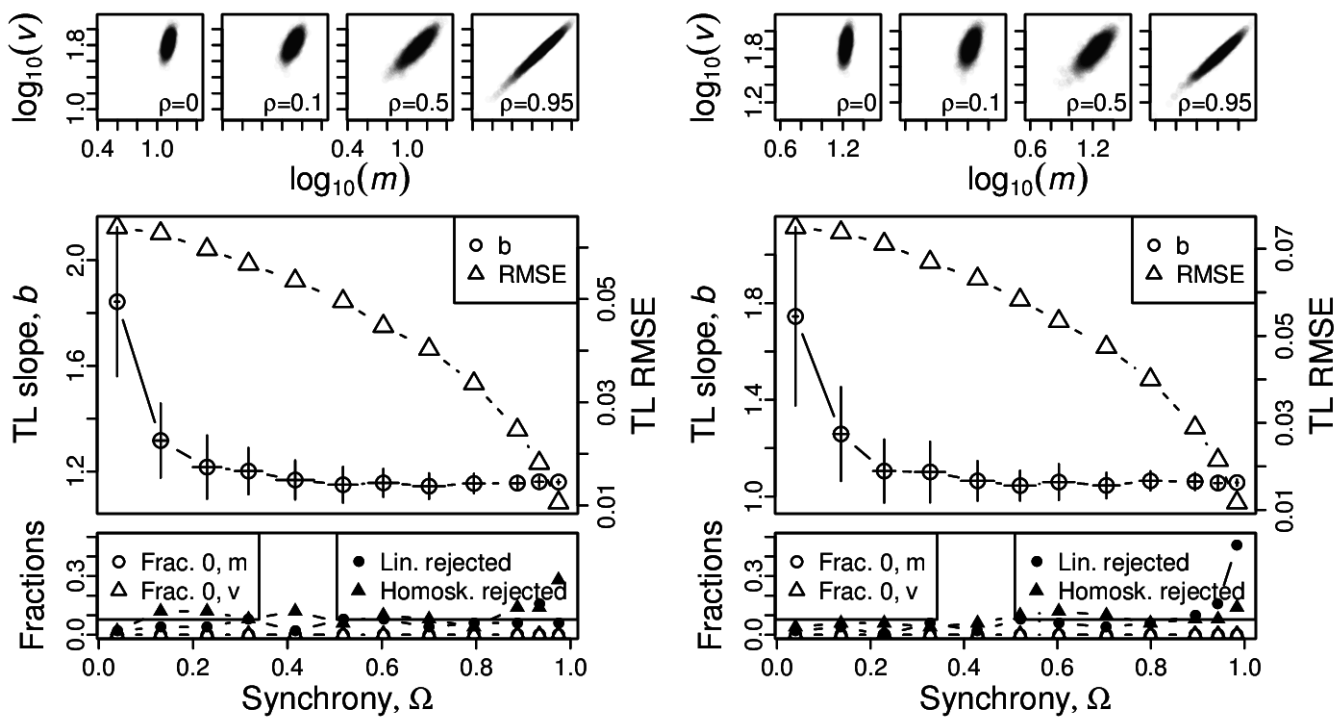


Figure S32: Omnibus plots (see section S6) for identically distributed log-normal marginals under the set up of section S3, for  $n = 100$  and  $\sigma = 1$ , for  $\mu = -1$  (A),  $\mu = 0$  (B),  $\mu = 1$  (C), and  $\mu = 2$  (D).

## S9 Figures, distributions constructed using Gaussian copulas and non-identically distributed marginals

A, B



C, D

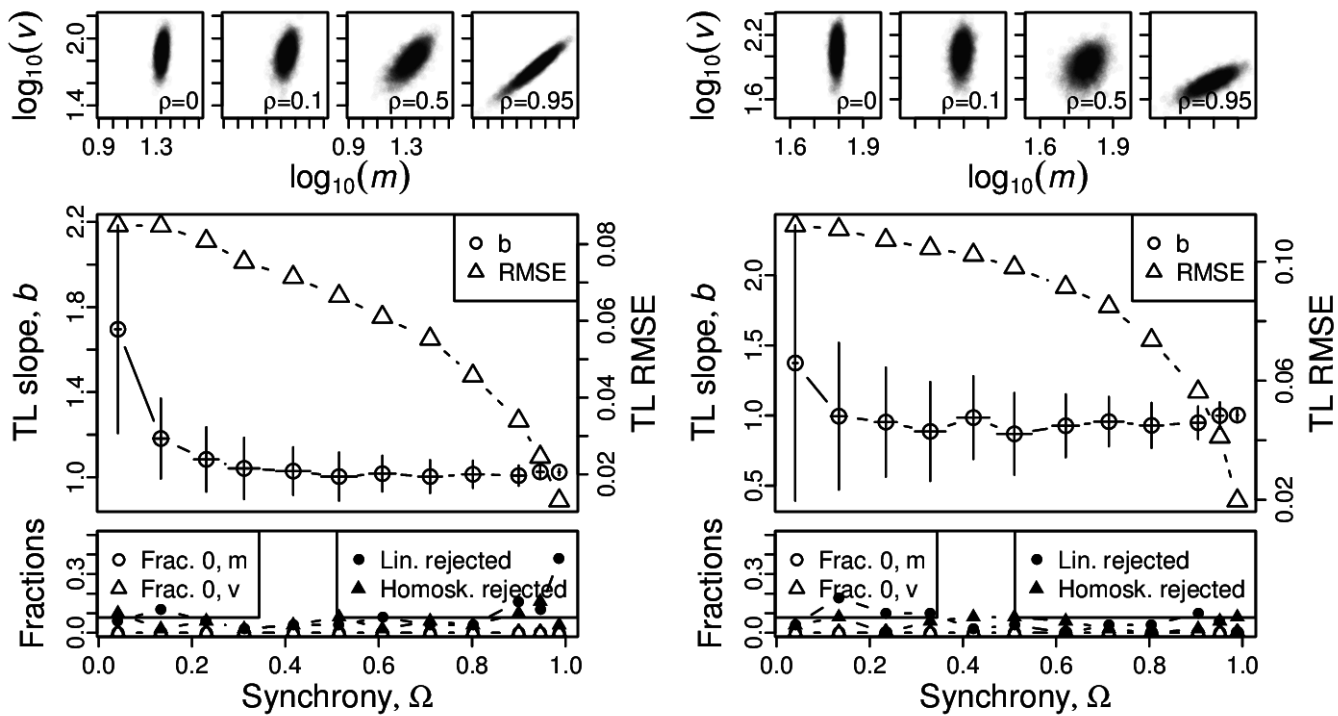
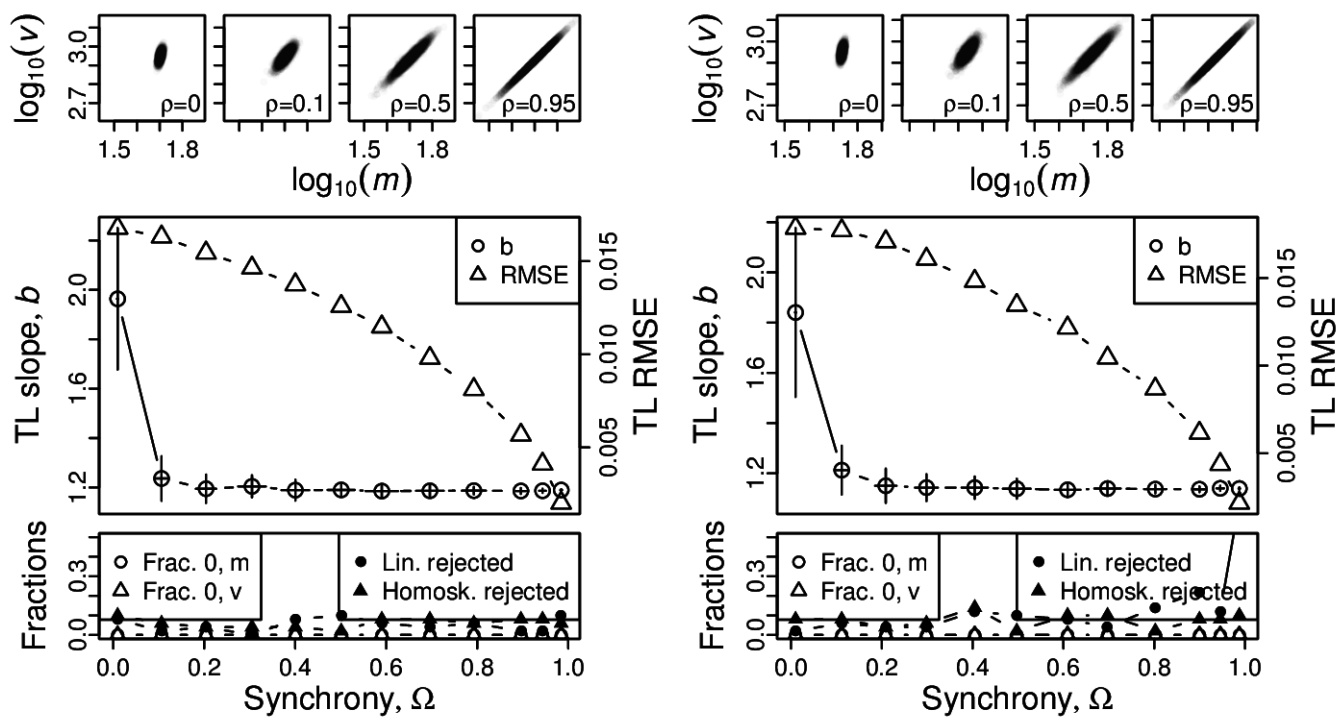


Figure S33: Omnibus plots (see section S6) for non-identically distributed Poisson marginals under the set up of section S4, for  $n = 25$  and  $Y_1$  with  $\lambda = 1$  (A),  $\lambda = 5$  (B),  $\lambda = 10$  (C), and  $\lambda = 50$  (D).

A, B



C, D

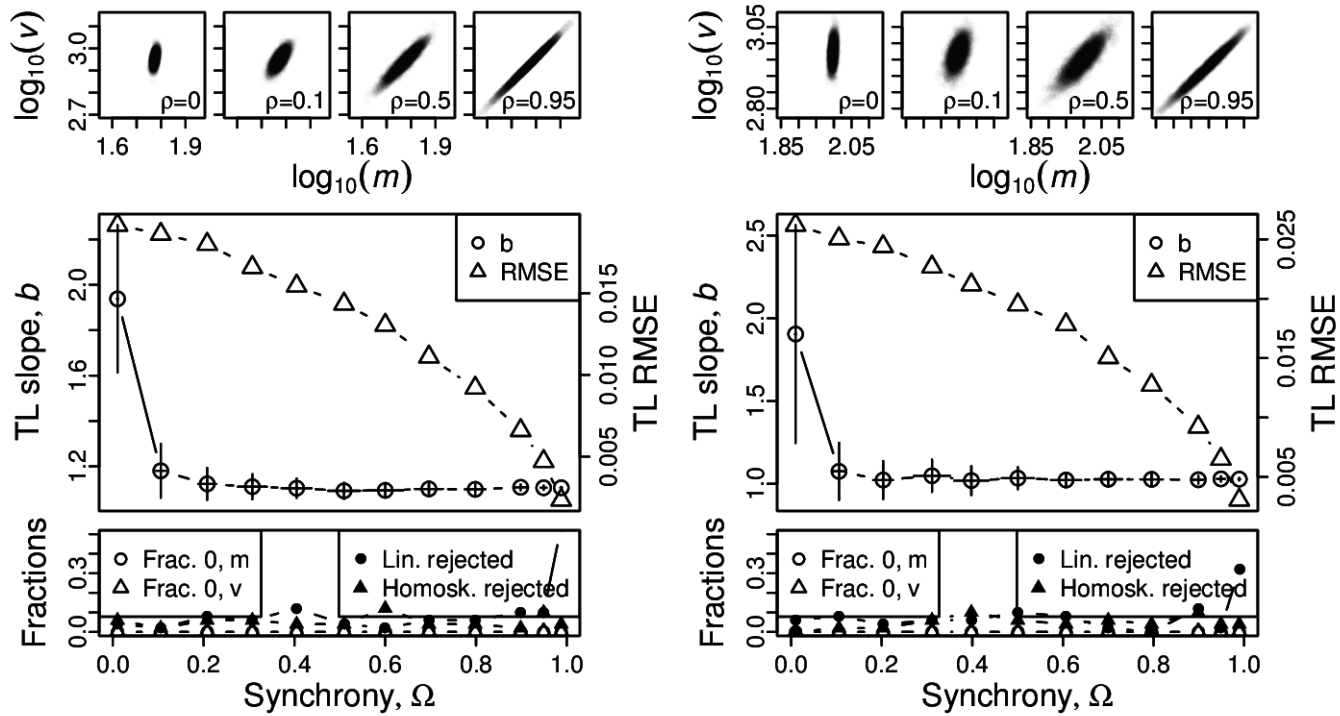
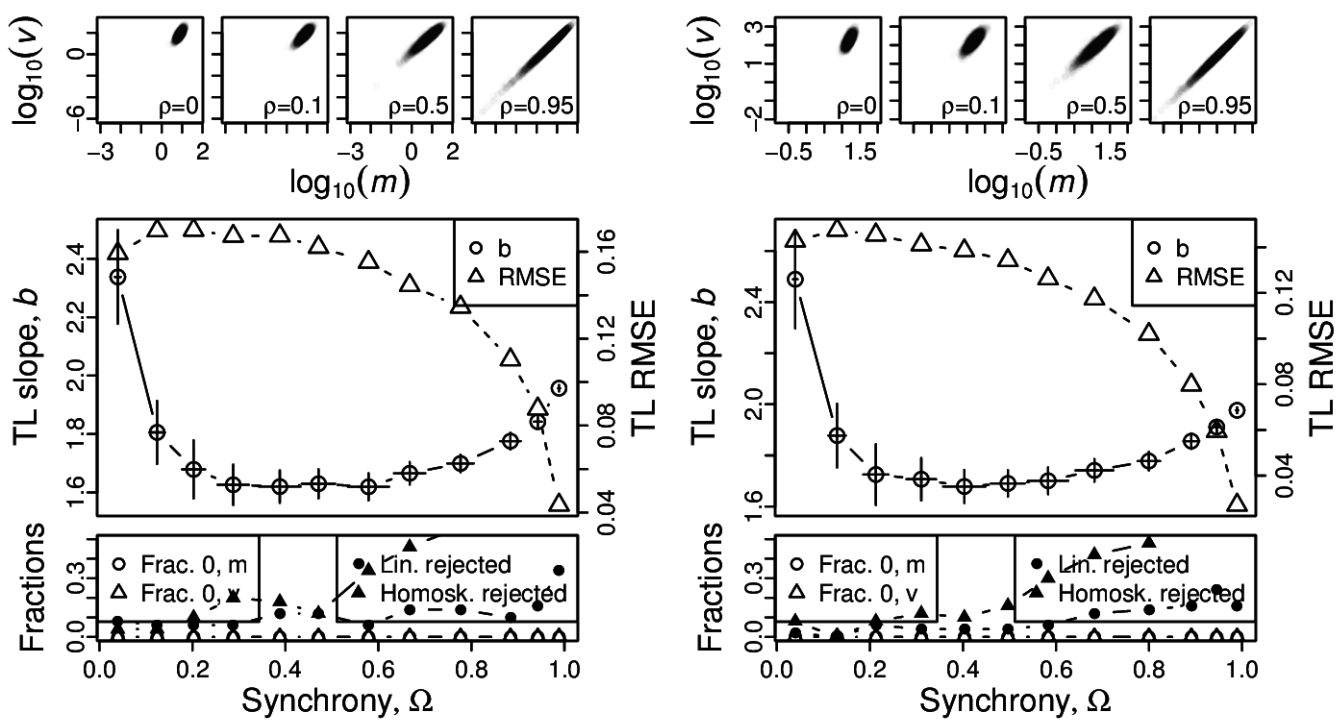


Figure S34: Omnibus plots (see section S6) for non-identically distributed Poisson marginals under the set up of section S4, for  $n = 100$  and  $Y_1$  with  $\lambda = 1$  (A),  $\lambda = 5$  (B),  $\lambda = 10$  (C), and  $\lambda = 50$  (D).

A, B



C, D

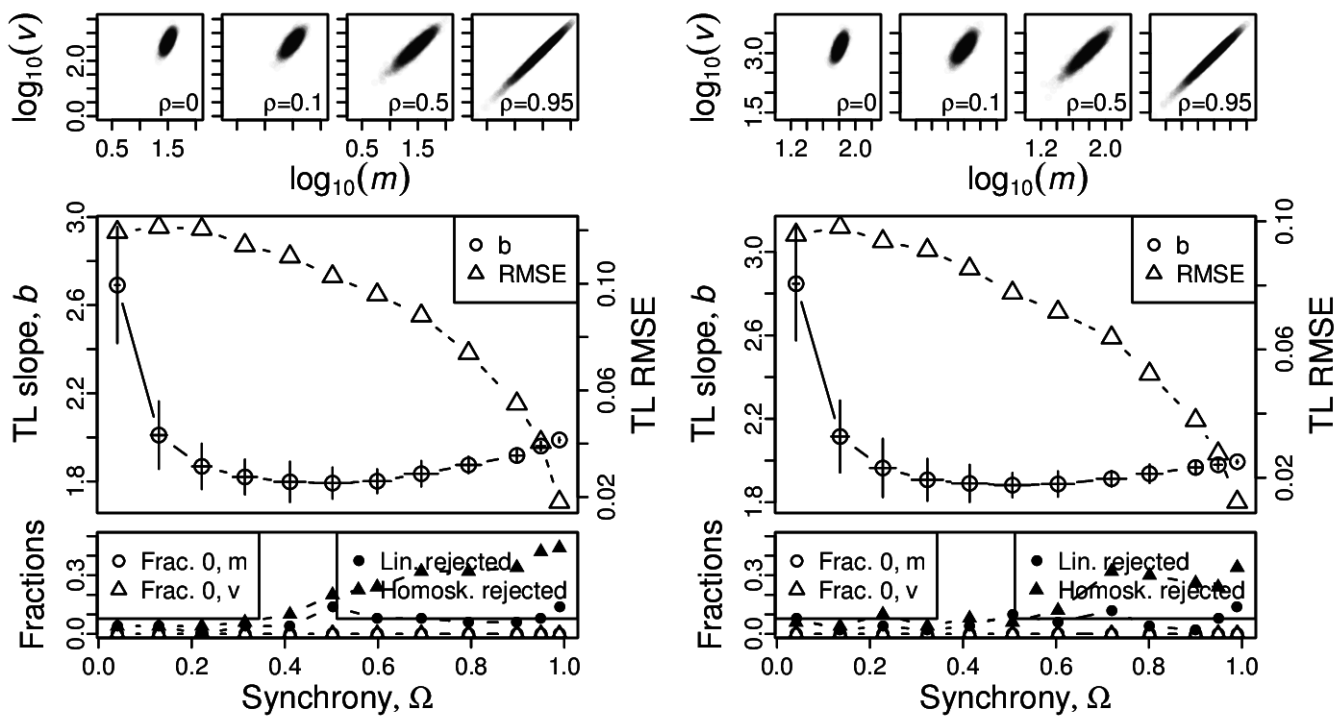
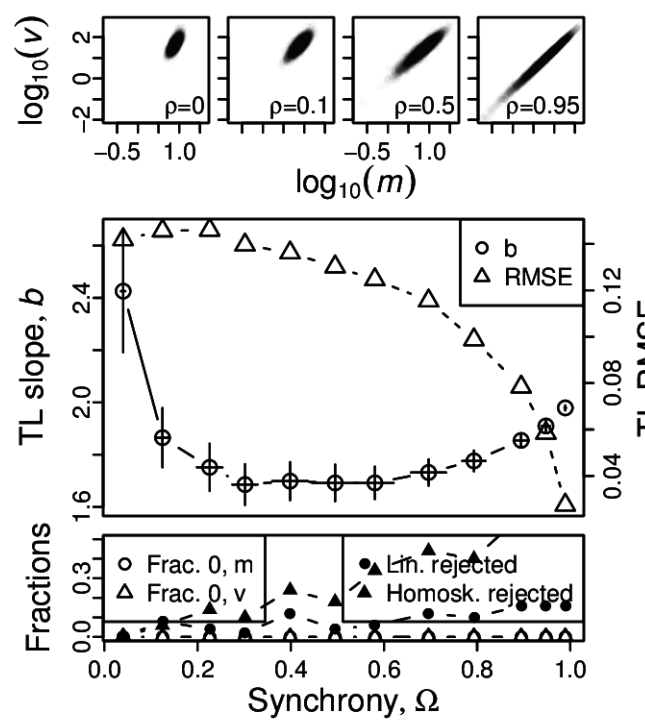
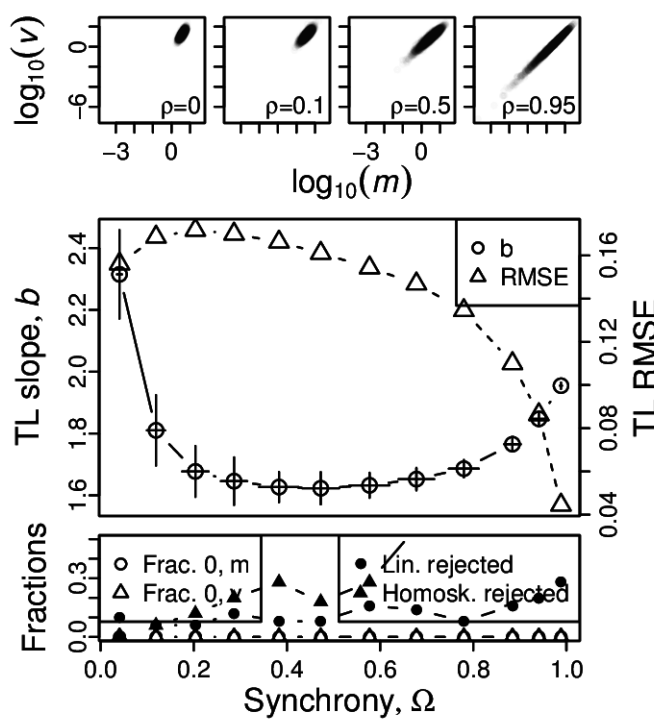


Figure S35: Omnibus plots (see section S6) for non-identically distributed gamma marginals under the set up of section S4, for  $n = 25$  and  $Y_1$  with  $\beta = 0.5$  and  $\alpha = 1$  (A),  $\alpha = 2$  (B),  $\alpha = 4$  (C), and  $\alpha = 8$  (D).

A, B



C, D

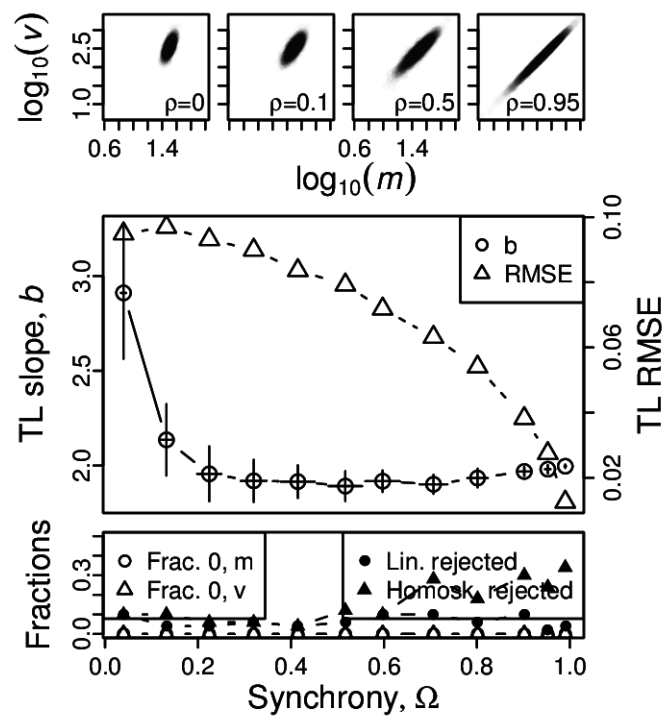
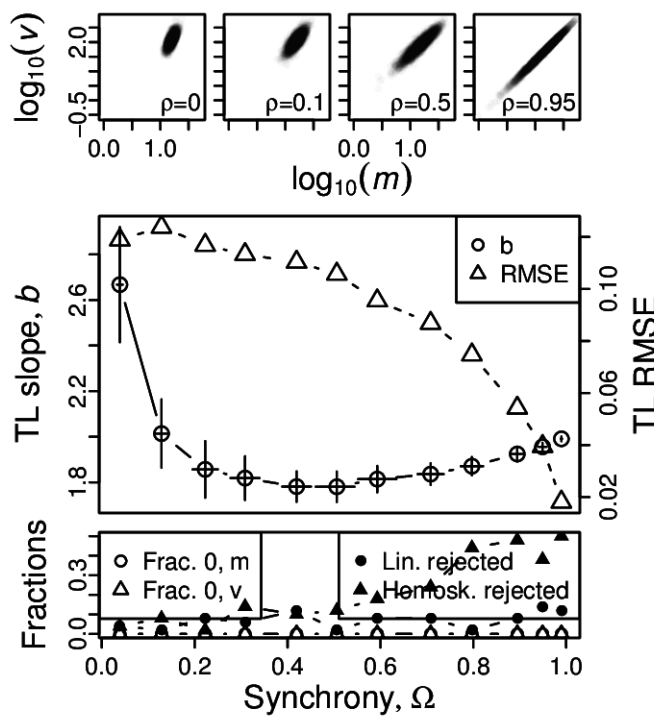
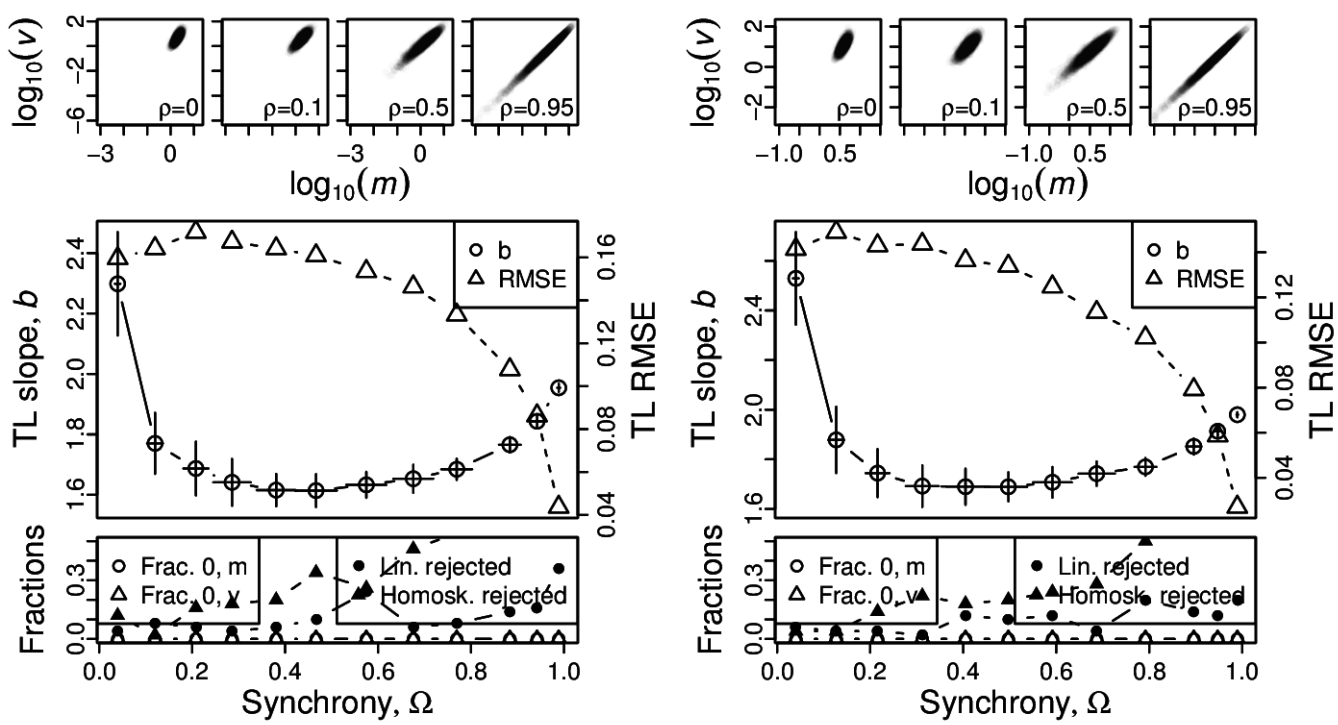


Figure S36: Omnibus plots (see section S6) for non-identically distributed gamma marginals under the set up of section S4, for  $n = 25$  and  $Y_1$  with  $\beta = 1$  and  $\alpha = 1$  (A),  $\alpha = 2$  (B),  $\alpha = 4$  (C), and  $\alpha = 8$  (D).

A, B



C, D

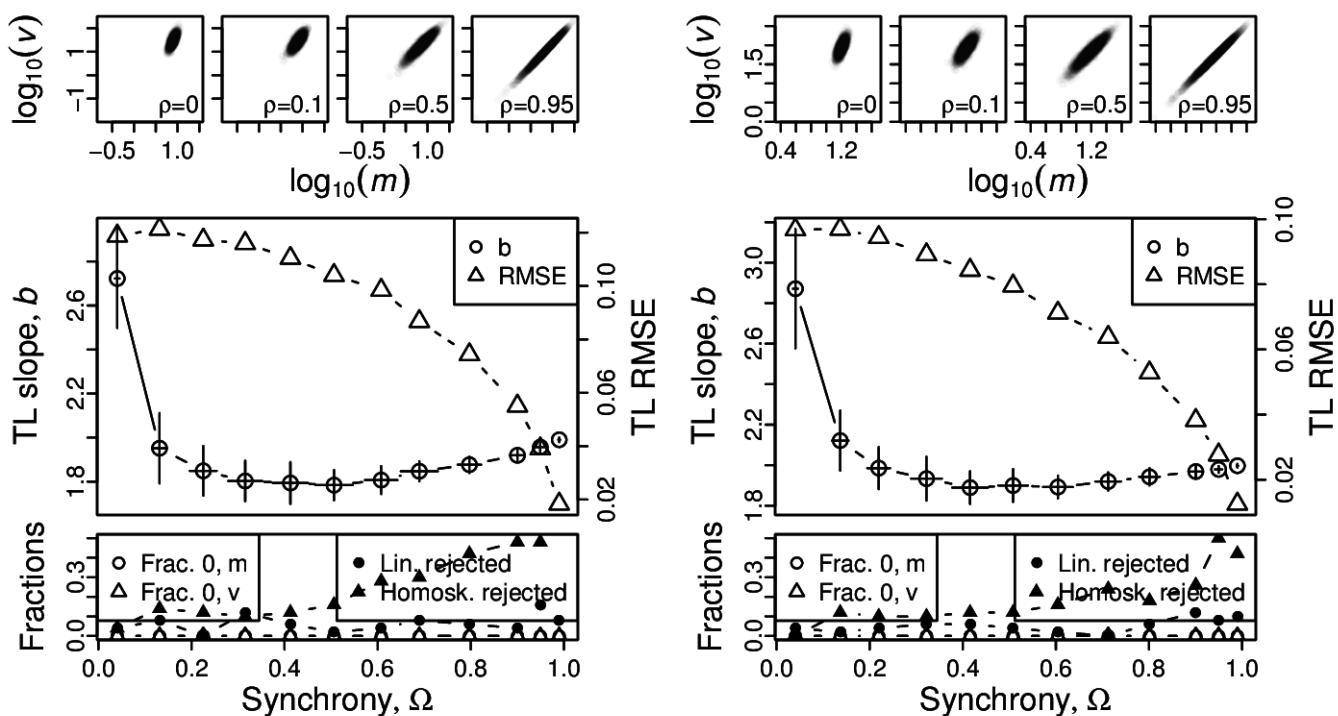
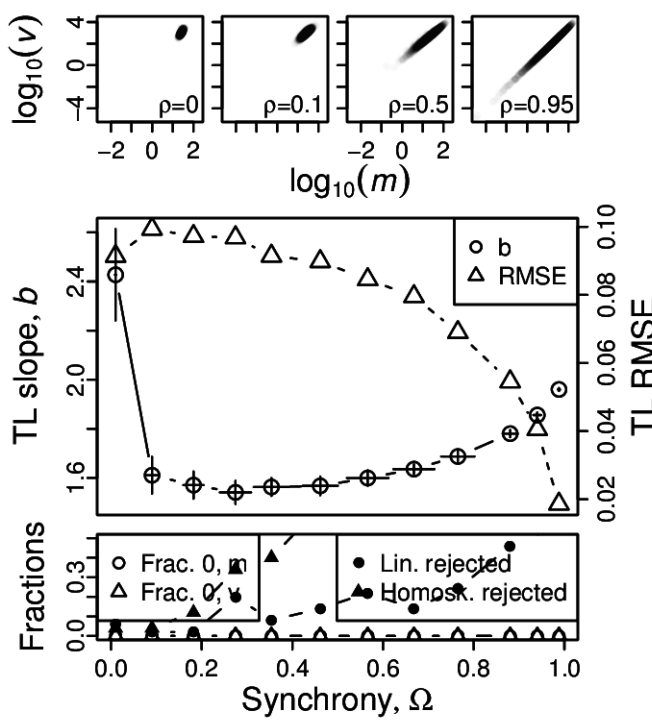


Figure S37: Omnibus plots (see section S6) for non-identically distributed gamma marginals under the set up of section S4, for  $n = 25$  and  $Y_1$  with  $\beta = 2$  and  $\alpha = 1$  (A),  $\alpha = 2$  (B),  $\alpha = 4$  (C), and  $\alpha = 8$  (D).

A, B



C, D

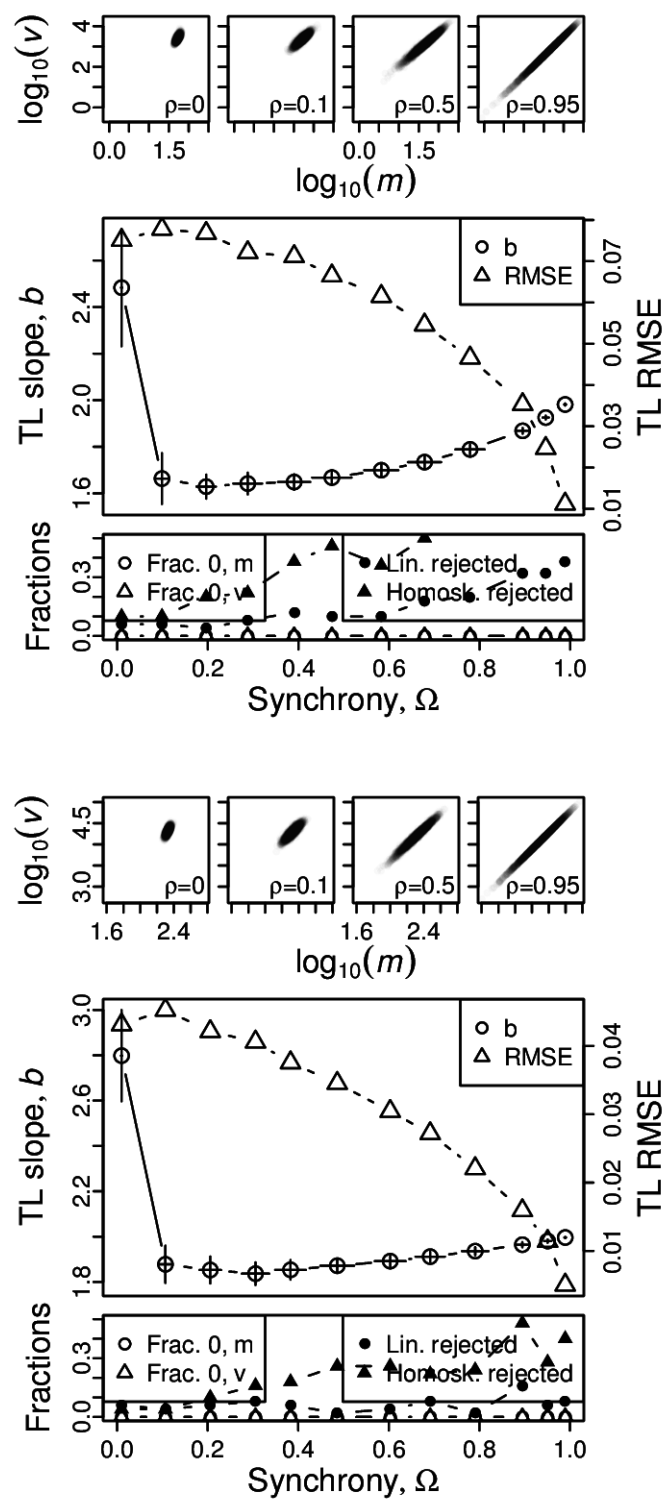
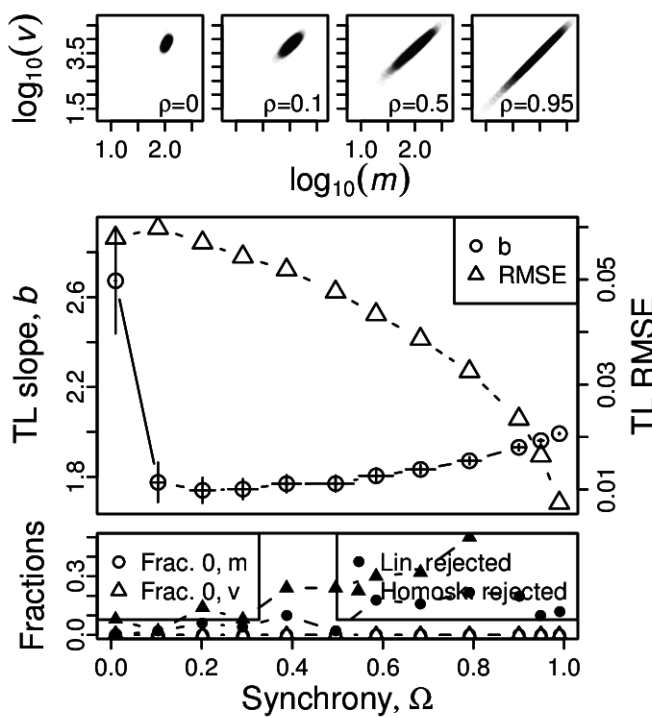
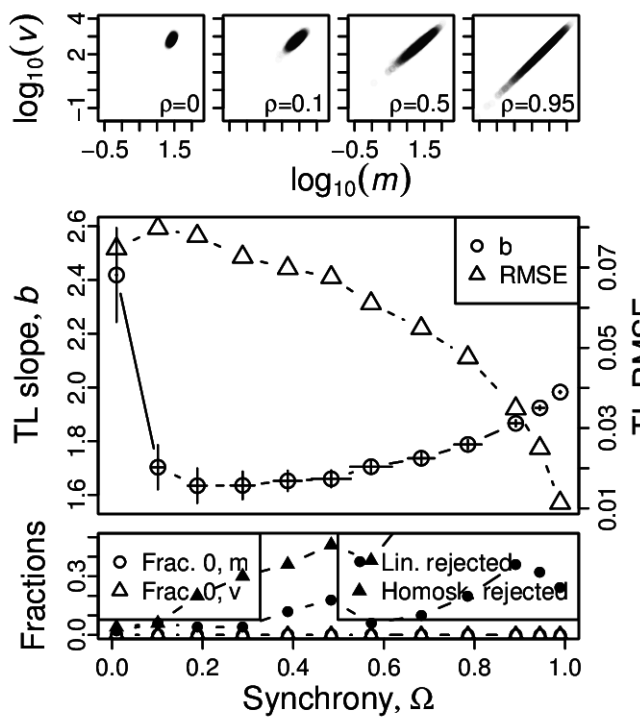
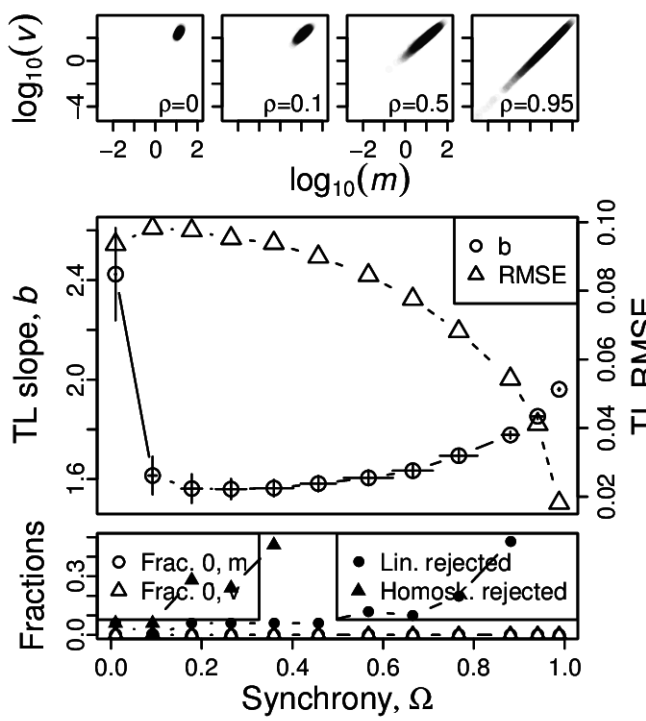


Figure S38: Omnibus plots (see section S6) for non-identically distributed gamma marginals under the set up of section S4, for  $n = 100$  and  $Y_1$  with  $\beta = 0.5$  and  $\alpha = 1$  (A),  $\alpha = 2$  (B),  $\alpha = 4$  (C), and  $\alpha = 8$  (D).

A, B



C, D

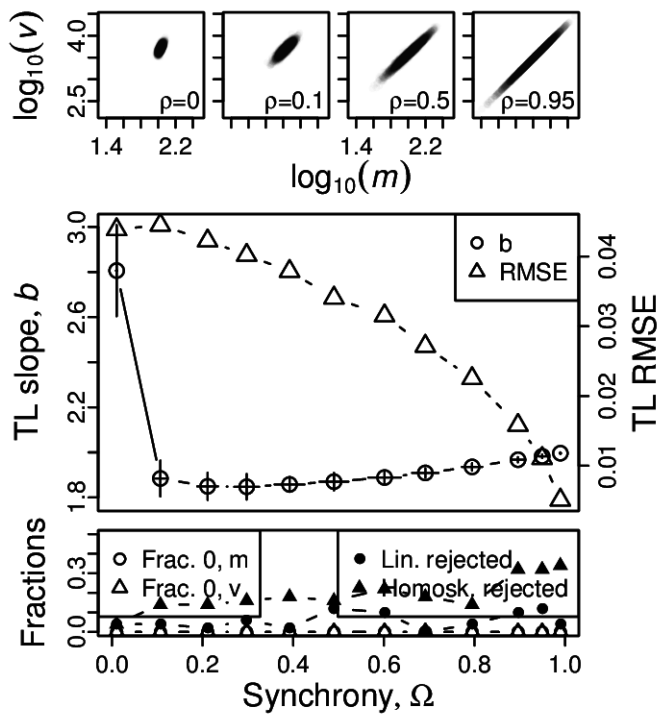
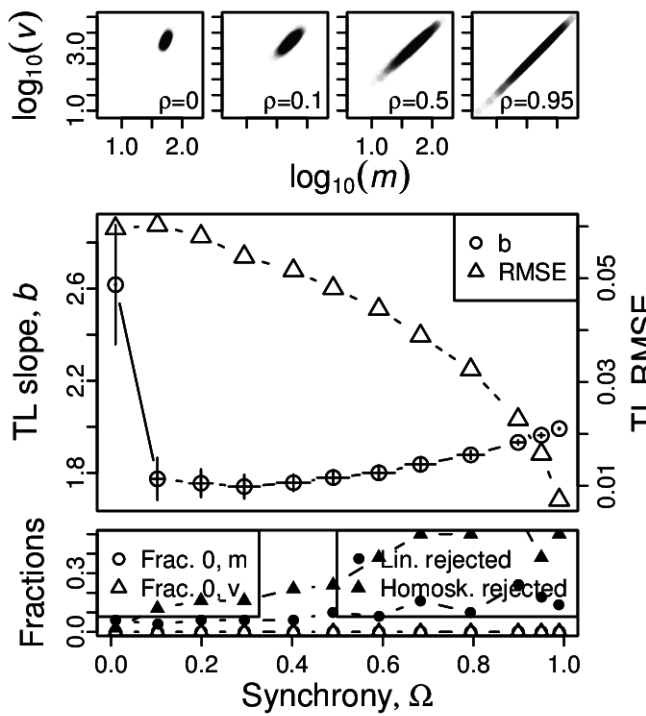
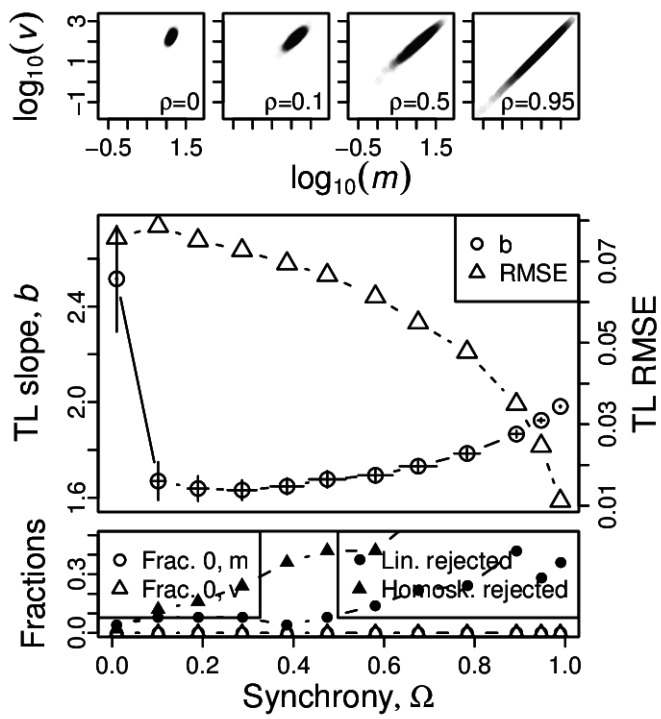
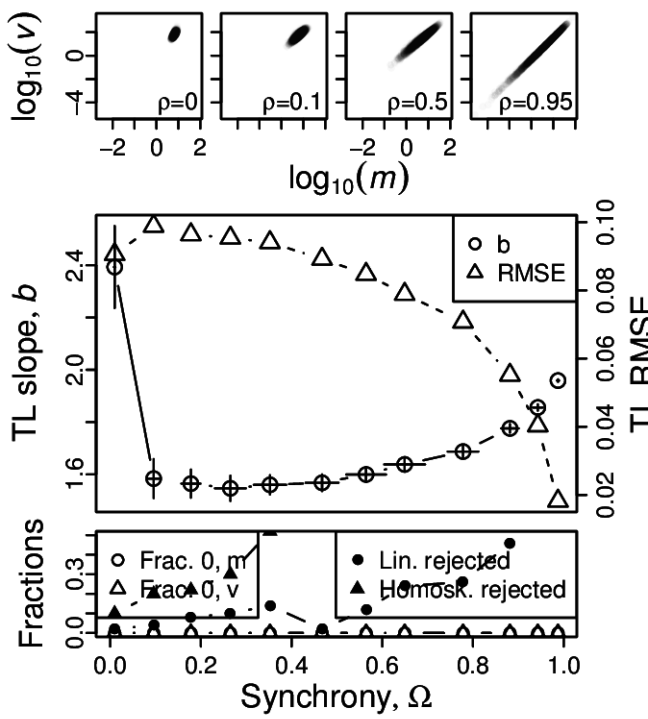


Figure S39: Omnibus plots (see section S6) for non-identically distributed gamma marginals under the set up of section S4, for  $n = 100$  and  $Y_1$  with  $\beta = 1$  and  $\alpha = 1$  (A),  $\alpha = 2$  (B),  $\alpha = 4$  (C), and  $\alpha = 8$  (D).

A, B



C, D

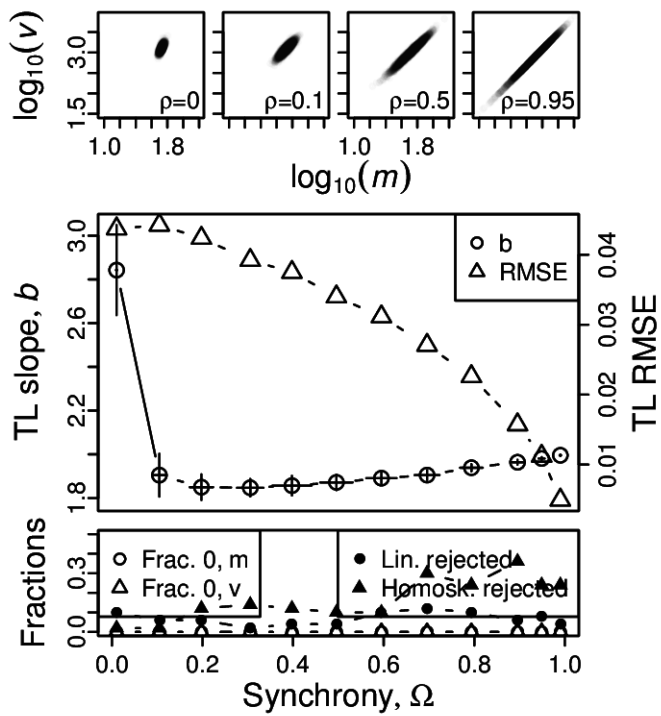
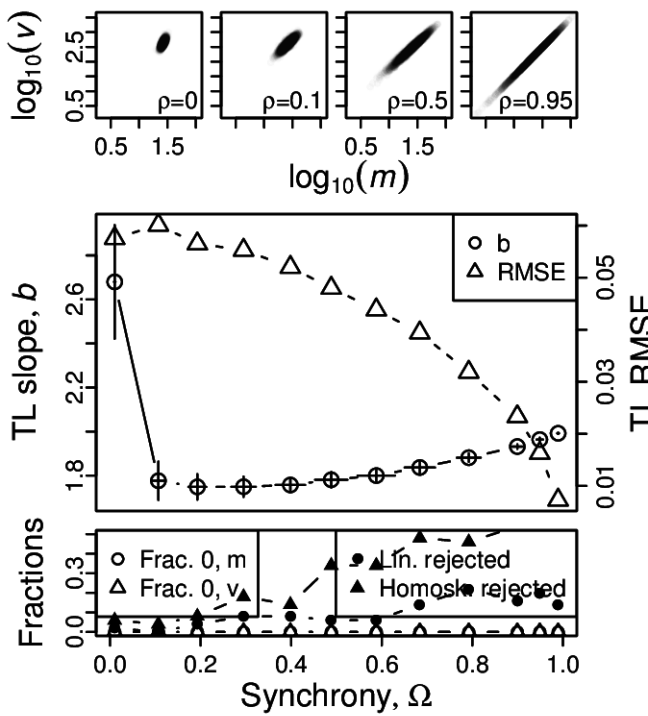
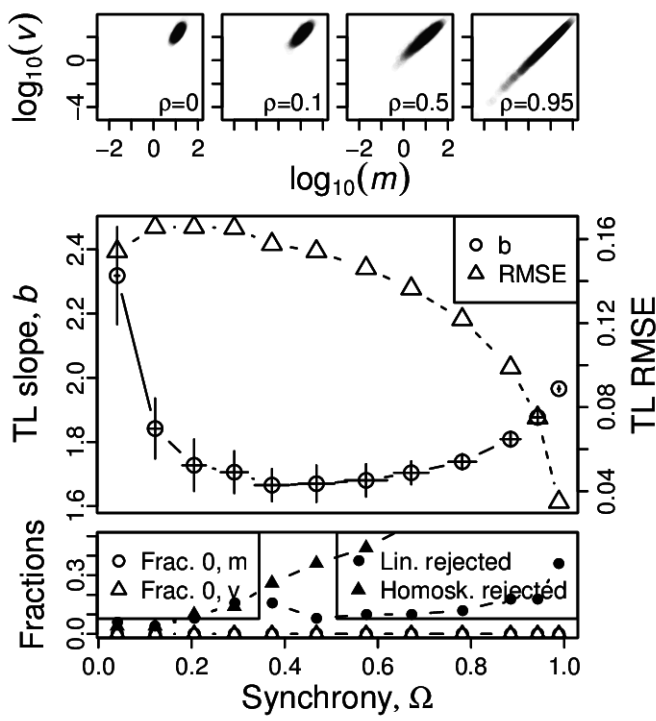


Figure S40: Omnibus plots (see section S6) for non-identically distributed gamma marginals under the set up of section S4, for  $n = 100$  and  $Y_1$  with  $\beta = 2$  and  $\alpha = 1$  (A),  $\alpha = 2$  (B),  $\alpha = 4$  (C), and  $\alpha = 8$  (D).

A, B



C, D

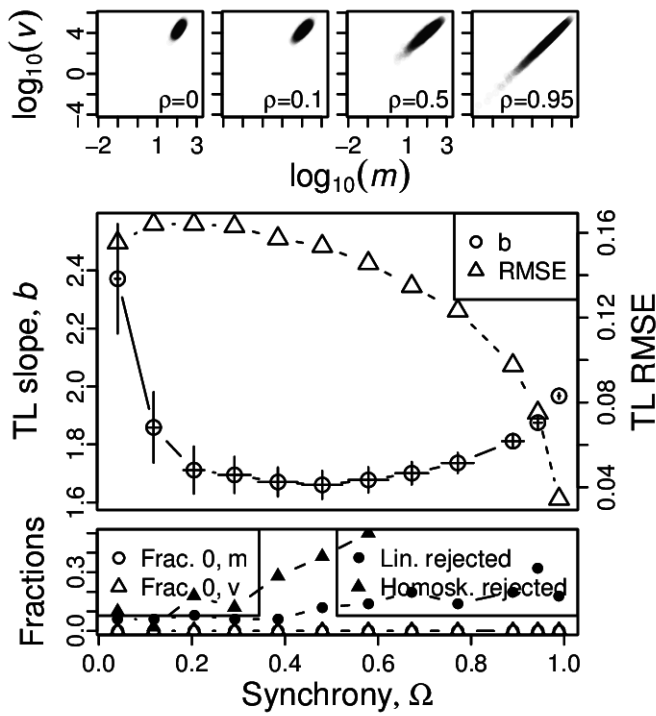
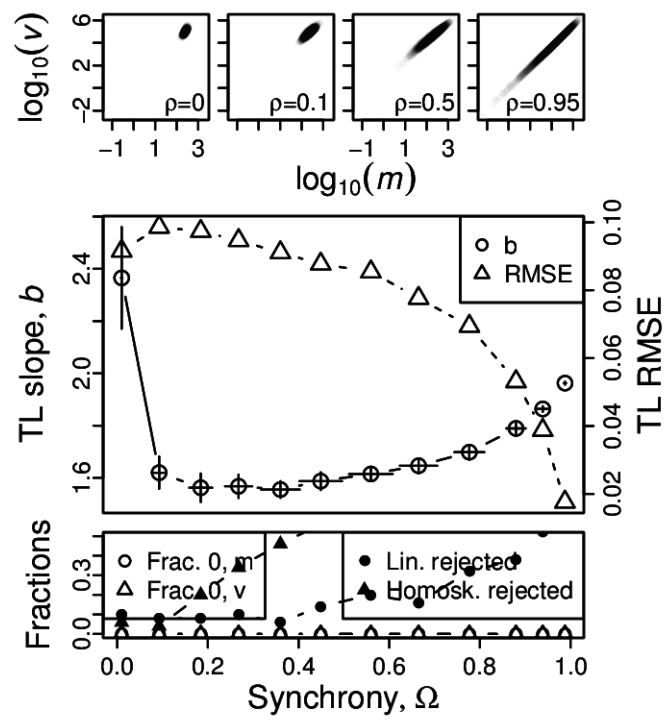
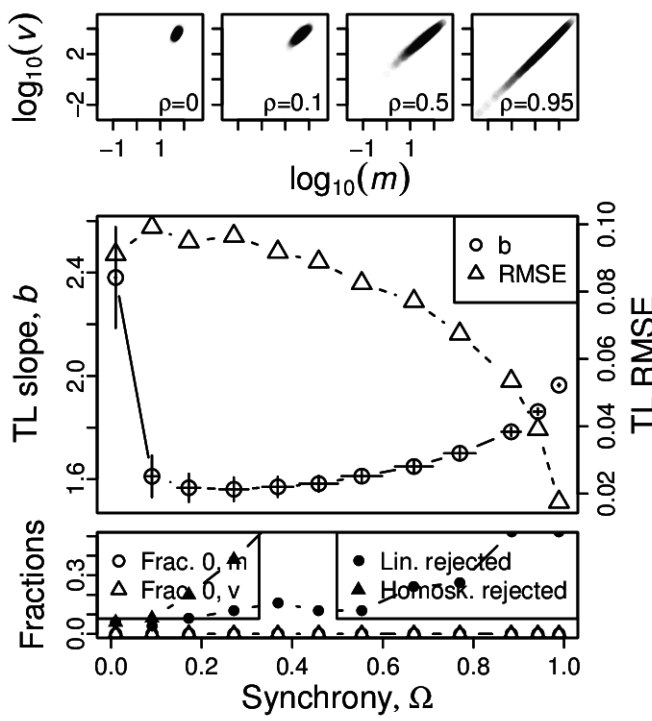


Figure S41: Omnibus plots (see section S6) for non-identically distributed exponentially distributed marginals under the set up of section S4, for  $n = 25$  and  $Y_1$  with  $1/\lambda = 1$  (A),  $1/\lambda = 5$  (B),  $1/\lambda = 10$  (C), and  $1/\lambda = 50$  (D).

A, B



C, D

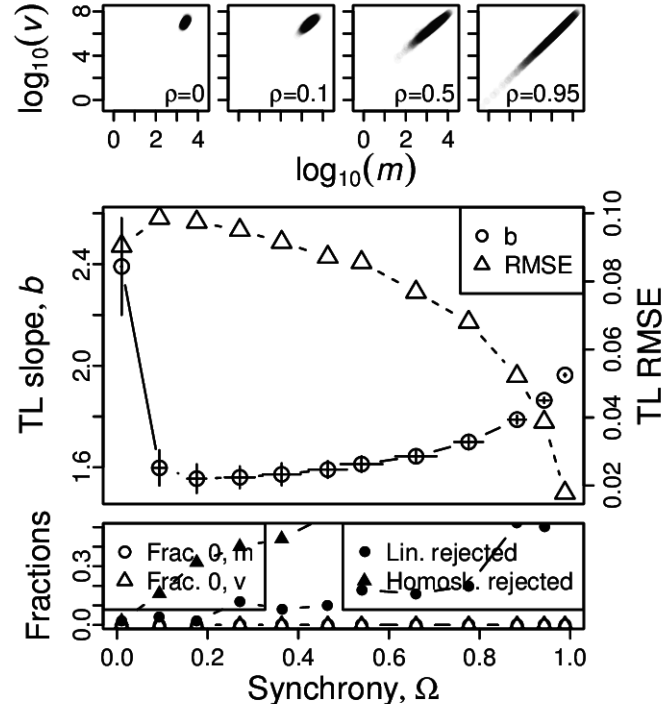
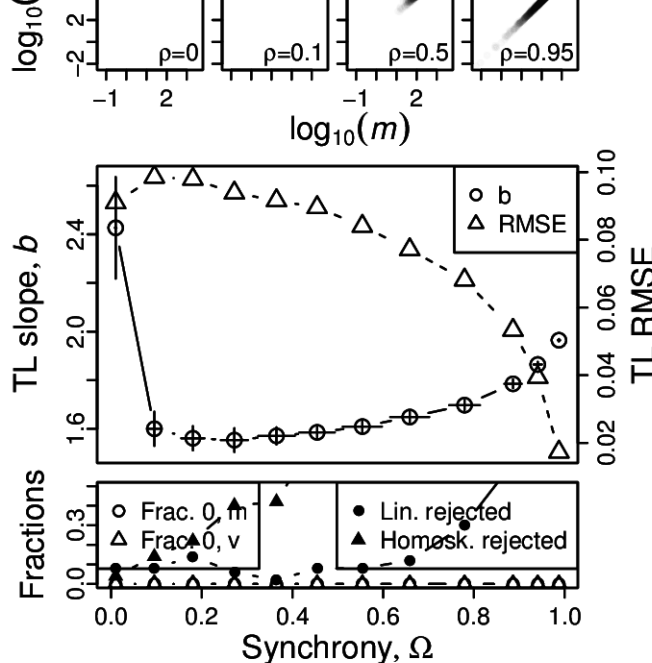
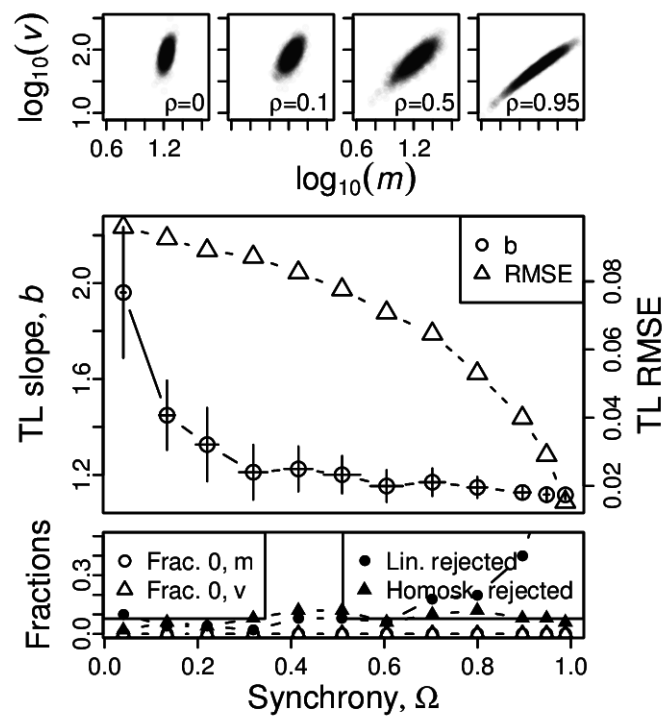
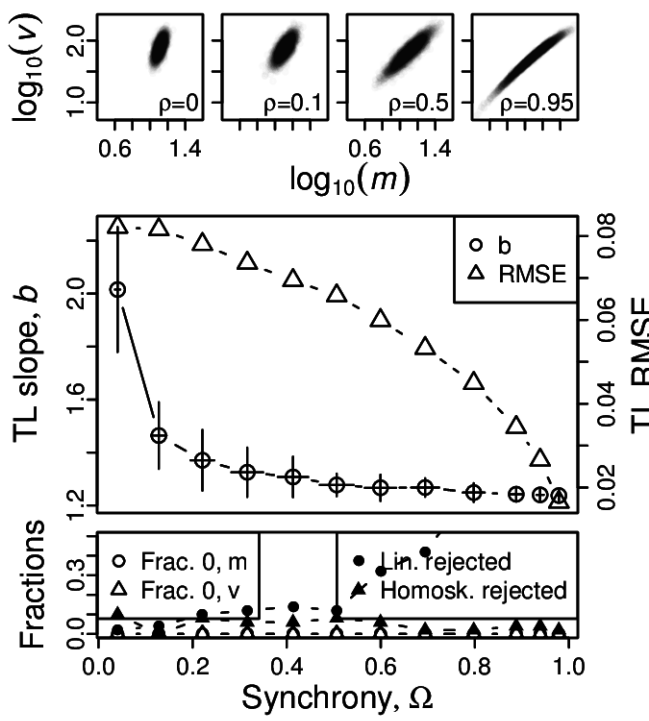


Figure S42: Omnibus plots (see section S6) for non-identically distributed exponentially distributed marginals under the set up of section S4, for  $n = 100$  and  $Y_1$  with  $1/\lambda = 1$  (A),  $1/\lambda = 5$  (B),  $1/\lambda = 10$  (C), and  $1/\lambda = 50$  (D).

A, B



C, D

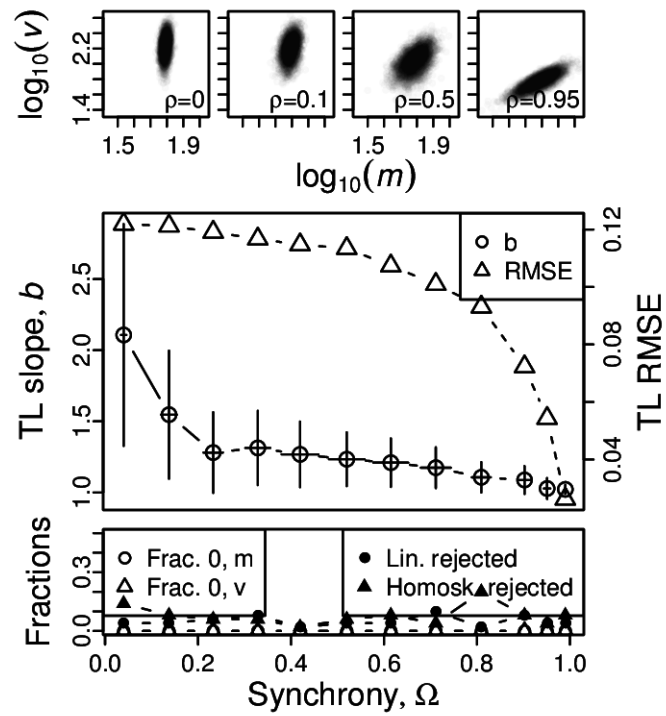
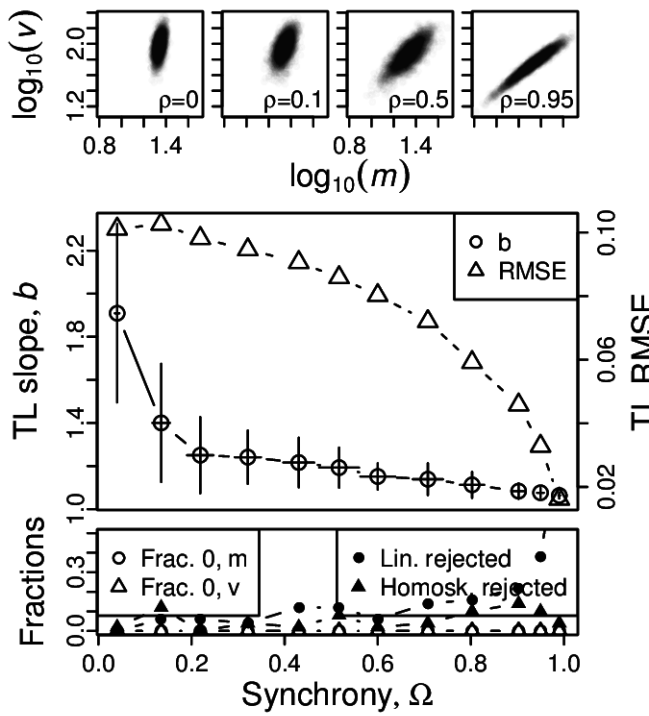
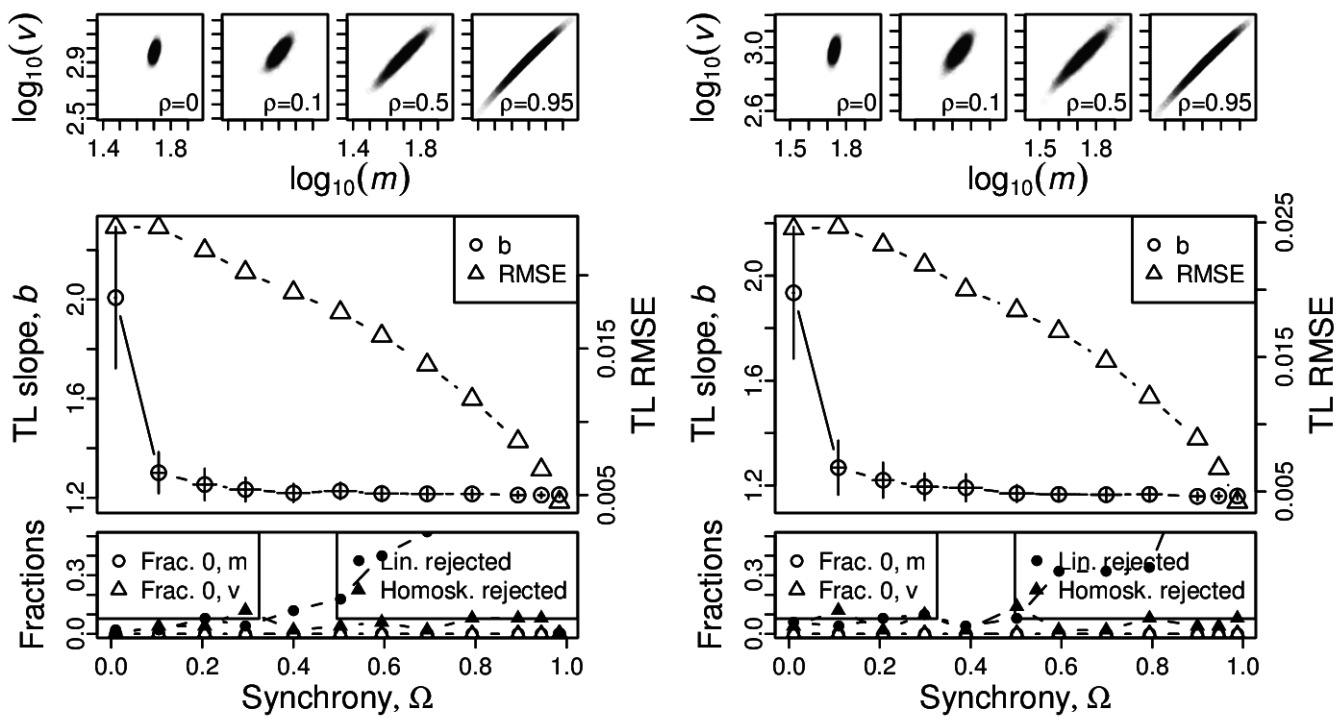


Figure S43: Omnibus plots (see section S6) for non-identically distributed chi-squared distributed marginals under the set up of section S4, for  $n = 25$  and  $Y_1$  with  $k = 1$  (A),  $k = 5$  (B),  $k = 10$  (C), and  $k = 50$  (D).

A, B



C, D

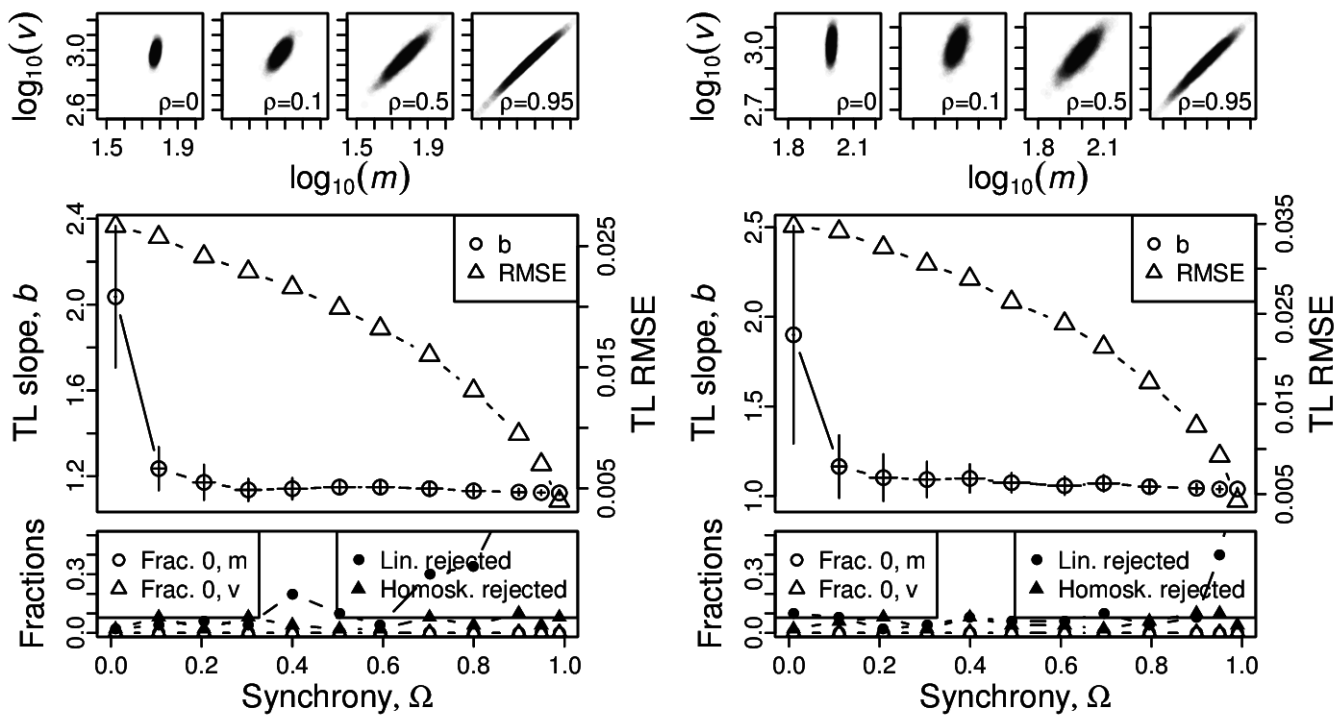


Figure S44: Omnibus plots (see section S6) for non-identically distributed chi-squared distributed marginals under the set up of section S4, for  $n = 100$  and  $Y_1$  with  $k = 1$  (A),  $k = 5$  (B),  $k = 10$  (C), and  $k = 50$  (D).

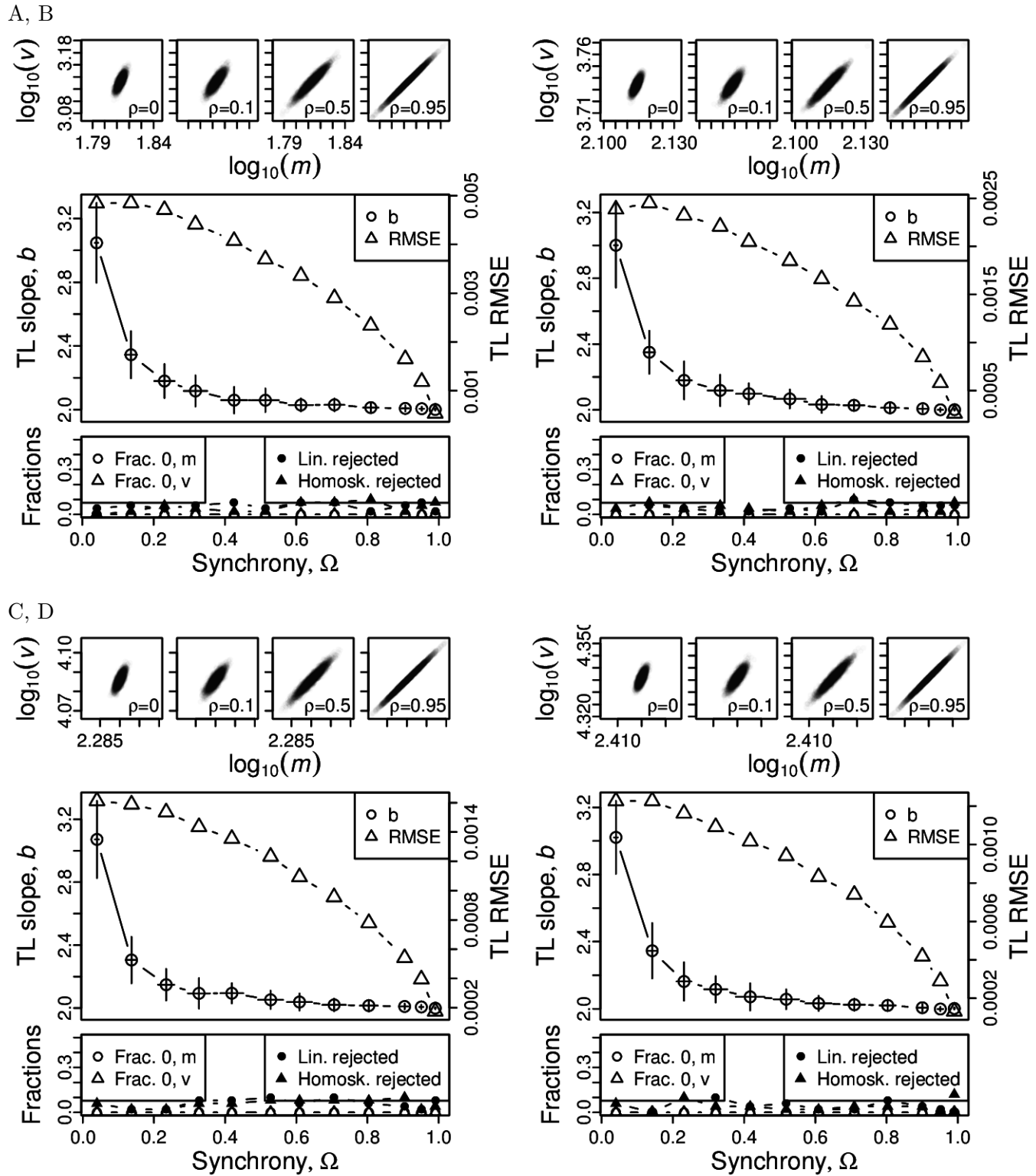
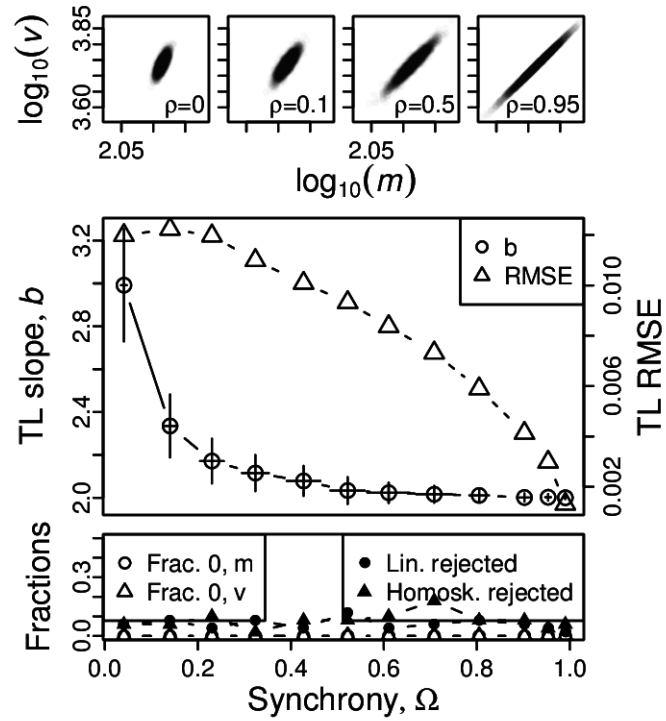
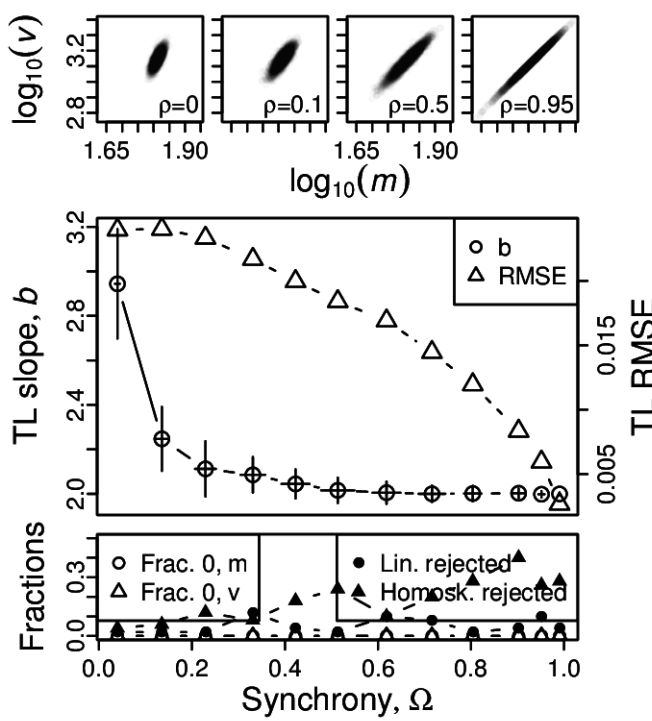


Figure S45: Omnibus plots (see section S6) for non-identically distributed normal marginals under the set up of section S4, for  $n = 25$  and  $Y_1$  with  $\sigma = 0.1$  and  $\mu = 5$  (A),  $\mu = 10$  (B),  $\mu = 15$  (C), and  $\mu = 20$  (D).

A, B



C, D

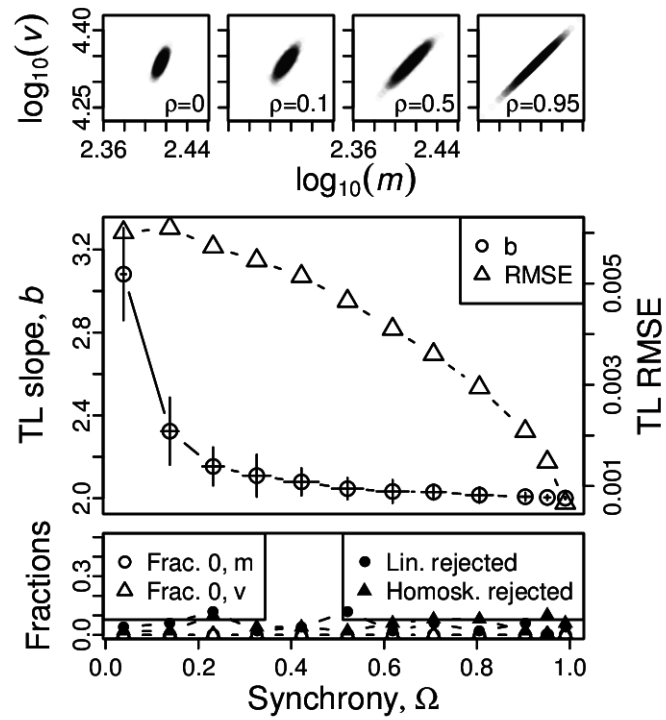
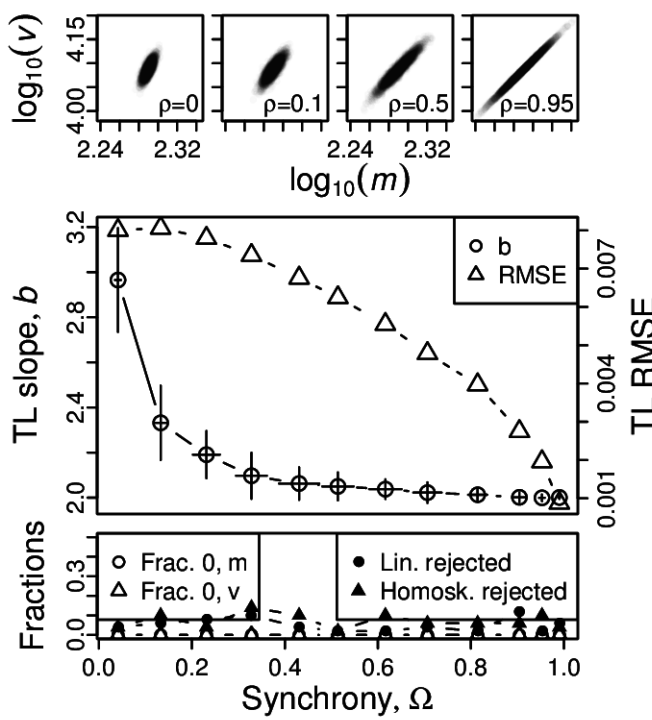
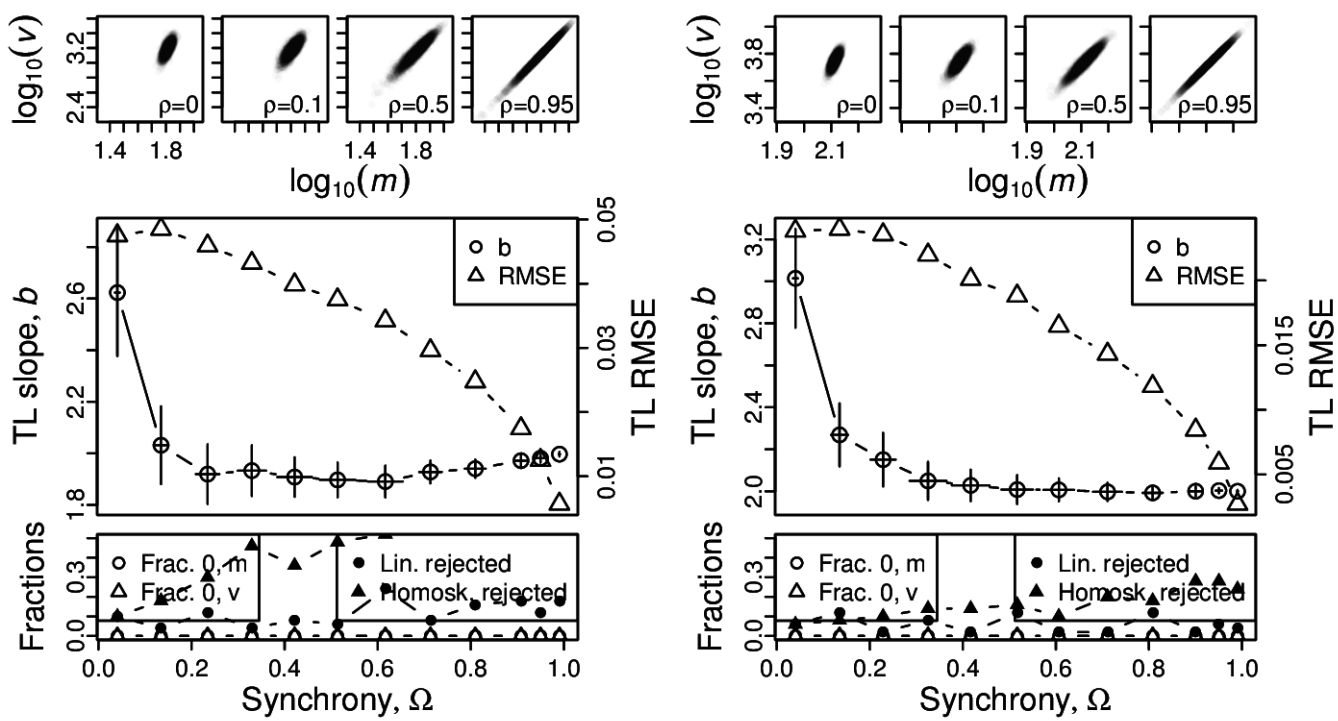


Figure S46: Omnibus plots (see section S6) for non-identically distributed normal marginals under the set up of section S4, for  $n = 25$  and  $Y_1$  with  $\sigma = 0.5$  and  $\mu = 5$  (A),  $\mu = 10$  (B),  $\mu = 15$  (C), and  $\mu = 20$  (D).

A, B



C, D

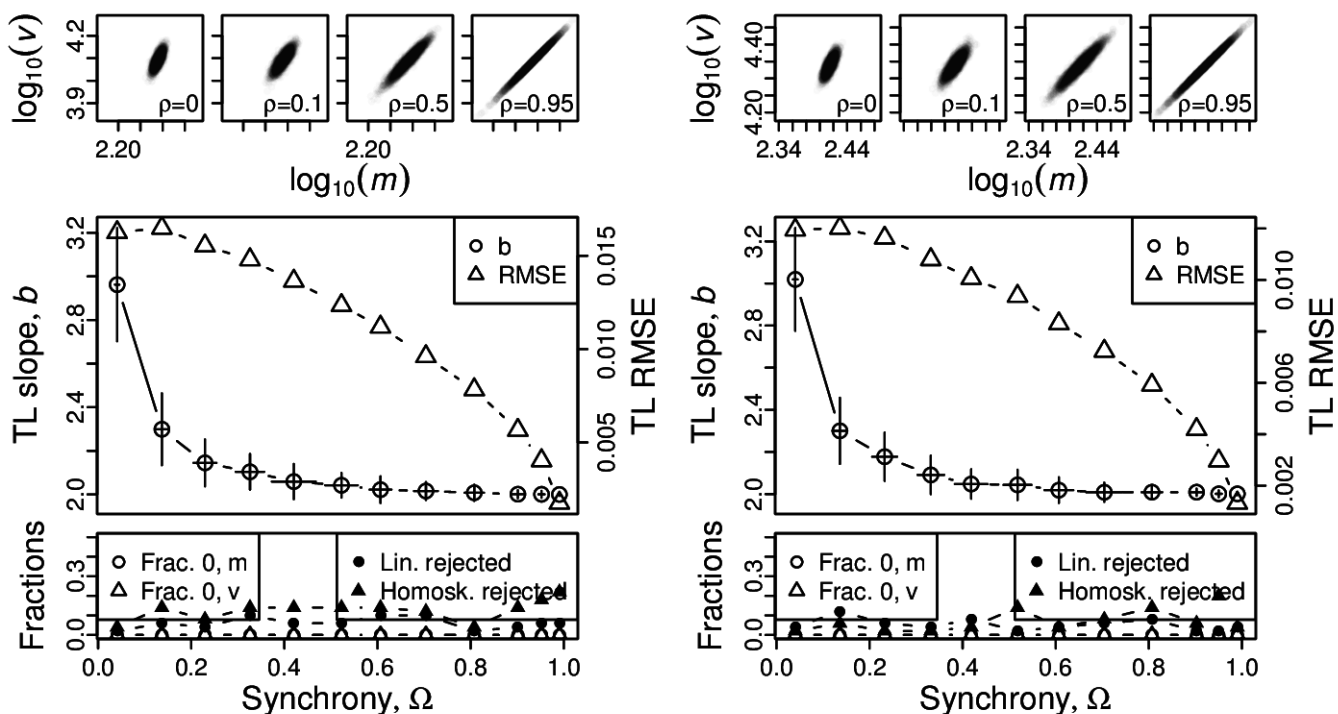
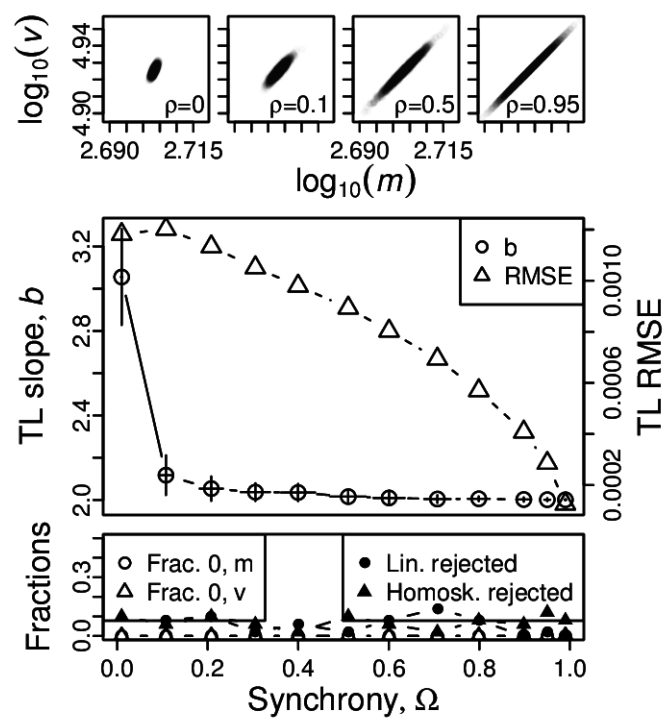
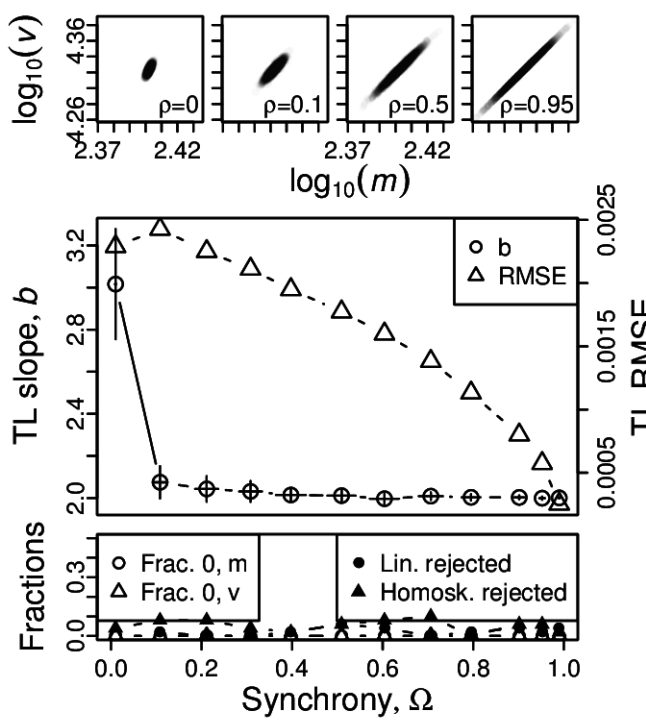


Figure S47: Omnibus plots (see section S6) for non-identically distributed normal marginals under the set up of section S4, for  $n = 25$  and  $Y_1$  with  $\sigma = 1$  and  $\mu = 5$  (A),  $\mu = 10$  (B),  $\mu = 15$  (C), and  $\mu = 20$  (D).

A, B



C, D

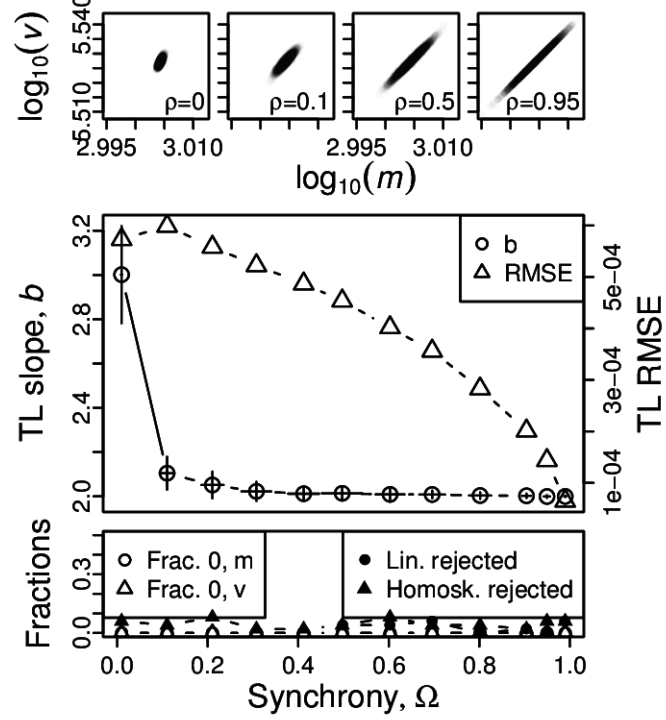
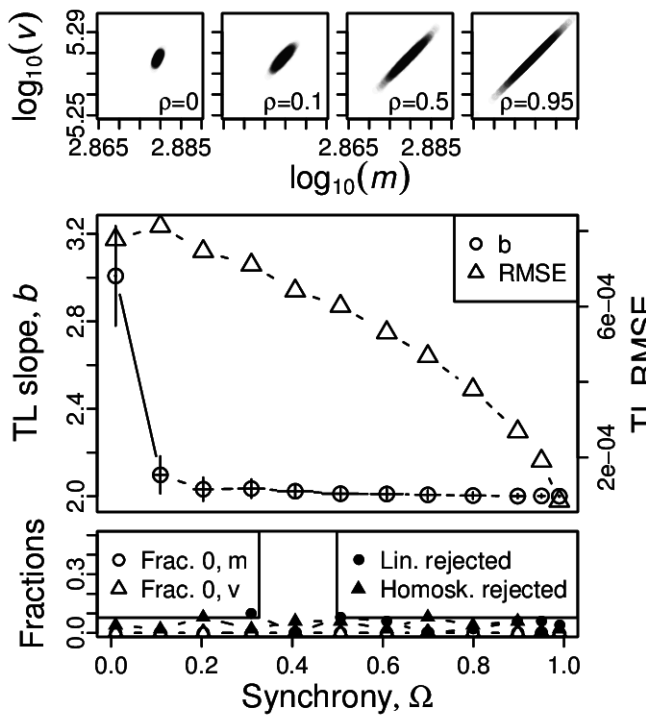
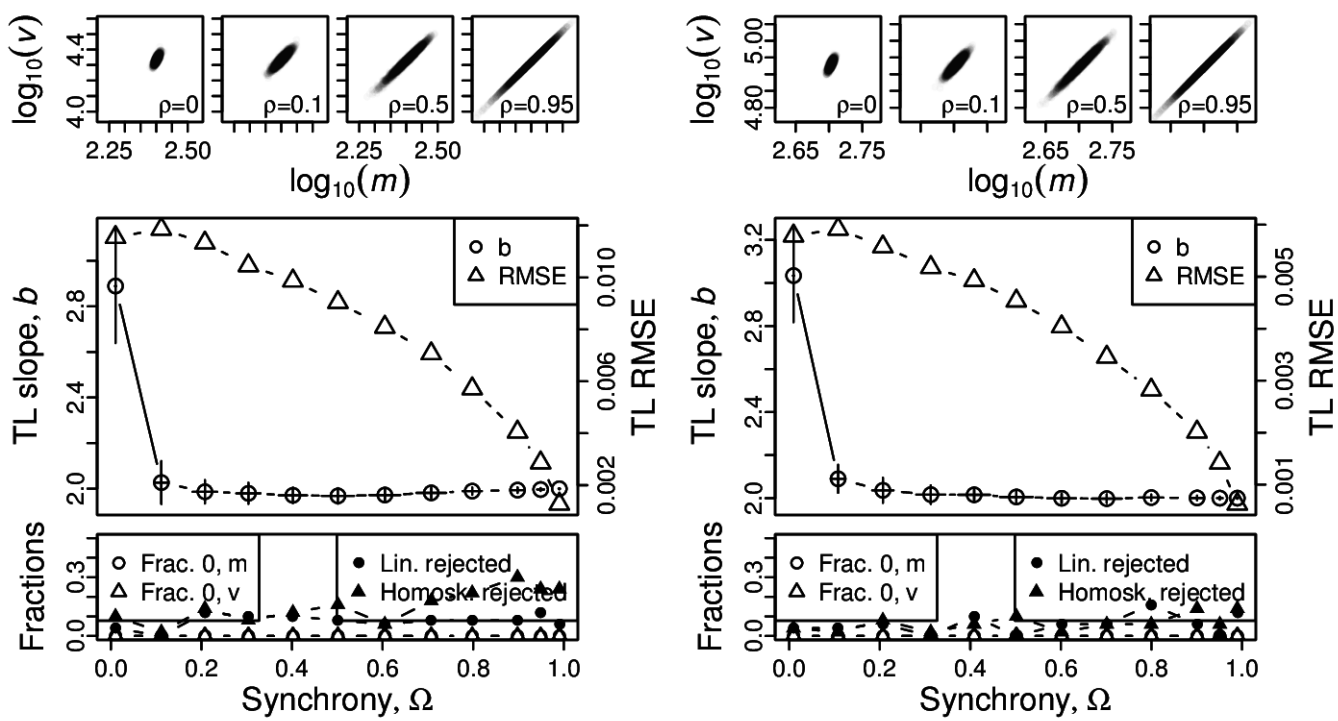


Figure S48: Omnibus plots (see section S6) for non-identically distributed normal marginals under the set up of section S4, for  $n = 100$  and  $Y_1$  with  $\sigma = 0.1$  and  $\mu = 5$  (A),  $\mu = 10$  (B),  $\mu = 15$  (C), and  $\mu = 20$  (D).

A, B



C, D

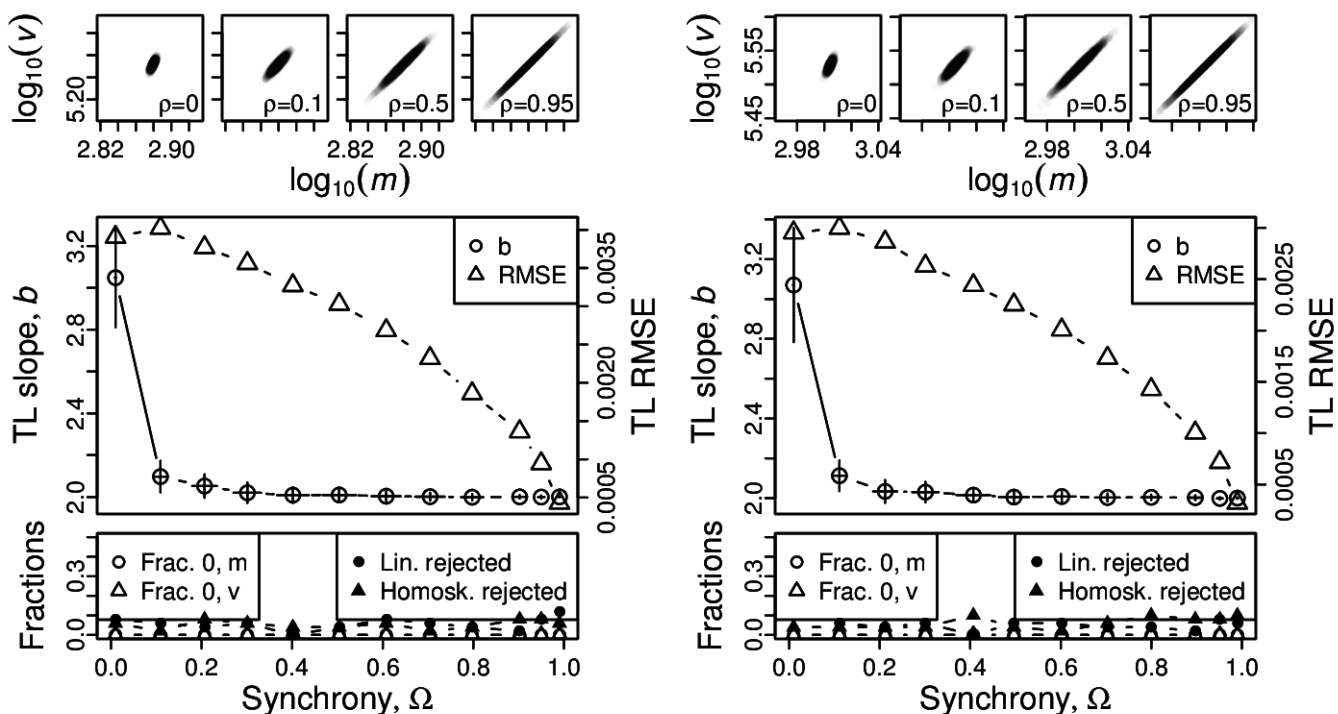
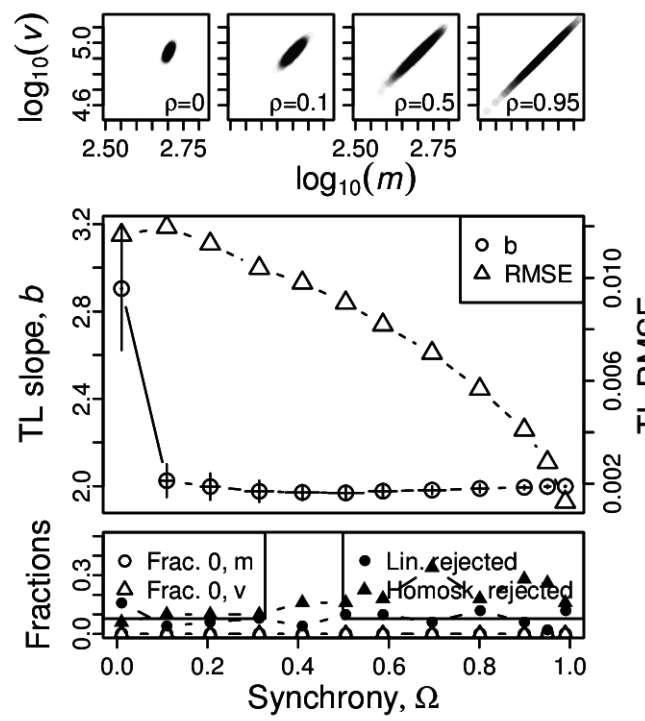
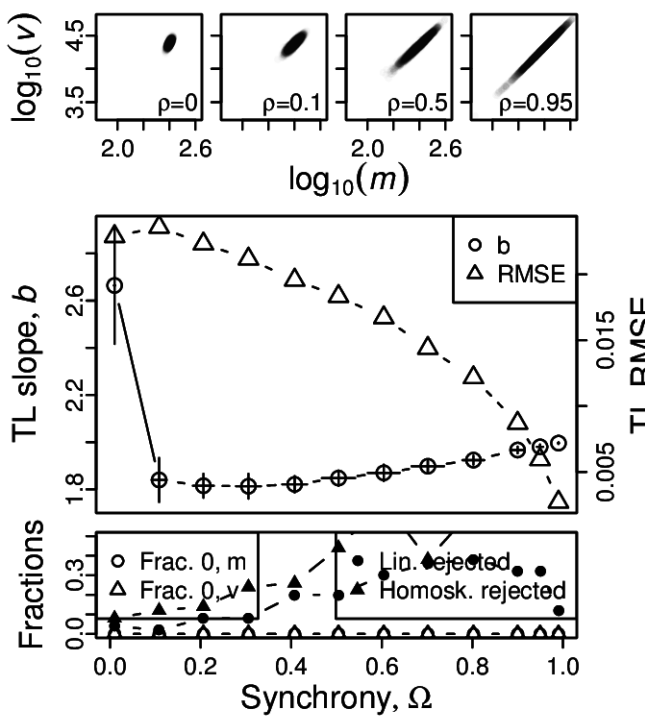


Figure S49: Omnibus plots (see section S6) for non-identically distributed normal marginals under the set up of section S4, for  $n = 100$  and  $Y_1$  with  $\sigma = 0.5$  and  $\mu = 5$  (A),  $\mu = 10$  (B),  $\mu = 15$  (C), and  $\mu = 20$  (D).

A, B



C, D

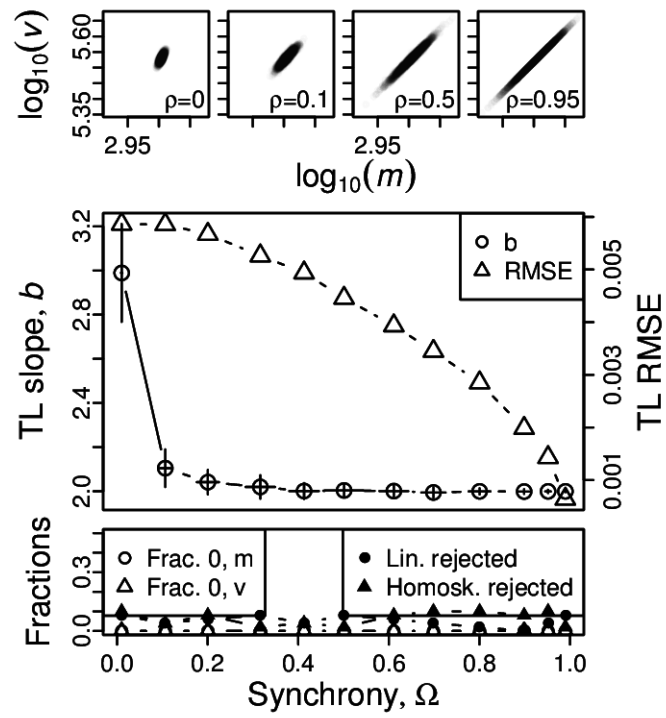
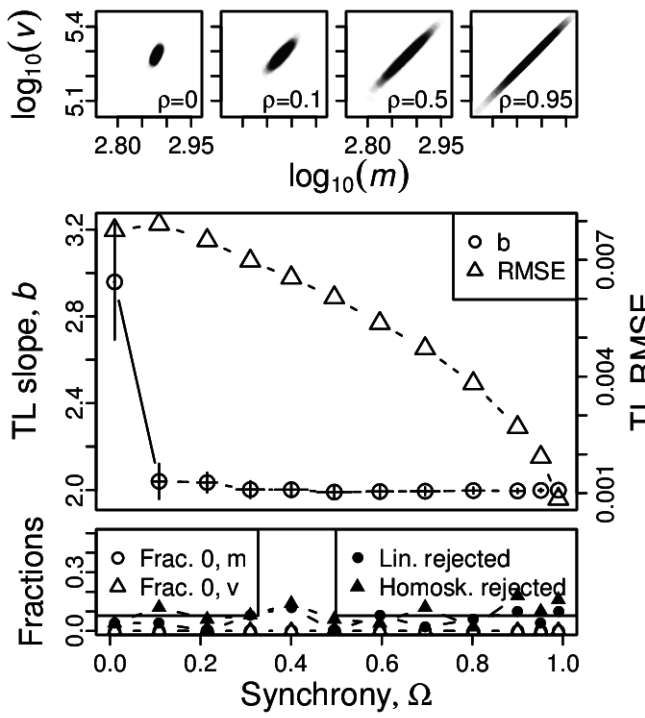
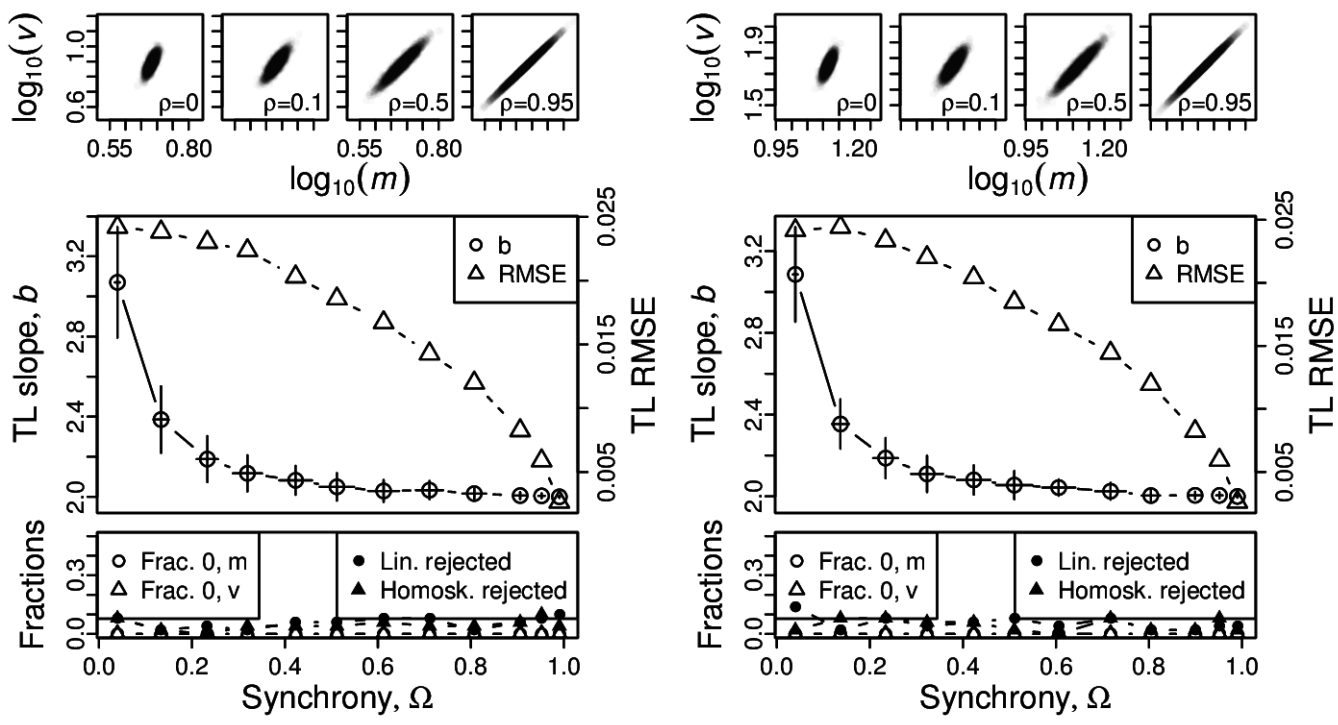


Figure S50: Omnibus plots (see section S6) for non-identically distributed normal marginals under the set up of section S4, for  $n = 100$  and  $Y_1$  with  $\sigma = 1$  and  $\mu = 5$  (A),  $\mu = 10$  (B),  $\mu = 15$  (C), and  $\mu = 20$  (D).

A, B



C, D

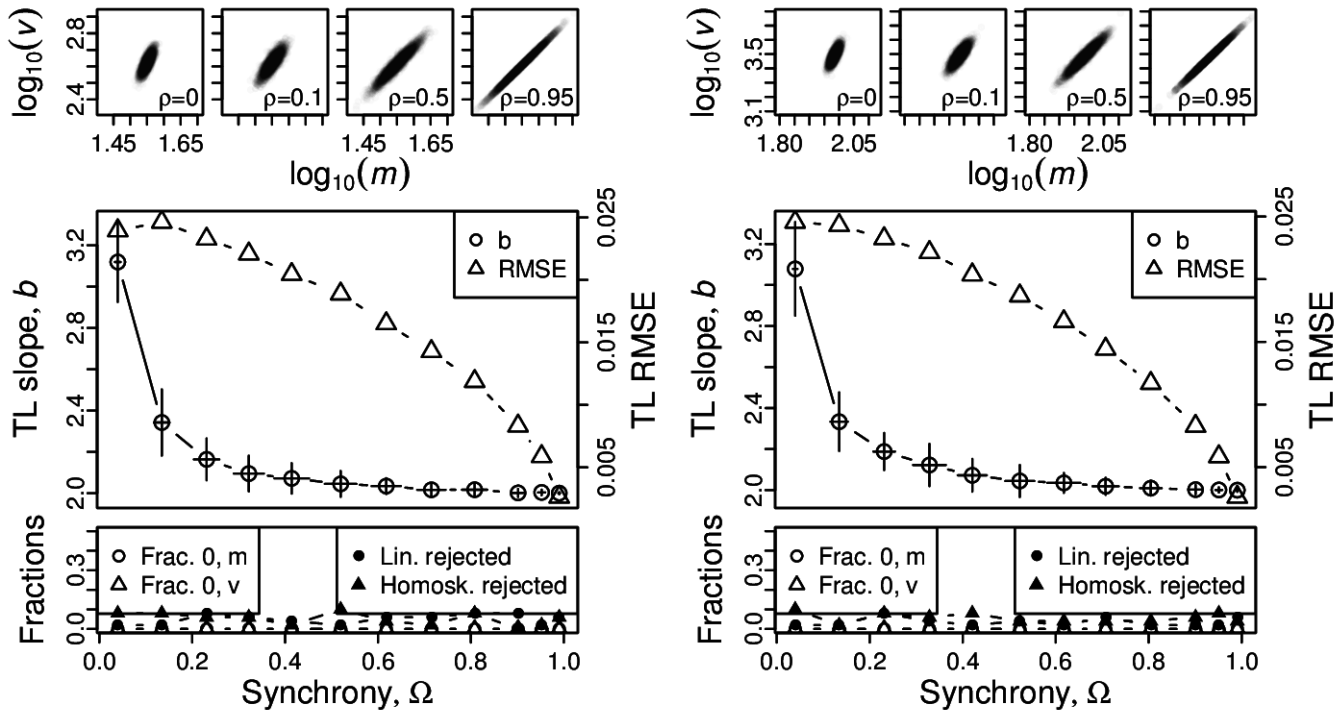
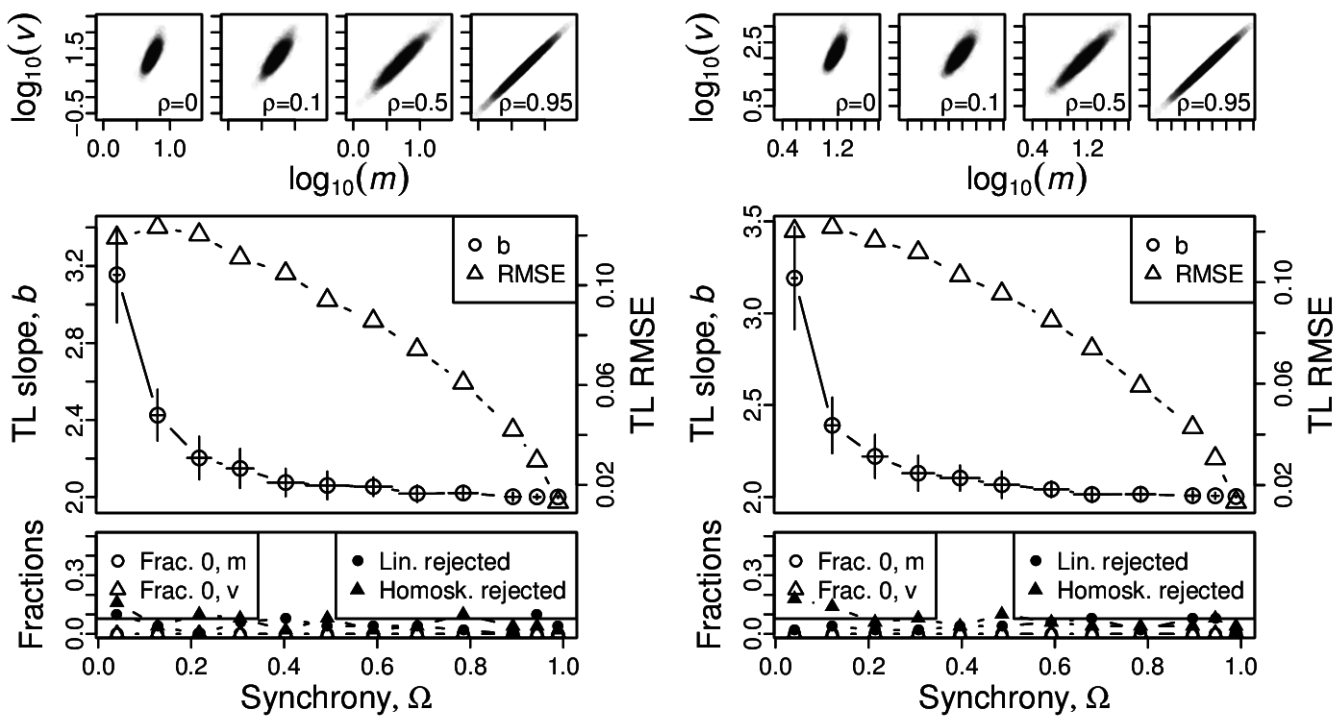


Figure S51: Omnibus plots (see section S6) for non-identically distributed log-normal marginals under the set up of section S4, for  $n = 25$  and  $Y_1$  with  $\sigma = 0.1$  and  $\mu = -1$  (A),  $\mu = 0$  (B),  $\mu = 1$  (C), and  $\mu = 2$  (D).

A, B



C, D

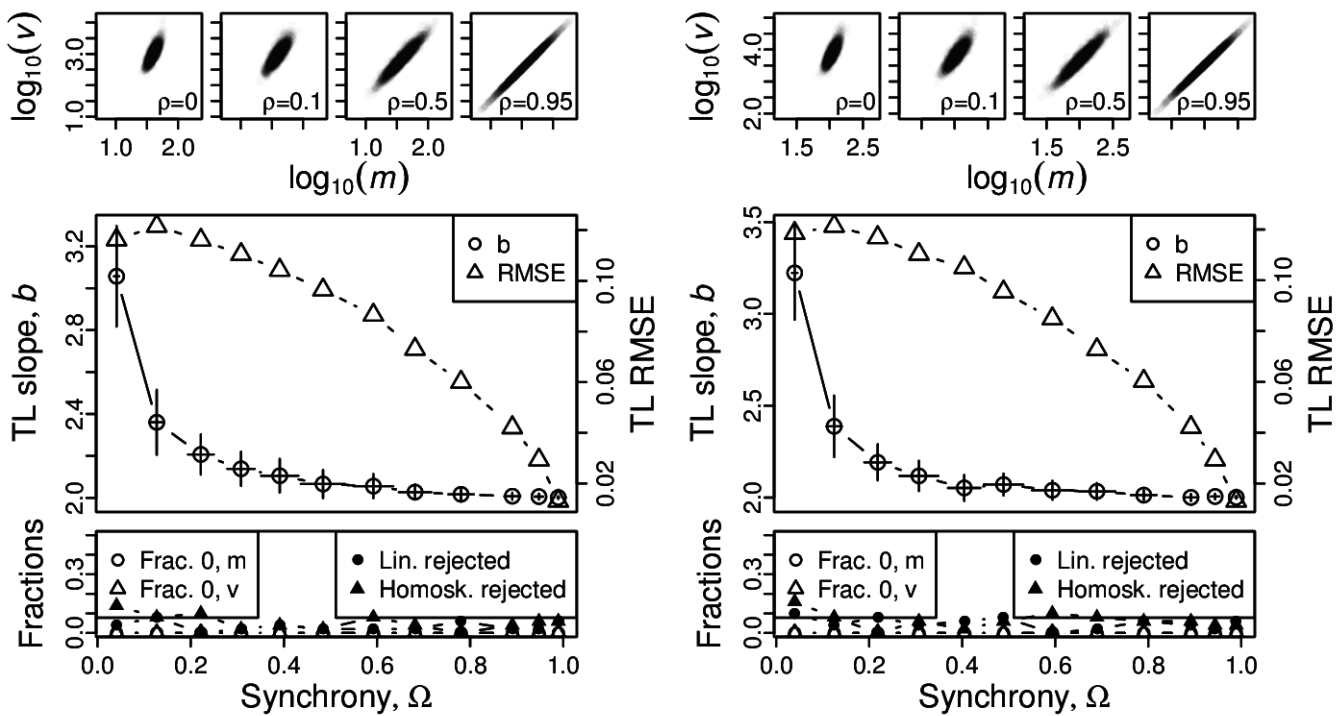
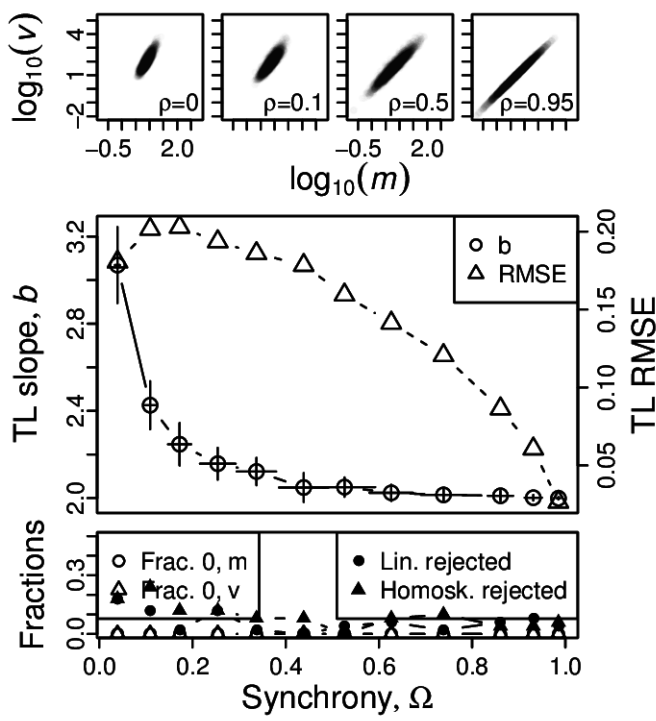


Figure S52: Omnibus plots (see section S6) for non-identically distributed log-normal marginals under the set up of section S4, for  $n = 25$  and  $Y_1$  with  $\sigma = 0.5$  and  $\mu = -1$  (A),  $\mu = 0$  (B),  $\mu = 1$  (C), and  $\mu = 2$  (D).

A, B



C, D

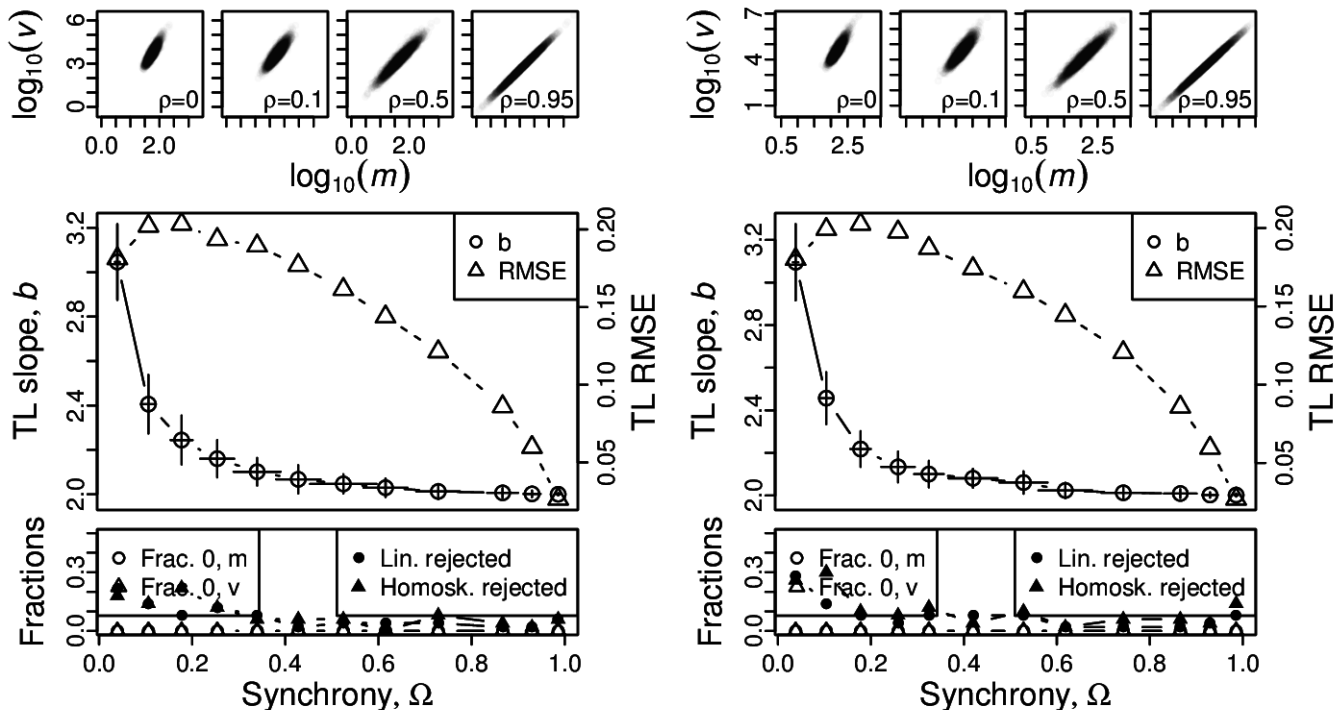
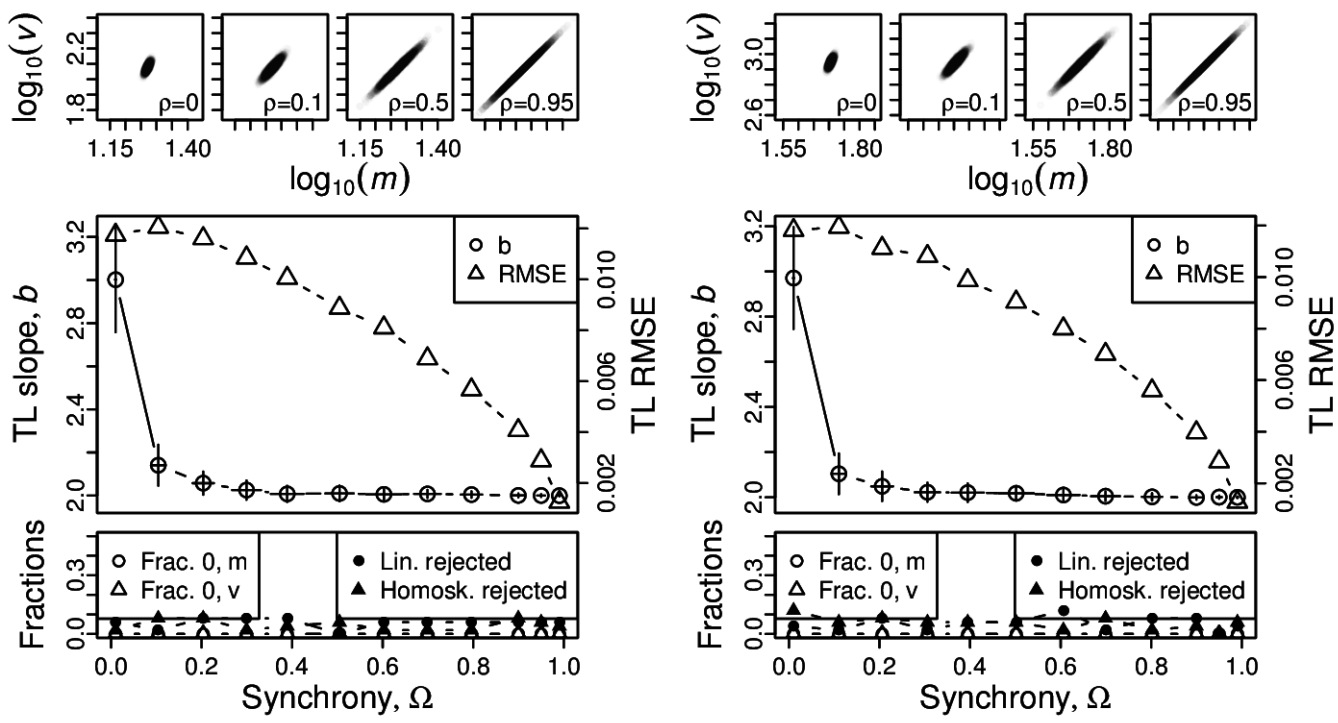


Figure S53: Omnibus plots (see section S6) for non-identically distributed log-normal marginals under the set up of section S4, for  $n = 25$  and  $Y_1$  with  $\sigma = 1$  and  $\mu = -1$  (A),  $\mu = 0$  (B),  $\mu = 1$  (C), and  $\mu = 2$  (D).

A, B



C, D

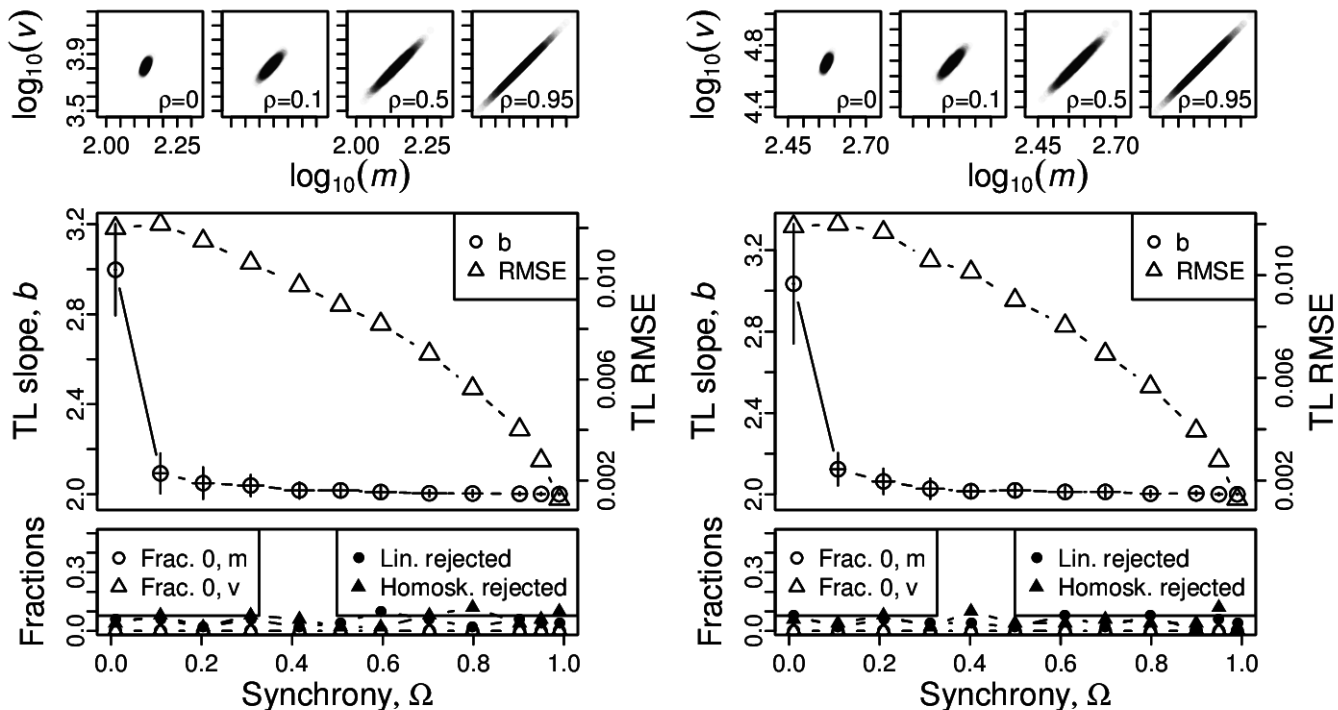
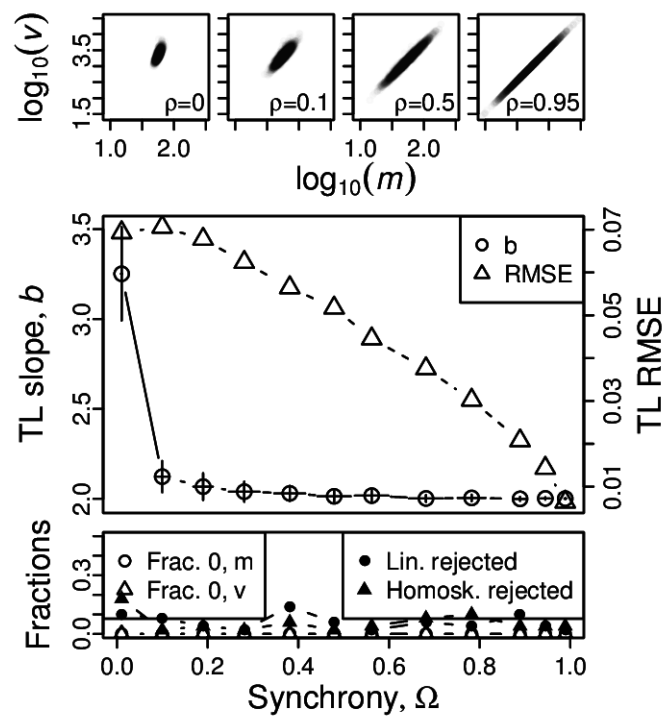
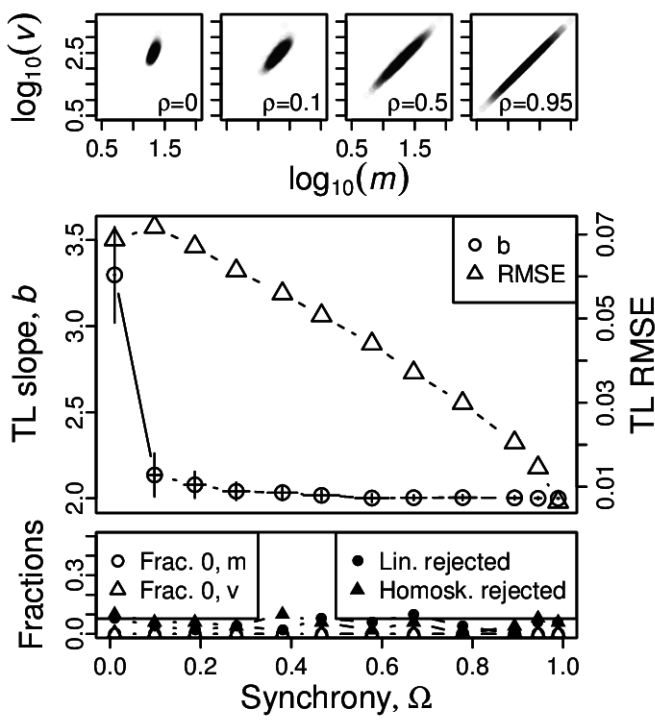


Figure S54: Omnibus plots (see section S6) for non-identically distributed log-normal marginals under the set up of section S4, for  $n = 100$  and  $Y_1$  with  $\sigma = 0.1$  and  $\mu = -1$  (A),  $\mu = 0$  (B),  $\mu = 1$  (C), and  $\mu = 2$  (D).

A, B



C, D

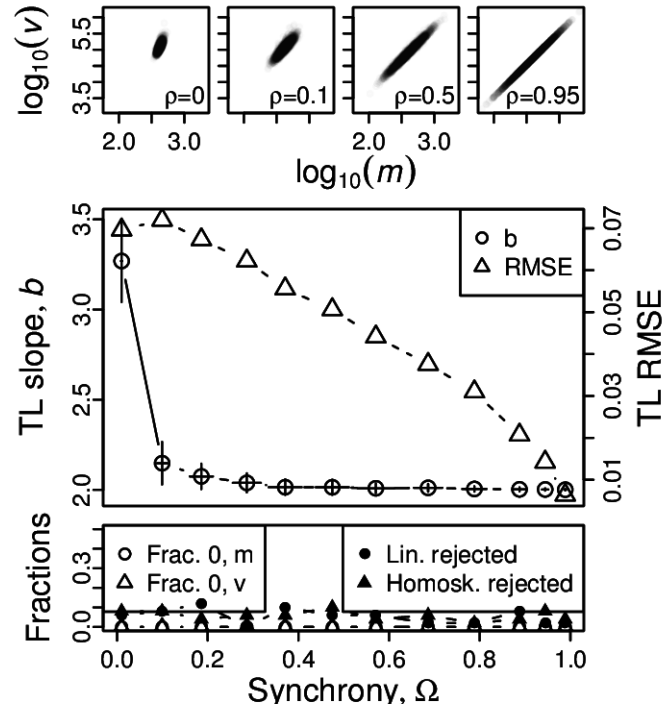
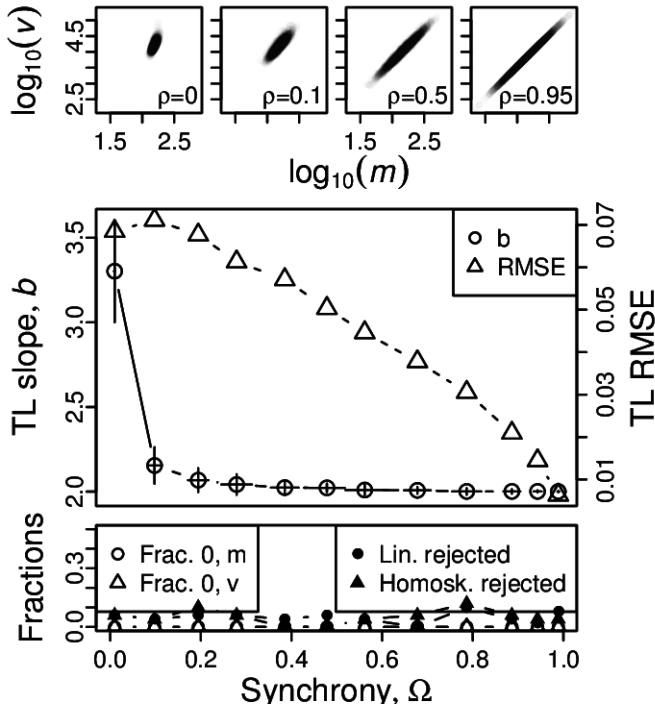
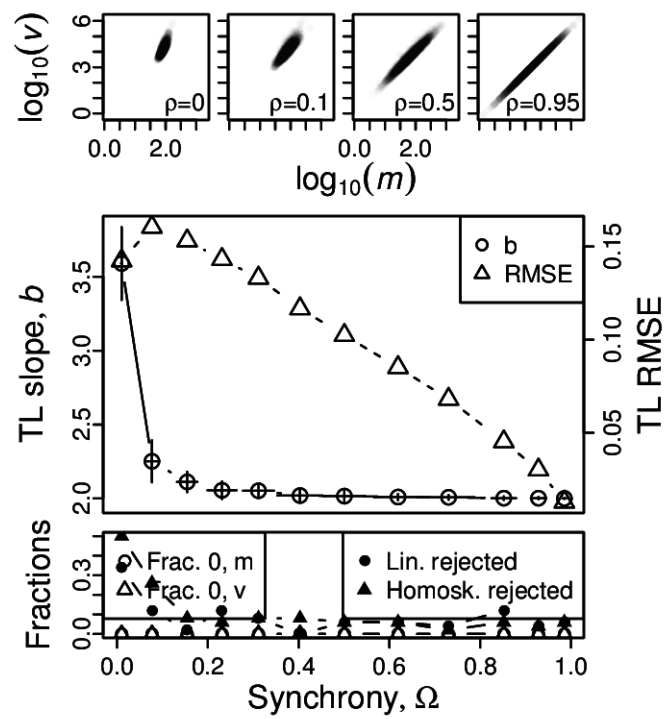
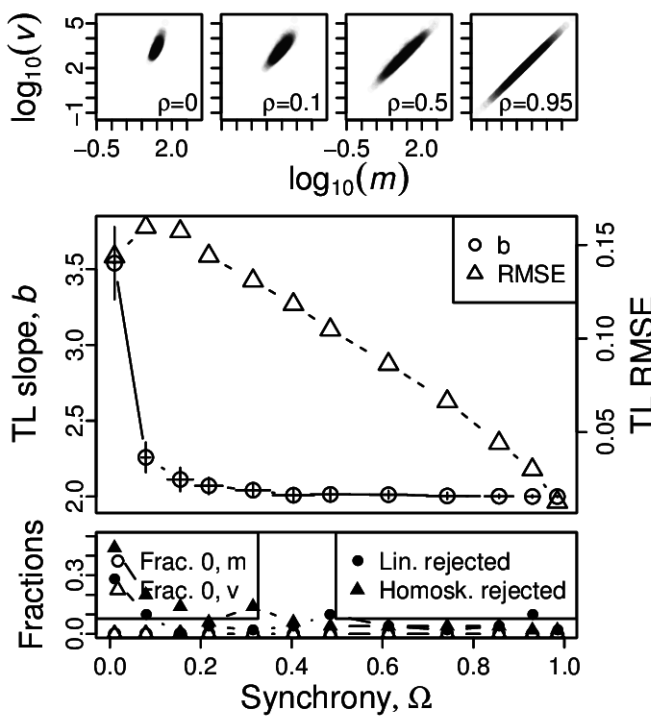


Figure S55: Omnibus plots (see section S6) for non-identically distributed log-normal marginals under the set up of section S4, for  $n = 100$  and  $Y_1$  with  $\sigma = 0.5$  and  $\mu = -1$  (A),  $\mu = 0$  (B),  $\mu = 1$  (C), and  $\mu = 2$  (D).

A, B



C, D

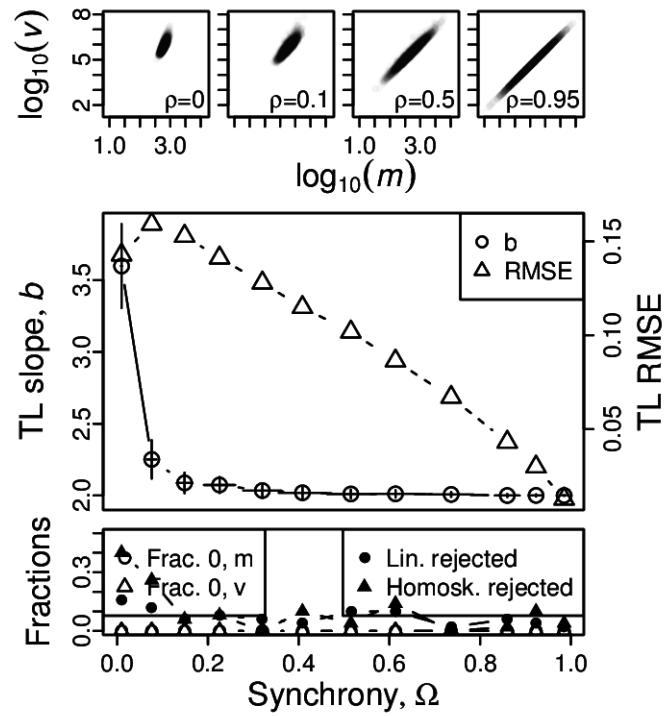
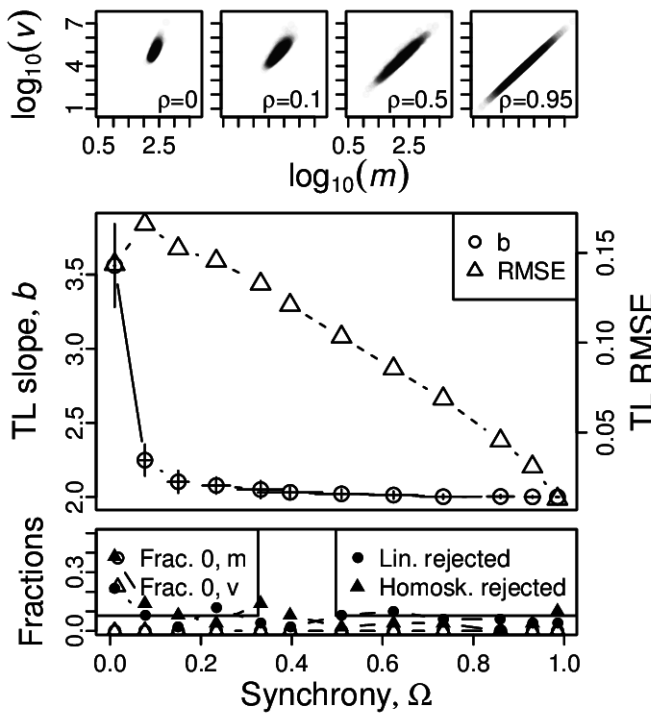


Figure S56: Omnibus plots (see section S6) for non-identically distributed log-normal marginals under the set up of section S4, for  $n = 100$  and  $Y_1$  with  $\sigma = 1$  and  $\mu = -1$  (A),  $\mu = 0$  (B),  $\mu = 1$  (C), and  $\mu = 2$  (D).

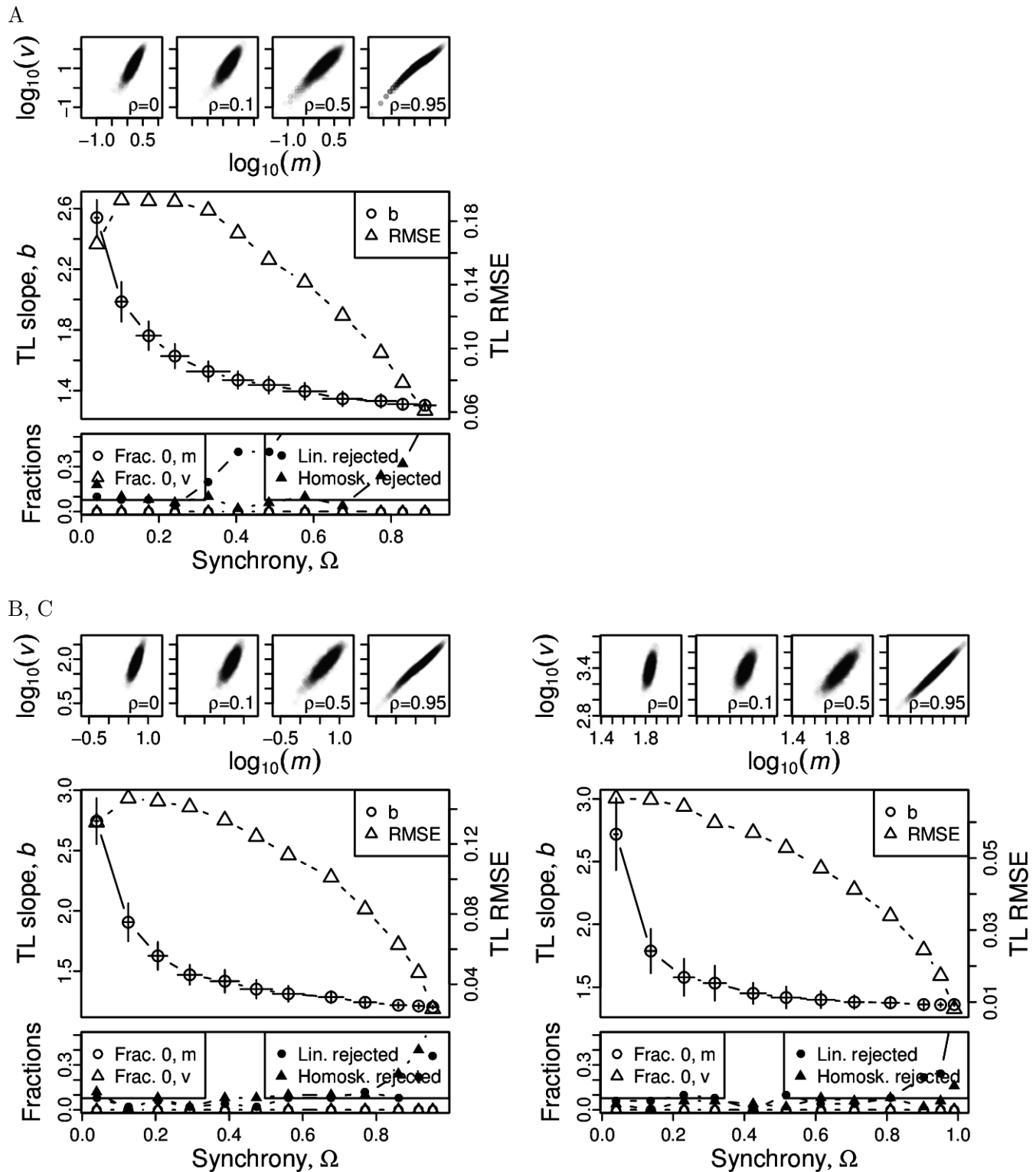


Figure S57: Omnibus plots (see section S6) for non-identically distributed negative binomial marginals under the set up of section S4, for  $n = 25$  and  $Y_1$  with  $p = 0.2$  and  $r = 5$  (A),  $r = 10$  (B),  $r = 50$  (C).

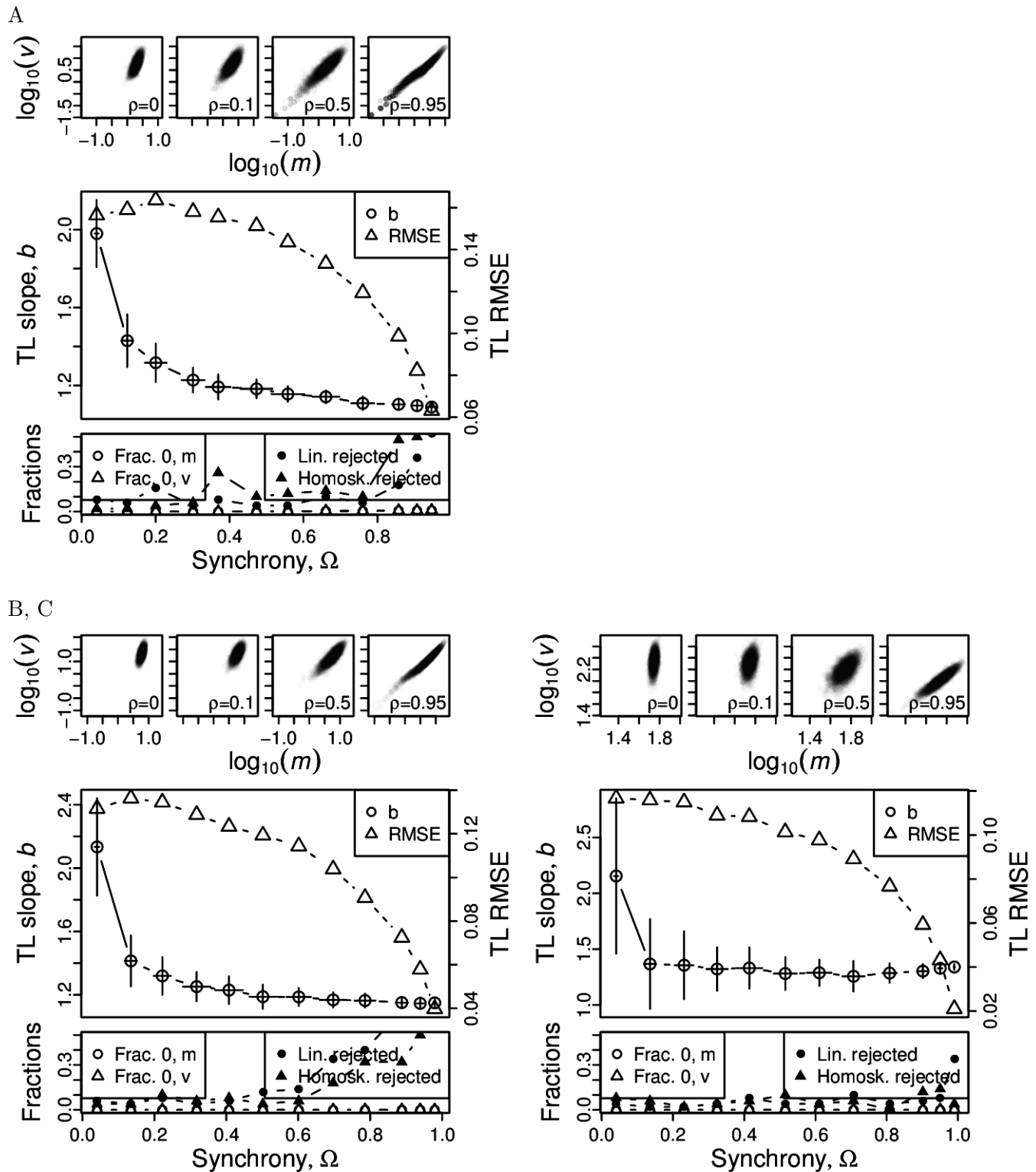


Figure S58: Omnibus plots (see section S6) for non-identically distributed negative binomial marginals under the set up of section S4, for  $n = 25$  and  $Y_1$  with  $p = 0.4$  and  $r = 5$  (A),  $r = 10$  (B),  $r = 50$  (C).

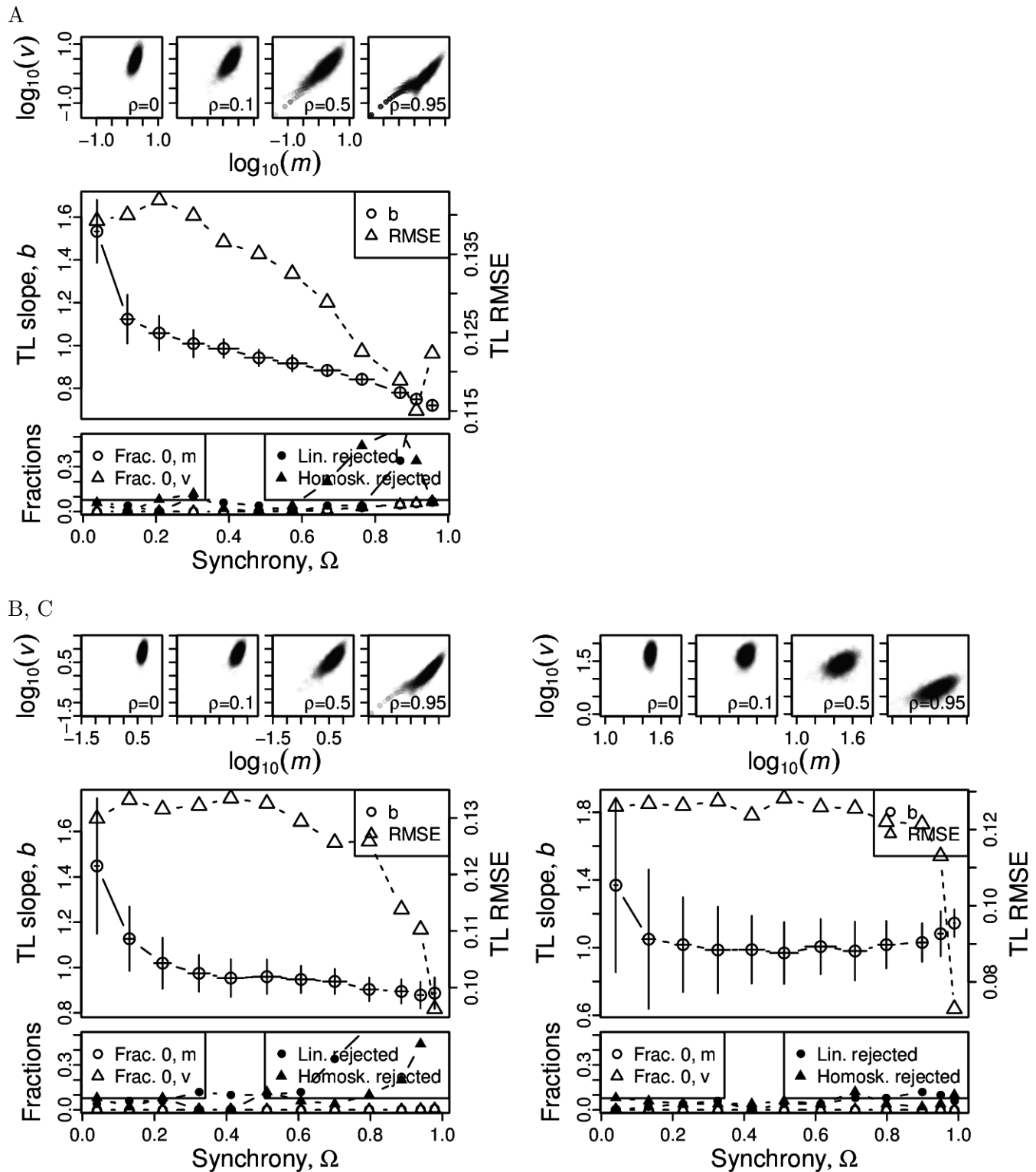


Figure S59: Omnibus plots (see section S6) for non-identically distributed negative binomial marginals under the set up of section S4, for  $n = 25$  and  $Y_1$  with  $p = 0.6$  and  $r = 5$  (A),  $r = 10$  (B),  $r = 50$  (C).

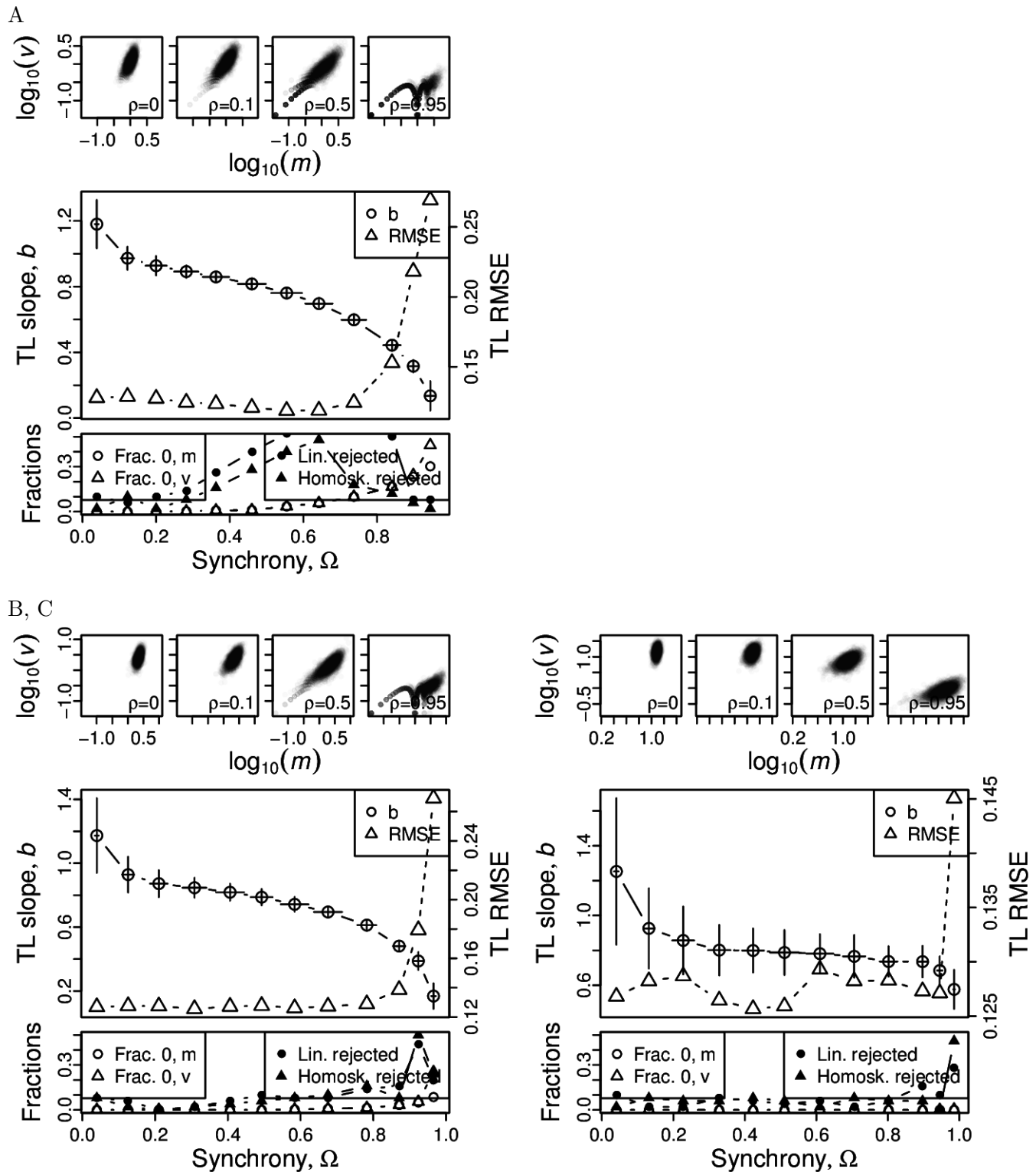


Figure S60: Omnibus plots (see section S6) for non-identically distributed negative binomial marginals under the set up of section S4, for  $n = 25$  and  $Y_1$  with  $p = 0.8$  and  $r = 5$  (A),  $r = 10$  (B),  $r = 50$  (C).

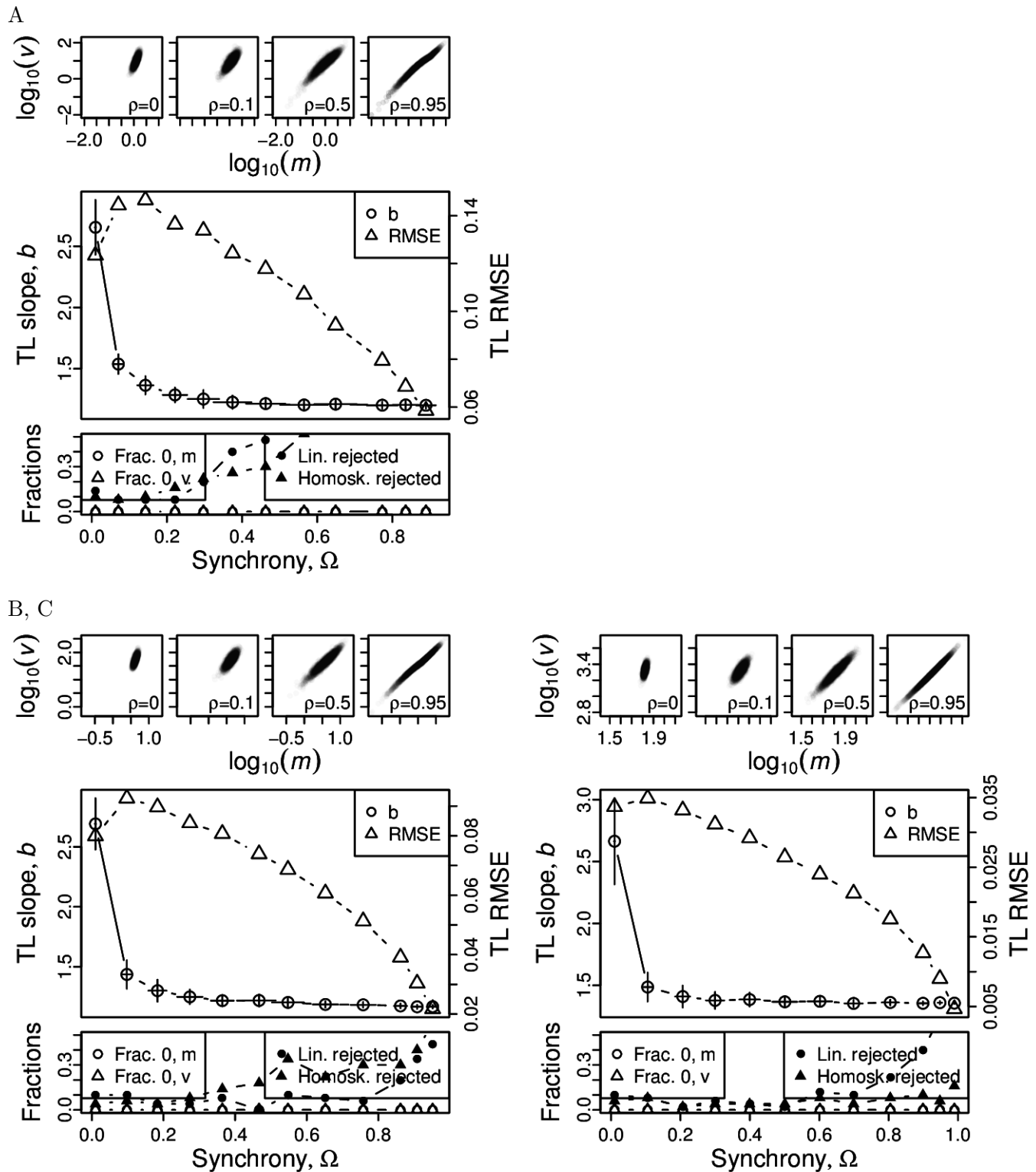


Figure S61: Omnibus plots (see section S6) for non-identically distributed negative binomial marginals under the set up of section S4, for  $n = 100$  and  $Y_1$  with  $p = 0.2$  and  $r = 5$  (A),  $r = 10$  (B),  $r = 50$  (C).

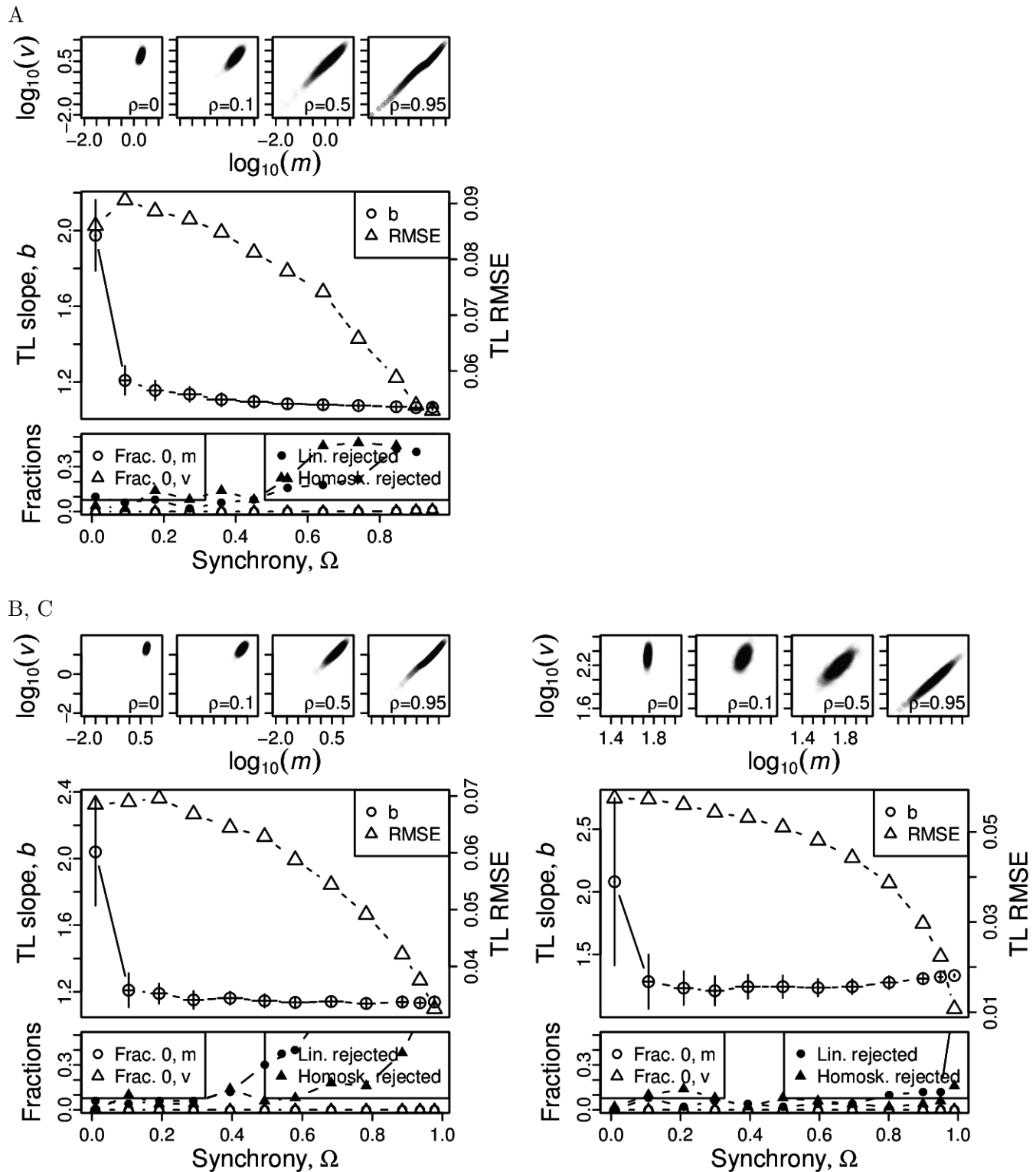


Figure S62: Omnibus plots (see section S6) for non-identically distributed negative binomial marginals under the set up of section S4, for  $n = 100$  and  $Y_1$  with  $p = 0.4$  and  $r = 5$  (A),  $r = 10$  (B),  $r = 50$  (C).

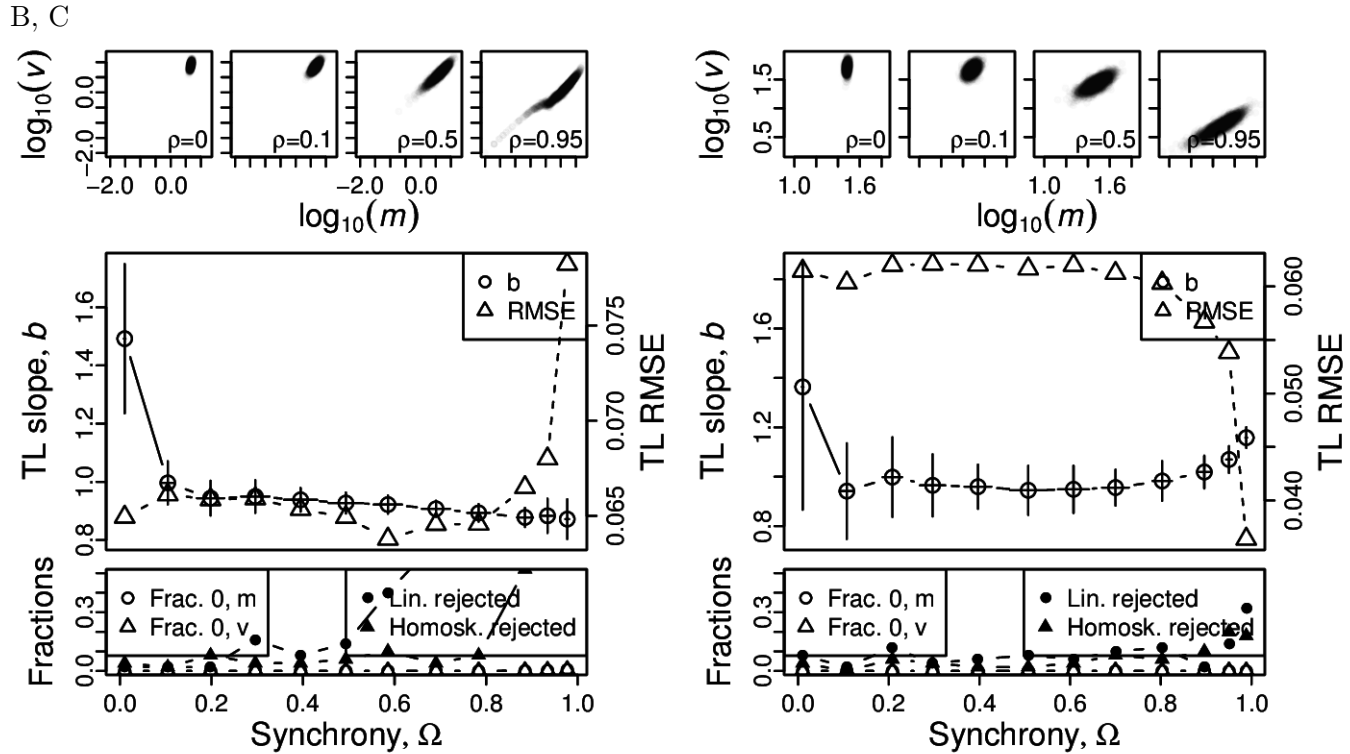
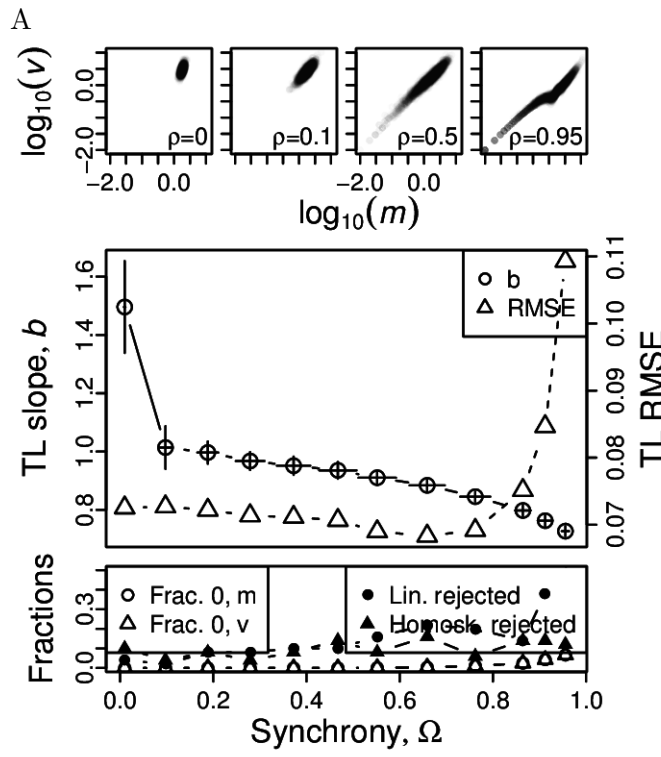


Figure S63: Omnibus plots (see section S6) for non-identically distributed negative binomial marginals under the set up of section S4, for  $n = 100$  and  $Y_1$  with  $p = 0.6$  and  $r = 5$  (A),  $r = 10$  (B),  $r = 50$  (C).

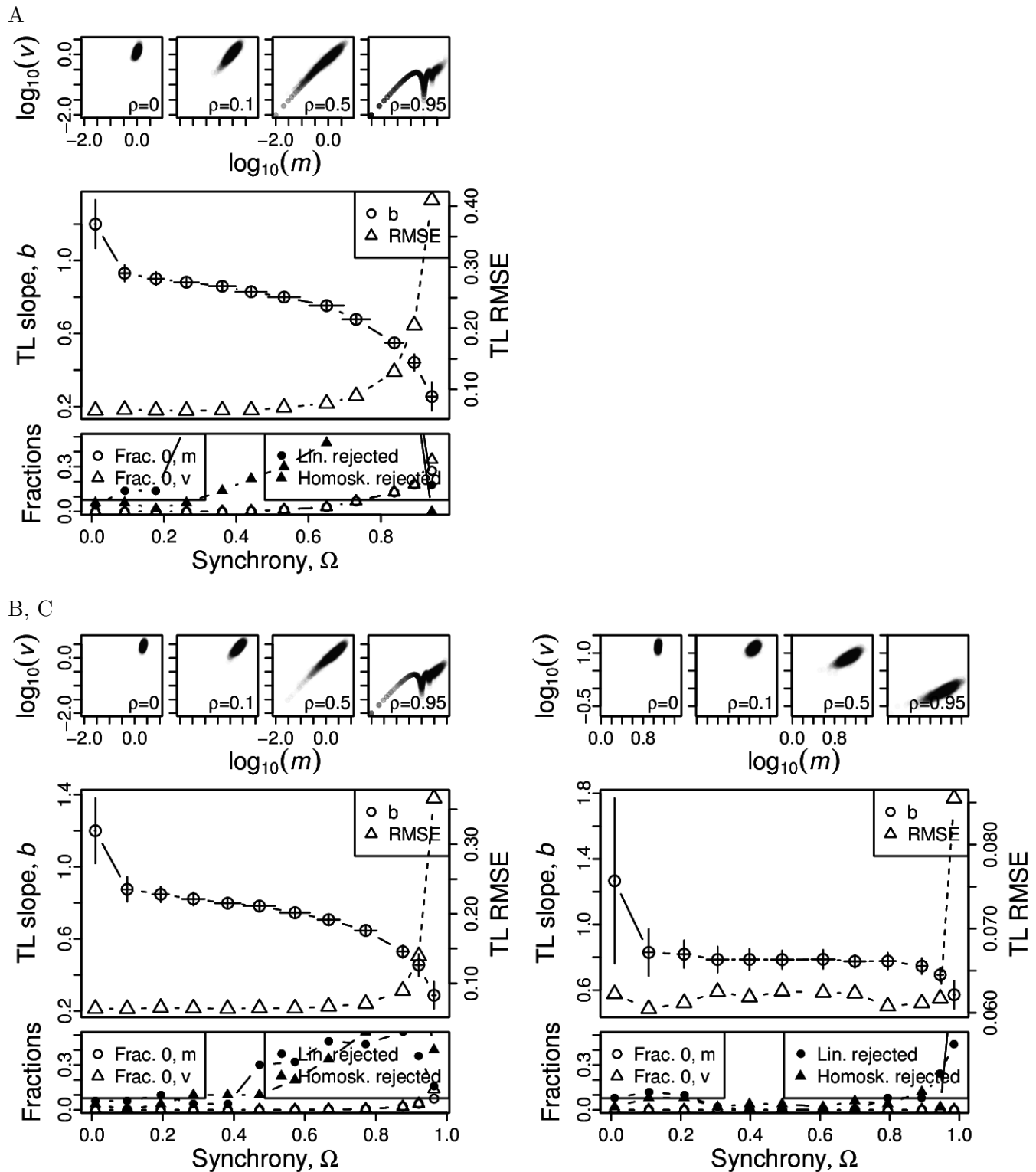
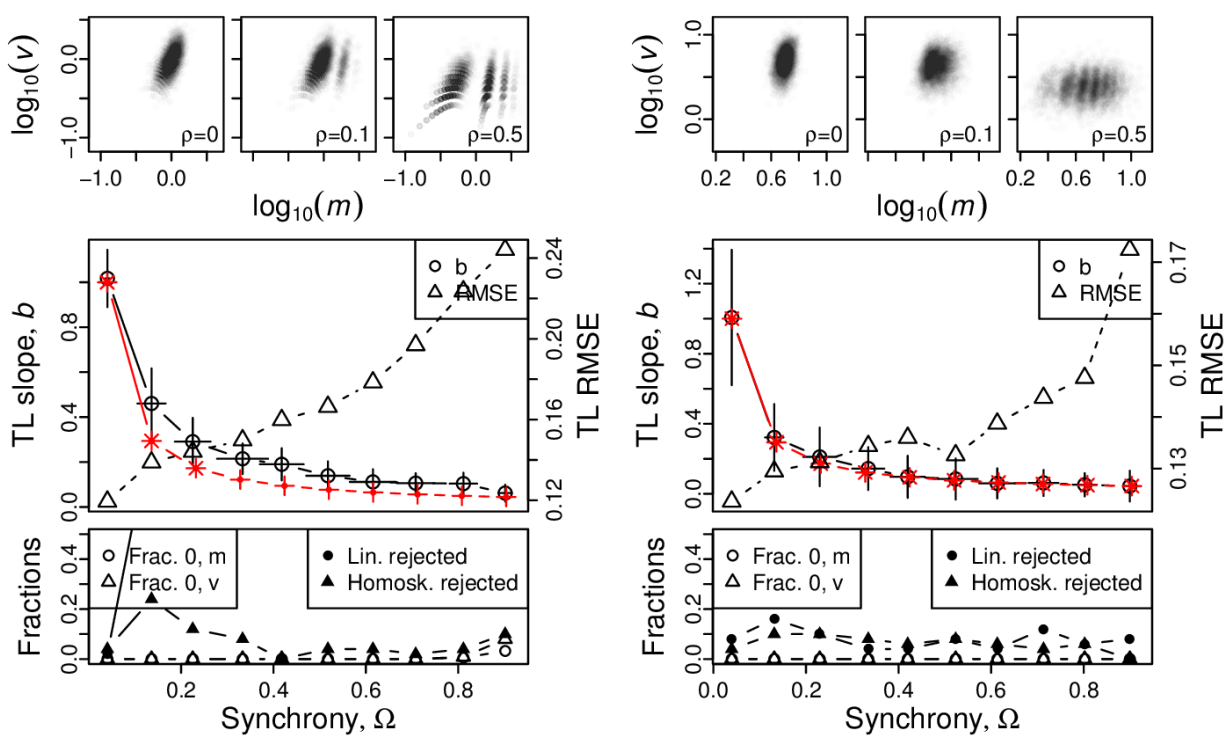


Figure S64: Omnibus plots (see section S6) for non-identically distributed negative binomial marginals under the set up of section S4, for  $n = 100$  and  $Y_1$  with  $p = 0.8$  and  $r = 5$  (A),  $r = 10$  (B),  $r = 50$  (C).

## S10 Figures, distributions constructed using sums and identically distributed marginals

A, B



C, D

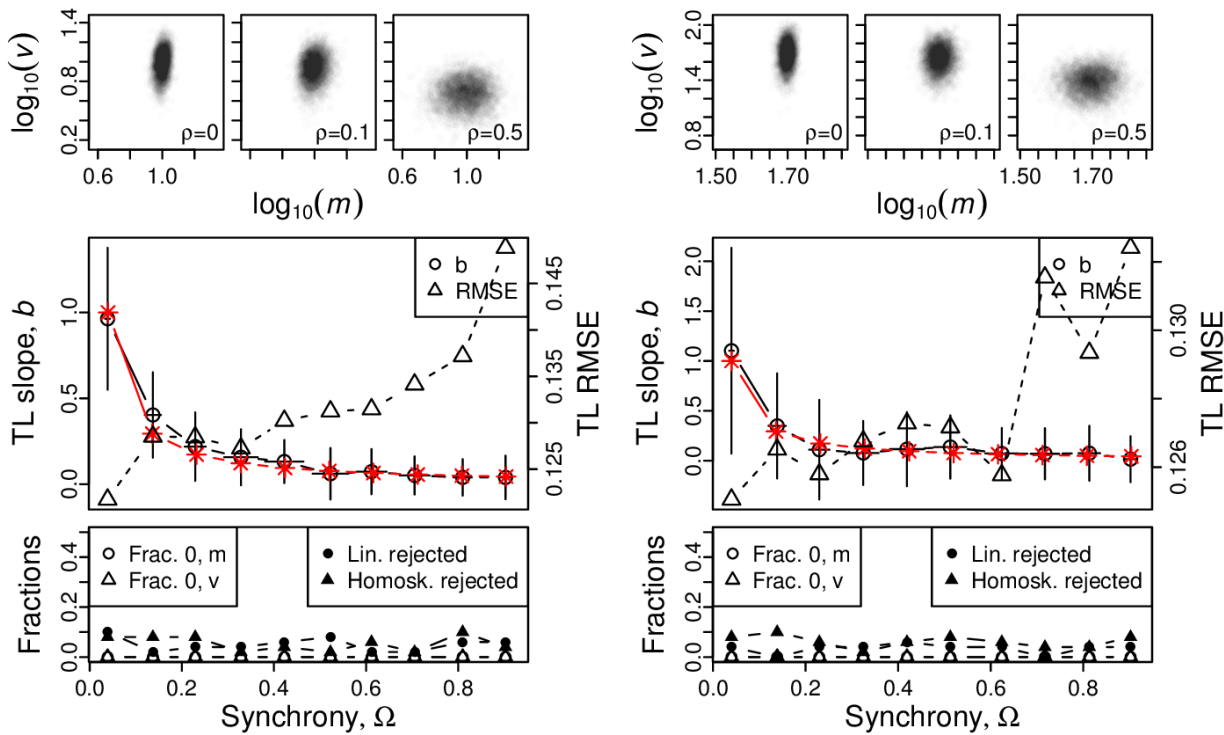
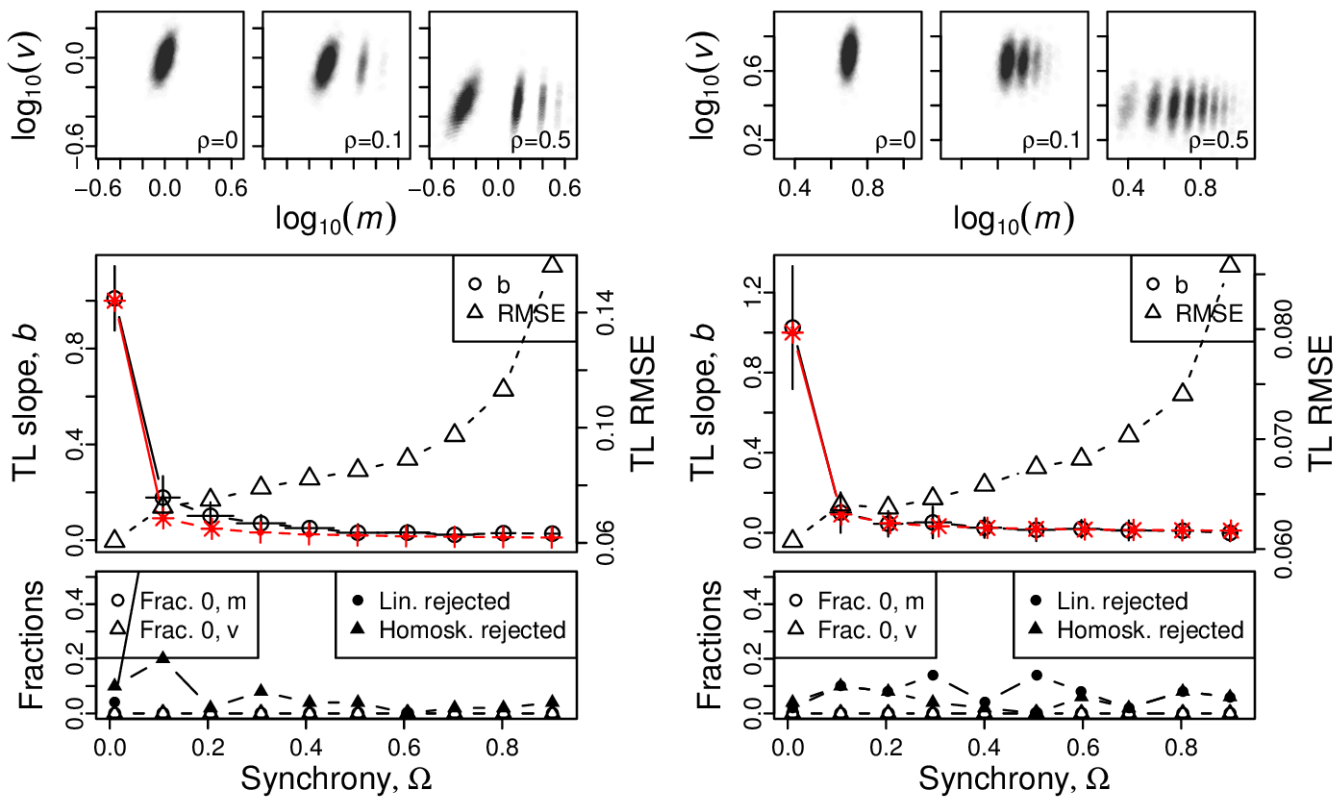


Figure S65: Omnibus plots (see section S6) for identically distributed Poisson marginals under the set up of section S5, for  $n = 25$ , for  $\lambda = 1$  (A),  $\lambda = 5$  (B),  $\lambda = 10$  (C), and  $\lambda = 50$  (D).

A, B



C, D

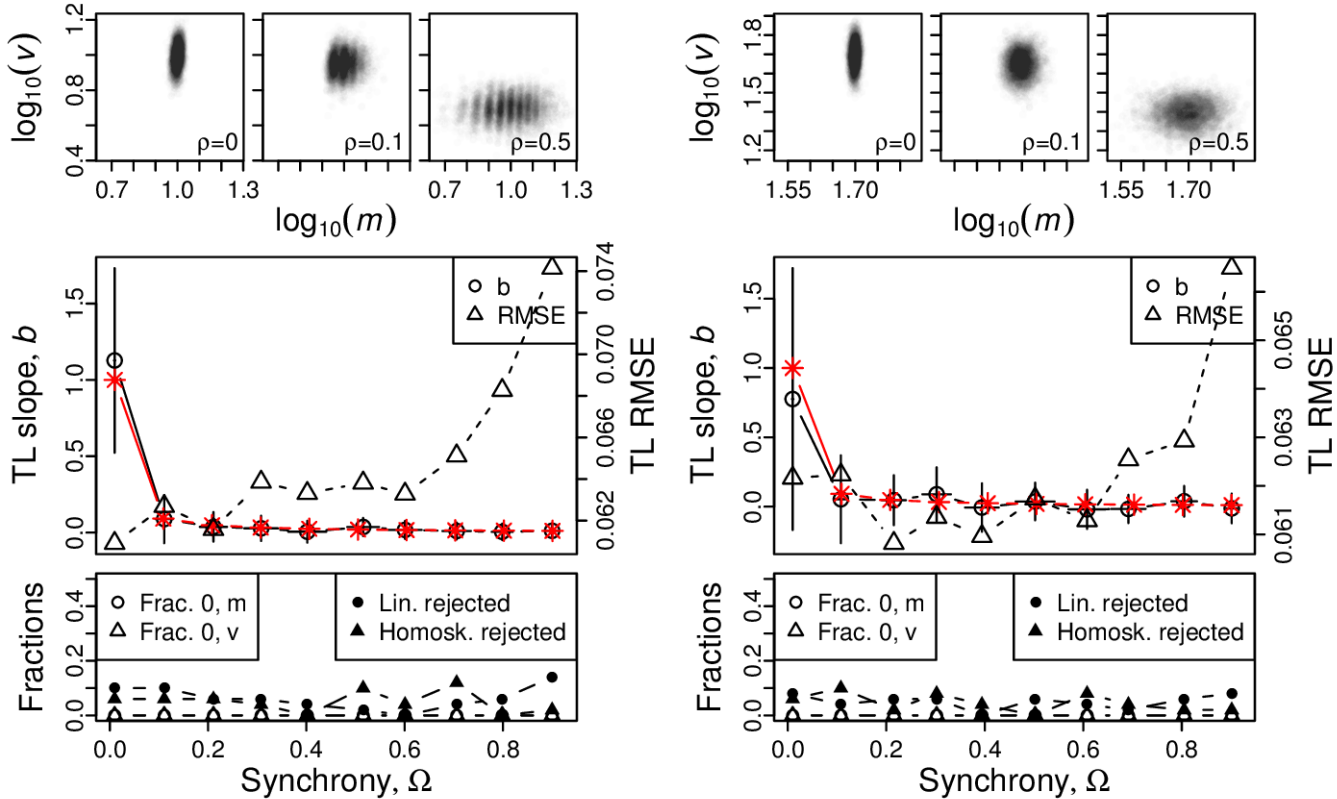
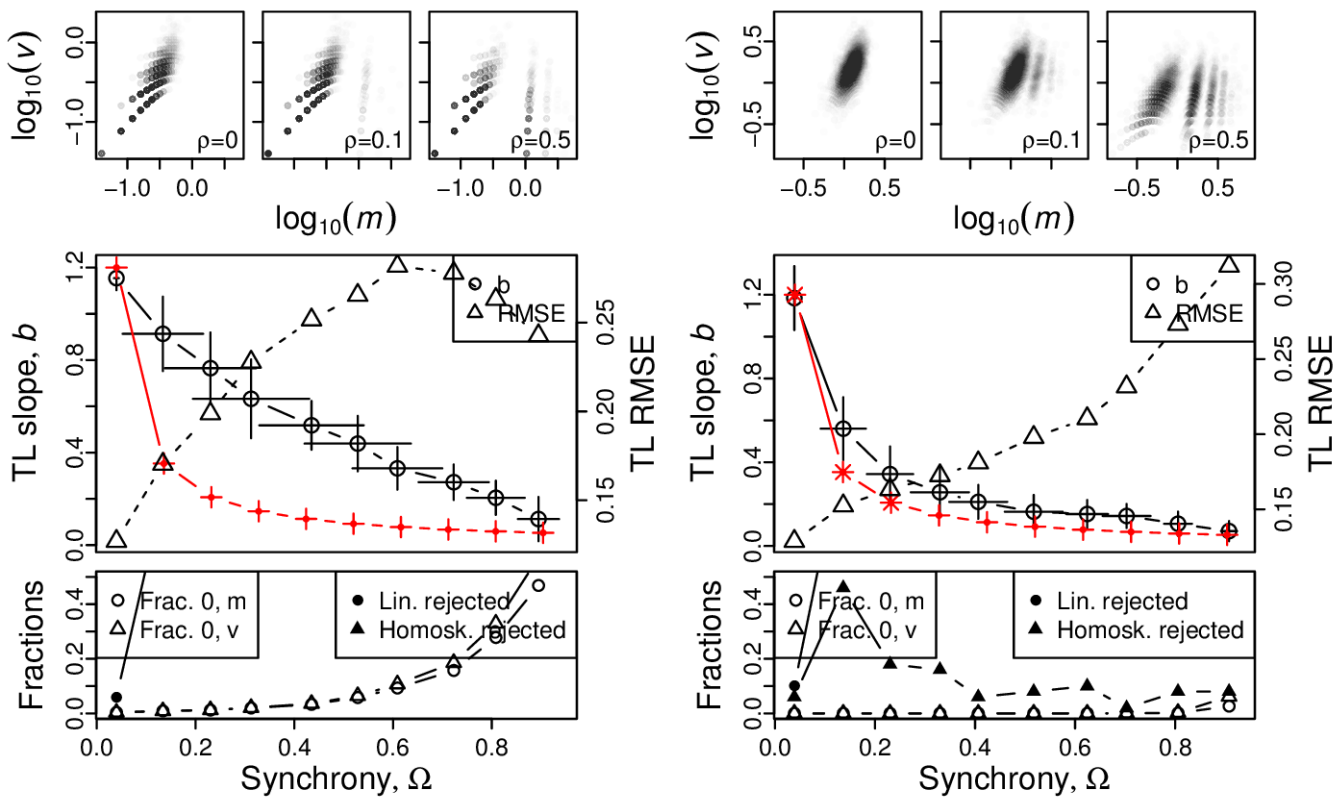


Figure S66: Omnibus plots (see section S6) for identically distributed Poisson marginals under the set up of section S5, for  $n = 100$ , for  $\lambda = 1$  (A),  $\lambda = 5$  (B),  $\lambda = 10$  (C), and  $\lambda = 50$  (D).

A, B



C, D

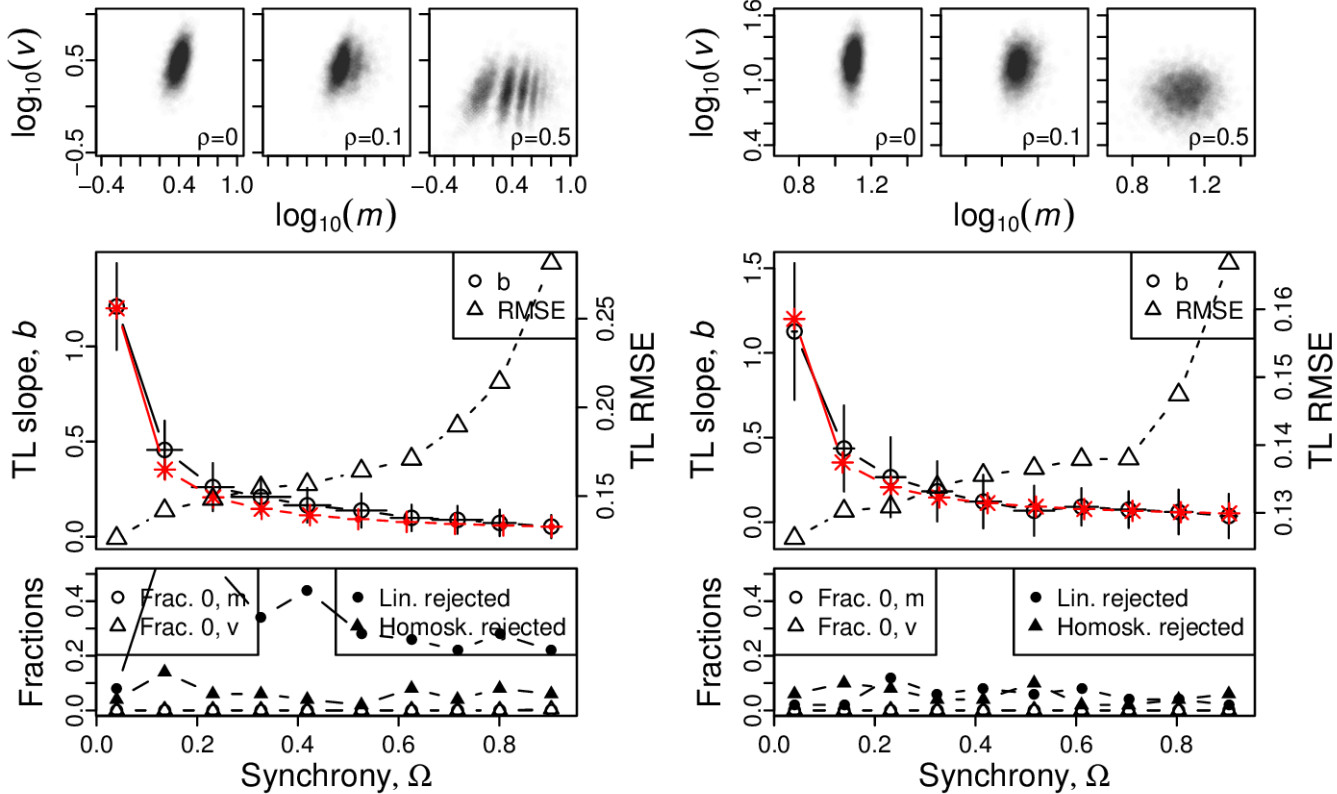
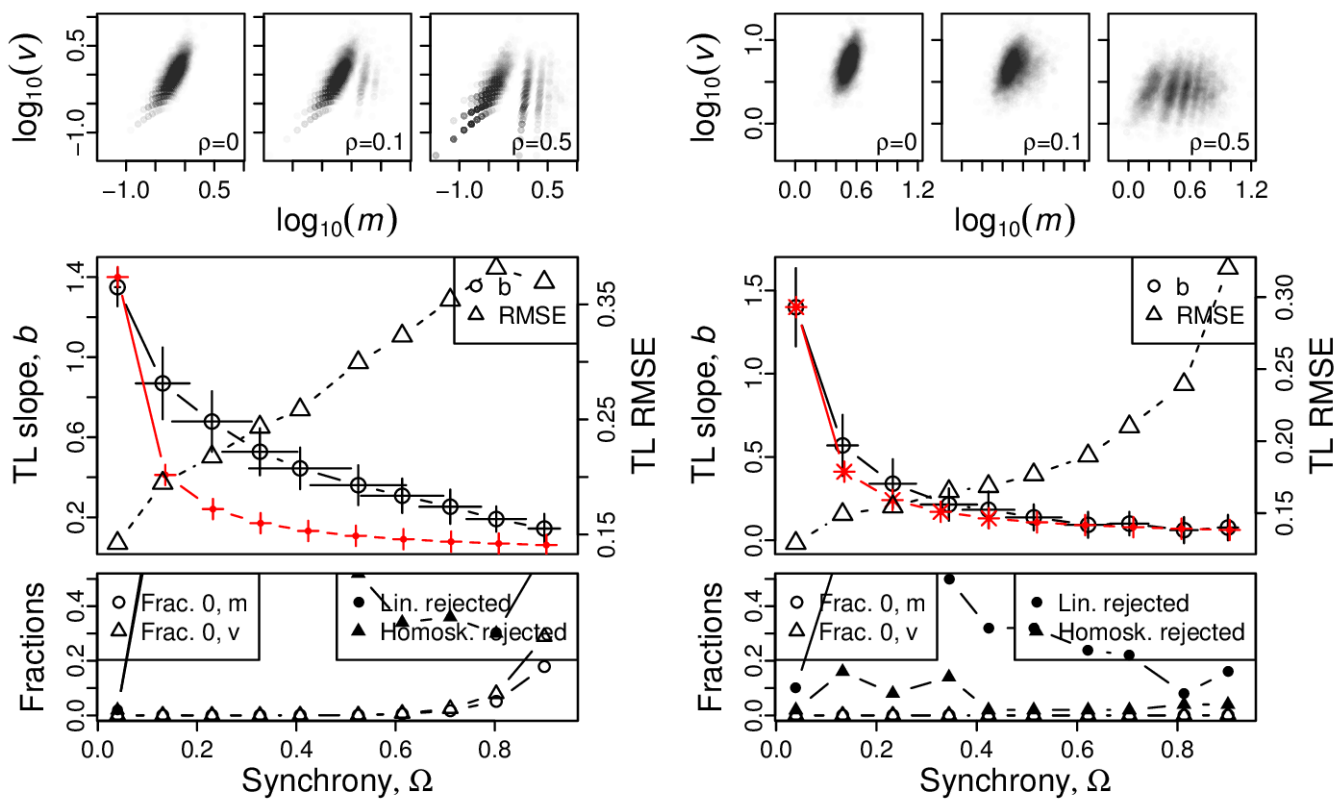


Figure S67: Omnibus plots (see section S6) for identically distributed negative binomial marginals under the set up of section S5, for  $n = 25$  and  $p = 0.2$ , for  $r = 1$  (A),  $r = 5$  (B),  $r = 10$  (C), and  $r = 50$  (D).

A, B



C, D

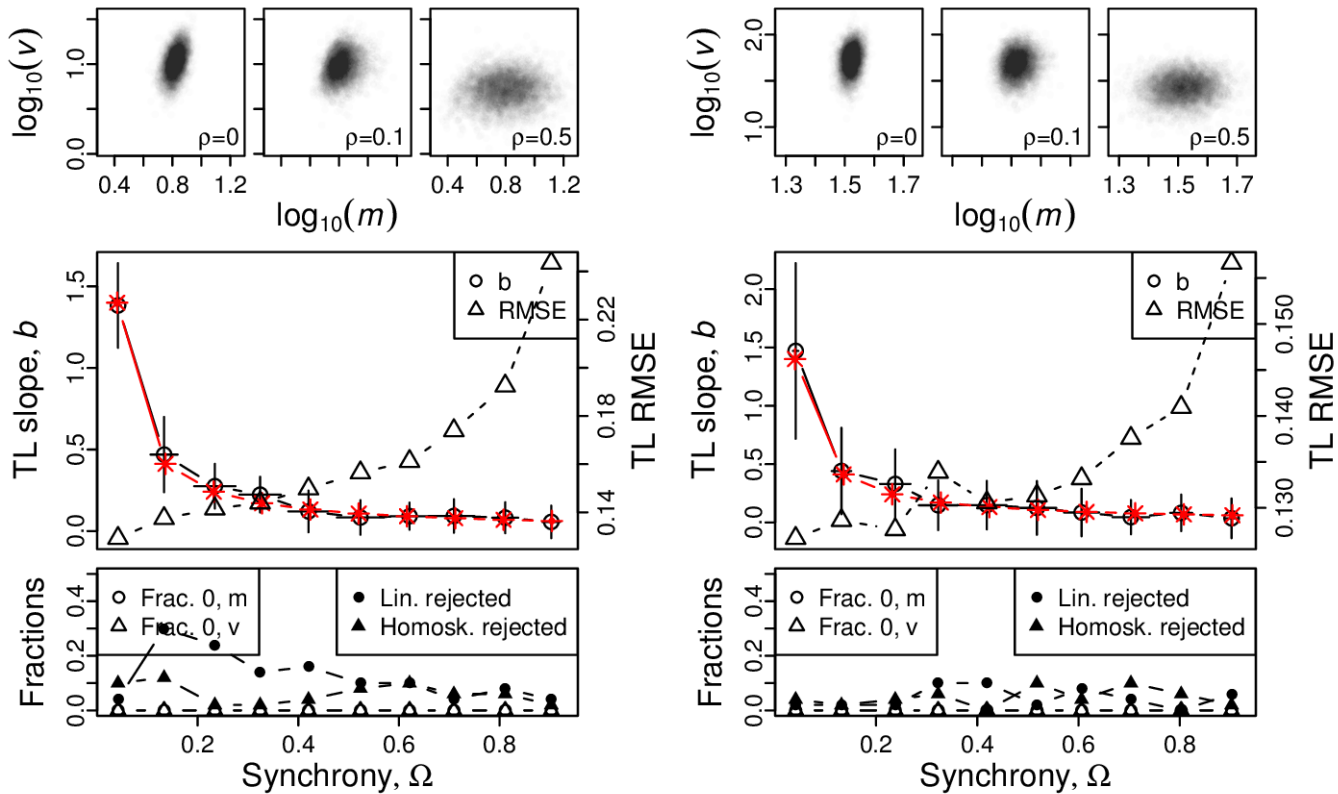
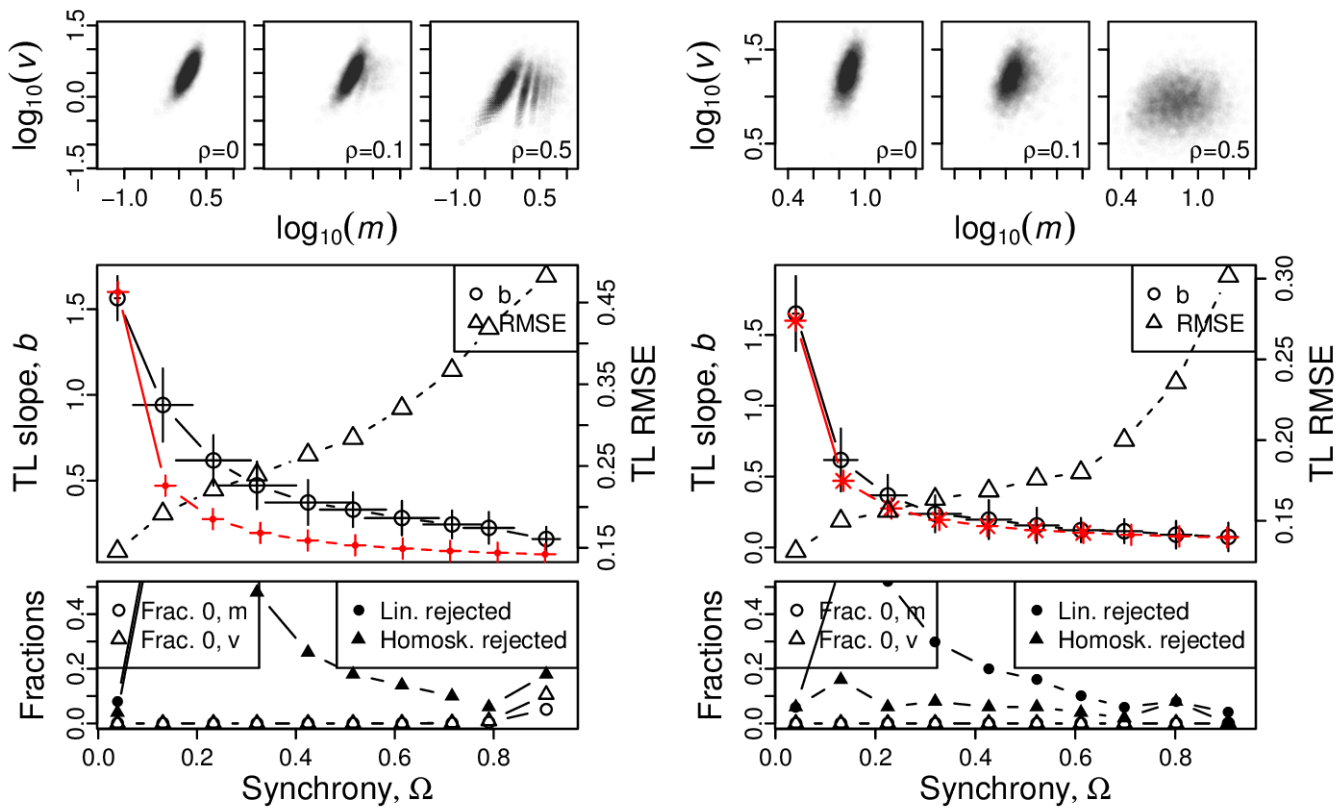


Figure S68: Omnibus plots (see section S6) for identically distributed negative binomial marginals under the set up of section S5, for  $n = 25$  and  $p = 0.4$ , for  $r = 1$  (A),  $r = 5$  (B),  $r = 10$  (C), and  $r = 50$  (D).

A, B



C, D

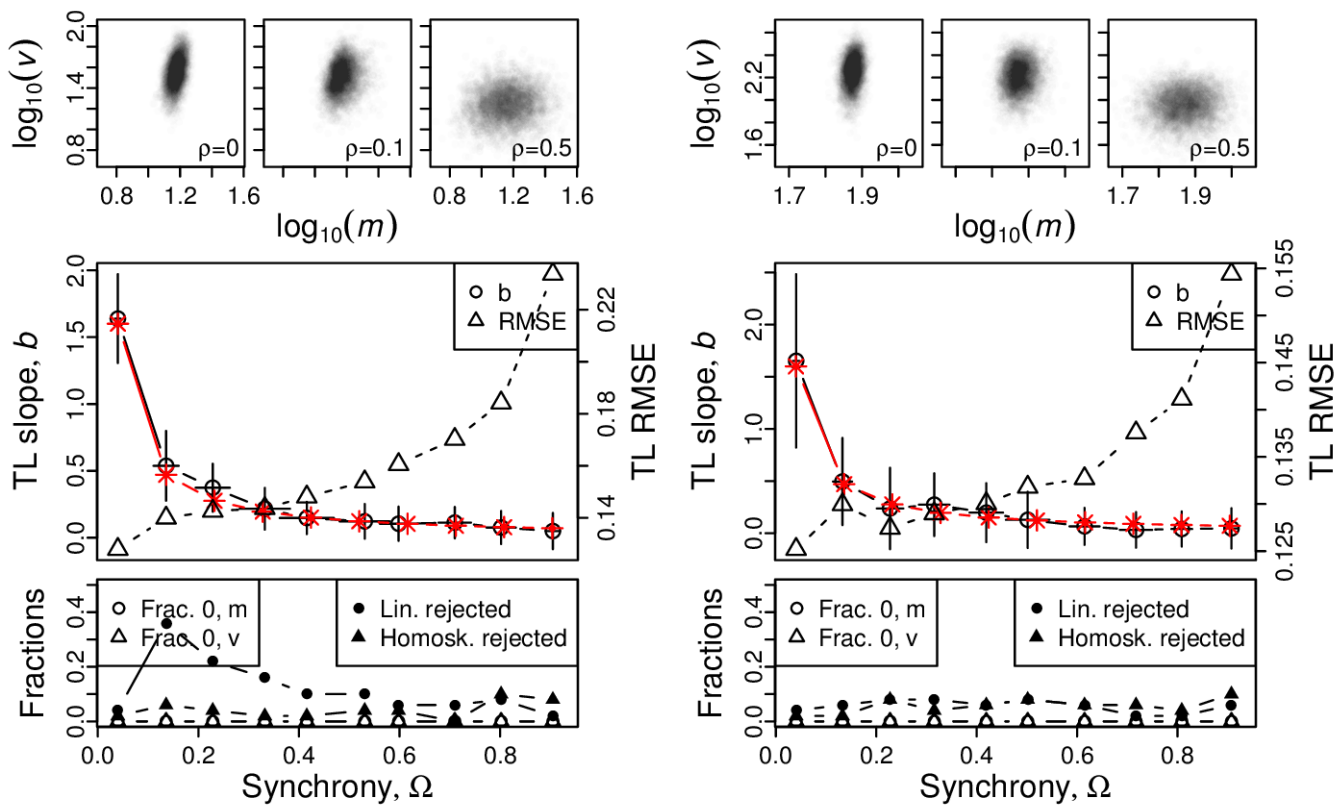
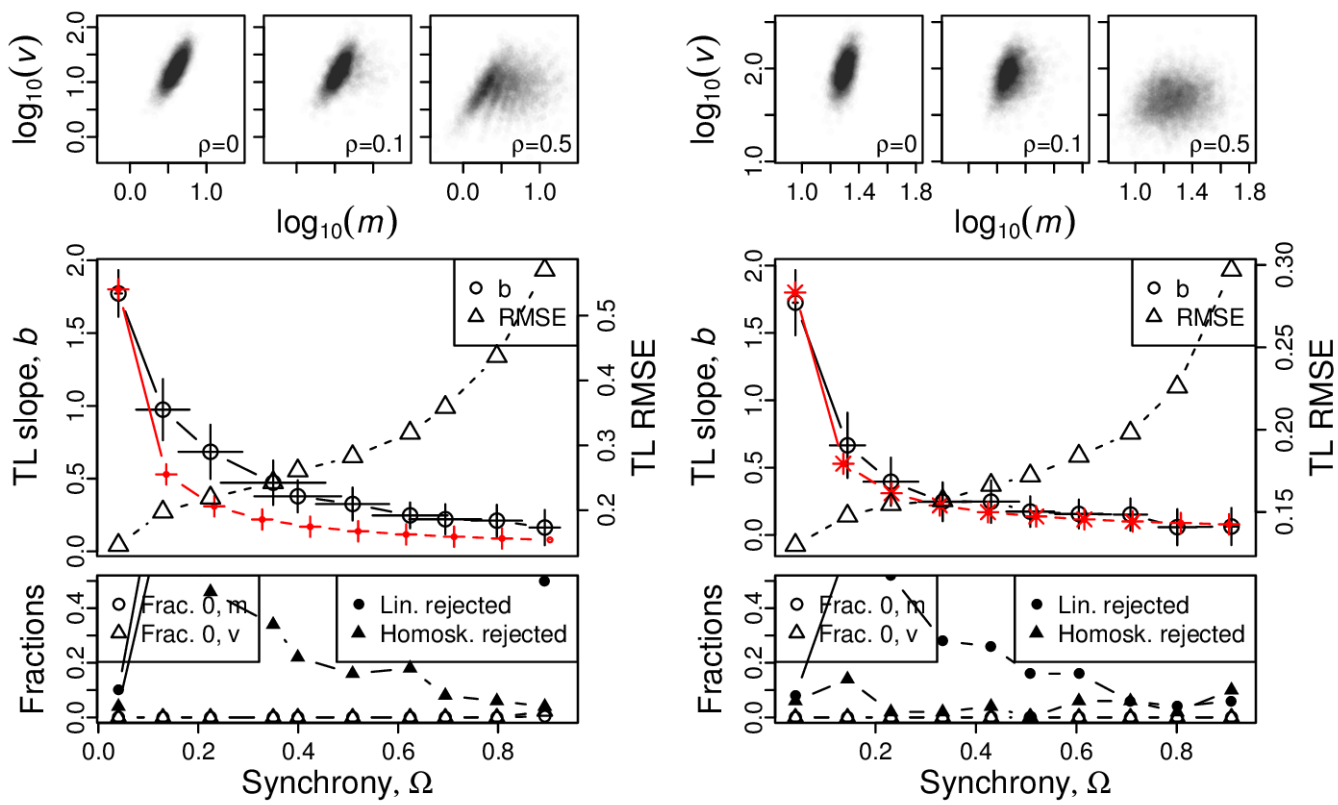


Figure S69: Omnibus plots (see section S6) for identically distributed negative binomial marginals under the set up of section S5, for  $n = 25$  and  $p = 0.6$ , for  $r = 1$  (A),  $r = 5$  (B),  $r = 10$  (C), and  $r = 50$  (D).

A, B



C, D

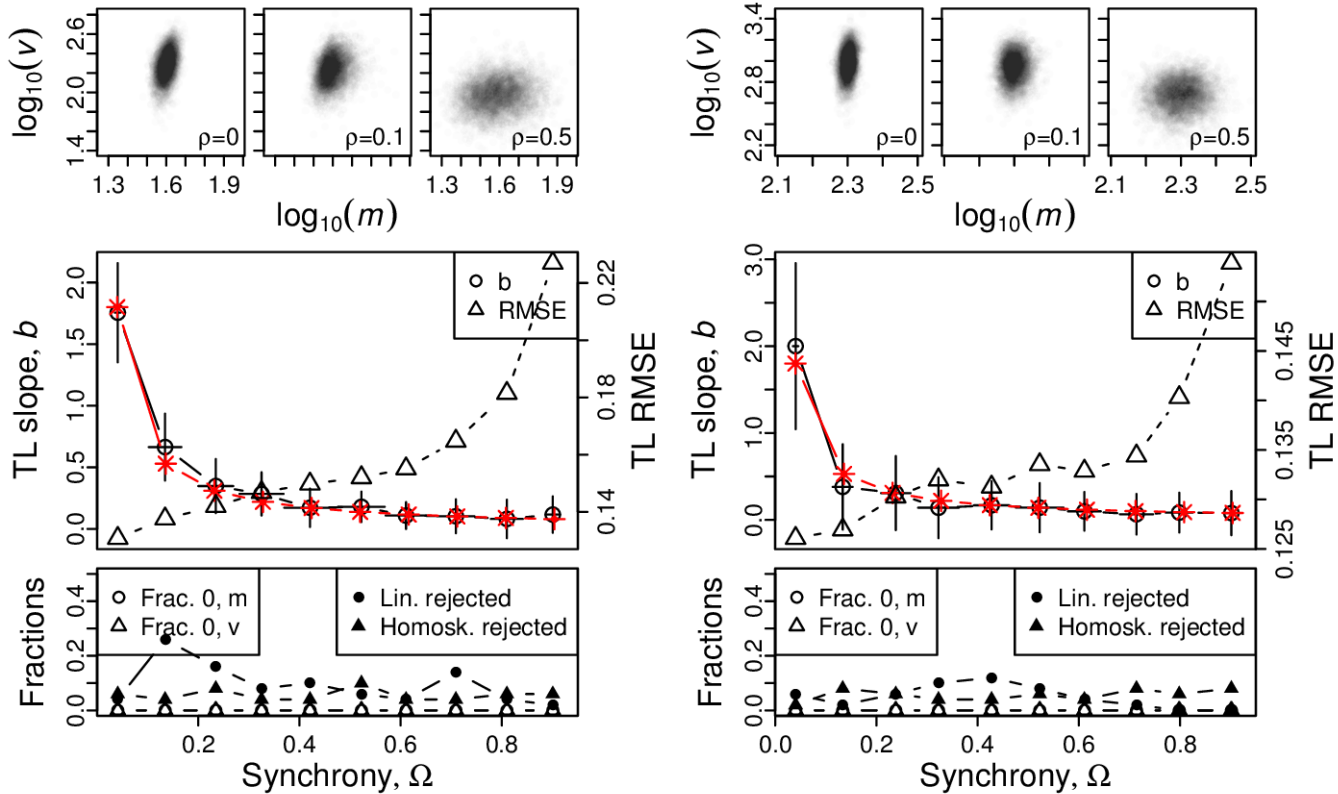


Figure S70: Omnibus plots (see section S6) for identically distributed negative binomial marginals under the set up of section S5, for  $n = 25$  and  $p = 0.8$ , for  $r = 1$  (A),  $r = 5$  (B),  $r = 10$  (C), and  $r = 50$  (D).

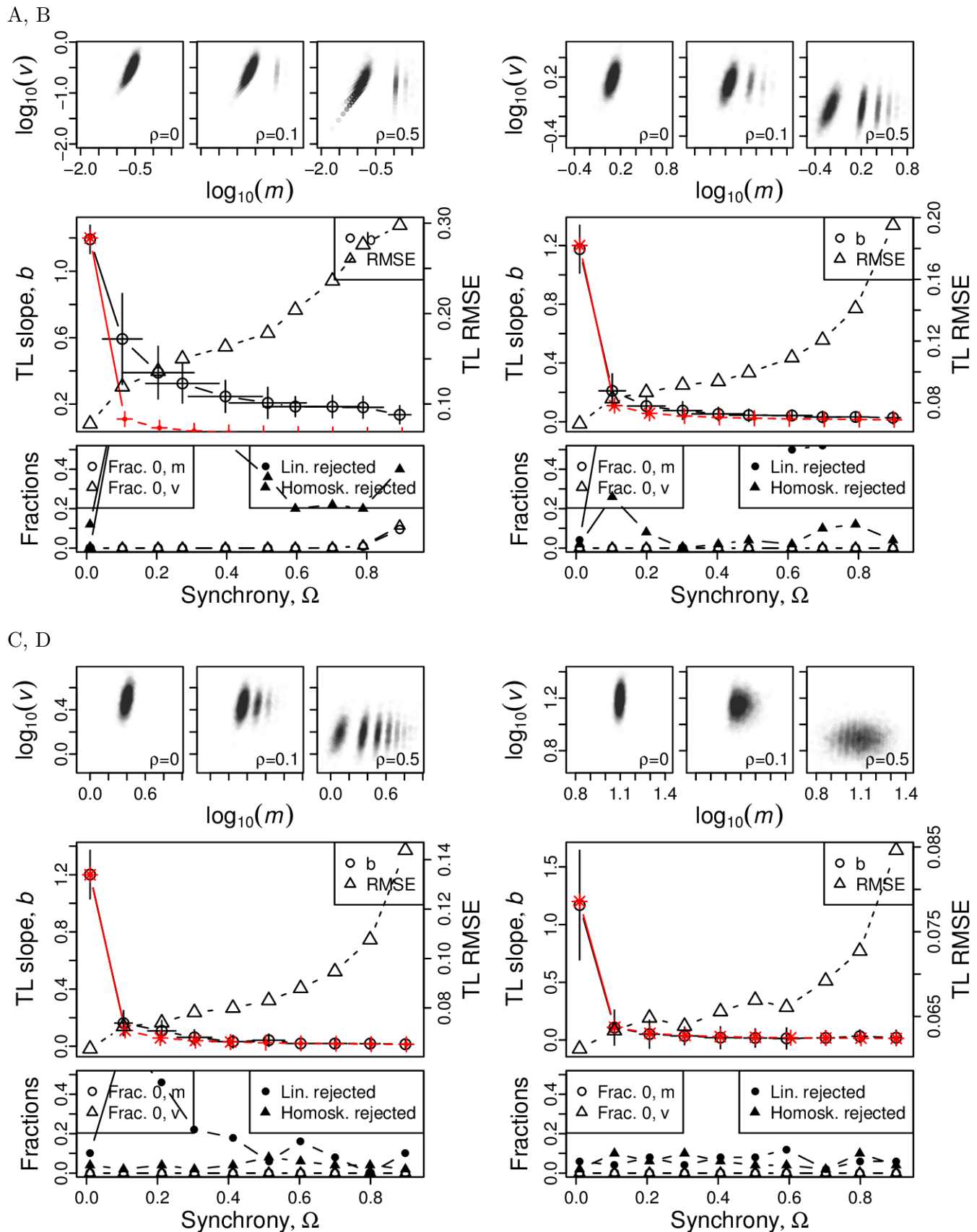
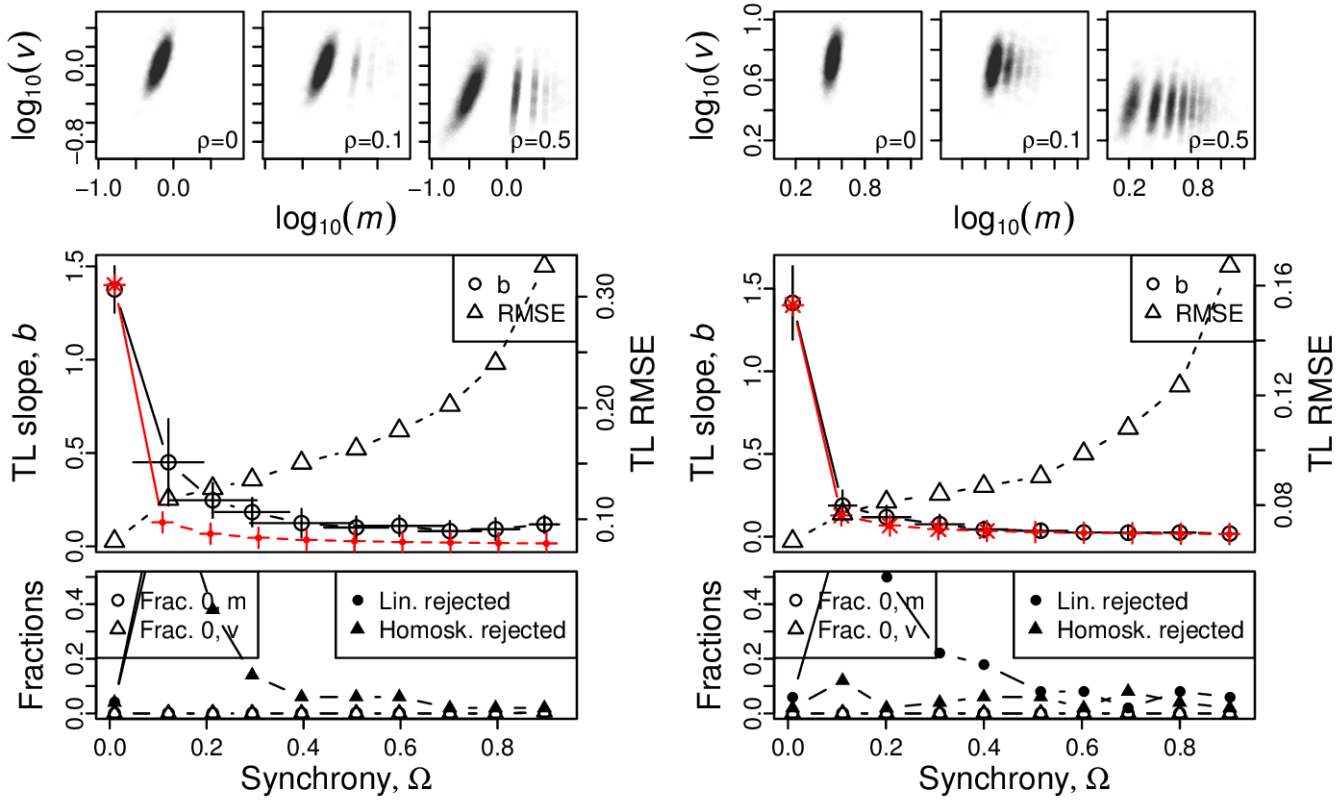


Figure S71: Omnibus plots (see section S6) for identically distributed negative binomial marginals under the set up of section S5, for  $n = 100$  and  $p = 0.2$ , for  $r = 1$  (A),  $r = 5$  (B),  $r = 10$  (C), and  $r = 50$  (D).

A, B



C, D

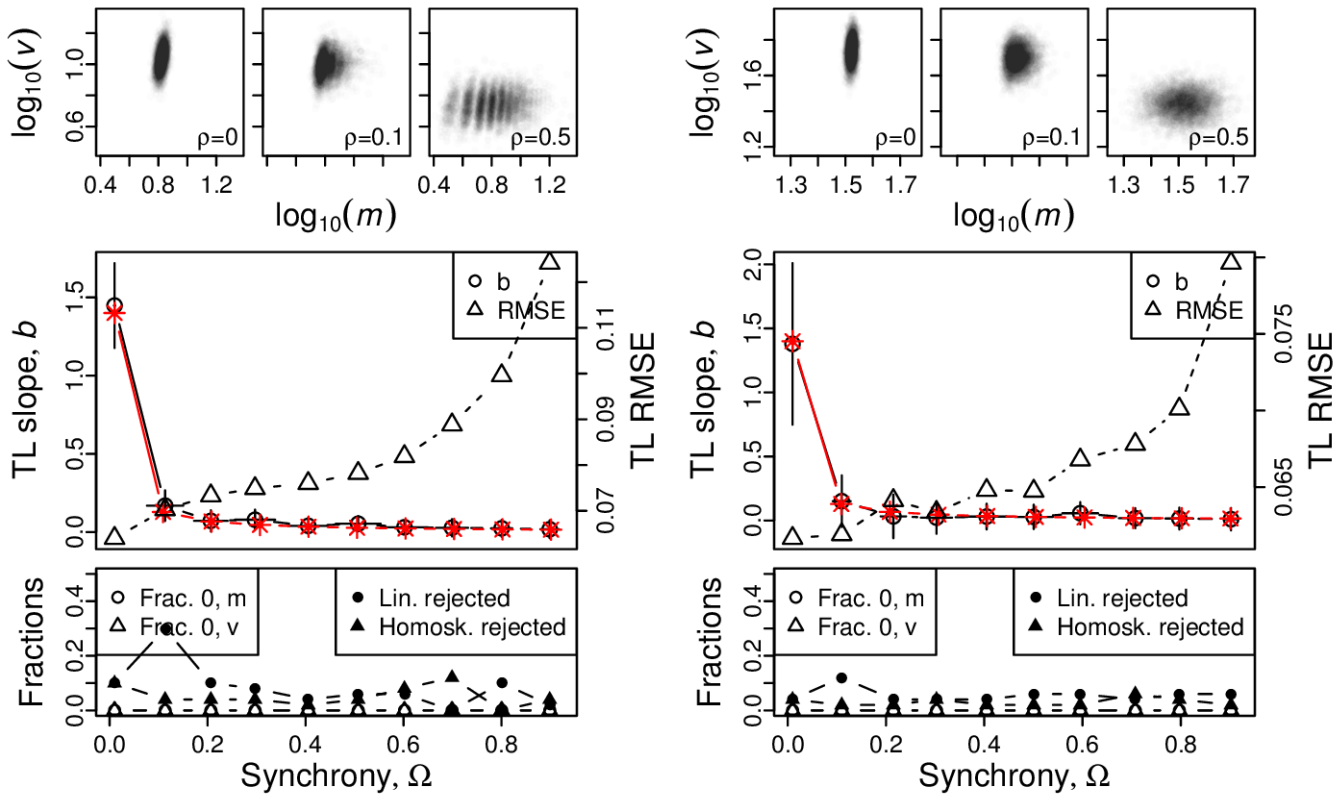
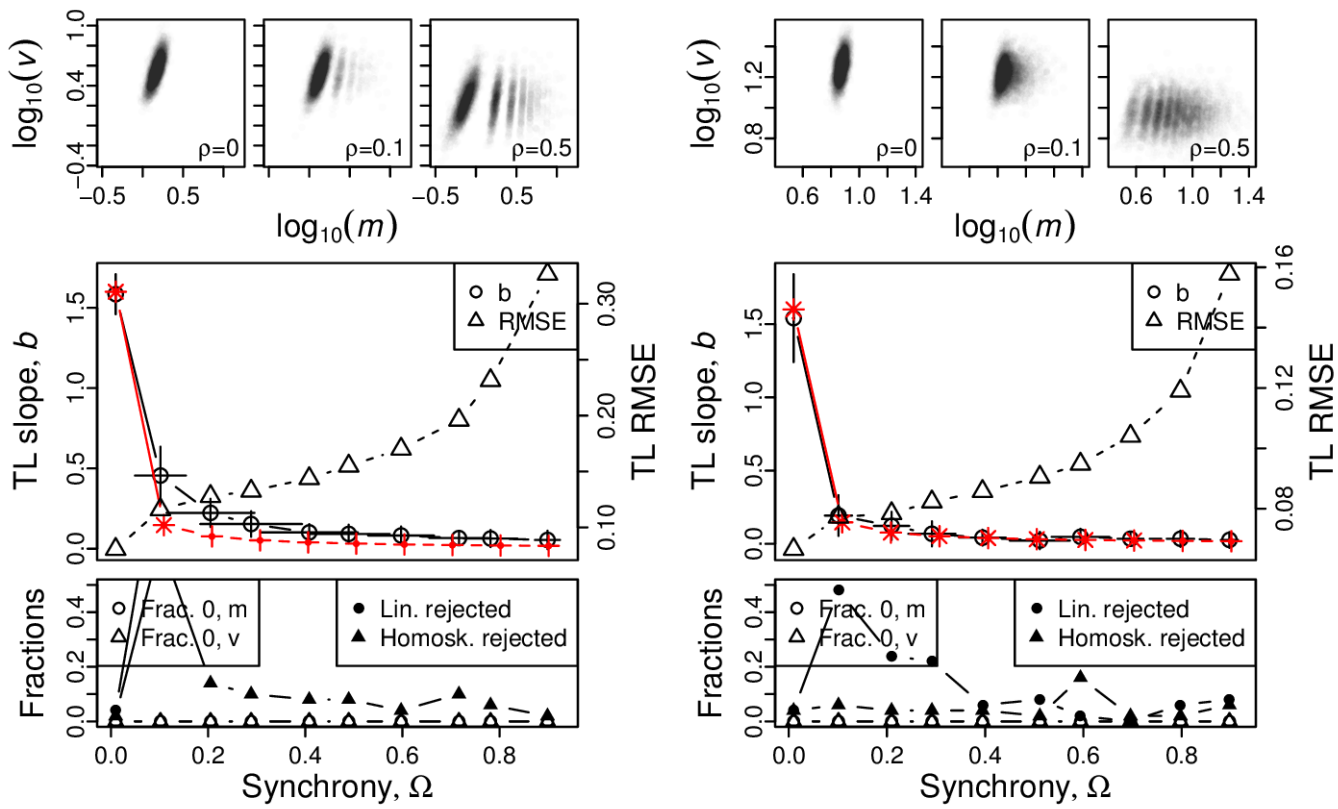


Figure S72: Omnibus plots (see section S6) for identically distributed negative binomial marginals under the set up of section S5, for  $n = 100$  and  $p = 0.4$ , for  $r = 1$  (A),  $r = 5$  (B),  $r = 10$  (C), and  $r = 50$  (D).

A, B



C, D

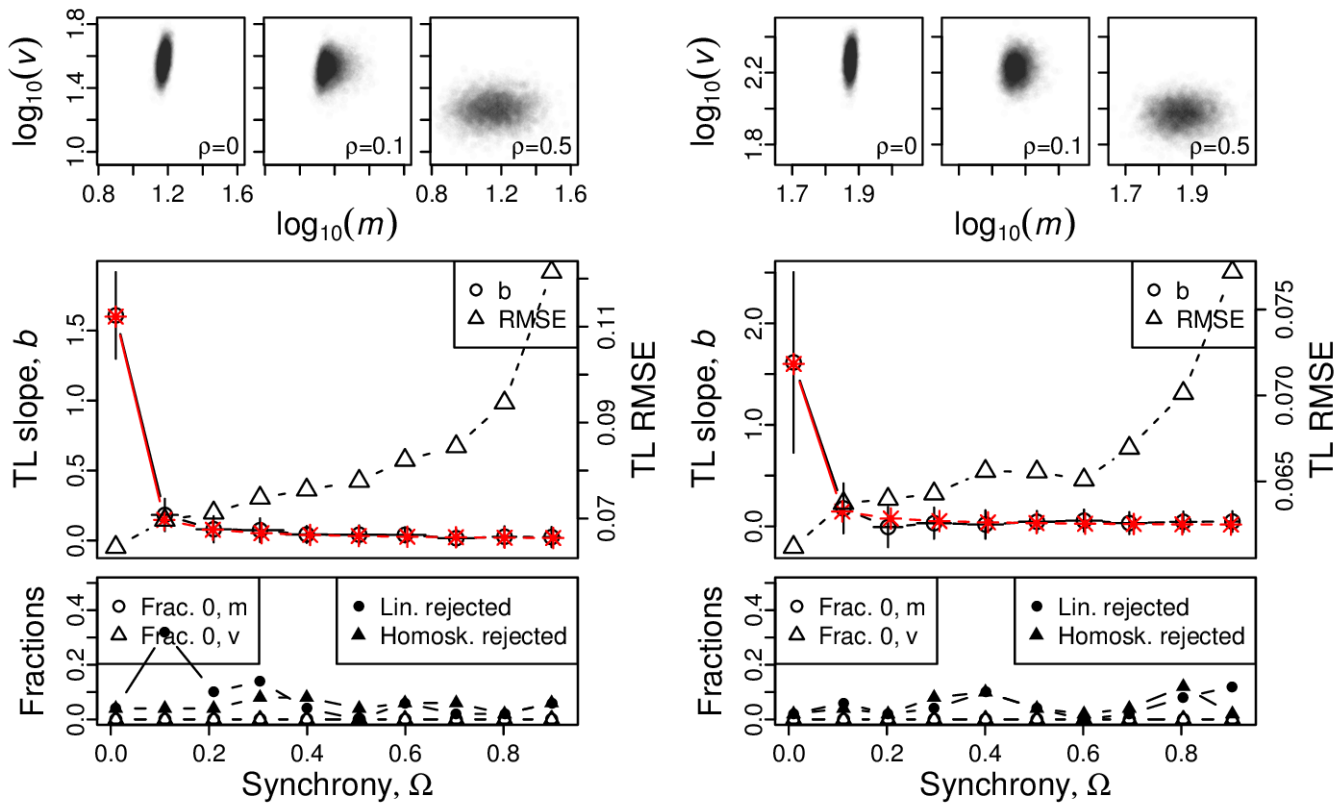
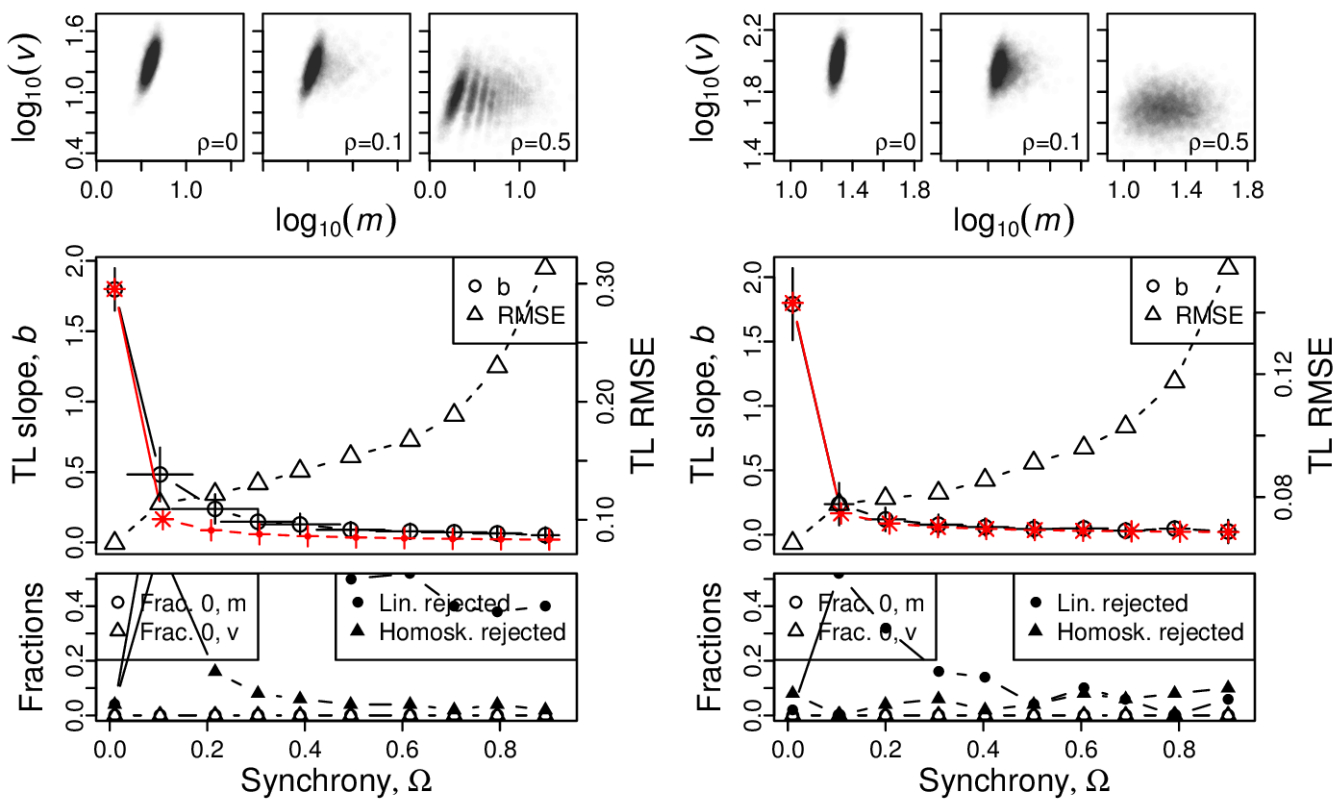


Figure S73: Omnibus plots (see section S6) for identically distributed negative binomial marginals under the set up of section S5, for  $n = 100$  and  $p = 0.6$ , for  $r = 1$  (A),  $r = 5$  (B),  $r = 10$  (C), and  $r = 50$  (D).

A, B



C, D

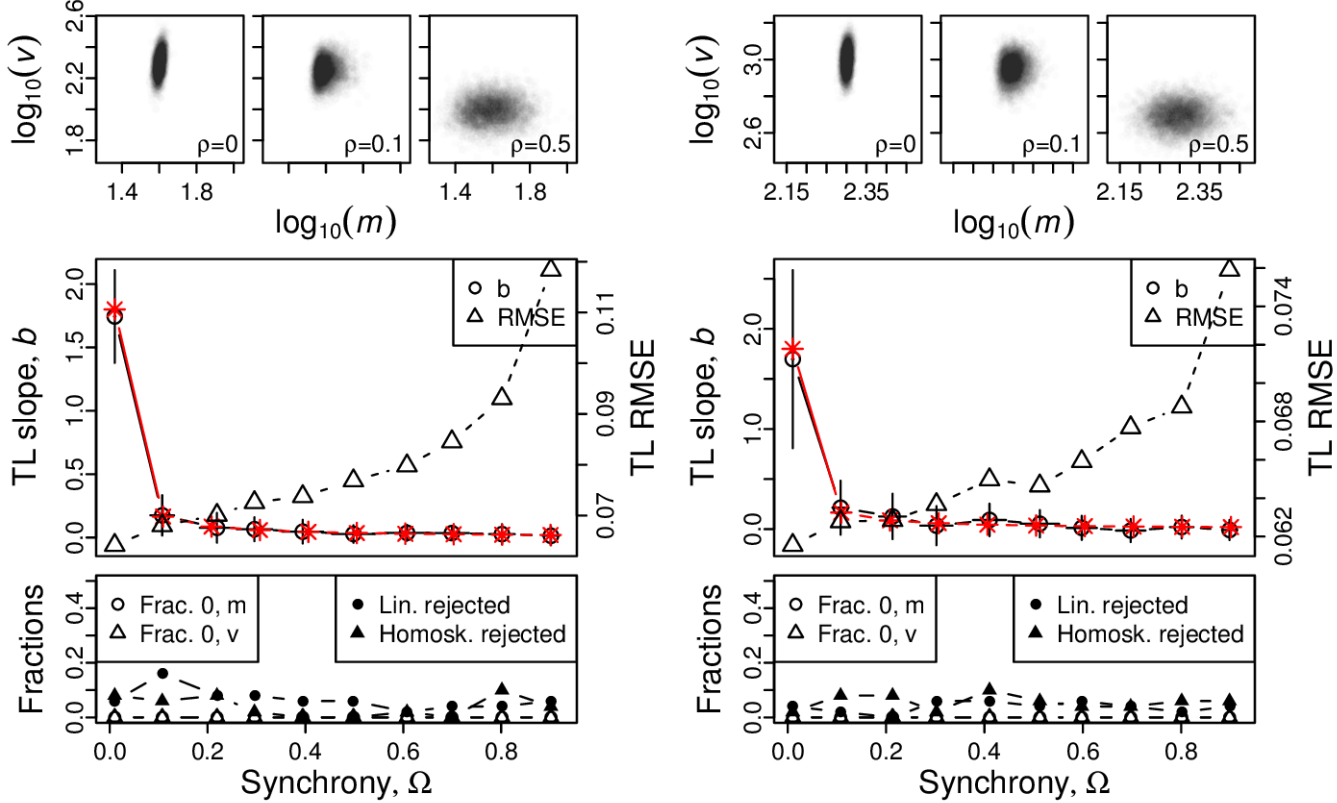


Figure S74: Omnibus plots (see section S6) for identically distributed negative binomial marginals under the set up of section S5, for  $n = 100$  and  $p = 0.8$ , for  $r = 1$  (A),  $r = 5$  (B),  $r = 10$  (C), and  $r = 50$  (D).

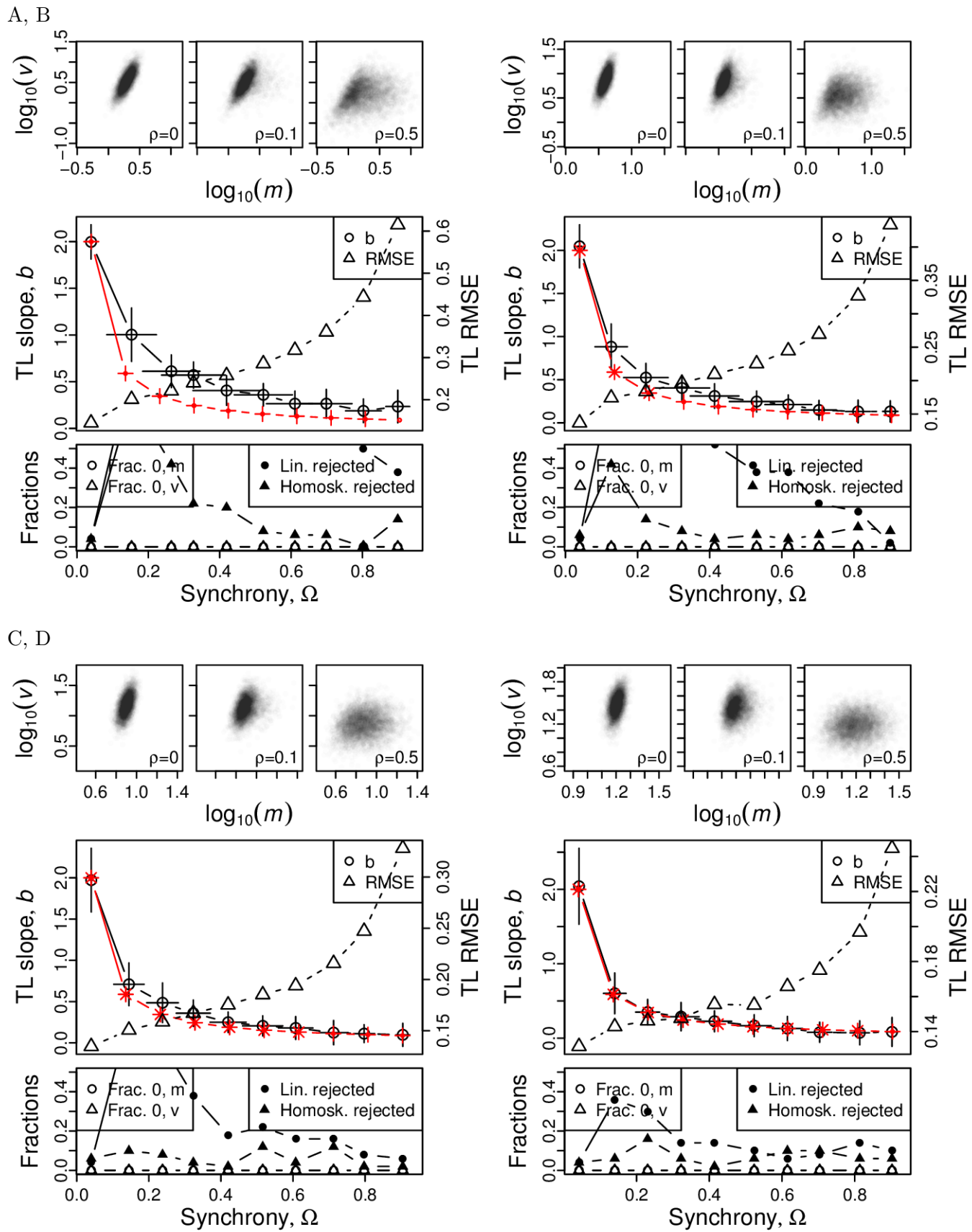
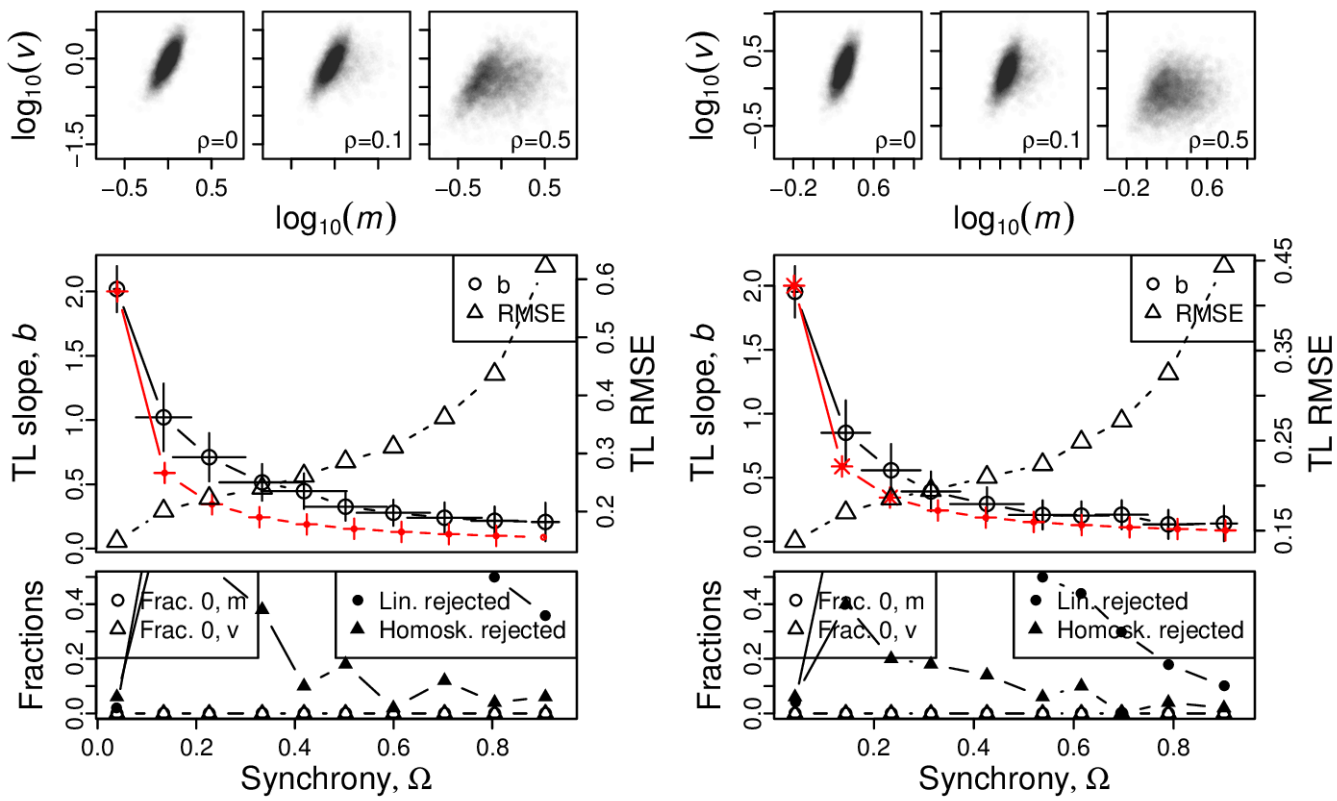


Figure S75: Omnibus plots (see section S6) for identically distributed gamma marginals under the set up of section S5, for  $n = 25$  and  $\beta = 0.5$ , for  $\alpha = 1$  (A),  $\alpha = 2$  (B),  $\alpha = 4$  (C), and  $\alpha = 8$  (D).

A, B



C, D

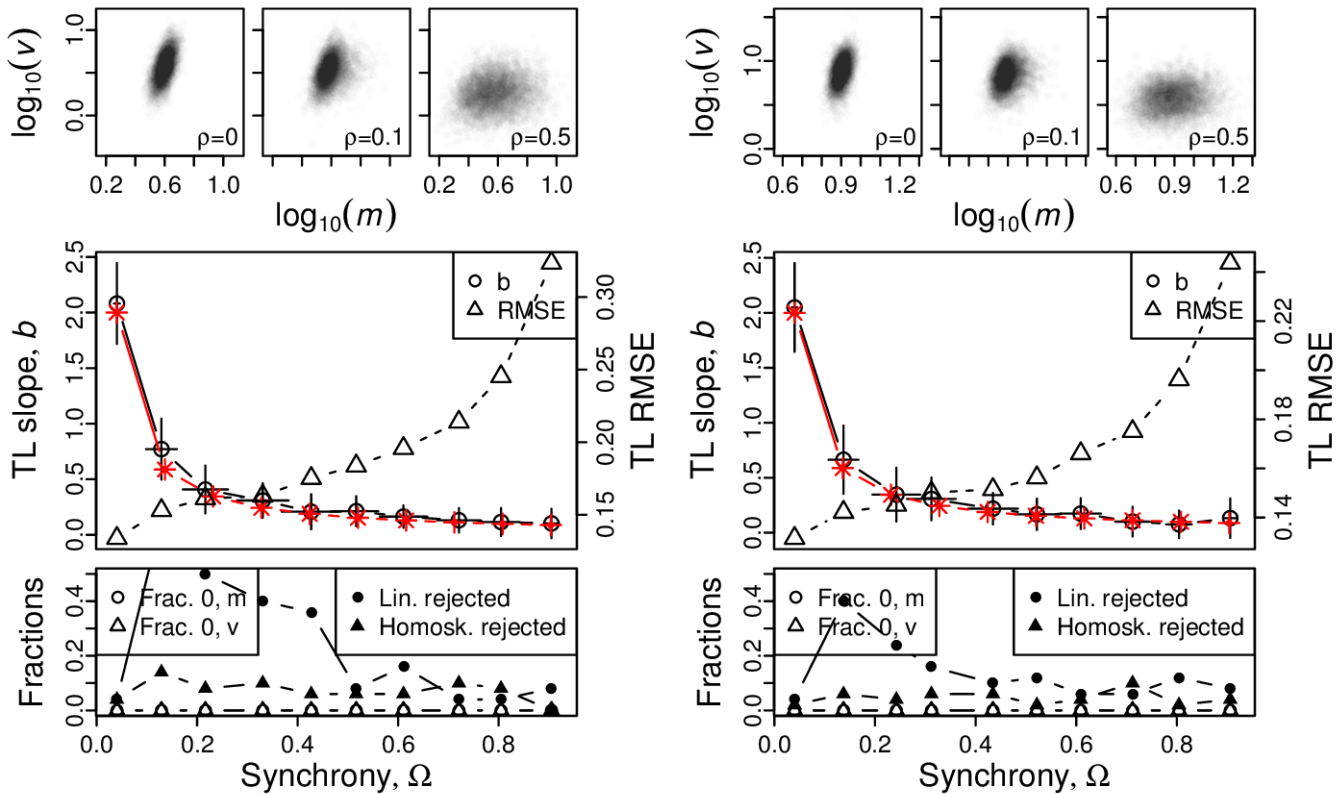
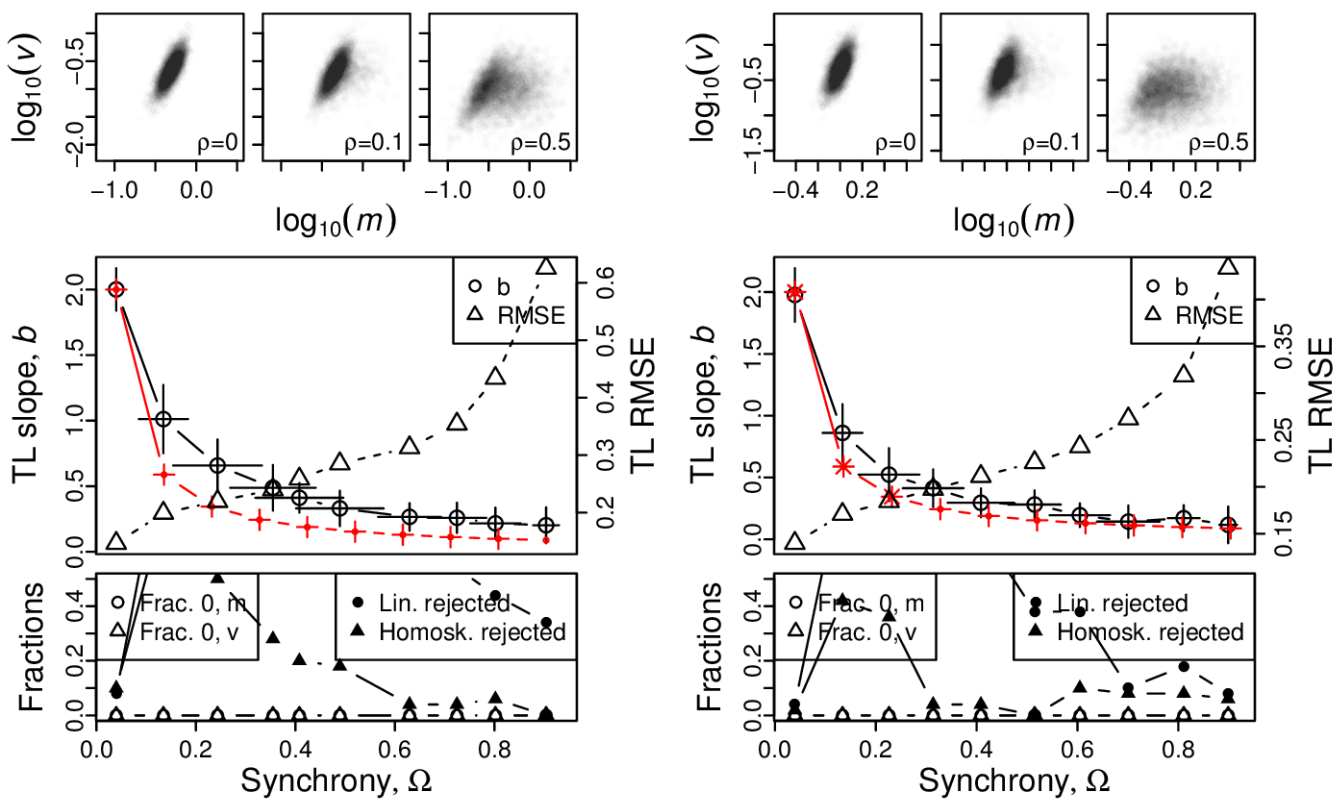


Figure S76: Omnibus plots (see section S6) for identically distributed gamma marginals under the set up of section S5, for  $n = 25$  and  $\beta = 1$ , for  $\alpha = 1$  (A),  $\alpha = 2$  (B),  $\alpha = 4$  (C), and  $\alpha = 8$  (D).

A, B



C, D

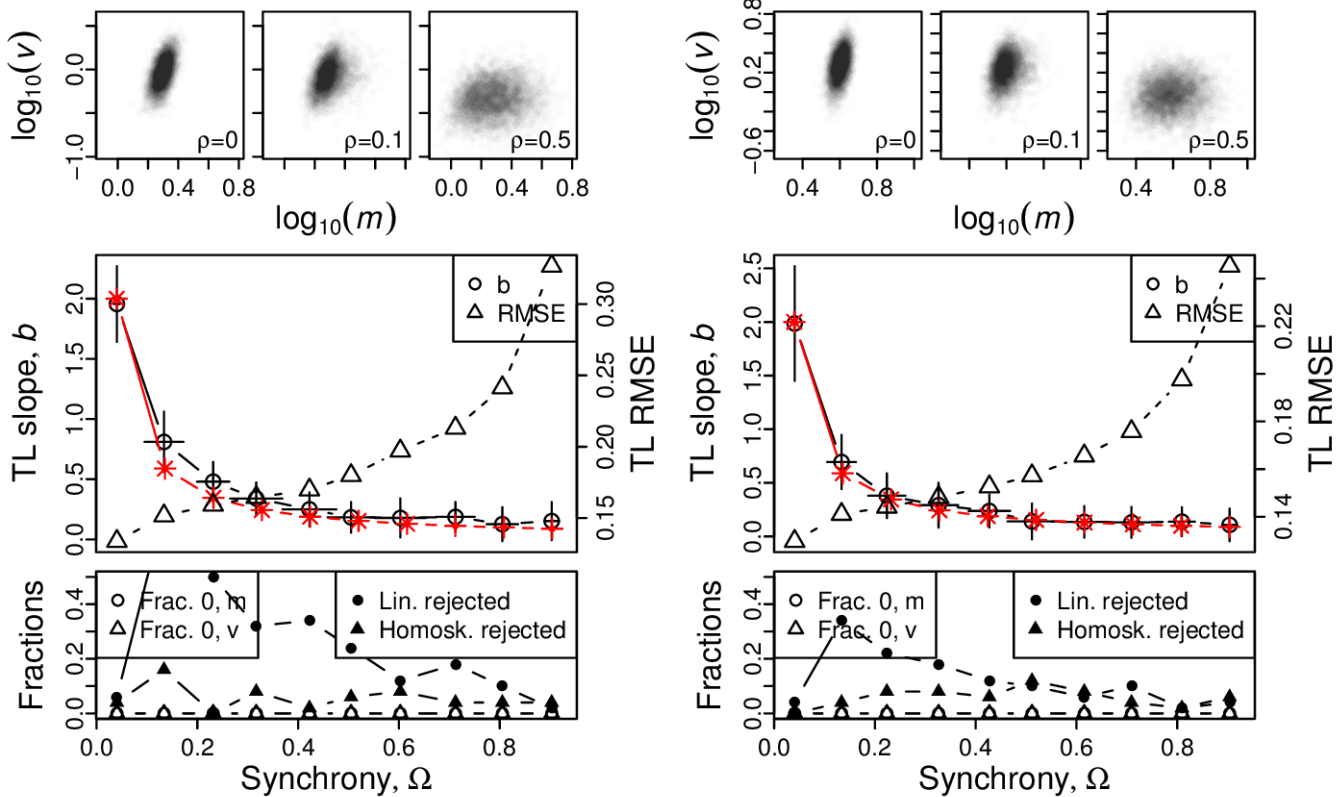
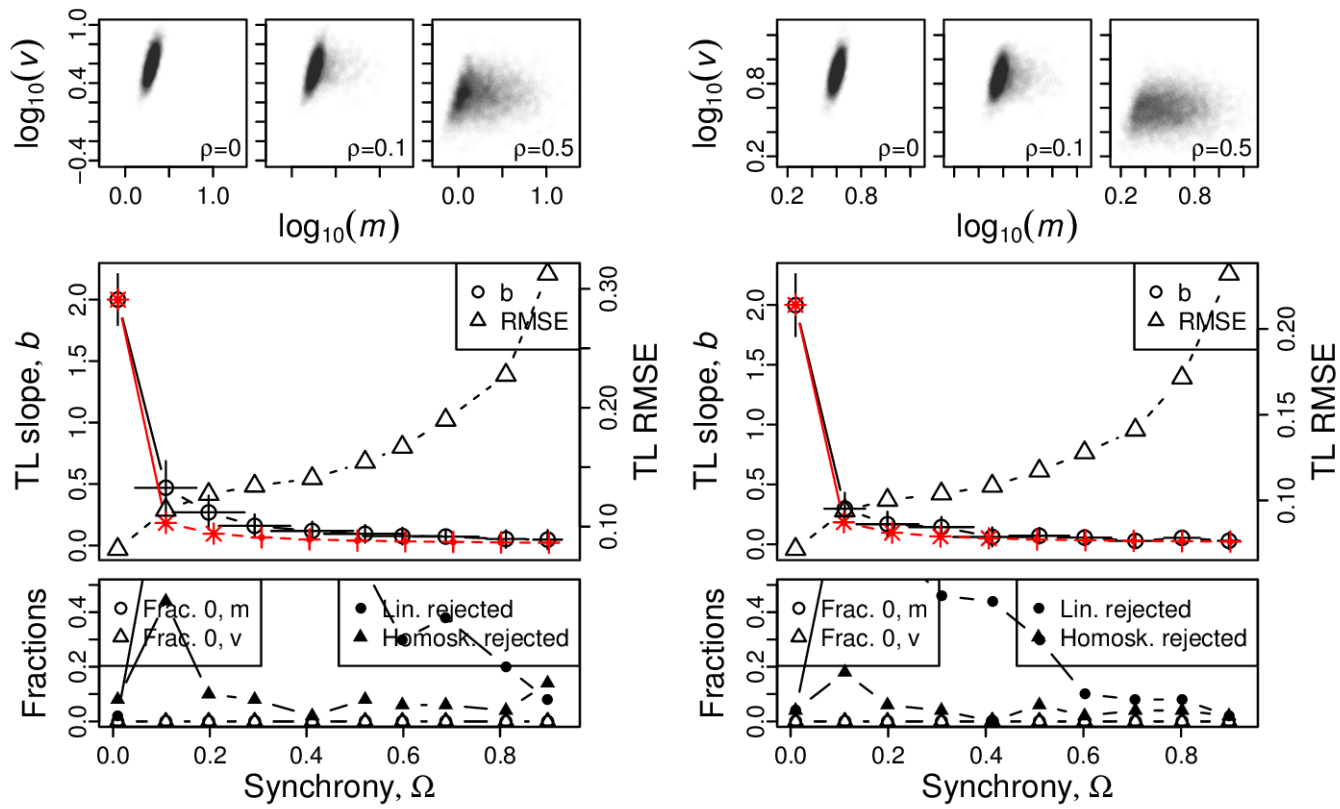


Figure S77: Omnibus plots (see section S6) for identically distributed gamma marginals under the set up of section S5, for  $n = 25$  and  $\beta = 2$ , for  $\alpha = 1$  (A),  $\alpha = 2$  (B),  $\alpha = 4$  (C), and  $\alpha = 8$  (D).

A, B



C, D

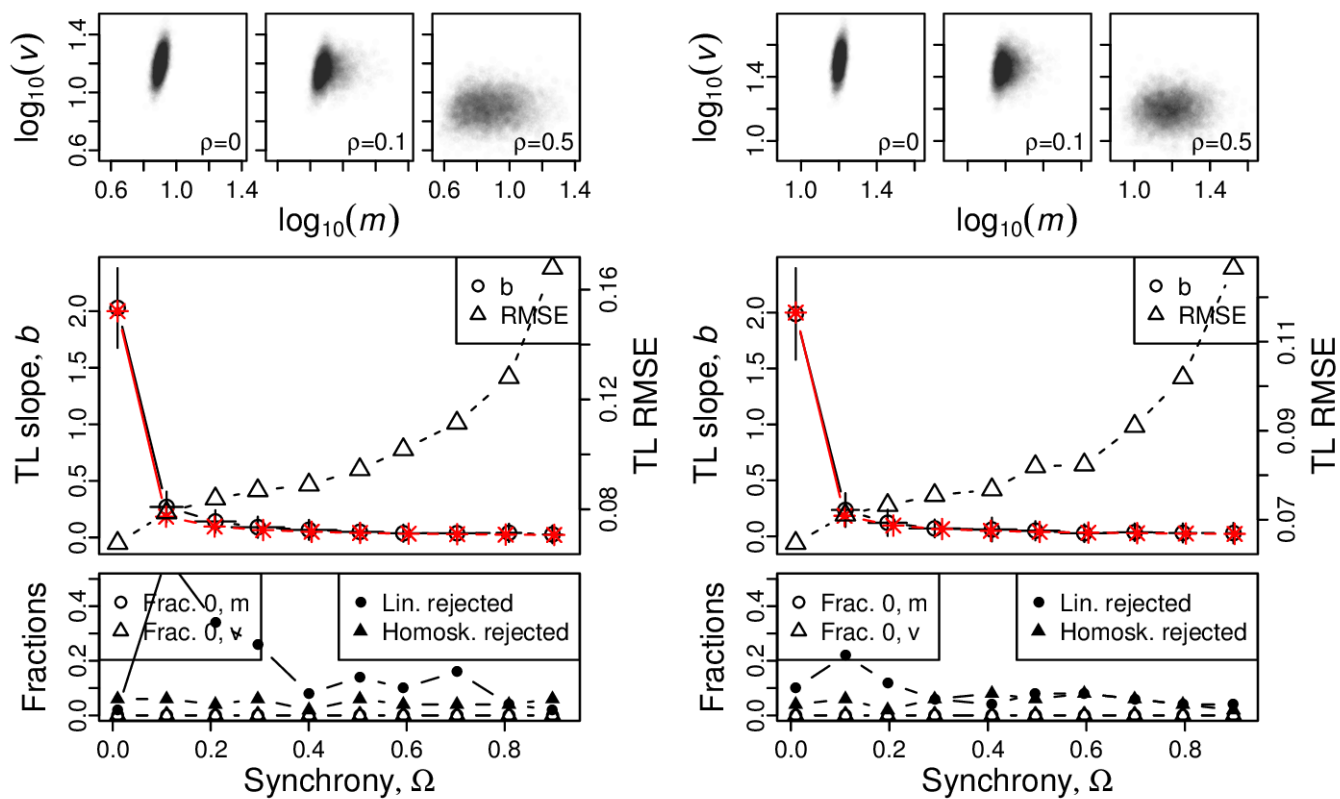
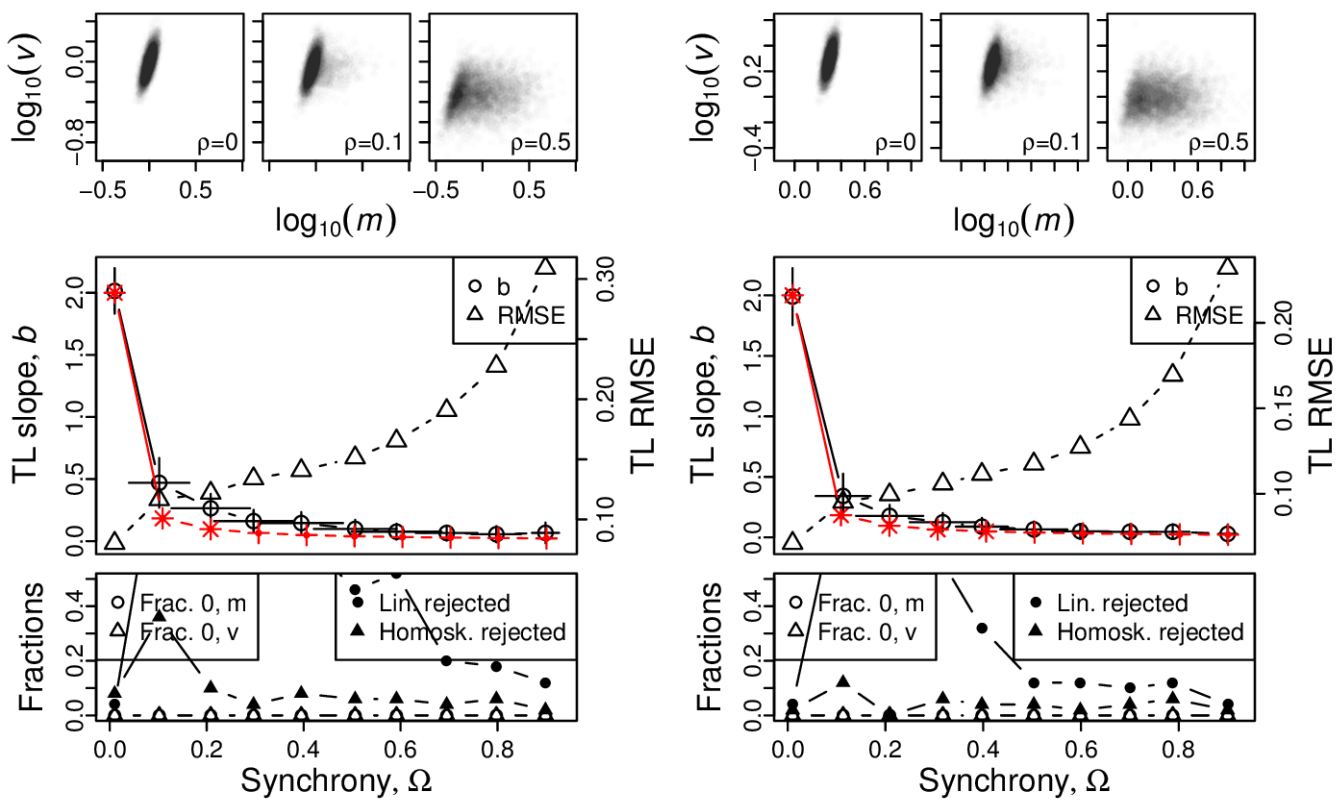


Figure S78: Omnibus plots (see section S6) for identically distributed gamma marginals under the set up of section S5, for  $n = 100$  and  $\beta = 0.5$ , for  $\alpha = 1$  (A),  $\alpha = 2$  (B),  $\alpha = 4$  (C), and  $\alpha = 8$  (D).

A, B



C, D

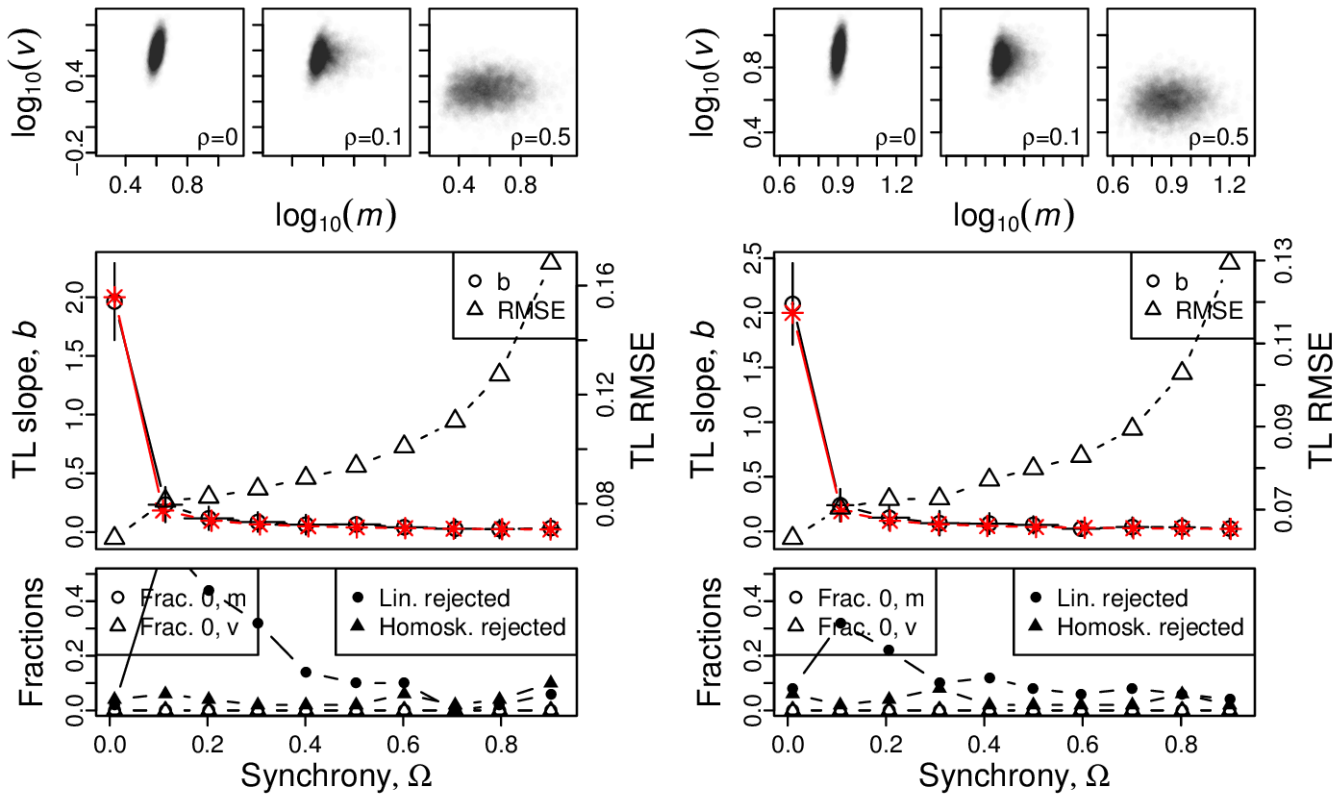
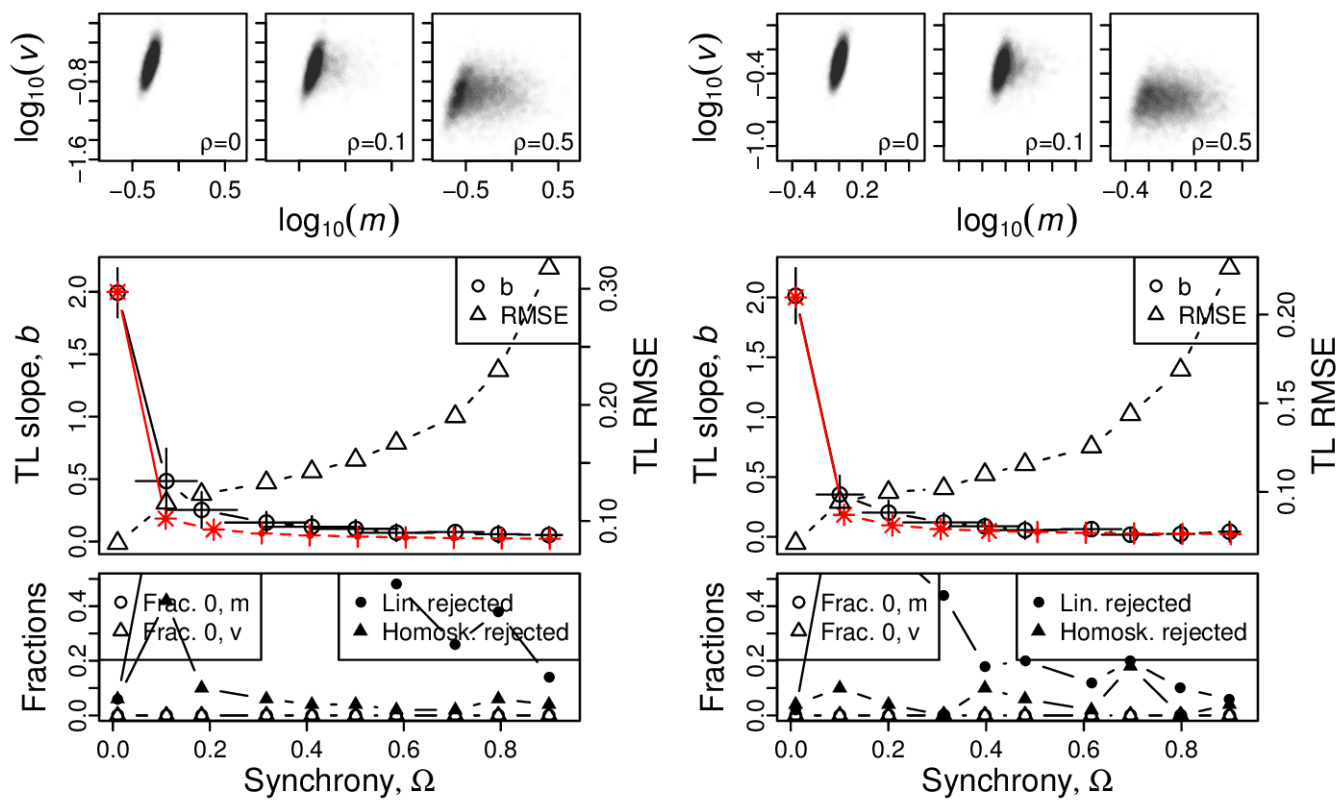


Figure S79: Omnibus plots (see section S6) for identically distributed gamma marginals under the set up of section S5, for  $n = 100$  and  $\beta = 1$ , for  $\alpha = 1$  (A),  $\alpha = 2$  (B),  $\alpha = 4$  (C), and  $\alpha = 8$  (D).

A, B



C, D

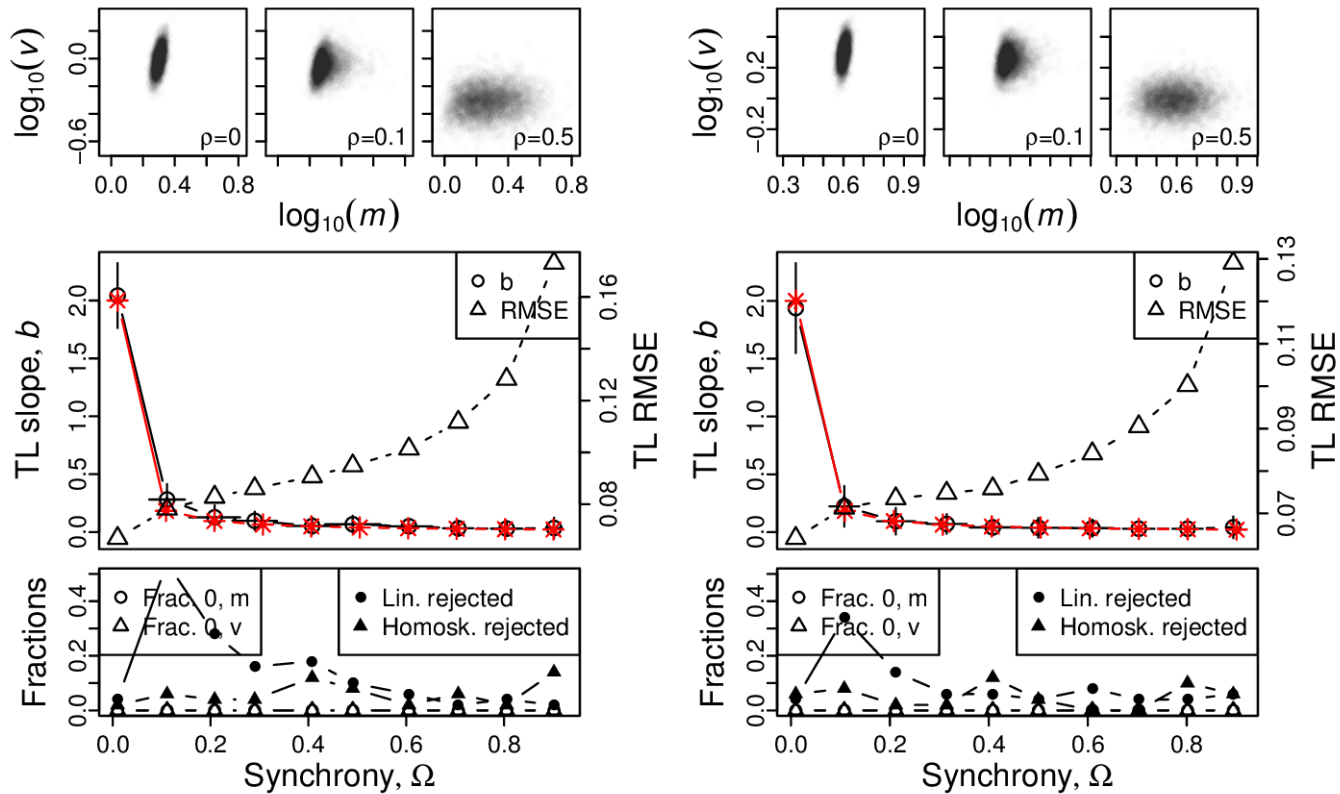
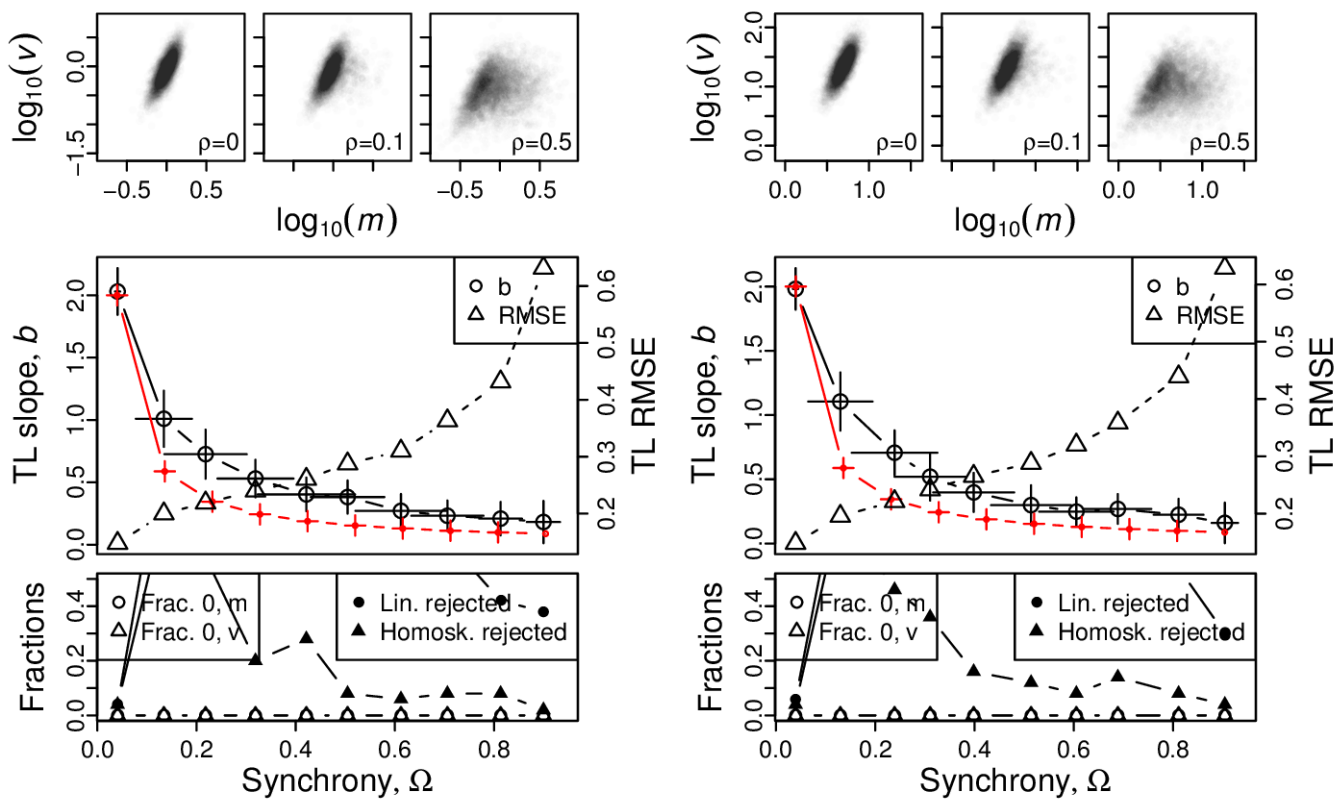


Figure S80: Omnibus plots (see section S6) for identically distributed gamma marginals under the set up of section S5, for  $n = 100$  and  $\beta = 2$ , for  $\alpha = 1$  (A),  $\alpha = 2$  (B),  $\alpha = 4$  (C), and  $\alpha = 8$  (D).

A, B



C, D

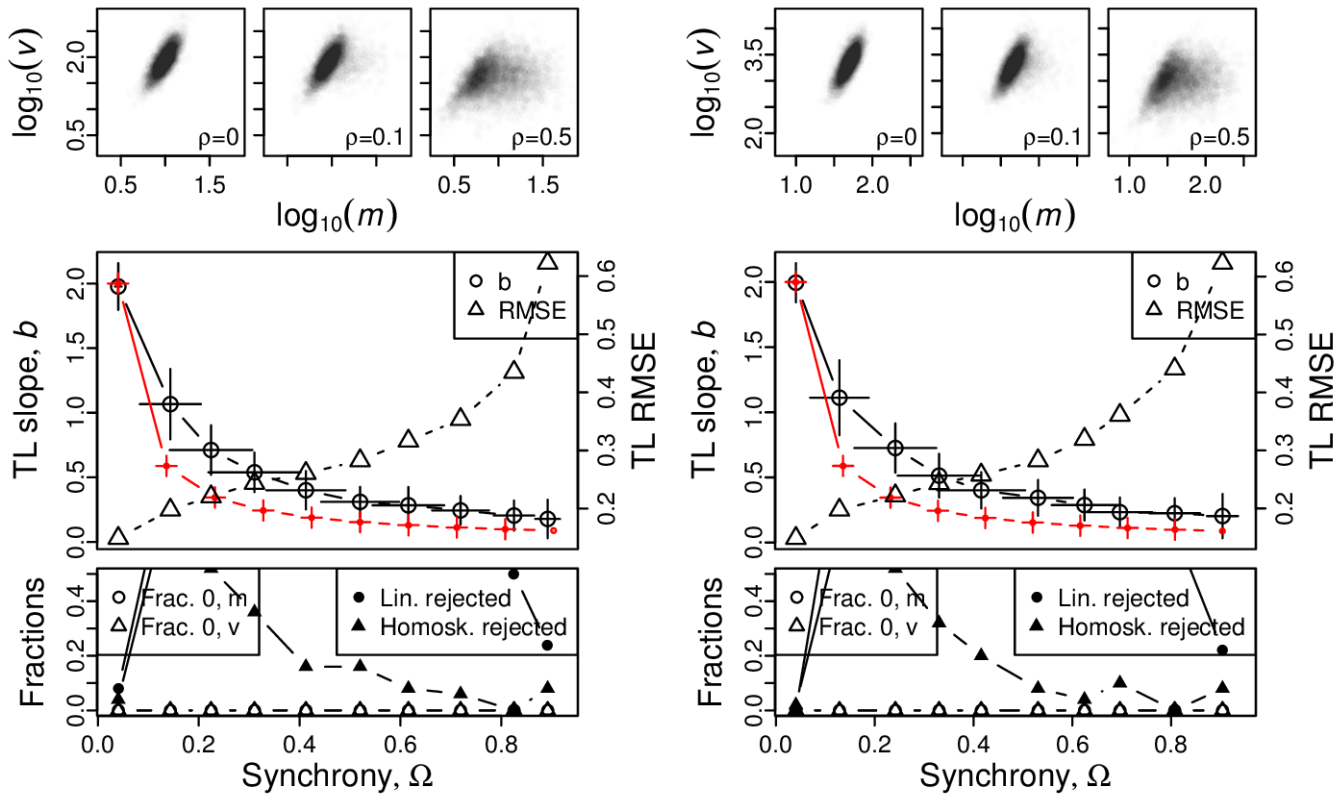
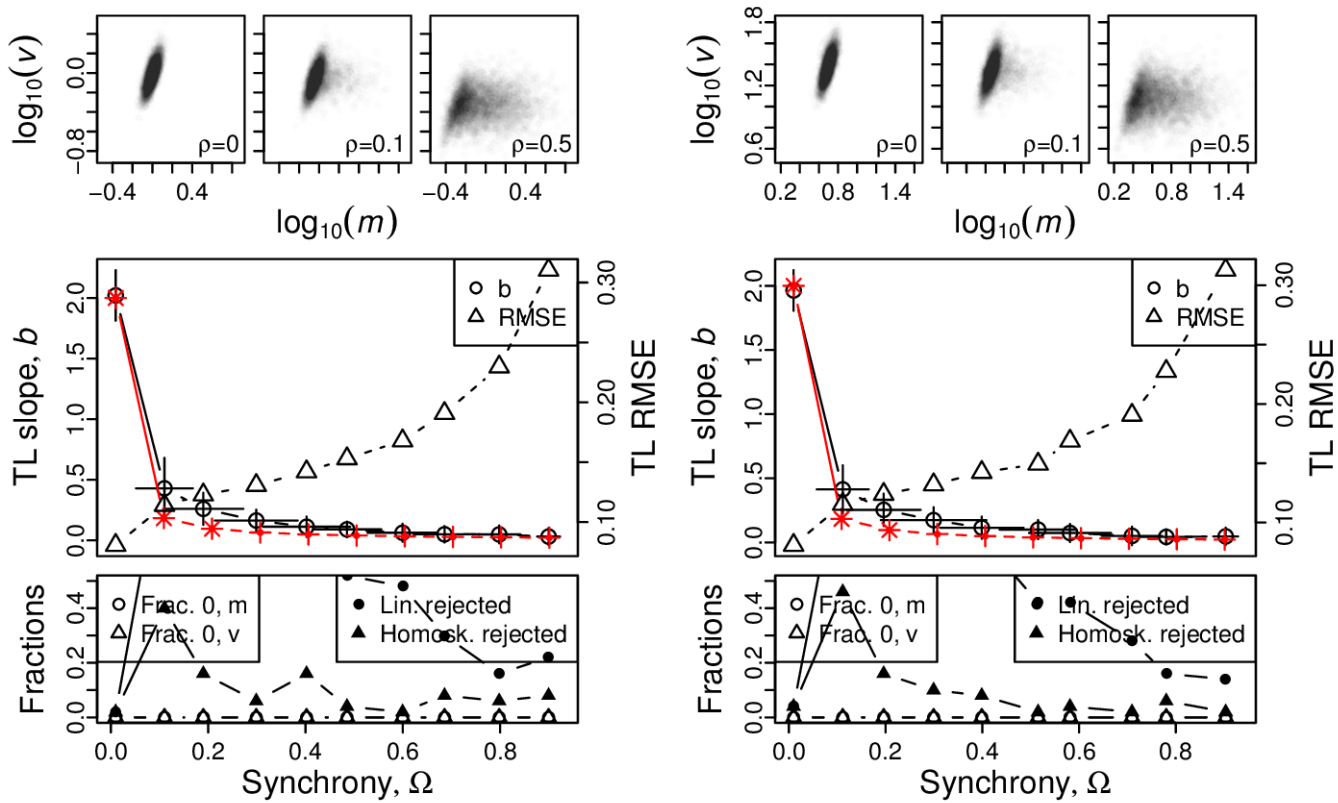


Figure S81: Omnibus plots (see section S6) for identically distributed exponentially distributed marginals under the set up of section S5, for  $n = 25$ , for  $1/\lambda = 1$  (A),  $1/\lambda = 5$  (B),  $1/\lambda = 10$  (C), and  $1/\lambda = 50$  (D).

A, B



C, D

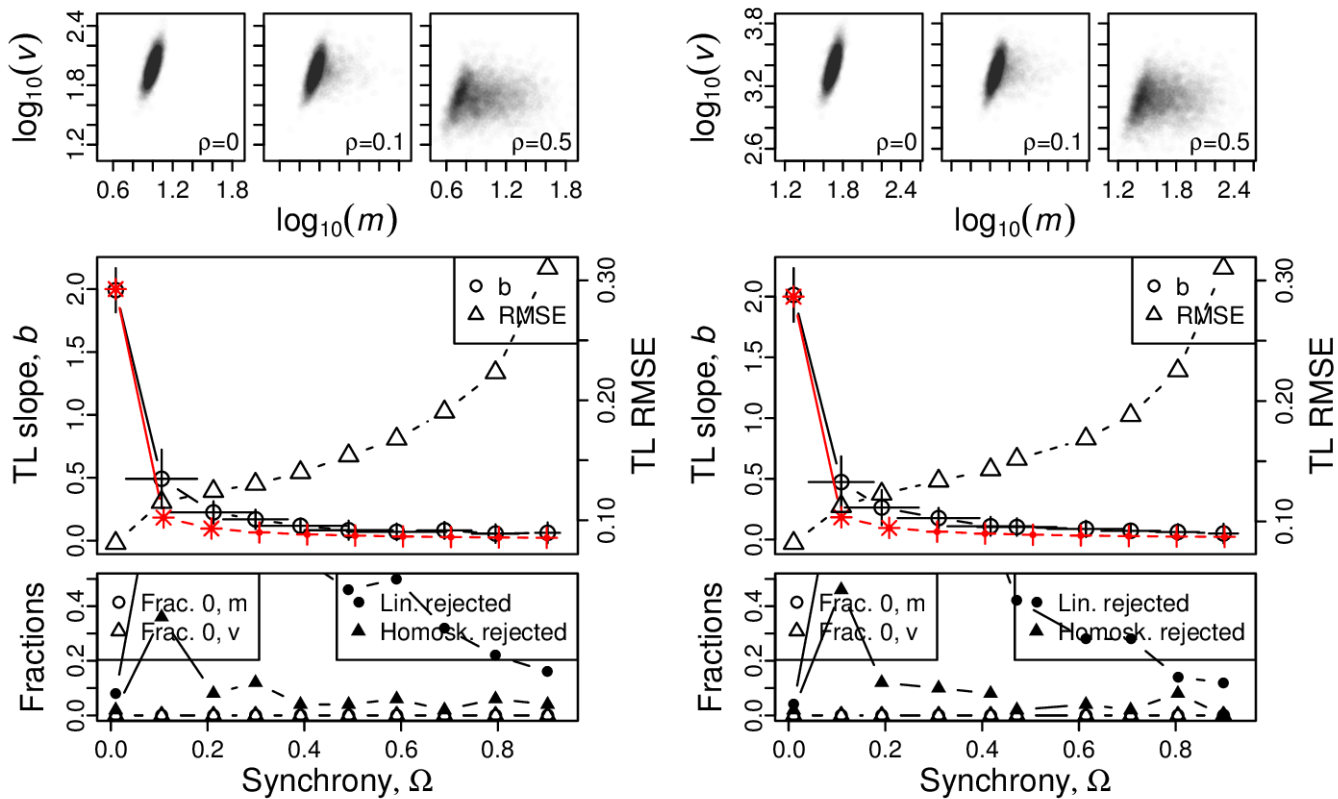
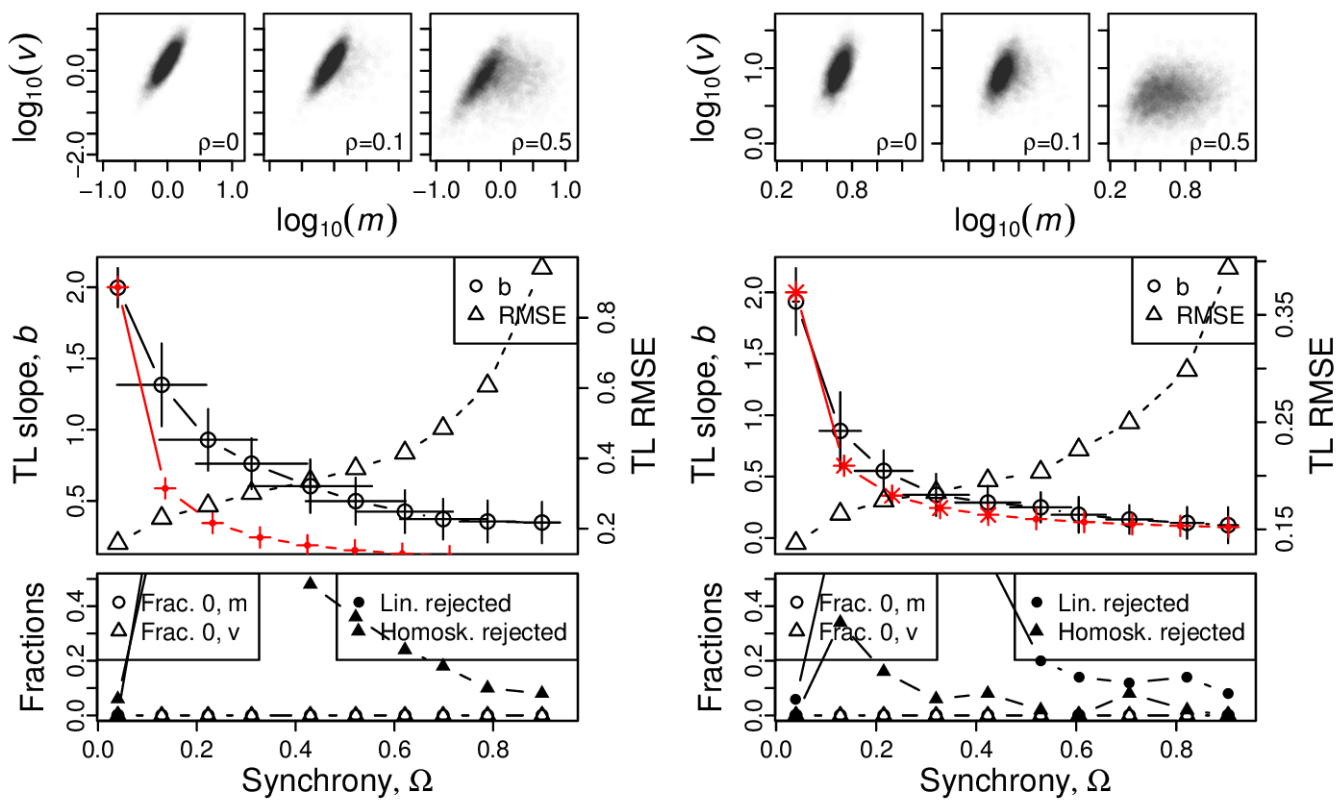


Figure S82: Omnibus plots (see section S6) for identically distributed exponentially distributed marginals under the set up of section S5, for  $n = 100$ , for  $1/\lambda = 1$  (A),  $1/\lambda = 5$  (B),  $1/\lambda = 10$  (C), and  $1/\lambda = 50$  (D).

A, B



C, D

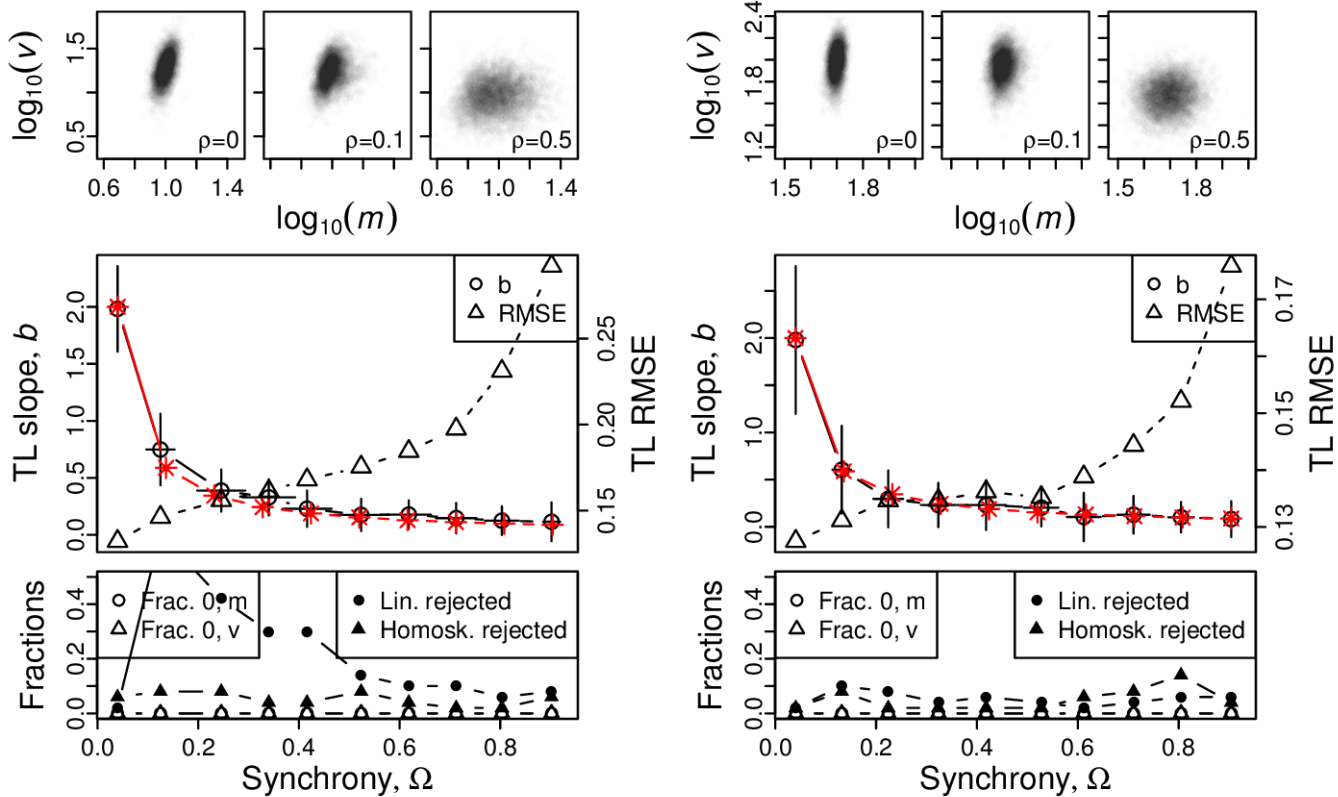
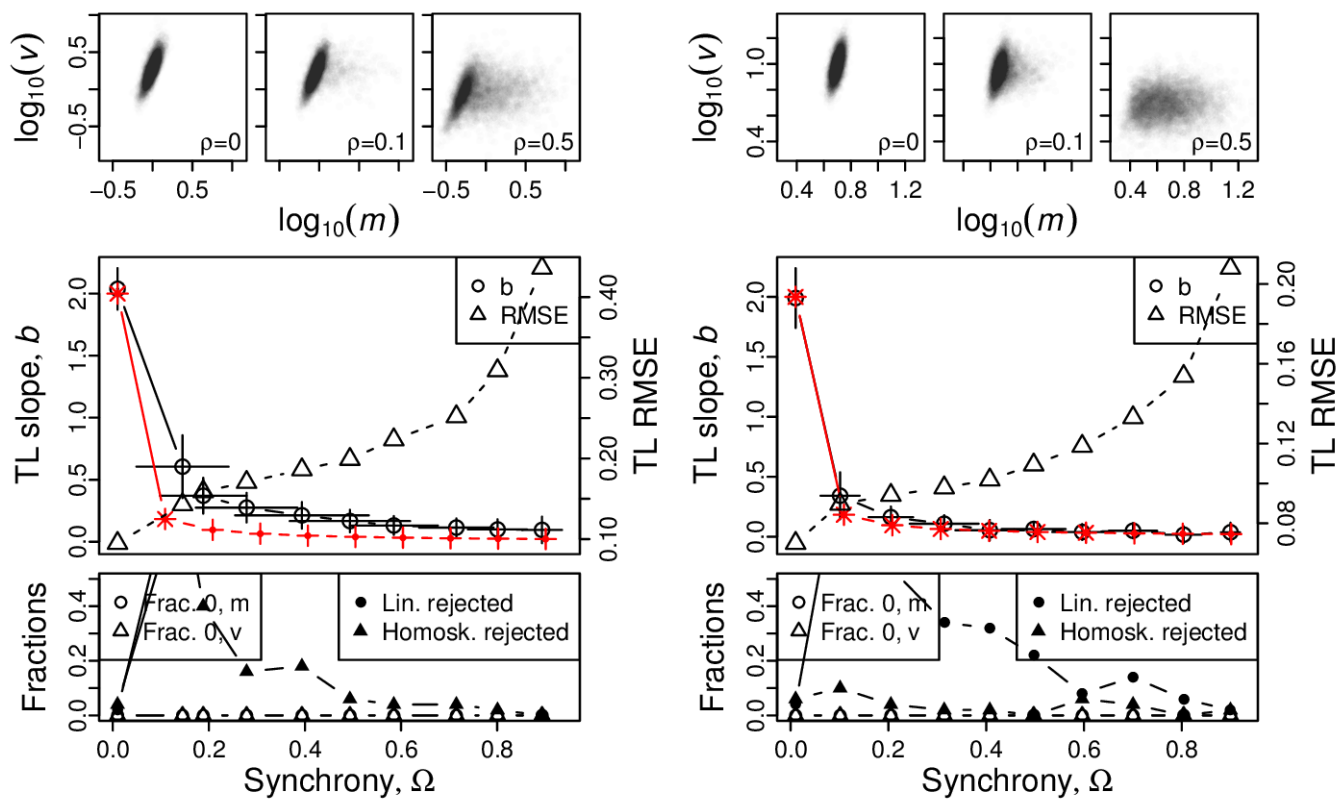


Figure S83: Omnibus plots (see section S6) for identically distributed chi-squared marginals under the set up of section S5, for  $n = 25$ , for  $k = 1$  (A),  $k = 5$  (B),  $k = 10$  (C), and  $k = 50$  (D).

A, B



C, D

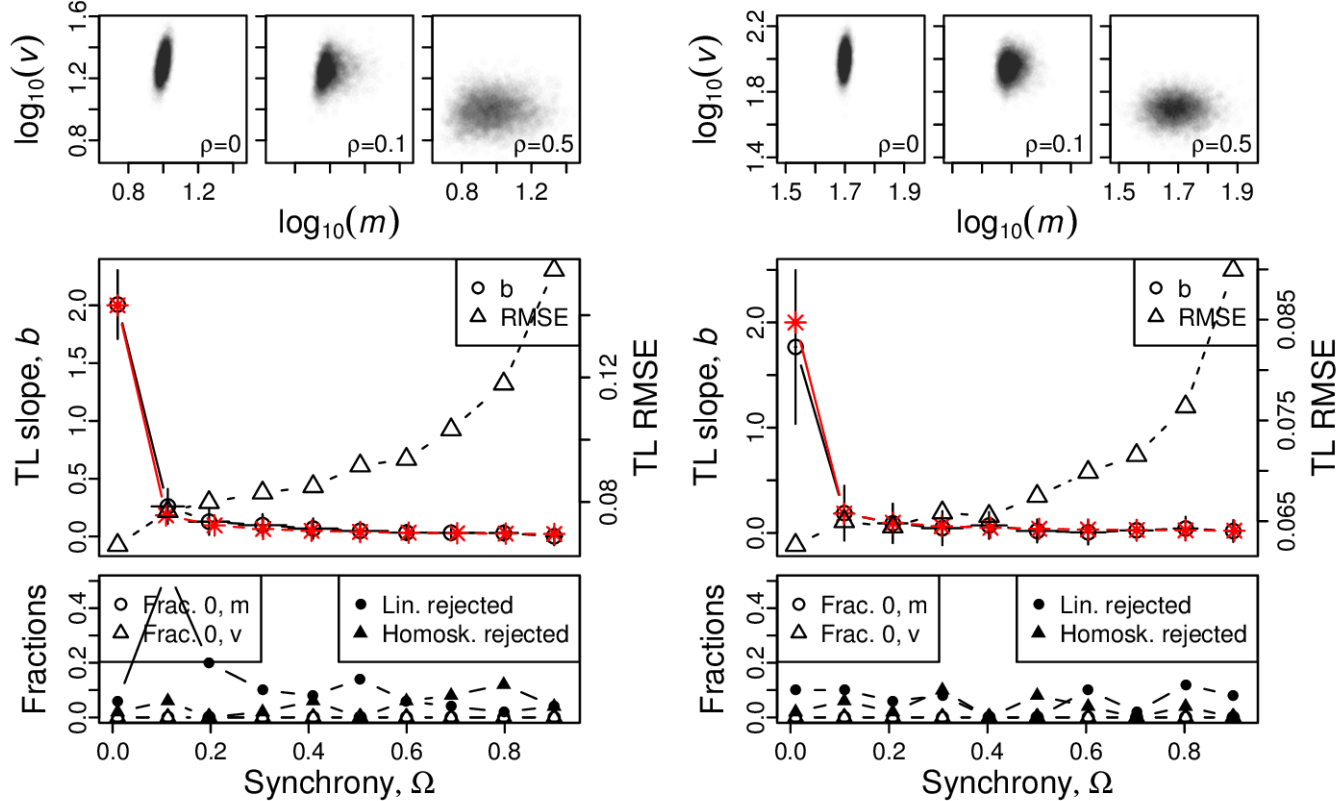
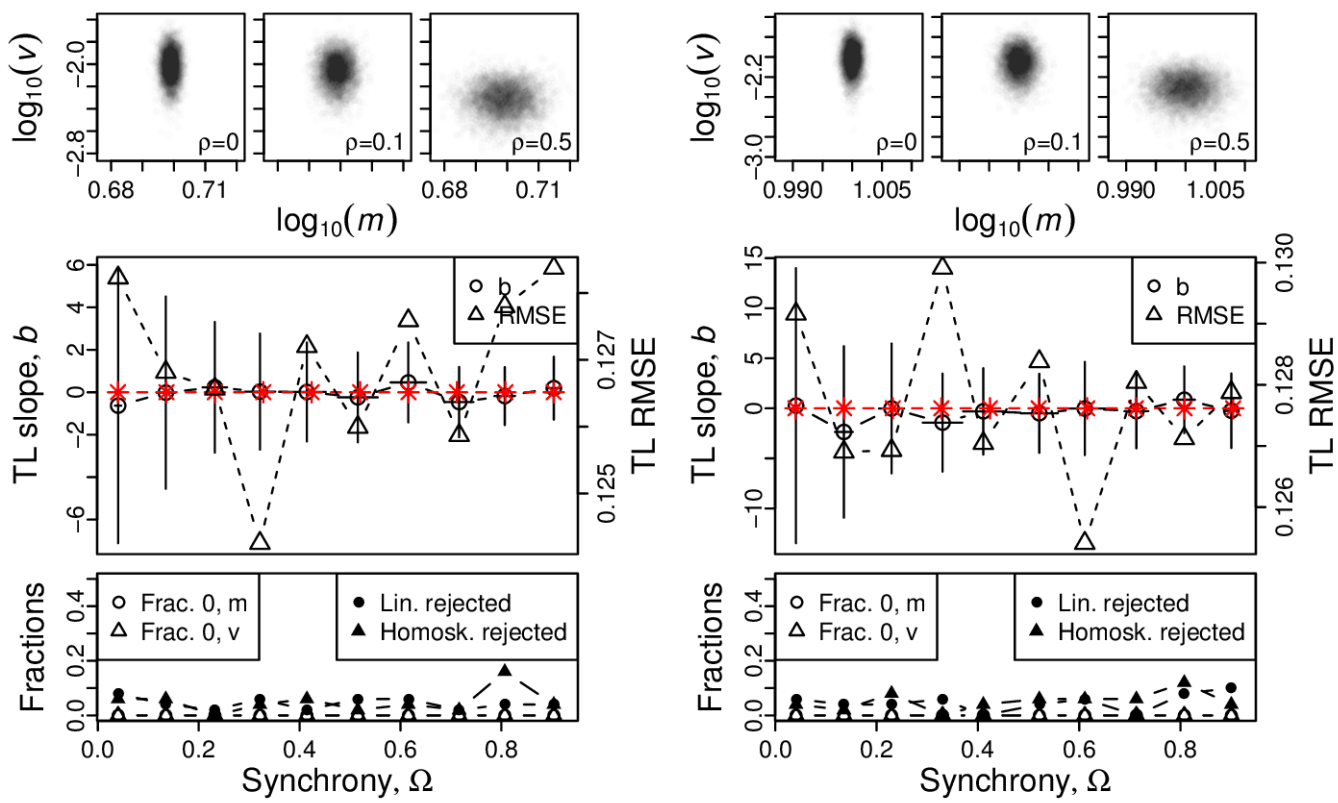


Figure S84: Omnibus plots (see section S6) for identically distributed chi-squared marginals under the set up of section S5, for  $n = 100$ , for  $k = 1$  (A),  $k = 5$  (B),  $k = 10$  (C), and  $k = 50$  (D).

A, B



C, D

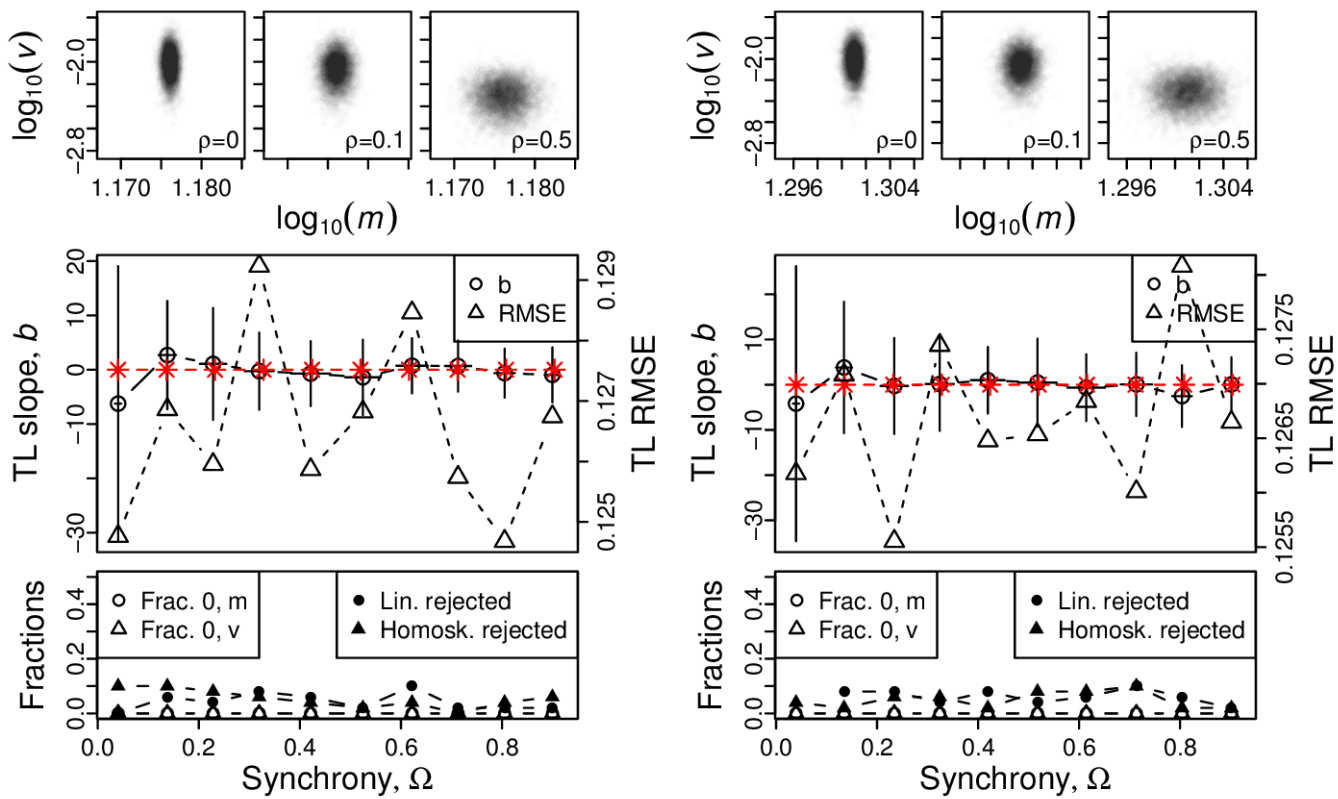
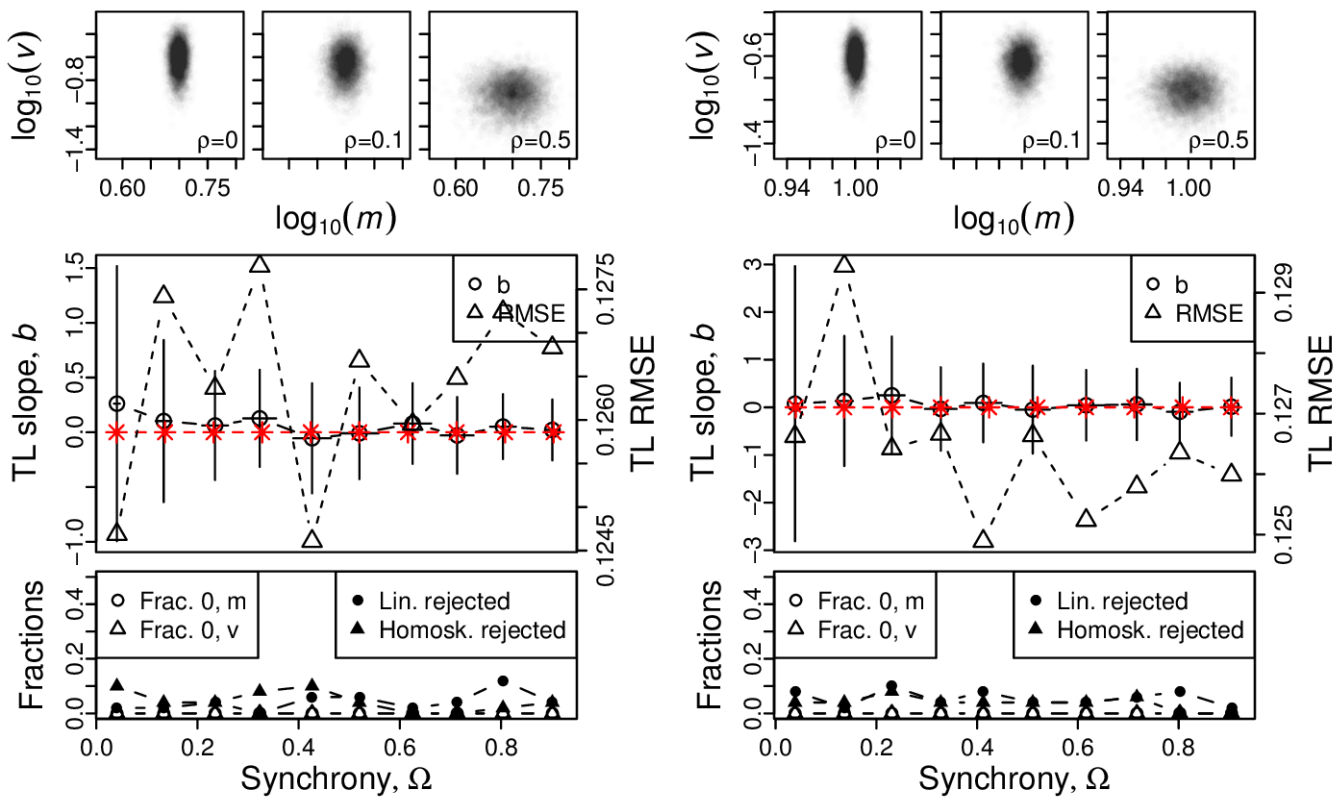


Figure S85: Omnibus plots (see section S6) for identically distributed normal marginals under the set up of section S5, for  $n = 25$  and  $\sigma = 0.1$ , for  $\mu = 5$  (A),  $\mu = 10$  (B),  $\mu = 15$  (C), and  $\mu = 20$  (D).

A, B



C, D

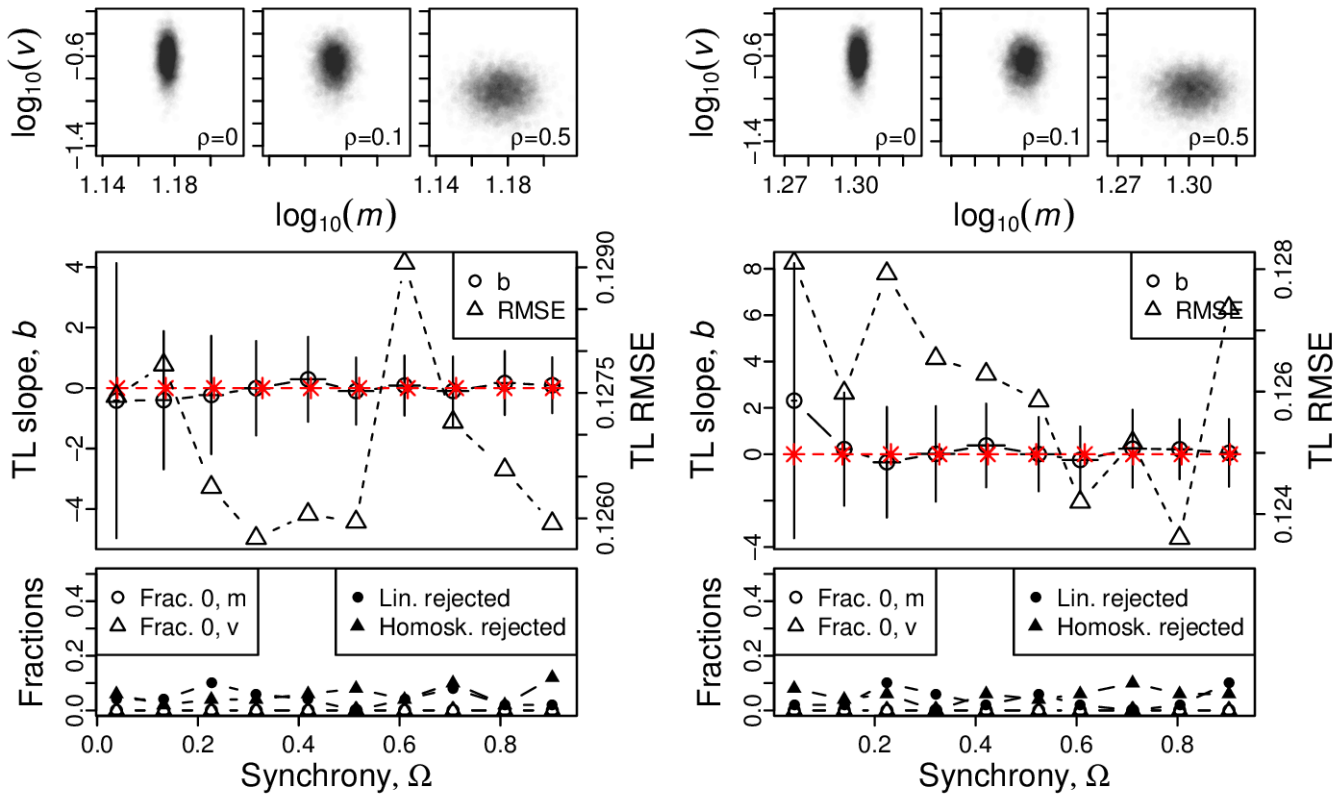
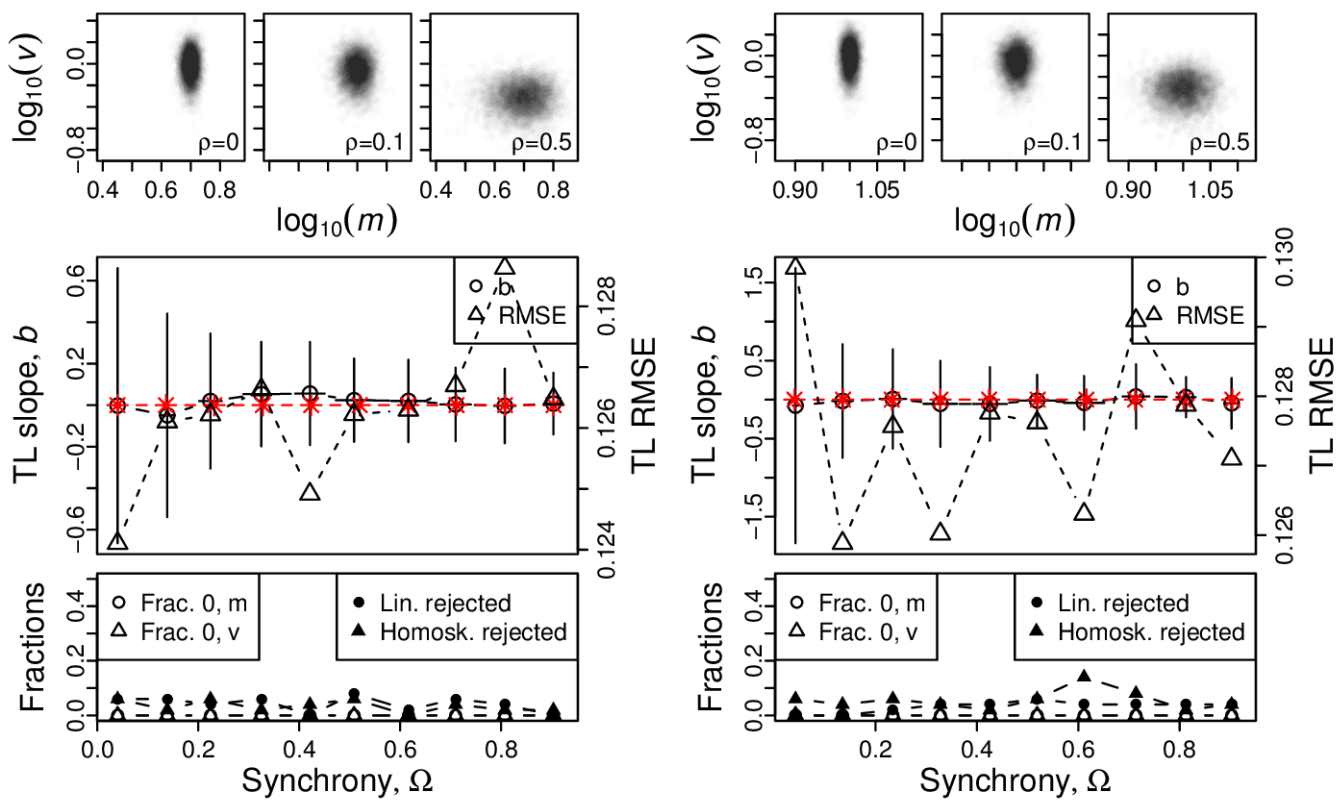


Figure S86: Omnibus plots (see section S6) for identically distributed normal marginals under the set up of section S5, for  $n = 25$  and  $\sigma = 0.5$ , for  $\mu = 5$  (A),  $\mu = 10$  (B),  $\mu = 15$  (C), and  $\mu = 20$  (D).

A, B



C, D

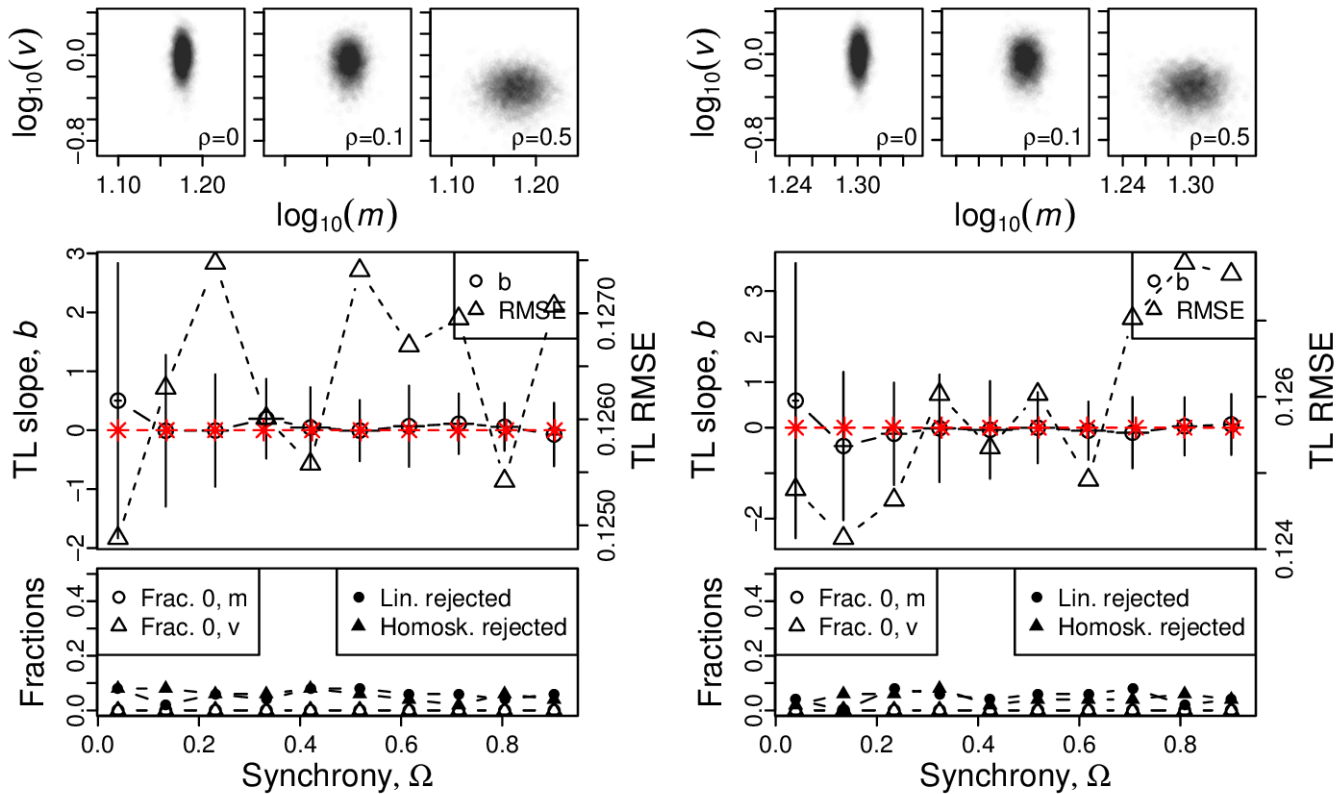
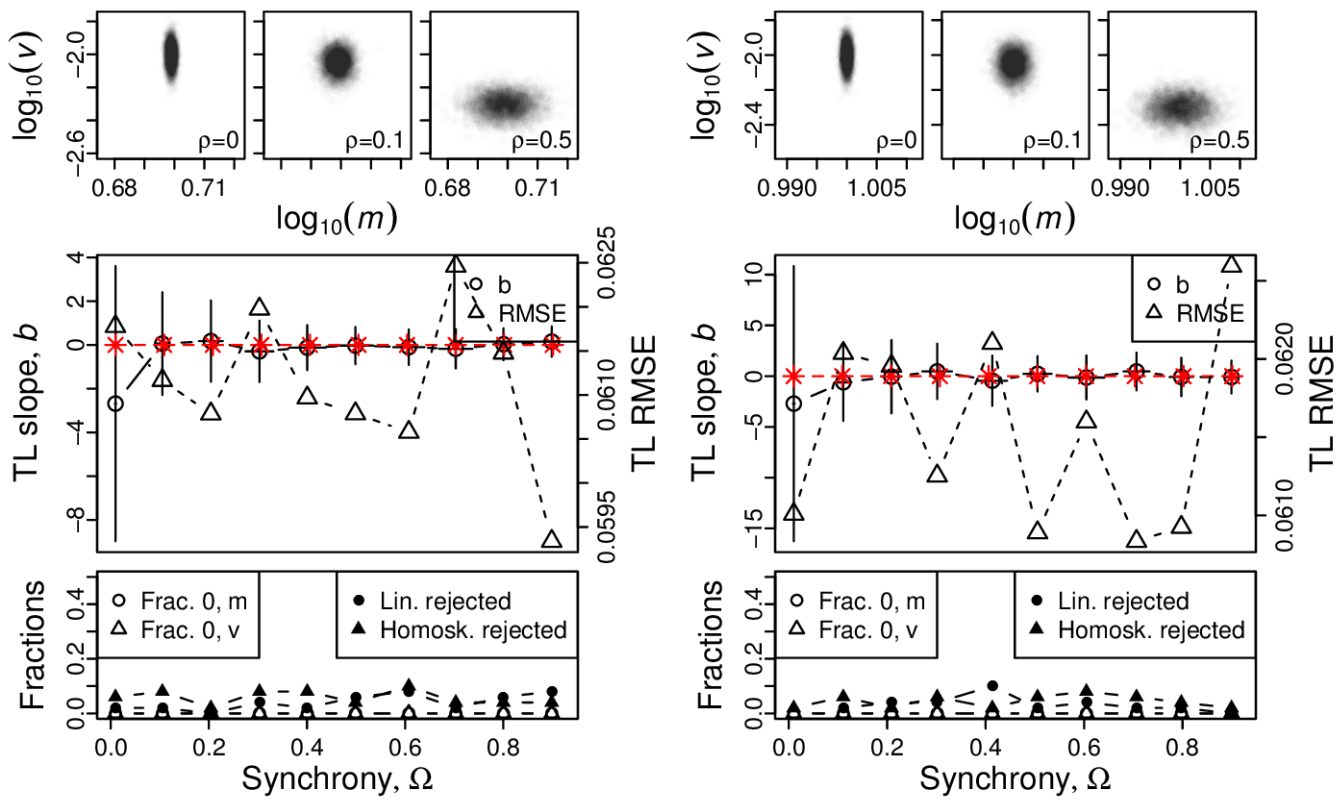


Figure S87: Omnibus plots (see section S6) for identically distributed normal marginals under the set up of section S5, for  $n = 25$  and  $\sigma = 1$ , for  $\mu = 5$  (A),  $\mu = 10$  (B),  $\mu = 15$  (C), and  $\mu = 20$  (D).

A, B



C, D

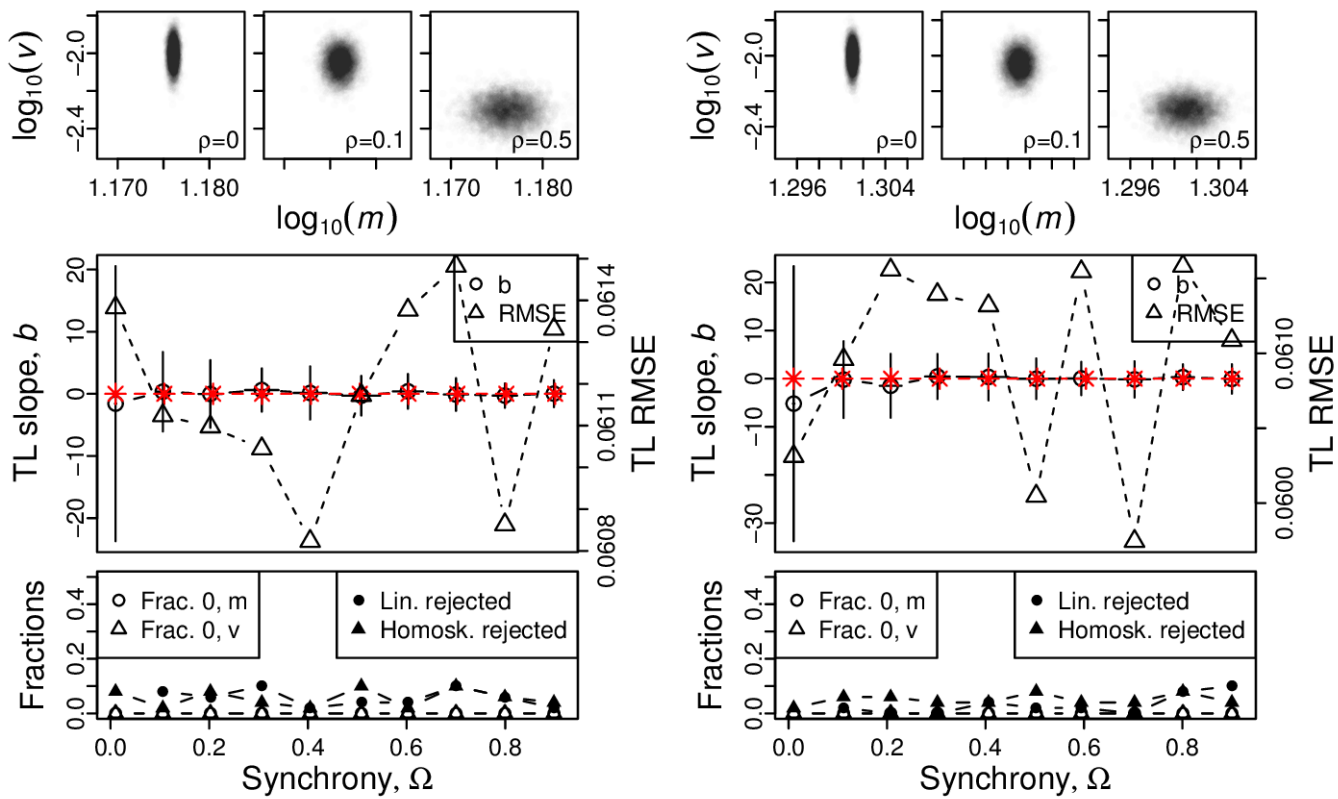
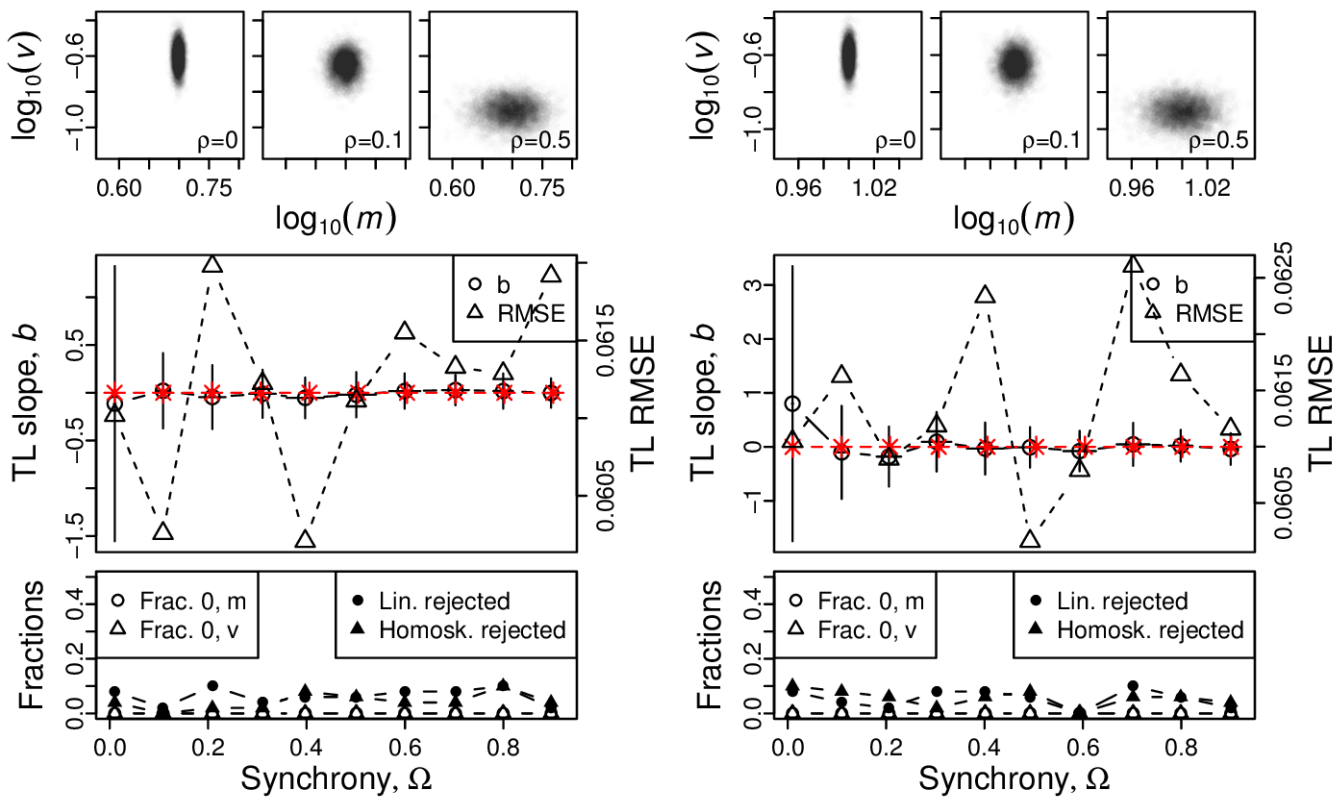


Figure S88: Omnibus plots (see section S6) for identically distributed normal marginals under the set up of section S5, for  $n = 100$  and  $\sigma = 0.1$ , for  $\mu = 5$  (A),  $\mu = 10$  (B),  $\mu = 15$  (C), and  $\mu = 20$  (D).

A, B



C, D

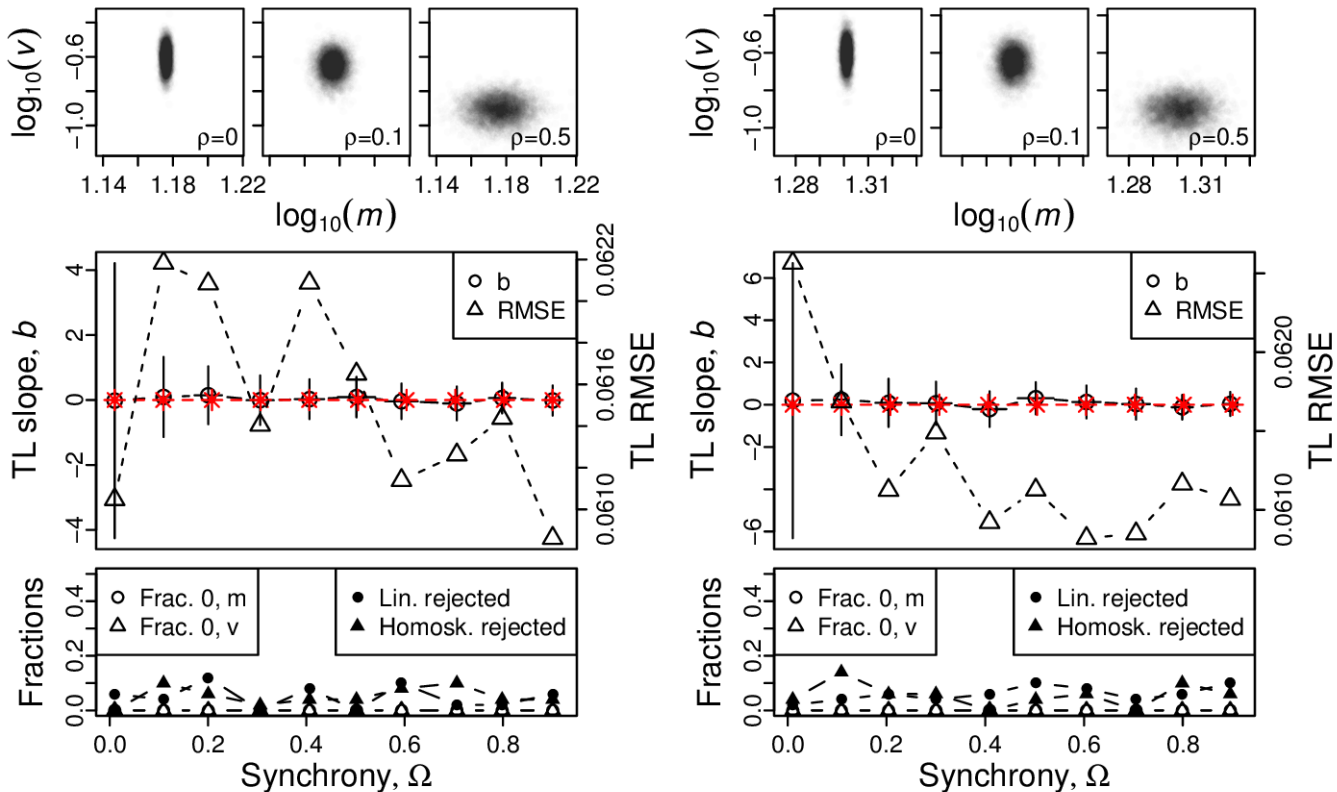


Figure S89: Omnibus plots (see section S6) for identically distributed normal marginals under the set up of section S5, for  $n = 100$  and  $\sigma = 0.5$ , for  $\mu = 5$  (A),  $\mu = 10$  (B),  $\mu = 15$  (C), and  $\mu = 20$  (D).

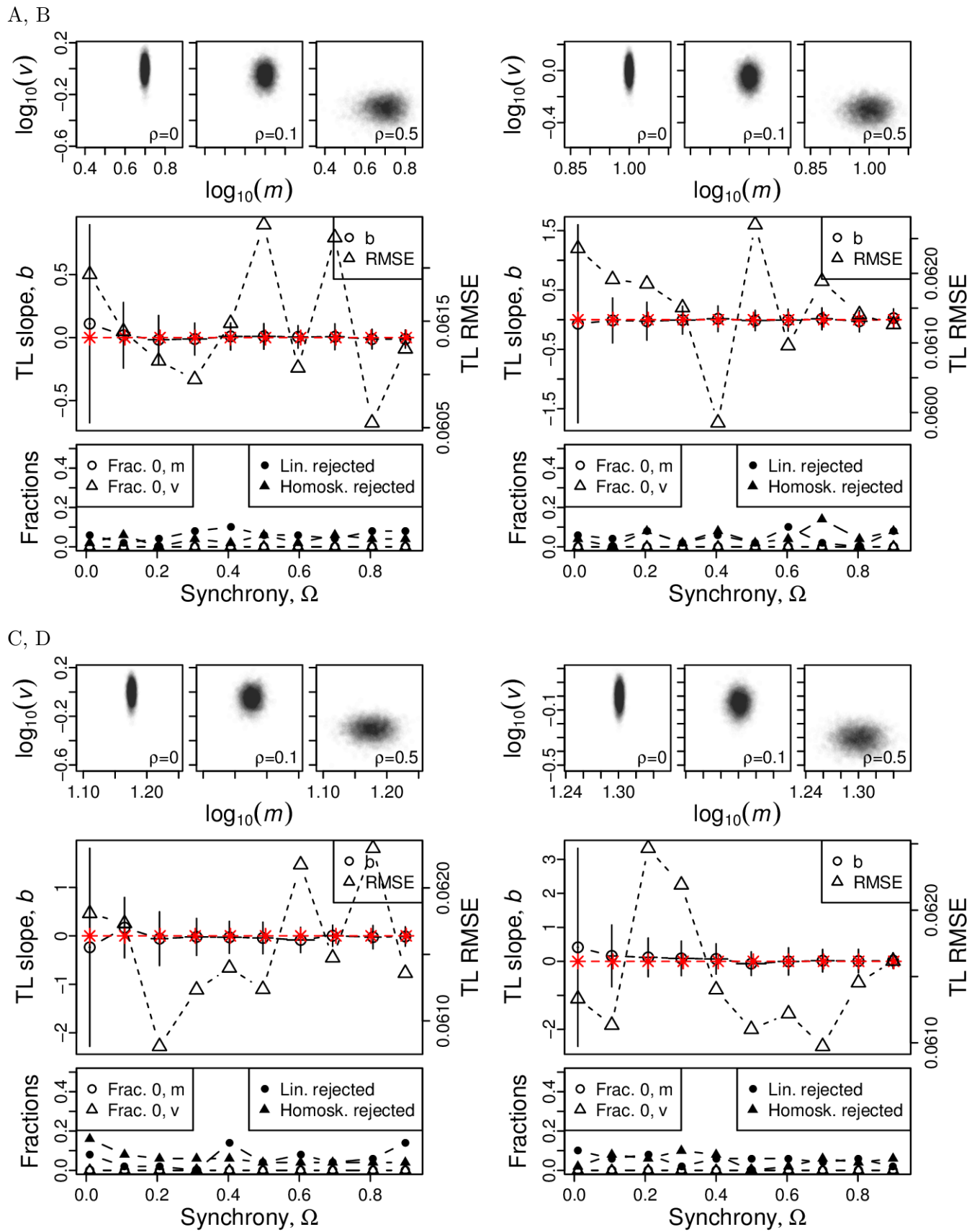


Figure S90: Omnibus plots (see section S6) for identically distributed normal marginals under the set up of section S5, for  $n = 100$  and  $\sigma = 1$ , for  $\mu = 5$  (A),  $\mu = 10$  (B),  $\mu = 15$  (C), and  $\mu = 20$  (D).

## S11 Figures testing spatial Taylor's law for empirical data

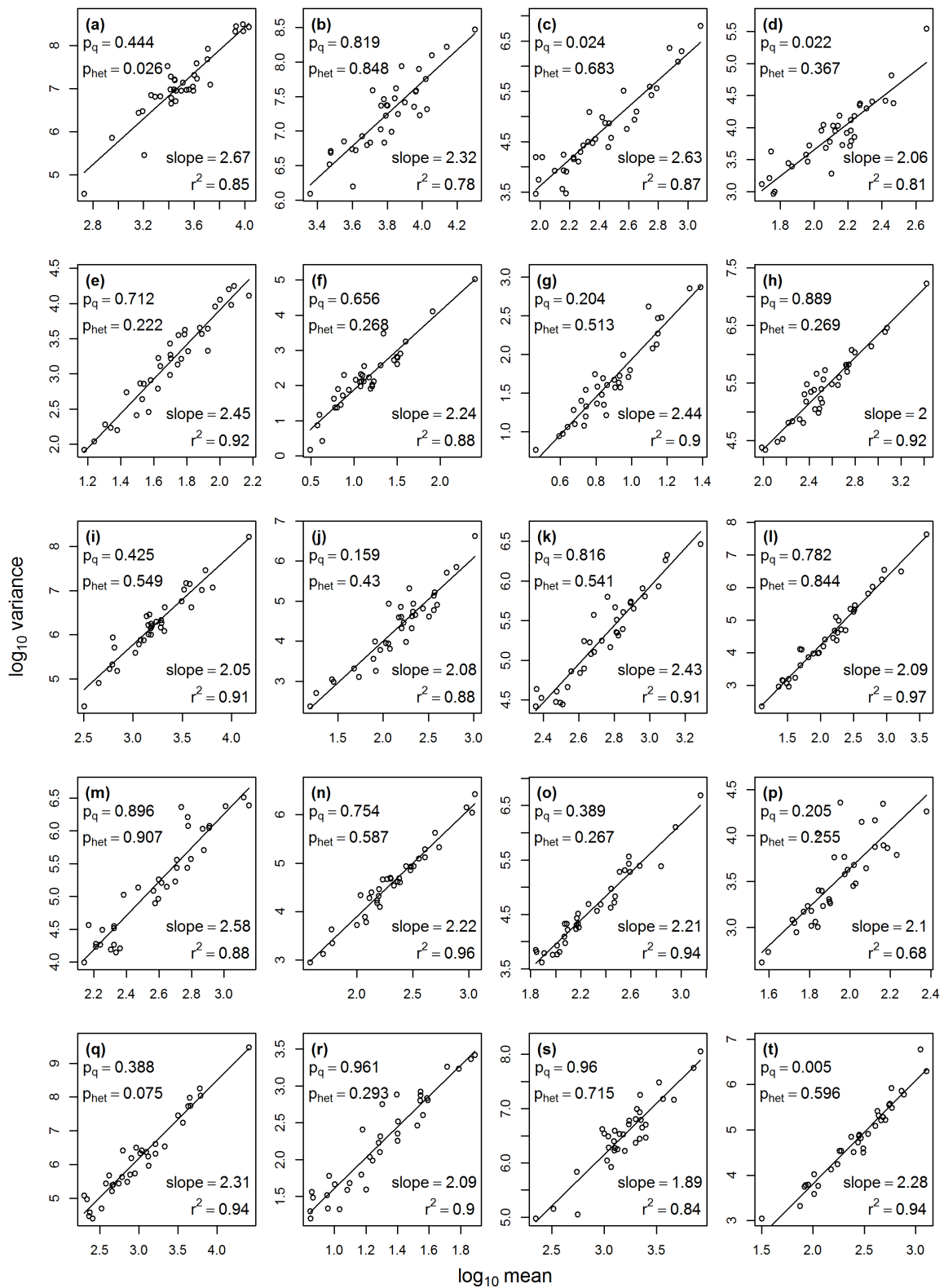


Figure S91: Plots of  $\log_{10}(\text{variance})$  versus  $\log_{10}(\text{mean})$  and results of statistical tests of whether data conformed to TL for 20 species of aphid from the UK (Methods). The value  $p_q$  tests linearity of the regression against a quadratic alternative;  $p_{het}$  tests for heteroskedasticity. Panels correspond to species listed in Table S1, in the same order.

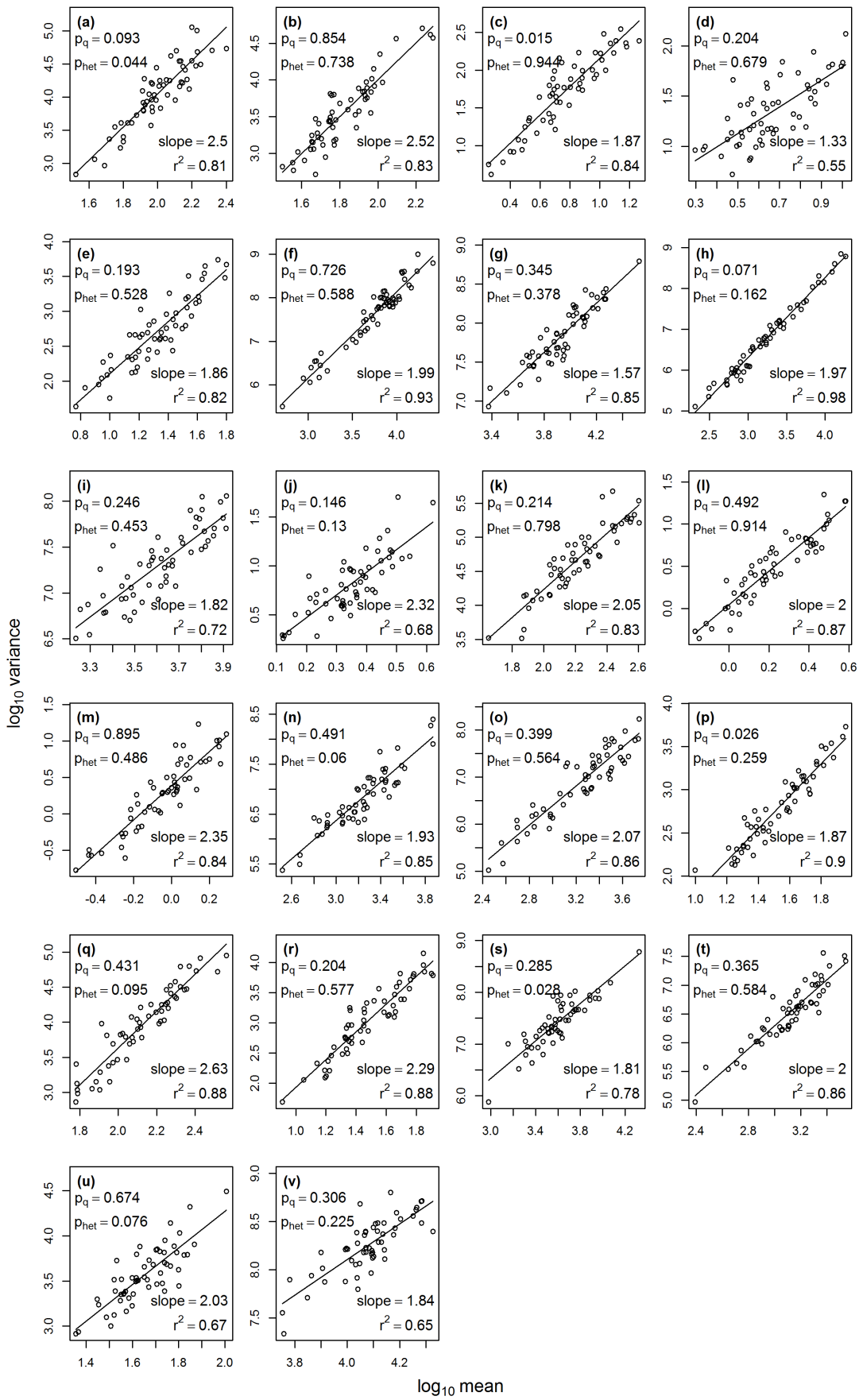


Figure S92: As for figure S91, but for plankton groups in the seas around the UK.

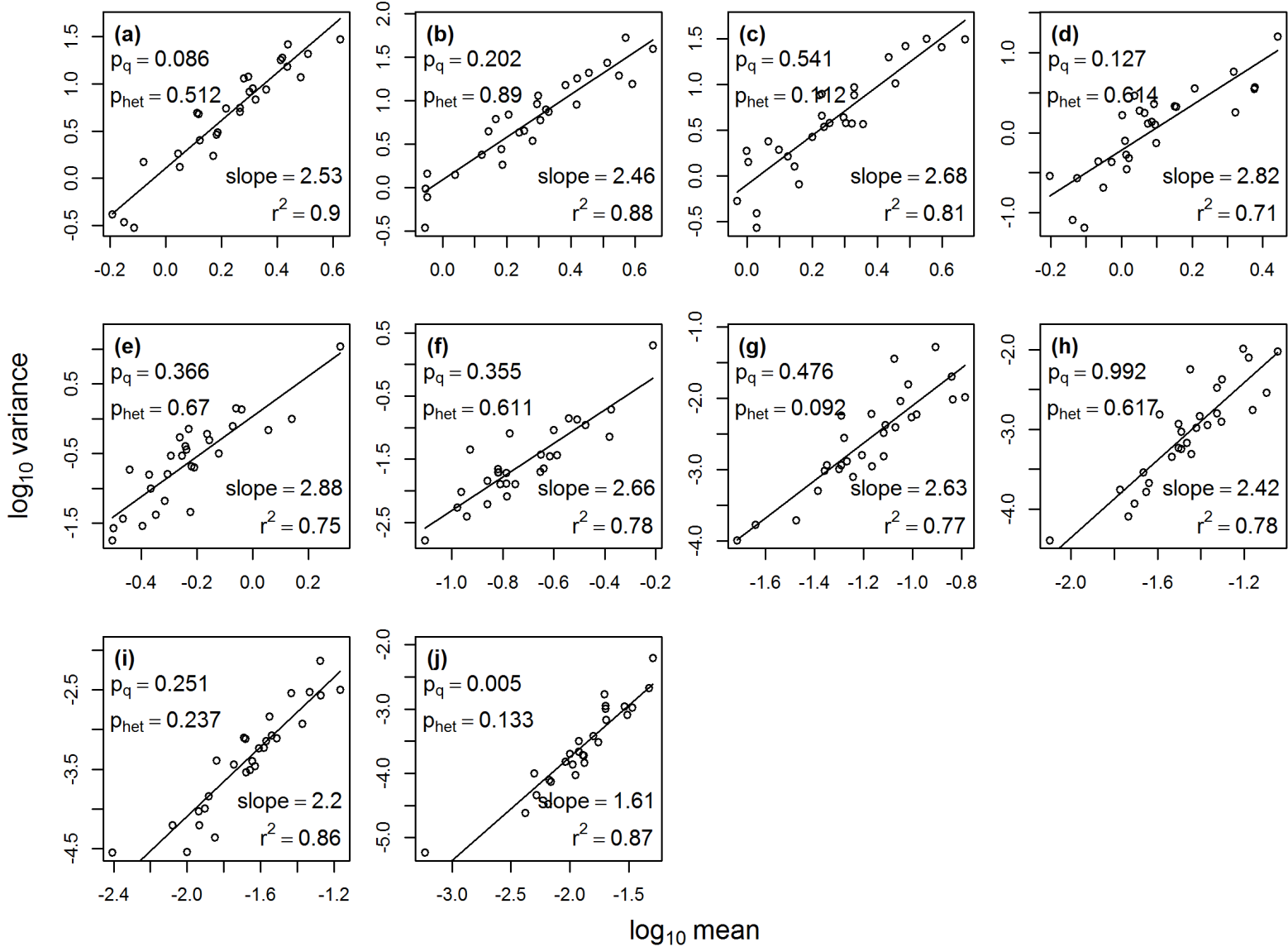


Figure S93: As for figure S91, but for chlorophyll-a abundances at different depths at sampling stations in the closest category to the shore (Methods).

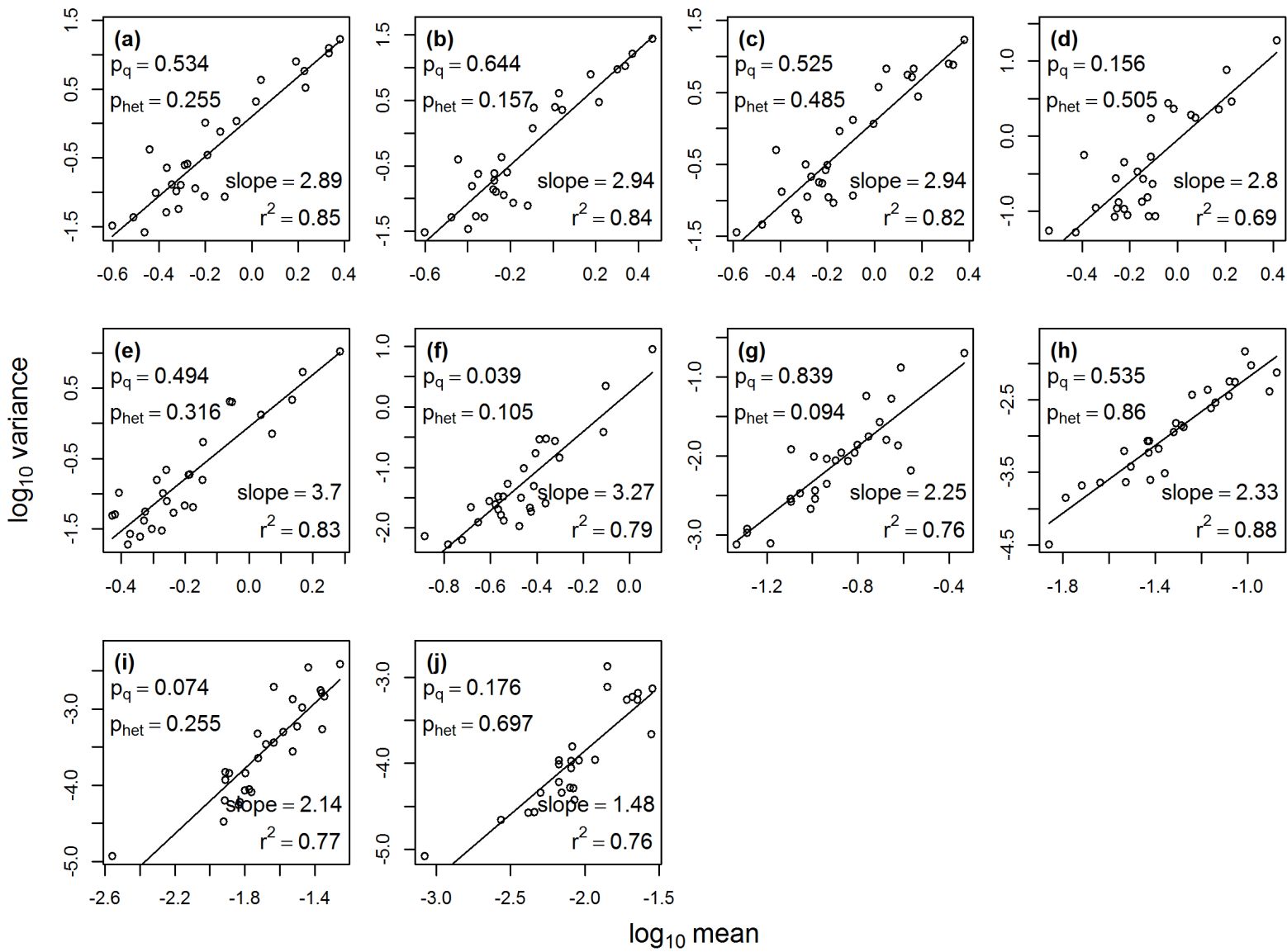


Figure S94: As for figure S91, but for chlorophyll-a abundances at different depths at sampling stations in the second closest category to the shore (Methods).

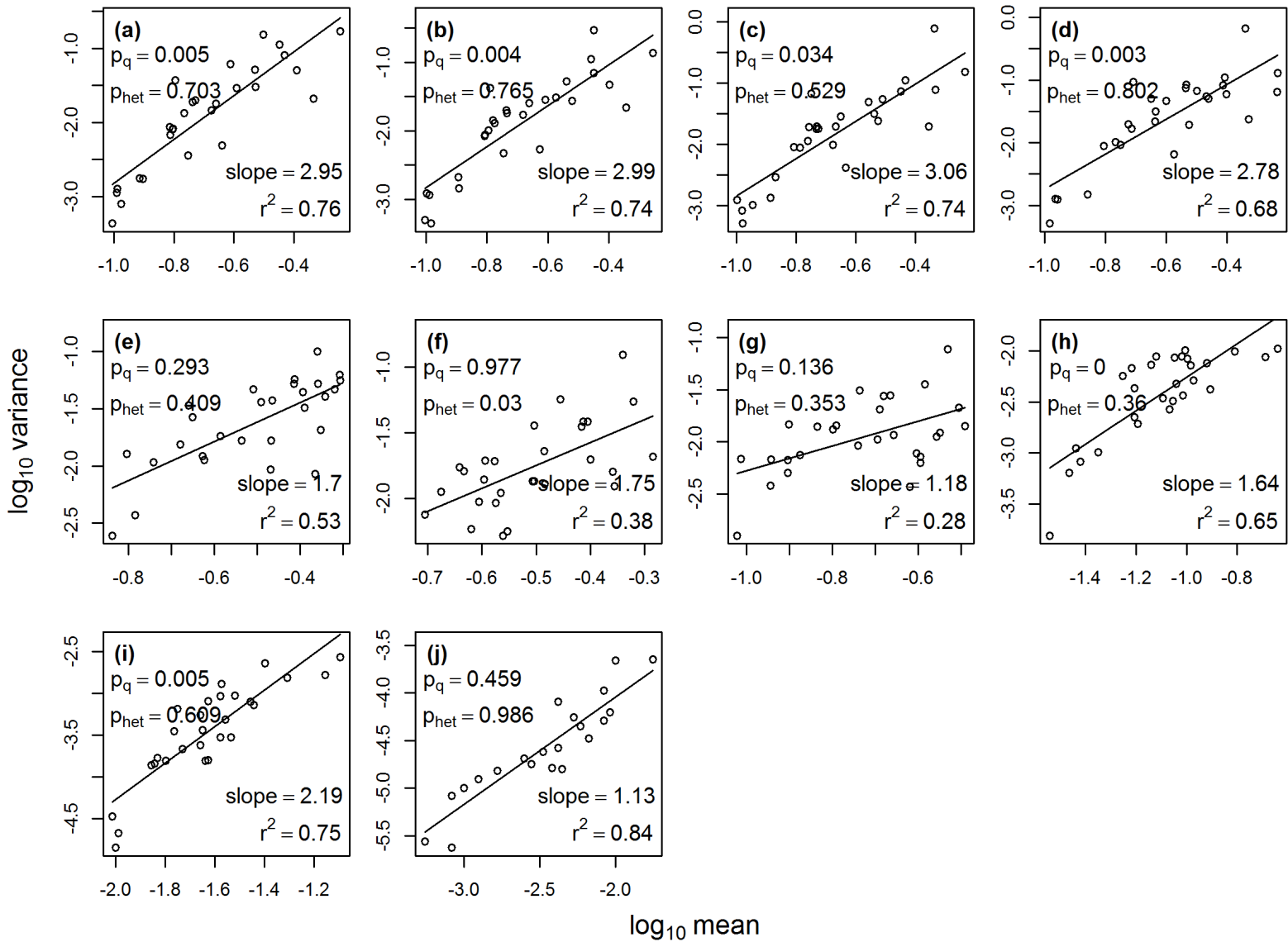


Figure S95: As for figure S91, but for chlorophyll-a abundances at different depths at sampling stations in the third closest category to the shore (Methods).

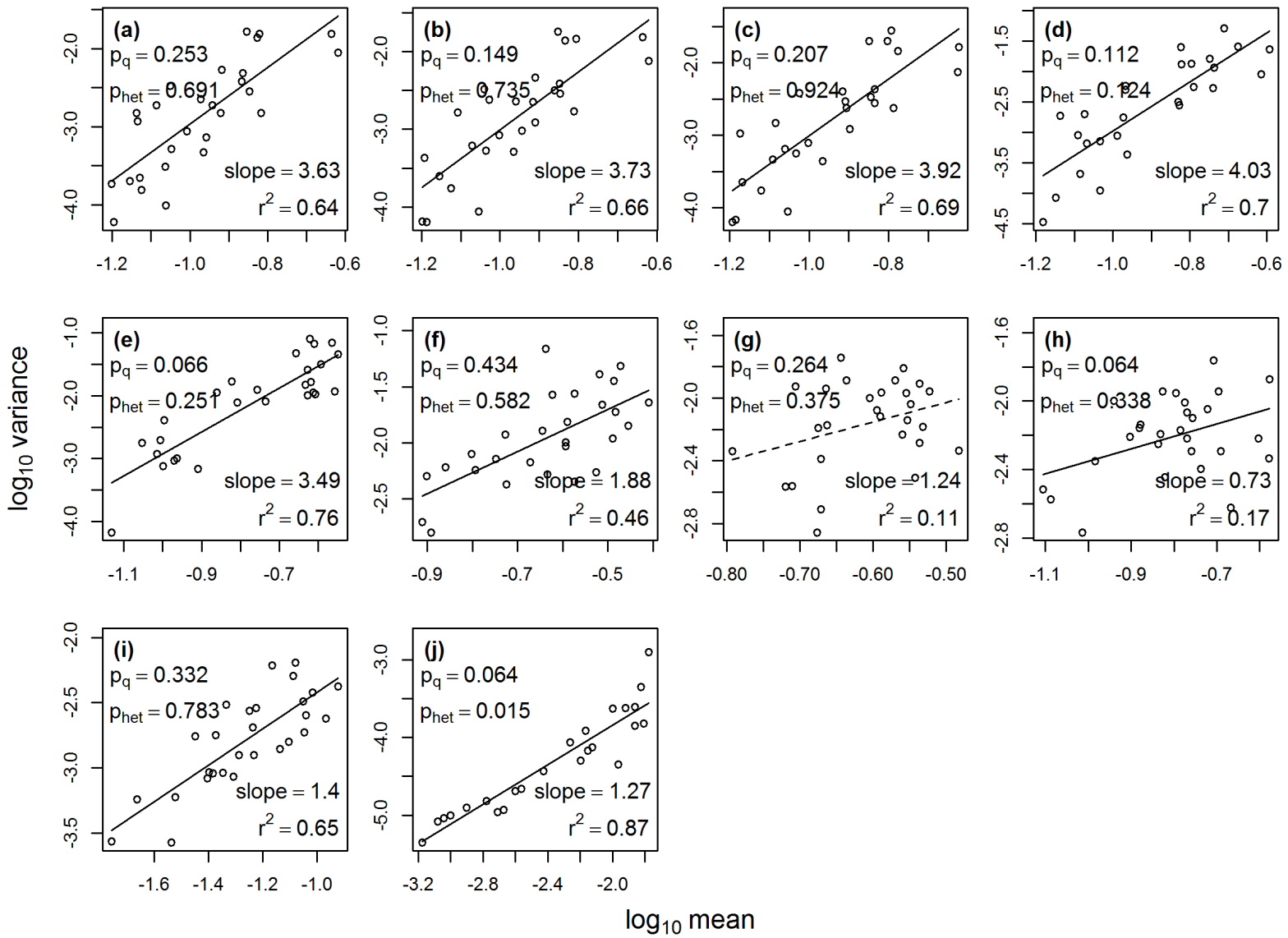


Figure S96: As for figure S91, but for chlorophyll-a abundances at different depths at sampling stations in the farthest category from the shore (Methods).

## S12 Figures testing spatial Taylor's law for randomized or partially sorted data

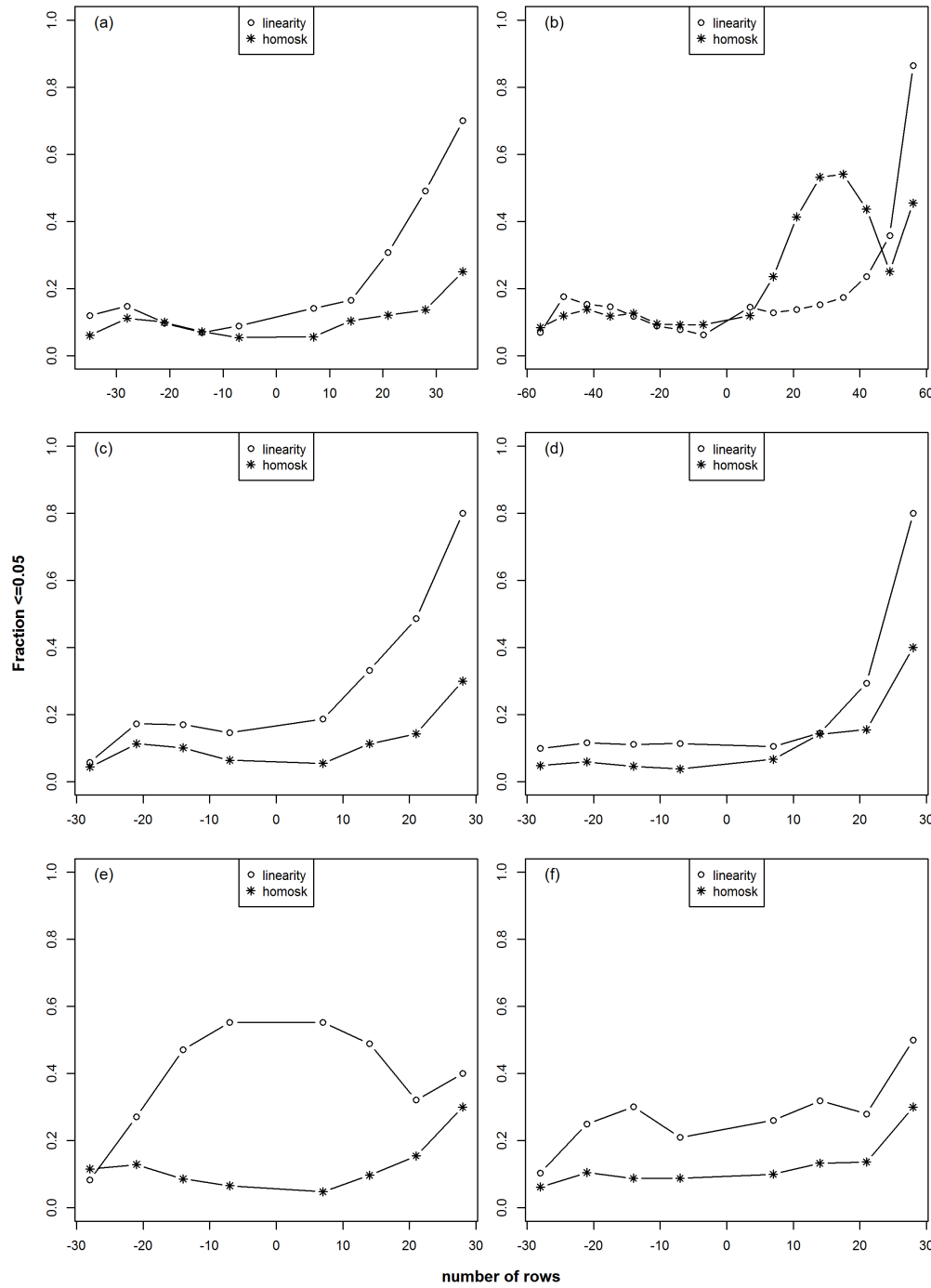


Figure S97: Statistical tests indicating whether the randomized or partially sorted data sets used in figure 3 in the main text conformed to TL. For each resampled/sorted dataset (Methods), conformity to TL was tested by testing linearity and homoskedasticity of the  $\log_{10}(\text{variance})$ -versus- $\log_{10}(\text{mean})$  pattern for that randomization (as in figures S91 -S11). Shown are the fraction of tests rejecting the null hypothesis (of linearity or homoskedasticity) with 95% confidence; thus when values substantially exceed 0.05, linearity or homoskedasticity were less acceptable hypotheses. See, however, figure S98. Positive values on the x-axis show numbers of random rows within which time series were randomized. Negative values on the x-axis show numbers of random rows within which time series were sorted. Thus the x-axis corresponds to strength of synchrony. Panels correspond to data sets in the same pattern as main text figure 3.

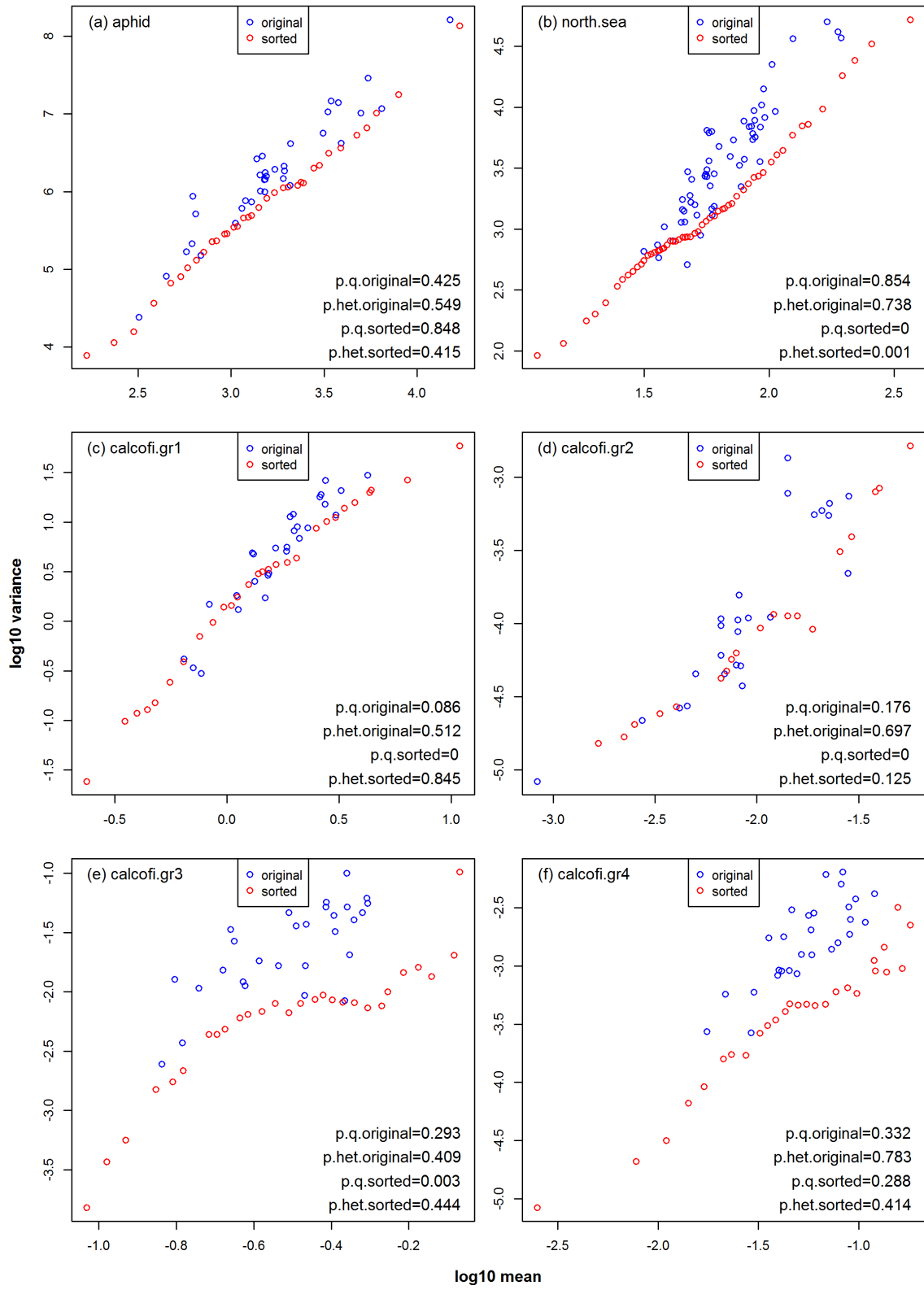


Figure S98: The  $\log_{10}(\text{variance})$ -versus- $\log_{10}(\text{mean})$  pattern for sorted time series. Sorting time series (Methods) produced the most synchronous resampled data sets we considered, but these resampled data sets were among the worst we considered in conformity to TL (figure S97, right side of each panel). Nevertheless, these plots show TL may be a useful approximation for some purposes even for these cases.

## S13 Other figures

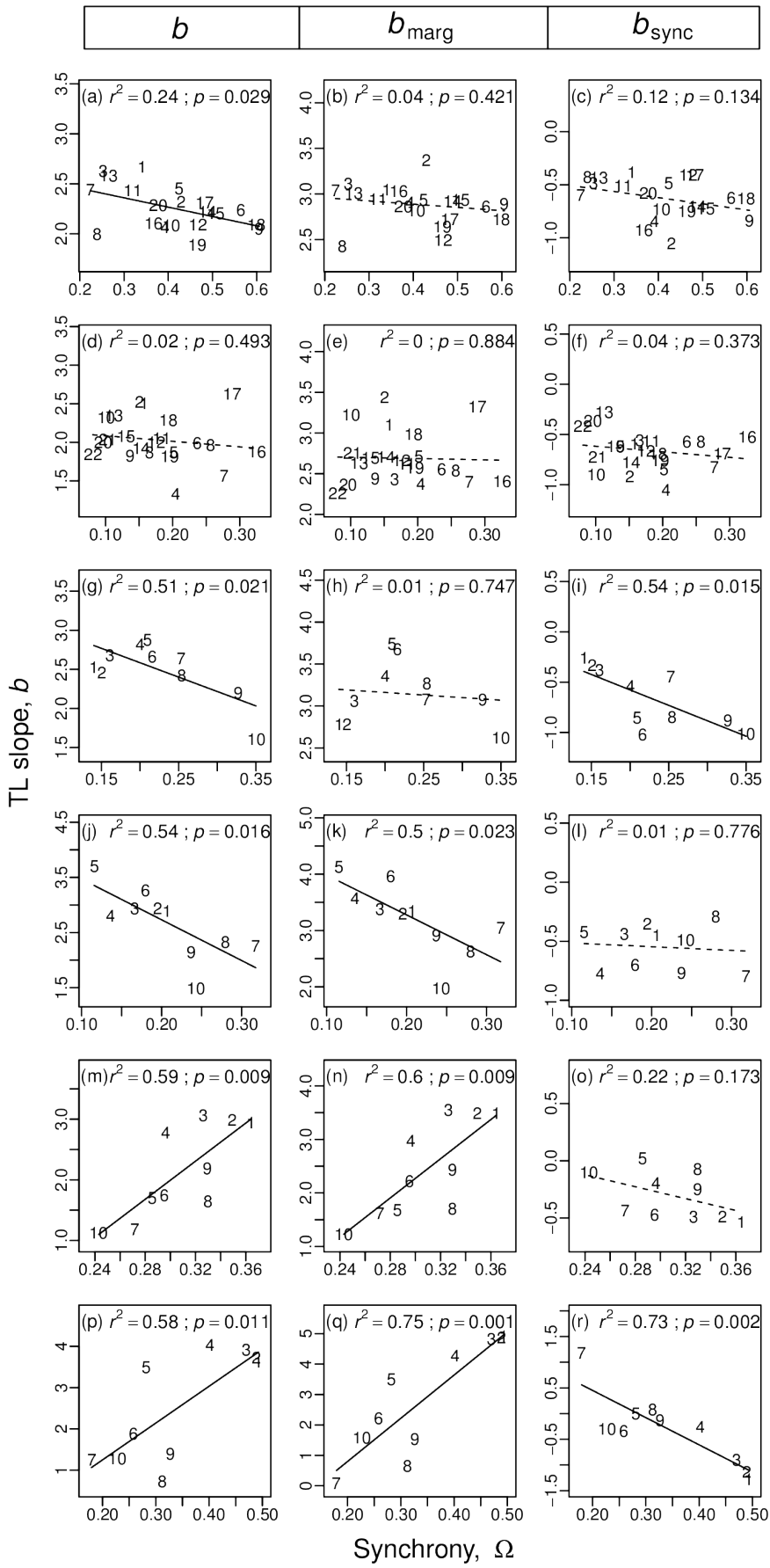


Figure S99: Same as main text figure 2, except points are numbered to identify aphid species, plankton groups, and depths, using the numbers of table S1.

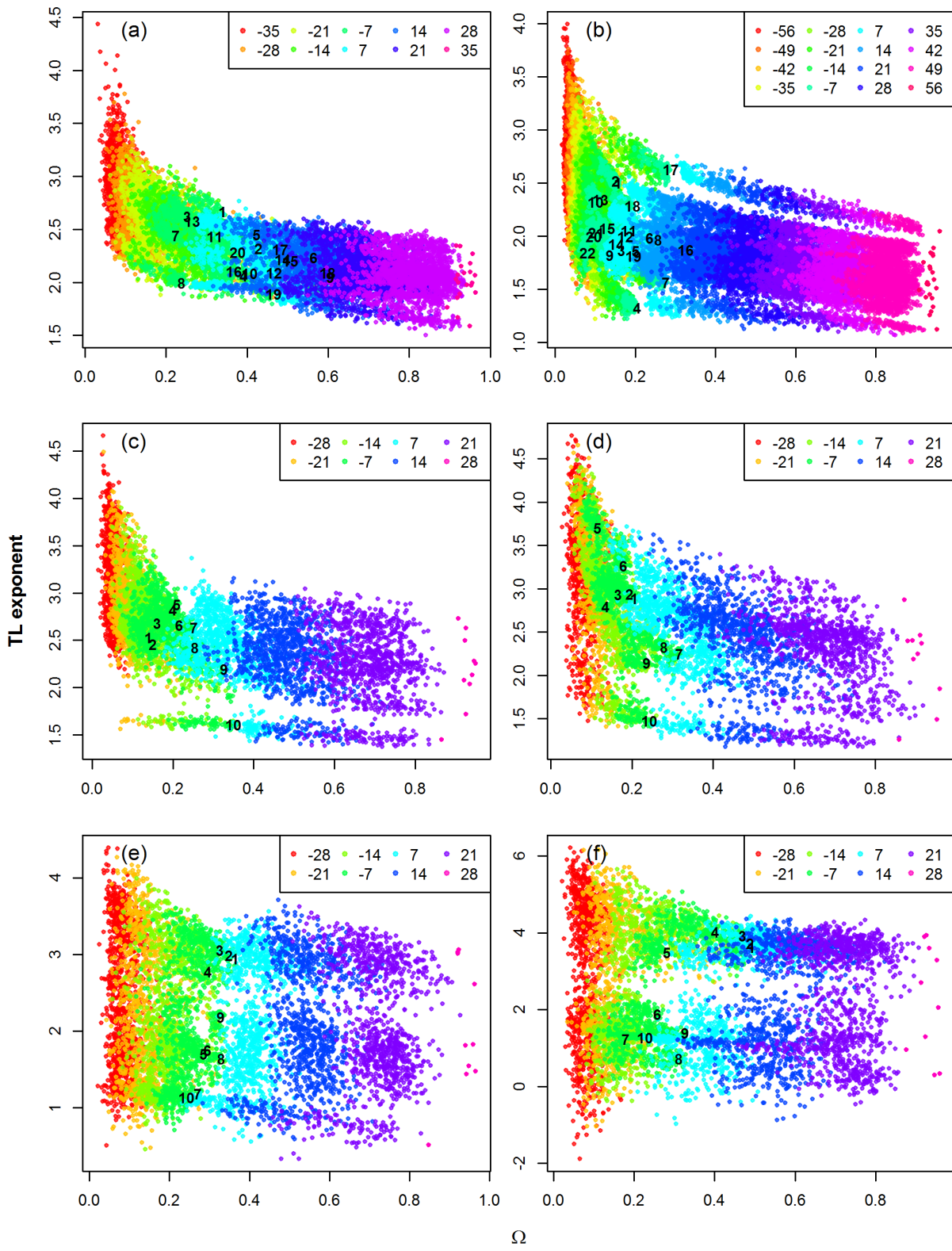


Figure S100: Points in figure 3 in the main text are averages over randomizations/sortings. This plot shows the individual randomizations/sortings. Colors correspond to numbers of rows within which time series were randomized or sorted, negative numbers of rows in figure legends corresponding to randomization and positive values to sorting. Panels correspond to data sets in the same pattern as main text figure 3.

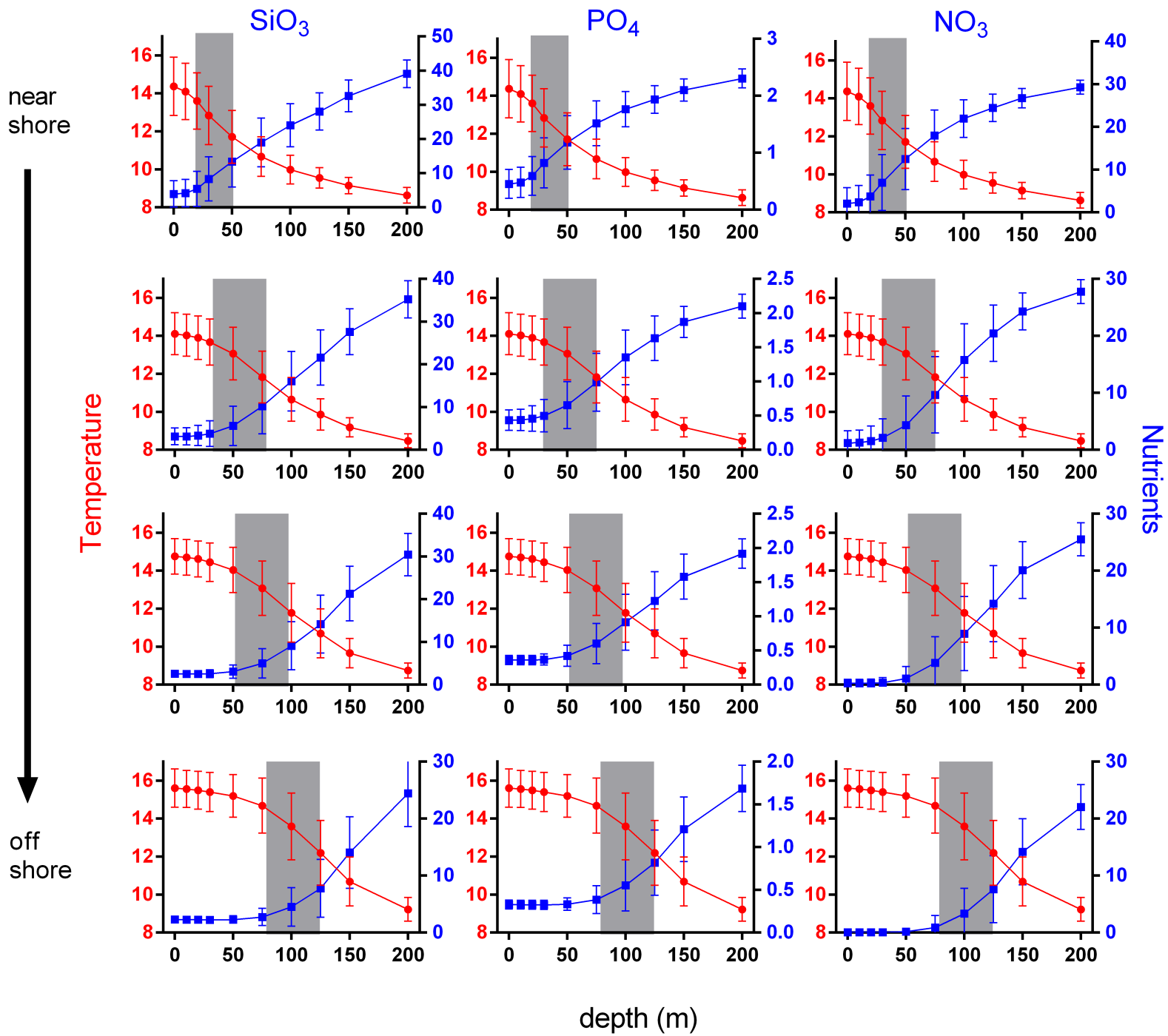


Figure S101: Temperature and nutrient depth gradients in near-shore, far-from-shore, and intermediate sampling stations for the CalCOFI data. Error bars give standard deviations across time and sampling location. Grey bars are put on by eye to approximately indicate the steepest part of the thermocline.

## S14 Tables

Aphids		UK seas		CalCOFI	
Index	Species name	Index	Group name	Index	Depth (m)
1	Apple-grass aphid	1	<i>Acartia</i> spp (unidentified)	1	0
2	Bird cherry-oat aphid	2	<i>Calanus</i> I-IV	2	10
3	Black bean aphid	3	<i>Calanus finmarchicus</i>	3	20
4	Blackberry-cereal aphid	4	<i>Calanus helgolandicus</i>	4	30
5	Blackcurrant-sowthistle aphid	5	<i>Centropages typicus</i>	5	50
6	Corn leaf aphid	6	<i>Ceratium furca</i>	6	75
7	Currant-lettuce aphid	7	<i>Ceratium fusus</i>	7	100
8	Damson-hop aphid	8	<i>Ceratium macroceros</i>	8	125
9	Grain aphid	9	<i>Ceratium tripos</i>	9	150
10	Green spruce aphid	10	Decapoda larvae (Total)	10	200
11	Leaf-curling plum aphid	11	Echinoderm larvae		
12	Mealy cabbage aphid	12	Euphausiacea Total		
13	Mealy plum aphid	13	<i>Metridia lucens</i>		
14	Pea aphid	14	<i>Nitzschia delicatissima</i>		
15	Peach-potato aphid	15	<i>Nitzschia seriata</i>		
16	Potato aphid	16	<i>Oithona</i> spp		
17	Rose-grain aphid	17	Para-Pseudocalanus spp		
18	Shallot aphid	18	<i>Pseudocalanus elongates</i> Adult		
19	Sycamore aphid	19	<i>Rhizosolenia alata</i> <i>alata</i>		
20	Willow-carrot aphid	20	<i>Rhizosolenia styliformis</i>		
		21	<i>Temora longicornis</i>		
		22	<i>Thalassiosira</i> spp		

Table S1: Indices used in plots to refer to specific aphid species, plankton groups, or sampling depths.

<b>Site</b>	<b>Latitude</b>	<b>Longitude</b>	<b>Operation dates through 2010</b>
<b>Ayr</b>	55.477	-4.567	30/8/1974 - 9/12/2001; 23/3/2003 - 25/12/2005
<b>Broom's Barn</b>	52.26	0.57	22/3/1965 - end
<b>Dundee</b>	56.457	-3.069	12/5/1965 - 10/12/2006; 17/2/2008 - 30/12/2008; 25/4/2010 - end
<b>Edinburgh</b>	55.949	-3.312	3/4/1969 - 2/10/1971; 1/1/1972 - 30/12/2005; 18/5/2004 - 13/12/2009
<b>Hereford</b>	52.125	-2.637	12/7/1971 - end
<b>Newcastle</b>	55.213	-1.682	21/5/1965 - end, excluding 2009
<b>Preston</b>	53.854	-2.763	29/4/1971 - end
<b>Rothamsted</b>	51.807	-0.356	29/4/1964 - end
<b>Starcross</b>	50.628	-3.454	5/2/1970 - 21/12/2008
<b>Writtle</b>	51.733	0.427	22/5/1975 - 29/7/1991; 1/1/1992 - end
<b>Wye</b>	51.185	0.939	30/11/1966 - end, excluding 2009

Table S2: Sampling sites used. Operating dates given in day/month/year format. Edinburgh is the combination of two very nearby sites, East Craigs and Gogarbank. East Craigs operating dates were 3/4/1969 to 2/10/1971 and 1/1/1972 to 30/12/2005. Gogarbank operating dates were 18/5/2004 to 13/12/2009. Data for Edinburgh were taken from 1/1/2006 forward from Gogarbank. This table was taken from [Sheppard et al. \[2015\]](#).

**Analytic results:** Appendices S1 and S2

Summary: Results apply when the  $Y_i$  are identically distributed.  $b$  depends on  $\Omega$  approximately as equation (44). The approximation will be worse for larger  $\Omega$ .  $b$  should decrease sharply as  $\Omega$  increases from 0. Skewness of  $Y_i$  is necessary in the identically distributed case to get  $b \neq 0$ .

Distribution	TL holds?	$b$ depends on $\Omega$ ?	$b \downarrow$ as $\Omega \uparrow$ from 0	$b \uparrow$ as $\Omega \uparrow$ further	eq. (44) a good approximation?
<b>Numeric results</b> for $Y_i$ identically distributed, Gaussian copula: Appendix S3 and figs S1 through S32					
Poisson, figs S1-S2	large $\lambda$ , yes; small $\lambda$ , approx'ly	yes	yes	no	NA
neg. binom., figs S3-S10	yes, except for larger $p$ and $\Omega$	yes	yes	no	NA
gamma, figs S11-S16	yes, but approx'ly for small $\alpha$ and large $\Omega$	yes	yes	sometimes no; sometimes slightly	qualitatively, yes; better for small $\Omega$
exponential, figs S17-S18	small $\Omega$ , yes; large $\Omega$ , approx'ly	yes	yes	sometimes no; sometimes slightly	qualitatively, yes; better for small $\Omega$
chi-squared, figs S19-S20	large $k$ , yes; small $k$ , approx'ly	yes	yes	sometimes no; sometimes slightly	qualitatively, yes; better for large $k$
normal, figs S21-S26	yes	no	no	no	yes
log-normal, figs S27-S32	yes, except when $\sigma$ is large and $\Omega$ small	yes	yes	no	only for small $\sigma$

**Numerical results** for  $Y_i$  non-identically distributed, Gaussian copula: Appendix S4 and figs S33 through S64

Poisson, figs S33-S34	yes	yes	yes	no	NA
neg. binom., figs S57-S64	small $\Omega$ yes; large $\Omega$ often no	yes	yes	usually no; sometimes yes	NA
gamma, figs S35-S40	small $\Omega$ yes; large $\Omega$ , approx'ly	yes	yes	yes	NA
exponential, figs S41-S42	small $\Omega$ yes; large $\Omega$ , approx'ly	yes	yes	yes	NA
chi-squared, figs S43-S44	small $\Omega$ yes; large $\Omega$ , approx'ly	yes	yes	no	NA
normal, figs S45-S50	yes, except for $\sigma = 1, \mu = 5$	yes	yes	no, except for $\sigma = 1, \mu = 5$	NA
log-normal, figs S51-S56	yes	yes	yes	no	NA

**Numeric results** for  $Y_i$  identically distributed, construction based on sums (common elements): Appendix S5 and figs S65 through S90

Poisson, figs S65-S66	large $\lambda$ yes ; small $\lambda$ no	yes	yes	no	yes
neg. binom., figs S67-S74	large $r$ approx'ly; small $r$ no	yes	yes	no	better for large $r$
gamma, figs S75-S80	only for smallest and largest $\Omega$	yes	yes	no	yes, but better for larger $\alpha$
exponential, figs S81-S82	only for smallest $\Omega$	yes	yes	no	qualitatively
chi-squared, figs S83-S84	only for small $\Omega$ or large $k$	yes	yes	no	qualitatively
normal, figs S85-S90	yes	no	no	no	yes

Table S3: Summary of analytic and numeric results. Color indicates hyperlinks that, when clicked inside a pdf viewer, will lead directly to the relevant material. A summary of randomization and empirical results is in table S14.

Empirical results: Main text, and main text fig. 2				
Data set	TL holds?	$b$ depends on $\Omega$ ?	$b_{\text{marg}}$ depends on $\Omega$ ?	$b_{\text{sync}}$ depends on $\Omega$ ?
Aphid data	yes, except 1 species	$b \downarrow$ as $\Omega \uparrow$ , signif'ly	$b_{\text{marg}} \downarrow$ as $\Omega \uparrow$ , non-signif'ly	$b_{\text{sync}} \downarrow$ as $\Omega \uparrow$ , non-signif'ly
SAHFOS data	yes	$b \downarrow$ as $\Omega \uparrow$ , non-signif'ly	$b_{\text{marg}} \downarrow$ as $\Omega \uparrow$ , non-signif'ly	$b_{\text{sync}} \downarrow$ as $\Omega \uparrow$ , non-signif'ly
CalCOFI gp. 1	yes, except 1 depth	$b \downarrow$ as $\Omega \uparrow$ , signif'ly	$b_{\text{marg}} \downarrow$ as $\Omega \uparrow$ , non-signif'ly	$b_{\text{sync}} \downarrow$ as $\Omega \uparrow$ , signif'ly
CalCOFI gp. 2	yes	$b \downarrow$ as $\Omega \uparrow$ , signif'ly	$b_{\text{marg}} \downarrow$ as $\Omega \uparrow$ , signif'ly	$b_{\text{sync}} \downarrow$ as $\Omega \uparrow$ , non-signif'ly
CalCOFI gp. 3	yes for 5 and no for 5 depths	$b \uparrow$ as $\Omega \uparrow$ , signif'ly	$b_{\text{marg}} \uparrow$ as $\Omega \uparrow$ , signif'ly	$b_{\text{sync}} \downarrow$ as $\Omega \uparrow$ , non-signif'ly
CalCOFI gp. 4	yes	$b \uparrow$ as $\Omega \uparrow$ , signif'ly	$b_{\text{marg}} \uparrow$ as $\Omega \uparrow$ , signif'ly	$b_{\text{sync}} \downarrow$ as $\Omega \uparrow$ , signif'ly

Randomization results: Main text, and main text fig. 3, figs S97 through S100				
Data set	TL holds?	$b$ depends on $\Omega$ ?	$b \downarrow$ as $\Omega \uparrow$ from 0	$b \uparrow$ as $\Omega \uparrow$ further
Aphid data	low sync., yes; high sync., approx'ly	yes	yes	no, except modestly for 1 case
SAHFOS data	low sync., yes; high sync., approx'ly	yes	yes	no, except modestly for 1 case
CalCOFI gp. 1	low sync., yes; high sync., approx'ly	yes	yes	no
CalCOFI gp. 2	low sync., yes; high sync., approx'ly	yes	yes	no, except modestly for 1 case
CalCOFI gp. 3	approx'ly	yes	yes	no, except modestly for a few cases
CalCOFI gp. 4	approx'ly	yes	yes, except 1 case	no, except a few cases

Table S4: Summary of randomization and empirical results. Color indicates hyperlinks that, when clicked inside a pdf viewer, will lead directly to the relevant material. For the empirical part of the table, TL was considered to hold except when linearity or homoskedasticity was rejected with 99% confidence. A summary of analytic and numeric results is in table S14.

## S15 References

- S.D. Batten, R. Clark, J. Flinkman, G.C. Hays, E. John, A.W.G. John, T. Jonas, J.A. Lindley, D.P. Stevens, and A. Walne. CPR sampling: the technical background, materials and methods, consistency and comparability. *Progress in Oceanography*, 58:193–215, 2003.
- G. Beaugrand and P.C. Reid. Long-term changes in phytoplankton, zooplankton and salmon related to climate. *Global Change Biology*, 9:801–817, 2003.
- J.R. Bell, L. Alderson, D. Izera, T. Kruger, S. Parker, J. Pickup, C.R. Shortall, M.S. Taylor, P. Verrier, and R. Harrington. Long-term phenological trends, species accumulation rates and climate: five decades of change in migrating aphids. *Journal of Animal Ecology*, 84:21–34, 2015.
- D. Brillinger. *Time Series: Data Analysis and Theory*. SIAM, Philadelphia, 2001.
- H. Caswell. *Matrix population models: Construction, analysis, and interpretation*. Sinauer Associated, Inc., Sunderland, MA, 2001.
- J.E. Cohen and M. Xu. Random sampling of skewed distributions implies Taylor's power law of fluctuation scaling. *Proceedings of the National Academy of Sciences*, 112:7749–7754, 2015. doi: 10.1073/pnas.1503824112.
- C. H. Fischer. On correlation surfaces of sums with a certain number of random elements in common. *Annals of Mathematical Statistics*, 4:103–126, 1933.
- R. Harrington. The Rothamsted Insect Survey strikes gold. *Antenna*, 38:158–166, 2014.
- D.W. Hosmer, S. Lemeshow, and S. May. *Applied Survival Analysis: Regression Modeling of Time-to-Event Data*. Wiley, New York, 2 edition, 2008.
- E. Macaulay, G. Tatchell, and L. Taylor. The Rothamsted Insect Survey 12-metre suction trap. *Bulletin of Entomological Research*, 78:121–129, 1988.
- A.W. Mantayla, S.J. Bograd, and E.L. Venrick. Patterns and controls of chlorophyll-*a* and primary productivity cycles in the Southern California Bight. *Journal of Marine Systems*, 73:48–60, 2008.
- R.M. Nisbet and S.C. Gurney. *Modelling fluctuating populations*. John Wiley and Sons, New York, 1982.
- G.W. Oehlert. A note on the delta method. *American Statistician*, 46:27–29, 1992.
- D.E. Raitsos, Y. Pradhan, S.J. Lavender, I. Hoteit, A. McQuatters-Gollop, P.C. Reid, and A.J. Richardson. From silk to satellite: half a century of ocean color anomalies in the Northeast Atlantic. *Global Change Biology*, 20:2117–2123, 2013.
- L.W. Sheppard, J.R. Bell, R. Harrington, and D.C. Reuman. Changes in large-scale climate alter spatial synchrony of aphid pests. *Nature Climate Change*, 6:610, 2015.
- P. Turchin. *Complex population dynamics: A theoretical/empirical synthesis*. Princeton University Press, Princeton, 2003.
- L. Zhang. Sample mean and sample variance: their covariance and their (in)dependence. *American Statistician*, 61:159–160, 2007.